AFCRL 64-197

ARCTIC METEOROLOGY RESEARCH GROUP
DEPARTMENT OF METEOROLOGY
McGILL UNIVERSITY, MONTREAL *

F. K. HARE, Chairman

Contributions to the

Seminars on the Stratosphere and Mesosphere and Polar Meteorology JULY 7-19, 1963

at Stanstead College. Stanstead, Quebec Province, Canada.

PUBLICATION IN METEOROLOGY No. 65 | January 1963

SCIENTIFIC REPORT No. 9*
Contract No. AF 19 (604)-8431
Project No. 8628 Task No. 862807

Prepared for

Air Force Cambridge Research Laboratories,
Office of Aerospace Research,
United States Air Force,
Bedford, Massachusetts.

BLANK PAGES IN THIS DOCUMENT WERE NOT FILMED

AFCRL 64-197

ARCTIC METEOROLOGY RESEARCH GROUP
DEPARTMENT OF METEOROLOGY
McGILL UNIVERSITY, MONTREAL

F. K. HARE, Chairman

Contributions to the

Seminars on the Stratosphere and Mesosphere and Polar Meteorology JULY 7-19, 1963

at Stanstead College. Stanstead, Quebec Province, Canada.

PUBLICATION IN METEOROLOGY No. 65 | January 1963

SCIENTIFIC REPORT No. 9
Contract No. AF 19 (604)-8431
Project No. 8628 Task No. 862807

Prepared for

Air Force Cambridge Research Laboratories,
Office of Aerospace Research,
United States Air Force,
Bedford, Massachusetts.

PREFACE

The 1963 Stanstead Seminar is over and done with, but it will not quickly be forgotten by those who took part. Many good papers were presented in the informal way that has become the usual Stanstead practice. Summaries of these papers are circulated in this report. As the list of authors shows, the group was a very distinguished one. We have never before had such a uniformly high level of performance.

In 1959, when we first devoted the Seminar in part to stratospheric questions, research at such levels was still something of a novelty. The McGill group felt itself to be among the pioneers. Four years later all is changed. Stratospheric and mesospheric problems occupy the centre of the stage. Moreover meteorologists have invaded the upper atmosphere, and can listen to papers like those by Colin Hines with dawning comprehension. The editorial policy of the Journal of Atmospheric Science has moved in this direction, and the Stanstead Seminars have followed suit. Nevertheless the main problems discussed were still the unresolved questions of meridional circulations, energy budget and diffusion mechanisms that have bothered us ever since the Brewer-Dobson model was first propounded.

This year we went back to our original plan of basing part of the program on polar meteorology. The Committee on Polar Meteorology of the American Geophysical Union invited us to do this; Dr. Svenn Orvig and Dr. M.J. Rubin (Chairman of this Committee) put together an excellent set of papers. We found, however, that it was impossible to separate the two activities. Much of the polar meteorology was stratospheric, and vice versa. Moreover we found that stratospheric specialists were obviously fascinated by boundary layer problems over cold surfaces, and we were forced to amalgamate the two groups for much of the period. It was salutary to remind ourselves that the troposphere and the boundary layer are not identical, as upper atmosphere specialists seem to assume !

Much of the success of a Seminar of this sort depends on the willing collaboration of those who take part : a willingness to talk first and think afterwards added zest to the discussion, and the rules of the game allowed one to admit one's error without loss of face. The four chairmen - Boville, Orvig, Rubin and Hare - would have got nowhere without this kind of attitude. They all owe a debt to the various members of the Seminar who were willing to talk.

Although much of the cost of the Seminar was borne by the USAF under Contract AF 19(604)8431, we must acknowledge with real gratitude a grant of $ 2,000 from the Committee on Research of McGill University. This enabled us to enlarge the program into fields not directly growing from our own contract research.

Director
Arctic Meteorology Research Group

ACKNOWLEDGEMENTS

Our warm thanks go to Mrs. V. MacDonald who collected and edited the scientific papers in this report, to Mrs. A. Kruczkowska who prepared the diagrams, to Mrs. V. Haar who was responsible for preparing the manuscript and processing the report and to Mr. P. Larsson who acted as registrar and bursar at the Conference.

B. W. Boville,
Project Director.

LIST OF PARTICIPANTS

* Dr. A.A. Barnes	A.F.C.R.L., G.R.D.
* Dr. B.W. Boville	McGill University
* Dr. A.W. Brewer	University of Toronto
Mr. H. Cameron	D.O.T., Meteorological Branch
* Dr. G.P. Cressman	U.S.W.B.
Dr. H.L. Croom	U.S.A.F.
* Dr. P.C. Dalrymple	Q.M. R. & E. Commd. US. Army
Dr. E. Danielson	Pennsylvania State University
Mr. J. Derome	McGill University
Maj. L. Devries	U.S.A.F.
Dr. P.J. Drevinsky	A.F.C.R.L., G.R.D.
* Dr. R.T. Duquet	Pennsylvania State University
* Mr. A. Eddy	McGill University
Mr. F.G. Finger	U.S.W.B.
Capt. W.A. Gallie	U.S.A.F.
* Dr. W.L. Godson	D.O.T., Meteorological Branch
Mr. Y. Gotaas	University of Alaska
* Mr. J. Hampson	C.A.R.D.E.
Mr. D.R. Haragan	University of Texas
Dr. F.K. Hare	McGill University
* Dr. B. Haurwitz	University of Colorado
Mr. T.J.G. Henry	D.O.T., Meteorological Branch
* Dr. W.S. Hering	A.F.C.R.L., G.R.D.
* Dr. C.O. Hines	University of Chicago
Maj. R.R. Hippler	U.S.A.F.
* Dr. W. Hitschfeld	McGill University
Capt. J.G. Joern	U.S.A.F.
Mr. E.L. Jones	U.S.A.F.

	Mr. M. Kwizak	D.O.T., Meteorological Branch
	Mr. P. Larsson	McGill University
	Mr. R. Lee	D.O.T., Meteorological Branch
*	Dr. H.H. Lettau	University of Wisconsin
*	Dr. J. London	University of Colorado
	Mrs V.D. MacDonald	McGill University
*	Dr. E.A. Martell	N.C.A.R.
	Mr. D.E. McClellan	D.O.T., Meteorological Branch
	Mr. P. Merilees	McGill University
	Capt. H.A. Million	U.S.A.F.
*	Mr. F.B. Muller	D.O.T., Meteorological Branch
*	Dr. F.W. Murray	Douglas Aircraft Co.
	Dr. G. Ohring	Geophysics Corp. of America
	Mr. A.H. Oort	Massachusetts Institute of Technology
*	Mr. B.E. O'Reilly	McGill University
*	Dr. S. Orvig	McGill University
*	Dr. S. Penn	A.F.C.R.L., G.R.D.
	Mr. A.B. Pittock	N.C.A.R.
	Mr. G.D. Prantner	U.S. Navy
*	Mr. A.J. Robert	McGill University
*	Mr. M.J. Rubin	U.S.W.B.
*	Dr. A. Schiff	McGill University
*	Mr. M. Shimizu	Japan Met. Agency
	Dr. D.B. Spiegler	Travelers Res. Center Inc.
	Mr. G.B. Spindler	C.A.R.D.E.
	Mr. L. Steinberg	McGill University
	Miss B. Taylor	McGill University
	Mr. H.J. Viebrock	U.S.W.B.
*	Dr. E. Vowinckel	McGill University
*	Dr. G. Warnecke	N.A.S.A.
*	Mr. W.M. Washington	Pennsylvania State University
*	Dr. W.S. Weyant	U.S.W.B.

* Dr. A. Wiin-Nielsen	N.C.A.R.
Mr. A.W. Wilson	University of Toronto
Miss C. Wilson	Laval University

* Speakers

TABLE OF CONTENTS

II

III

V

SOME COMMENTS ON THE INTERACTION OF ATMOSPHERIC LAYERS

B. W. Boville

The wave activity and final warmings of the winter stratospheric vortices, in both hemispheres, represent perturbations whose amplitudes increase with time in the presence of large horizontal temperature gradients. They are thus manifestations of baroclinic instability, in its most general sense. Whether their properties can be likened to the more classical concept of baroclinic instability, that is the growth of a small disturbance through a potential to kinetic energy conversion in the tropospheric thermal field which extends down to the solid lower boundary, is quite another question. It is doubtful whether our present levels of theoretical and observational specifications are sufficient to resolve the various wave possibilities.

Before looking at wave types, it is useful to consider the implications of the second law of thermodynamics. From the viewpoint of a heat engine (i.e. to have a hemispheric generation of available potential energy) a positive correlation between the meridional temperature profile and the diabatic heating function is required. On the basis of generally accepted values for the northern hemisphere winter, one finds a source layer from the surface to 10 km, a sink from 10 to 20 km; another source from 20 - 50 km and a sink from 50 - 80 km. Just as the lower stratosphere must obtain its energy supply from the troposphere, so it appears that the mesosphere must obtain its supply from the middle and upper stratosphere, or else from the troposphere. Dynamical studies of the 20 - 50 km layer should then reveal the crude nature of the stratospheric -mesospheric energetics in much the same fashion as tropospheric studies have done at low levels. One difficulty with generalising too far in regard to the upper layers is their relatively small energy storage. In the stratospheric winter, computations suggest that wave activity can destroy the available energy in less than 10 days. Also, observations suggest that high static stability pervades the polar and mid-latitude mesosphere. It is thus possible that a disturbed stratosphere could result in several vertically layered systems rather than a single maximum temperature and maximum wind system.

If one considers the possibility of an independent stratospheric system then the most recent formulation concerns the stability of an internal jet, treated by Charney and Stern (1962) . Under their criterion the jet will be stable unless there are maxima and minima in the latitudinal profile of absolute potential vorticity. A number of computed profiles, based on hemispherically averaged geopotential heights at 25 mb, indicate that the middle stratosphere is stable during the fall and early winter but some late winter profiles do meet the instability criterion. There are however, two factors difficult to reconcile in these cases. First, the singular neutral wave speed for these cases is about 45 m/sec which is far from the observed phase speed of the unstable mode which moves slowly or even retrogrades; and second, Fourier analyses at those times yield heat transports at lower levels, which is not consistent with the internal jet boundary conditions. Another factor, which seems to be against the internal jet mechanism is the apparent lack of early development in the southern hemisphere where stratospheric wind speeds are much stronger. However, preliminary profiles for the 700 K potential temperature surface suggest that the southern wind system is much too broad to attain the required horizontal wind shears. The possible importance of this type of instability cannot then be dismissed.

Many of the synoptic and dynamical studies carried out at McGill indicate that the stratospheric developments in the planetary waves one and two. are closely associated with tropospheric events. These suggest a closely coupled or strongly forced system. In a recent study on stationary planetary waves in a non-uniform basic current Eliassen and Plamer (1961) have shown that the upward propagation of wave energy is associated with a northward heat transport. This is also the characteristic of a classical baroclinic wave and the condition required to maintain a baroclinic wind profile. These factors show that the various baroclinic processes cannot be readily separated; they also indicate that a detailed study of horizontal heat transports would provide a simple and effective diagnostic tool.

A further analysis by Charney and Drazin on the upward propagation of planetary waves provides an additional criterion. Besides the suppression of vertical propagation in zero or easterly zonal wind regimes they find that strong west winds also inhibit vertical flux. Quasi-geostrophic waves with phase velocity less than the Rossby critical velocity do not penetrate the tropospheric jet. The vertical propagation of planetary wave two is suppressed by a west wind speed of about 40 m sec^{-1}. It appears that the zonal wind systems must change their vertical structure so as to inhibit the upward propagation of significant amounts of planetary wave energy into the upper atmosphere. The summer easterlies provide this barrier. Strong westerlies in the mesosphere and upper stratosphere setting in during the fall prior to the decay of the lower stratospheric easterlies would play a similar role. The apparent downward propagation of some of the wave activity might be explained by a maximum amplification rate in the regions of strong vertical wind shear. The apparent lack of early developments in the southern hemisphere may be related to the stronger west winds and the much lower amplitude of the tropospheric planetary waves in that hemisphere.

One is thus led to consider an upward propagation or strongly (tropospherically) forced baroclinic mechanisms for much of

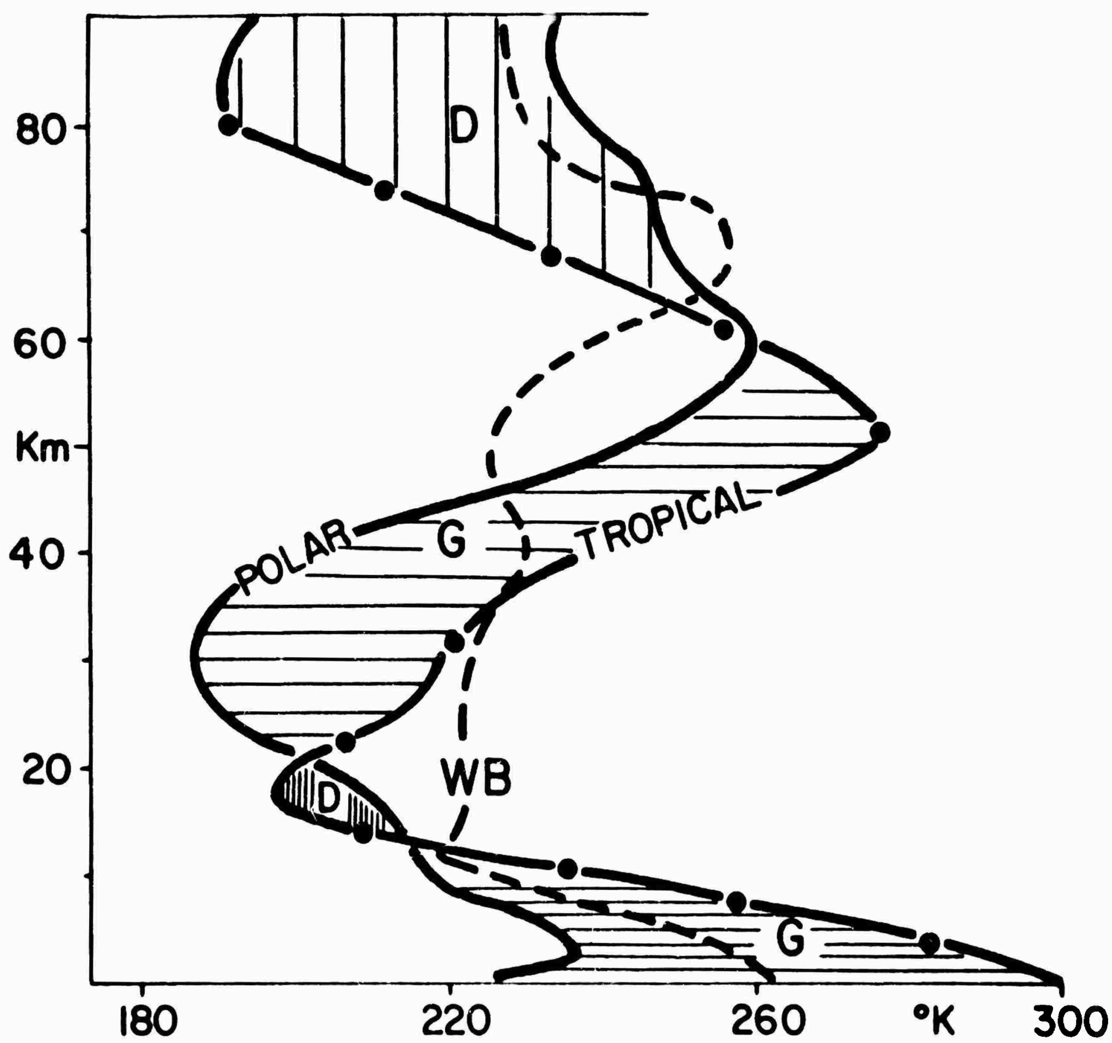

Figure 1. The solid curves are schematic mid-winter temperature profiles for tropical and polar regions. The horizontal hatching shows the probable generation regions (G) for zonal available potential energy and the vertical hatching the destruction regions (D). Note, however, that the introduction of a probably mid-latitude warm-belt profile complicates the picture both thermally and radiatively.

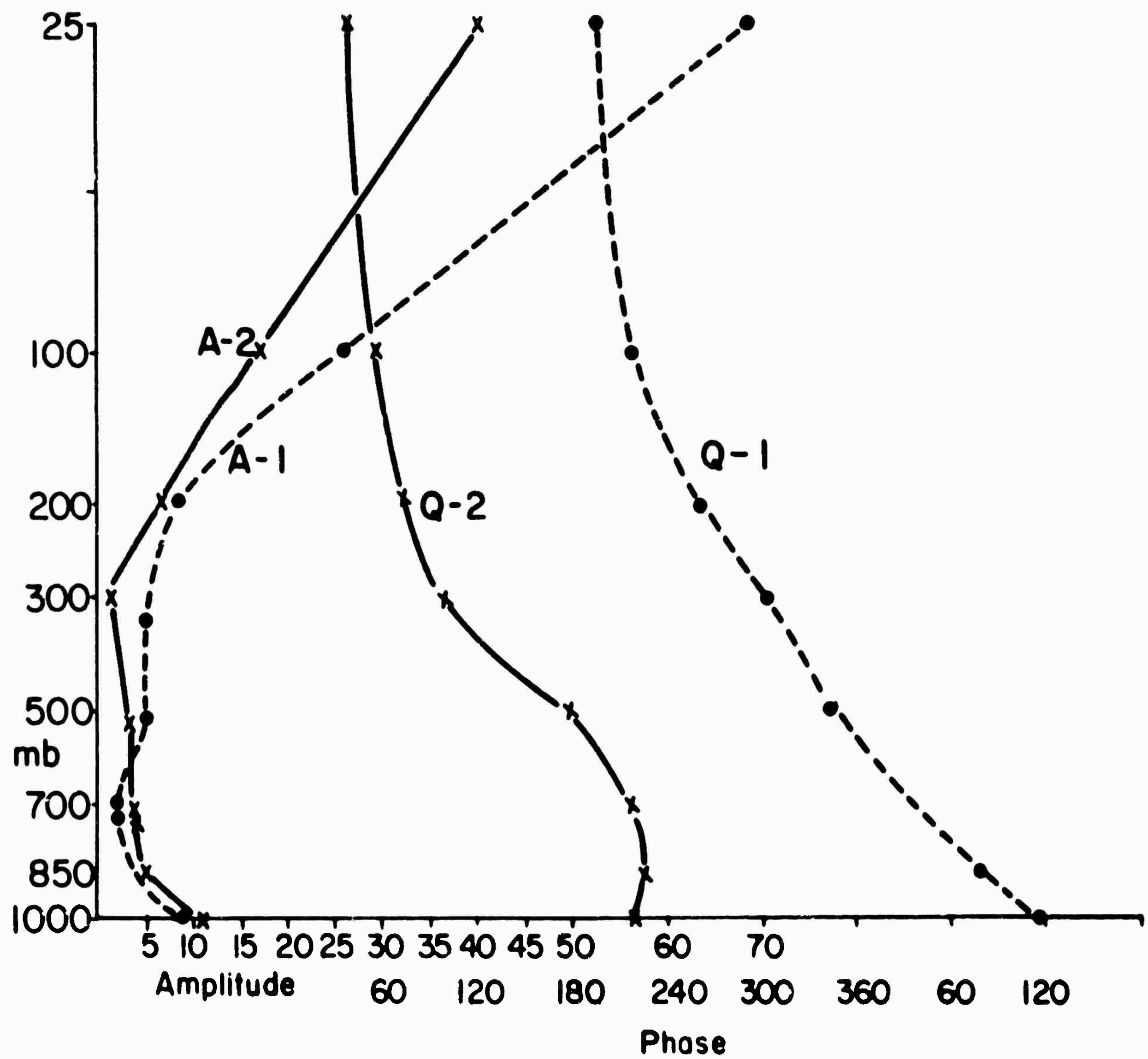

Figure 2. The amplitudes, A , and phase angles, Q, of planetary waves one and two at latitude 60 N on Jan 16, 1959 during a development period. Note the rapid increase in amplitude above the tropospheric jet stream level and the westward tilt of the waves with height.

the wave activity in the winter stratosphere. Internal instability may become an important contributing factor in late winter and spring.

REFERENCES :

Boville, B.W. : 'A dynamical study of the 1958-59 stratospheric polar vortex'. Arct. Met.Res.Gp. Pub. in Met. 36, McGill University, 1961.

Charney, J.G. and P.G. Drazin : 'Propagation of planetary scale disturbances from the lower into the upper atmosphere', J. Geophys. Res., 66, 83-109, 1961.

Charney, J.G. and M.E. Stern : ' On the stability of internal baroclinic jets in a rotating atmosphere', J. Atmos. Sc., 19,159 - 172, 1962.

Eliassen, A. and E. Palm : ' On the transfer of energy in stationary mountain waves', Geof. Pub., 22/3, 1-23, 1961.

Van Mieghem, J. 'New aspects of the general circulation of the stratosphere and mesosphere', Met. Abhandl. Inst. f. Meteor. u. Geophys. Freien Universitat Berlin, XXXVI , 5 -62, 1963.

THE ROLE OF THE STRATOSPHERE IN THE TROPOSPHERIC DEVELOPMENTS

G.P. Cressman

In order to understand the possible stratospheric influences in developing tropospheric systems, it will be necessary to examine closely the nature of tropospheric development. We should, for this purpose, exclude those systems whose behavior is essentially equivalent barotropic in nature, and define development as an event which in mid-troposphere is not described by the conservation of absolute vorticity. Such events are often characterized by the appearance of strong cyclonic systems.

We can write the vorticity equation as

$$\frac{\partial \zeta}{\partial t} + V \cdot \nabla (f + \zeta) - (f + \zeta) \frac{\partial \omega}{\partial p} + k \cdot \nabla \times \omega \frac{\partial V}{\partial p} = 0 \quad (1)$$

where ζ is relative vorticity, f is the coriolis parameter, V is the horizontal wind vector, and ω is the individual pressure derivative, dp/dt, referred to as the vertical velocity (in pressure coordinates). The evaluation of the term $k \cdot \nabla \times \omega \partial V/\partial p$ with reasonable accuracy is not difficult in any two or more parameter model, and shows that this term is not ordinarily of much importance in describing development. It remains then to consider the third term, arising from horizontal divergence. This can be done by deriving an equation for ω.

The adiabatic equation can be used for this purpose, stating

$$\frac{\partial}{\partial t} \left(\frac{\partial \Phi}{\partial p}\right) + V \cdot \nabla \frac{\partial \Phi}{\partial p} + \omega \sigma = 0 \quad (2)$$

where ϕ is geopotential, and σ is a measure of the static stability given by $\sigma = -\alpha\partial \ln \theta / \partial p$, where α is specific volume and θ is potential temperature. Without damaging the results of the discussion we can assume that

$$\frac{\partial}{\partial t}\left(\nabla^2 \frac{\partial\phi}{\partial p}\right) = f \frac{\partial}{\partial t}\left(\nabla^2 \frac{\partial\psi}{\partial p}\right), \text{ (geostrophic approx. for local change)} \quad (3)$$

and that σ is a function of pressure only. We then obtain, after differentiating (1) with p and taking the curl of (2), an equation for ω,

$$\nabla^2\omega + \frac{f\eta}{\sigma}\frac{\partial^2\omega}{\partial p^2} = \frac{1}{\sigma} f \frac{\partial}{\partial p}\left(V.\nabla\eta\right) - \nabla^2\left(V.\nabla\frac{\partial\phi}{\partial p}\right) \quad (4)$$

The term involving $k.\nabla \times \omega \frac{\partial V}{\partial p}$ was dropped, as being of little importance.

Before using this equation for evaluations of data, let us consider certain implications of the equation in a simplified form. Let

$$\nabla^2\omega = -k^2\omega \quad ,$$

$$\frac{\partial^2\omega}{\partial p^2} - A\,\omega = F, \quad (5)$$

where $A = \frac{k^2\sigma}{f\eta}$, and F is a forcing function made up of the terms on the right hand side of (4). This equation has a vertically symmetric solution for ω if F is invariant with pressure. However, if F varies markedly with pressure, the maximum value of ω is found far from mid-troposphere, giving large mid-tropospheric divergence associated with development.

The component terms of F are seen to depend on the Laplacian of temperature advection and on variations with height of the advection of absolute vorticity. If we consider a typical strong cold frontal situation, we recall that the strong cold advection is concentrated at low levels and weakens with height, finally going over to a warm advection at higher levels as the warm stratospheric bulge moves in over the cold dome. Also the sign of the vertical shear reverses at the tropopause, giving a change in sign of the vorticity advection. Consequently, we see that in such a situation F not only varies with height, but changes sign at the tropopause. Under these conditions the curve of ω against p will usually have a maximum (sinking) at low levels and a minimum (rising) at high levels, with a maximum slope (convergence) in mid-troposphere.

In accord with the extensive literature in synoptic meteorology we find that the important factors in producing this developmental situation are (a) the low level cold push, (b) the strong high tropospheric jet stream associated with the strong temperature gradient, and (c) the stratospheric warm bulge above the low-level cold air dome.

The energetics of this process can be displayed by a cross-section technique using equation (4) to evaluate atmospheric data. If we separate the horizontal wind into rotational and divergent components, $\mathbb{V}'$ and $\mathbb{V}''$ respectively, we have continuity expressed as

$$\nabla \cdot \mathbb{V}'' + \frac{\partial \omega}{\partial p} = 0 \tag{6}$$

We then display $\mathbb{V}''$ and ω on cross sections of temperature to observe the sense of the energy producing or destroying circulation. A typical cross section of this type shows the circulation to be vigorous and direct in the troposphere and neutral in the lower stratosphere (below 100 mb).

The above evidence suggests that the role of the stratosphere in the tropospheric development is exerted through the existence of the downward warm stratospheric bulge above the cold dome. This encourages a vertically asymmetric distribution of ω, with the appearance of strong mid-tropospheric divergence and convergence areas. However, the energy supply for the development appears to come from the tropospheric circulation, with the stratosphere playing a passive role. It may be that the role of the stratospheric and tropopause perturbation could be best described as catalytic, facilitating the release of the available energy in the tropopause, but otherwise contributing nothing.

REFERENCE :

Cressman, G.P. : 'A diagnostic study of mid-tropospheric development', Monthly Wea. Rev., 74-82, March 1961.

SOME SYNOPTIC FEATURES OF STRATOSPHERIC CIRCULATION

G. Warnecke

By means of hemispheric maps showing the semi-annual temperature change between January and July 1958, as well as July through December 1958, it was pointed out that within the layers between 20 and 30 kilometers there are existing remarkable deviations from a mere radiation controlled temperature variation throughout the year, especially over the northern North Pacific Ocean. This is caused by the appearance of a strong Aleutian anticyclone prevailing during the winter season, which is additionally responsible for the small annual temperature variation over Japan, shown by the course of monthly mean 50 and 20 mb temperatures over Tateno during the period of 1954 - 1960.

The various forms and changes of stratospheric circulation throughout the year were demonstrated by a series of daily synoptic maps :

(a) The summer-winter transition was discussed by the example of July through December 1961. The cooling of the stratosphere, amounting to about 0.27° per day on the average over ten years, starts in the middle of July, when the temperature maximum of the 10 mb level is found with about - 30°C at the North Pole. The first cyclonic curvature in the summer anticyclone appeared one month later. The first closed cyclone could be found about August 20th. During the first half of September the polar vortex is already established. Its strongest deepening occurs during October and in December when temperatures of about - 80°C appear over the Pole at

10 mb. This pressure level dropped from 32.3 to 29.7 km within five months.

(b) The interruptions of the westerly flow during winter were demonstrated by the examples of the formation of an Aleutian anticyclone during the first half of January 1962, and similar formations of an Atlantic anticyclone about two weeks later. However, whereas the Pacific anticyclone was established as a quasi-stationary anticyclonic circulation center, the Atlantic high pressure center moved rapidly eastward and vanished somewhere over the Near East.

(c) The winter-summer transition is widely characterized by the well-known phenomenon of the sudden stratospheric warmings or so called "break-downs" of the polar vortex. For example: the tremendous sudden warming of January 1963 was discussed in detail using the synoptic map series of the Berlin Group up to 10 mb and numerous evaluations of Rocket Network data provided by the Stratospheric Research Project, USWB . This warming shows obvious similarities with the strong warmings of 1957 and 1958 , with respect to its migration across the stream or even upstream. Its beginning was detected on 16 January 1963, southeast of Newfoundland. The rapid temperature increase then travelled northwestwardly to Canada, reaching its temperature maximum with 10 mb values close to $0^{\circ}C$ over Mould Bay on January 27, 1963. During the warming period an extensive mesospheric anticyclone was built up in the mesopeak region, as shown by the rocket network data. With respect to the causes of this warming, a process detected by Scherhag was discussed, which seems to be important for the described formation of the Aleutian and Atlantic anticyclones or for this warming. All three cases show that just at the time of the beginning of sudden stratospheric temperature increase, the warm air which usually covers the 100 mb troughs begins to move out eastwardly into the preceding ridge, which becomes warm by this process and is consequently strengthened with height. Finally, it results in a closed anticyclone at 30 or more kilometers height, lately caused by vertical motions which were initiated from below. It was shown that usually a cooling period follows these warmings, the cooling rate being slightly smaller than those observed in early winter.

(d) The formation of the summer anticyclone was demonstrated briefly. Around May 10 the reversal of winds and temperature gradients takes place at the 10 mb level. At this time the contour heights are varying between 3110 and 3150 geop. decameters over the entire hemisphere, the temperature being found between - 36 and - 46°C.

A short comment was made as to the problem of stratospheric compensation and its deviations in correlation with the behaviour of the polar vortex.

The probable existence of a stratospheric singularity in the occurrence of easterly wind components at 20 mb over Berlin, Germany was demonstrated by Scherhag's diagram.

The differences between the Antarctic and Arctic late winter warmings were additionally demonstrated by long-period data over Alert, Ellesmere Land (1950 -60) Amundsen-Scott , (South Pole) (1957 - 59). Most of the Arctic warmings occur during the polar night while the Southern Hemisphere warmings apparently appear after sunrise.

REFERENCES :

Finger, F.G. and S. Teweles : 'The midwinter stratospheric warming of 1963', to be published.

Met. Abhandl. Inst. f. Meteor. u. Geophys. Freien Universitat Berlin, X, XII, XIII, XV, XVI, XVIII, XIX, XX, XXIII, XXIV, XXV, XXVI (1960 - 1962.)

Scherhag R., et al : Met. Abhandl . Inst. f. Meteor. u. Geophys. Freien Universitat Berlin , XX, 2, 1961.

Warnecke, G. : 'Ueber die zustandsaenderungen der nordhemisphaerischen stratosphaere', Met . Abhandl. Inst. f. Meteor. u Geophys. Freien Universitat Berlin, XXVIII, 3.

Warneche, G. : 'Ueber den temperaturverlauf in der stratosphaere der polargebiete', Polarforschung Zeitschrift der Deutchen Gesellschaft fuer Polarforschung, Holzminden, Germany (in print).

THE YEARLY AND LONG-PERIOD CHANGES OF STRATOSPHERIC CIRCULATION

G. Warnecke

The summer circulation is obviously very similar from year to year, characterized by a pronounced hemispheric anticyclone centered over the North Pole. Contour heights and temperatures at 10 mb are nearly identical on all maps around the middle of July, being almost identical with the normal monthly mean map.

The winter and spring seasons however, show very large differences in the stratospheric circulation patterns, as demonstrated by various map series throughout the last seven years. Even monthly mean maps show tremendous differences in contour heights between comparable times of different years. These irregular circulation changes were illustrated and discussed for the period of 1958-1963.

Regular changes in stratospheric circulation are represented by a 26-month period, as treated by W. Godson during this seminar, and by an approximate 6-year period in hemispheric temperatures, which was shown by Figs. 1 and 2. Apparently, the annual mean temperatures at the 20 or 50 mb level, over some key stations over tropical, subtropical , temperate and polar latitudes show a pronounced double wave within the sunspot-cycle.[1] However, as only one period can be shown now, a proof for the reality of such a temperature oscillation is to be given by further years of homogeneous observations. Most striking is the parallelism of the temperature variation with the geomagnetic A_p indices (planetary amplitude), which has a pronounced double period within a sunspot cycle.

---

1 Warnecke, G. Met. Abhandl. , Inst. f. Meteor. u. Geophys. Freien Universitat Berlin, XXVIII, 3, 1962.

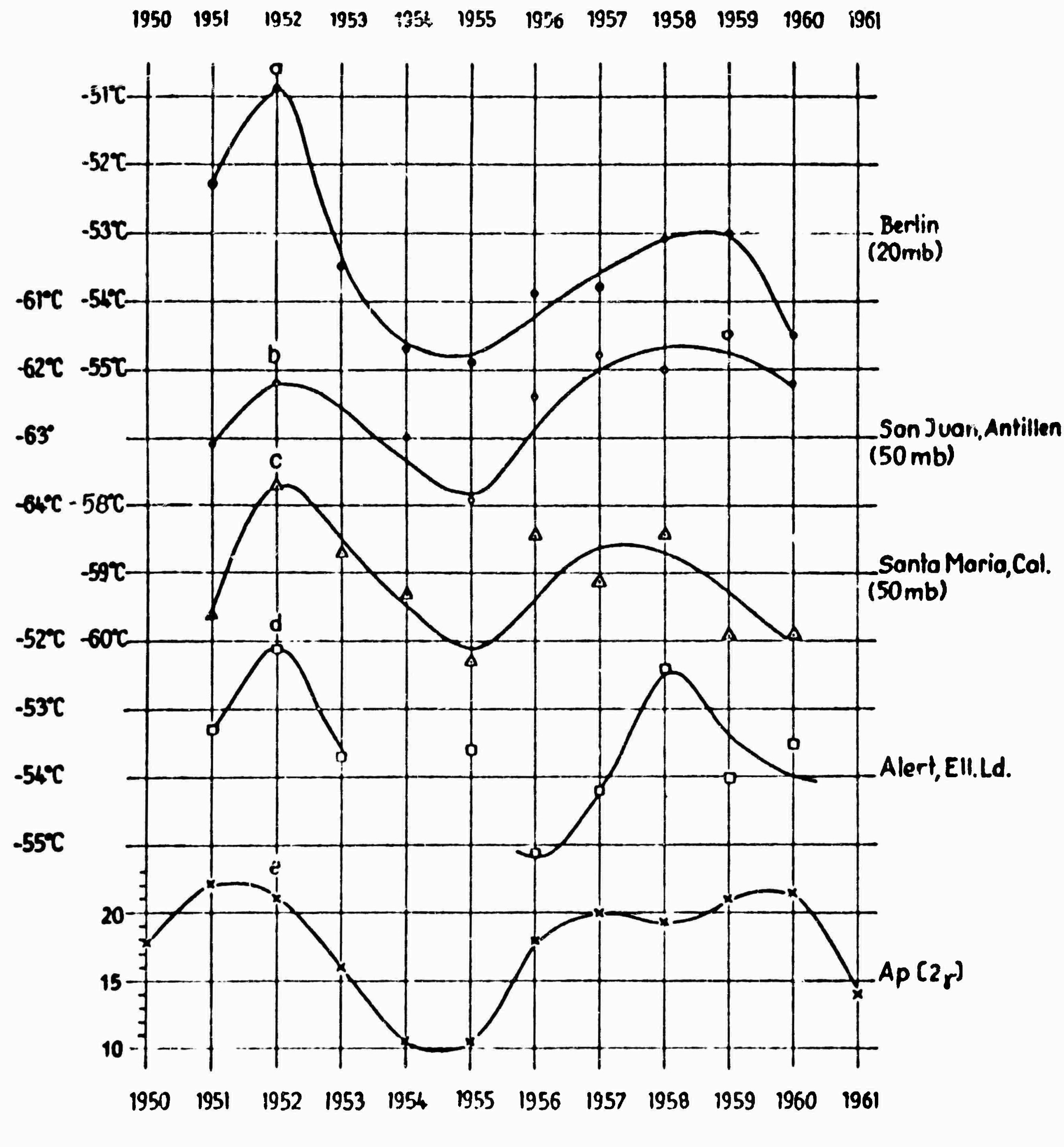

Figure 1. Annual mean stratospheric temperature over Berlin, Germany (a), San Juan, Antilles (b), Santa Maria, California (c), and Alert, Ellesmere Land (d), and annual mean values of geomagnetic 'planetary amplitude' (e) for the period 1950-61.

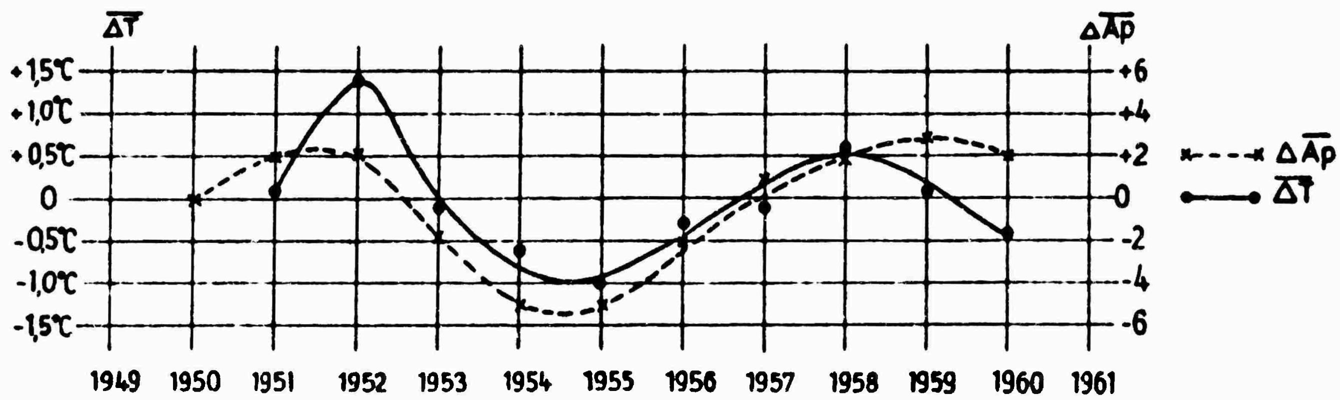

Figure 2. Deviation of annual mean stratospheric temperature from the ten years mean value averaged over Berlin, San Juan, Santa Maria, and Alert ($\overline{\Delta T}$), and deviation of three times overlapping annual mean values of geomagnetic planetary amplitude from the average over the period 1949-61 ($\overline{\Delta A}_p$) .

TIME SERIES STUDY OF STRATOSPHERIC-TROPOSPHERIC RELATIONS

F.B. Muller

As a preliminary to the development of a model of interaction between troposphere and middle stratosphere a project is underway within the Research and Training Division of the Canadian Meteorological service to study time series consisting of evaluations of various terms which enter the differentiated equations of motion, or which are subjectively evaluated by the synoptic meteorologist.

Basic data for this study consist of grid point values (on a hemispheric and North American grid) of height and temperature fields at 24 hour intervals for two tropospheric pressure surfaces and three stratospheric surfaces for a number of winter half years. Large scale phenomena are studied on the hemispheric grid with 13.2 degrees of latitude spacing, and smaller scale processes on the 6.6 degree grid length over North America.

The data are being assembled sequentially on tape so that a large number of evaluations from all levels and combinations of levels may be made once per day, and these evaluations may then be rearranged as a set of time series, each 180 days in length, and representing the march of these evaluations through a number of half years.

Although data preparation is well advanced, only one level, the 50 mb level, has been completed to date. The other levels being collected are the 1000, 500, 30 and 10 mb levels, for the years 1961-62 and 1962-63. Automation of the data preparation will allow working forward and backward from these years

Specific evaluations being chosen for the first pass through the data include averages, over areas varying from one grid square to hemispheric, of the following: meridional and zonal wind components, angular momentum and kinetic energy, vorticity and its advection, temperature and its advection, thermal vorticity, vertical motion indicators. Thus one pass through the data produces hundreds of time series.

For the study of these series and their relationships use is made of spectral analysis, cross spectral analysis, filtration and multiple regression.

Cross spectral analysis may be used to reveal the time scale, and for transient effects, the space scale of the fluctuations and relationships under study. It also provides an indication as to whether relationships are lagged, implying motion or propagation of disturbances, or whether the relationship is of direct, pressure-type linkage.

Difficulties in this method include the need to remove any large amounts of variance at sharply tuned frequencies, and over bands of frequency which obscure detail in the neighbouring frequency bands. Specially designed filters are required for this purpose. One direct pressure type relationship being studied is indicated by the regression equation

$$\Delta_{1\,day} Z_{1000} = \underbrace{A_1 V_T \cdot \nabla \zeta_{a_T} + A_2 V_T \cdot \nabla T_T}_{\text{Evaluated in the troposphere}} + \underbrace{B_1 V_s \cdot \nabla \zeta_{a_s} + B_2 V_s \cdot \nabla T_s}_{\text{Evaluated in the middle stratosphere}}$$

Processing the many series requires a type of macro-programming which allows the performance in arbitrary sequence of the required routing steps such as parameterization, filtering, combining-differencing, scaling, normalizing and plotting. A preliminary test run on the 1961-62 50 mb North American grid provided series and plots of daily values (averaged over six different areas on the North American grid) of mean vorticity, thermal vorticity, temperatures and heights and also daily values of a North American zonal index. The individual spectra all showed more than 95% of the variance in periods longer than nine days, although all spectra showed significant peaks in periods between two and three days. These results, weighted according to frequency can be used to give a measure of an upper limit to predictability as a function of the time scale up to which detail is completely predicted in both amplitude and phase. An example of this is the predictability during 1961-62 winter of the mean temperature in Alaska over an area "a" which is three grid lengths square; for a two day forecast to explain 75% of the change in this parameter complete detail would have been needed up to a time scale of 18 day periods, and only 15% of the change would be forecast by prediction up to a 7 day time scale.

Coherence between mean vorticities and mean temperatures (averaged over 16 grid points in areas which were separated in respect to their centres by 2000 nautical miles on the same mean stream line) was low for short periods and near .5 above periods of 3 -4 days. The phase by which the downstream area differed from the upstream area could be interpreted as a displacement time for disturbances moving from one area to the other. For all periods up to 7 days this corresponded to a speed of about 25 knots, while the North American zonal index for the entire winter six months averaged about 32 knots between 45 degrees and 75 degrees North. Data from tropospheric levels will establish whether these are true stratospheric short and medium waves or simply upward propagation of tropospheric disturbances.

See Figures.

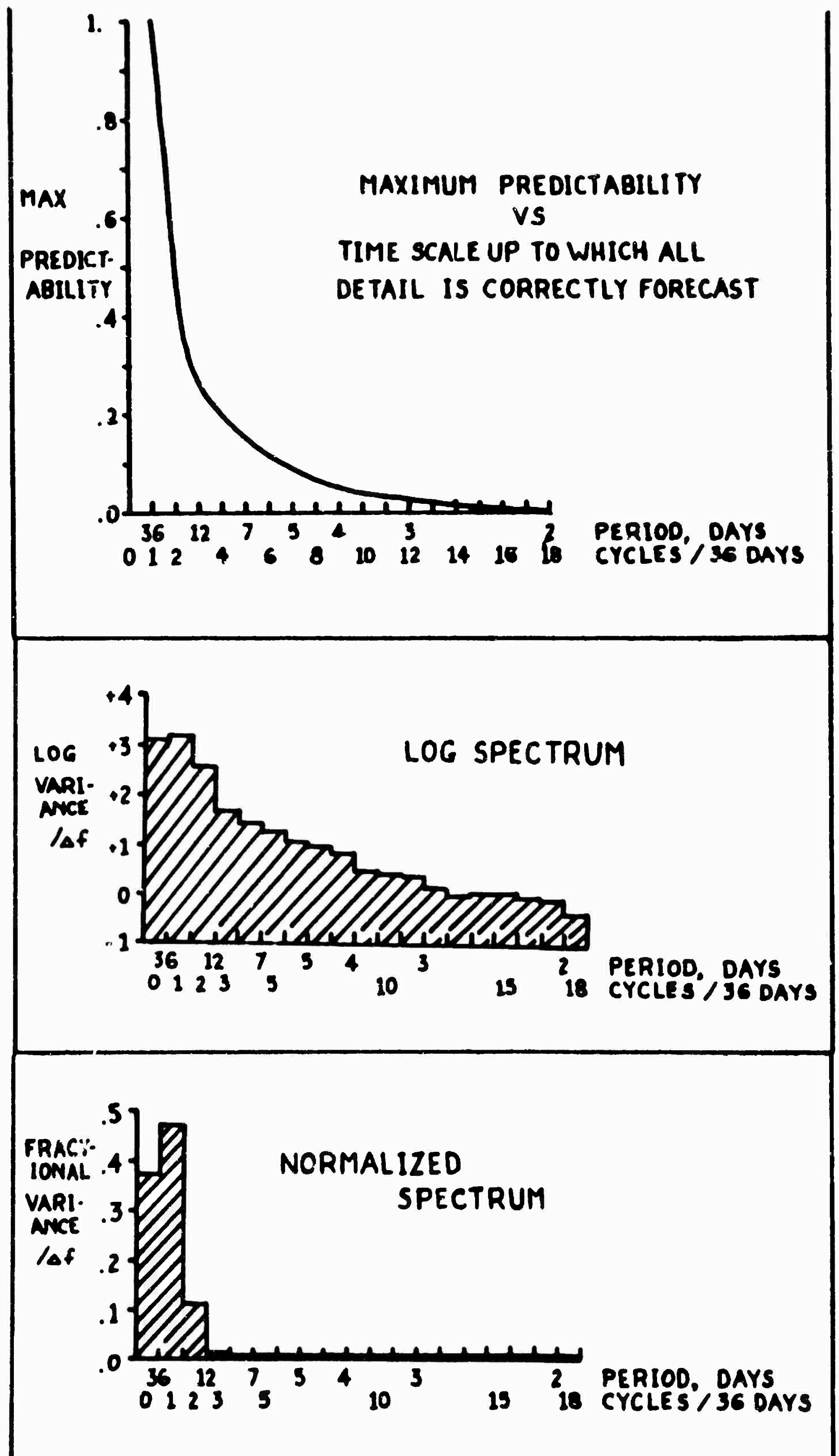

AREA "a" NORTHERN ALASKA 50mb. 1961 - 62
WINTER SPACE MEAN TEMPERATURE

THE ANTARCTIC STRATOSPHERE

W.S. Weyant

Dissimilarities between the Arctic and Antarctic regions were discussed. In particular, the presence of a nearly landlocked ocean covering most of the Arctic as opposed to a high continental mass in the regions surrounding the South Pole creates considerable differences in the atmospheric behaviour of the two polar regions, although the astronomical factors are essentially the same except for the six month phase difference.

Some of the first results of the "opening-up" of Antarctica beginning with the IGY period were reviewed and discussed in the light of later data. Time cross-sections of temperature from three Antarctic Stations illustrated the persistence of the surface inversion layer, a small annual variation of tropospheric temperatures, and the large annual variation of stratospheric temperatures. These cross-sections also showed the higher winter tropopause (as opposed to summer) and the weakening of the tropopause in winter.

The spring stratospheric warming was illustrated by graphs of the annual course of 50-mb temperatures at Amundsen-Scott (South Pole) Station for six years and, in particular, during the spring months from September to December. In most of the years from 1957 through 1962 the spring warming at this level was quite abrupt, with the most rapid temperature increases occurring in late October or early November. However, in 1959 and, to a lesser extent, in 1961, the warming was much more gradual with typical summer values of 50-mb temperatures not being attained until December. The growth and structure of the circumpolar stratospheric vortex, as well as its spring breakdown, was related to the temperature field and its changes. The wind speed of the polar night jet associated with this vortex reaches a mean value of over 200 knots at 30 km. (Phillpot 1962).

In the 1962 winter, radiosondes released at Byrd Station (80 S 120 W) consistently reached greater altitudes than had hitherto been attained during the polar night. Mean soundings for the stratospheric layers from 15 to 40 km. for each month from April through August show the transition from nearly isothermal temperature structure in April to a developing and gradually lowering inversion with the inversion height at about the 20 km. level by August. The actual cooling in this layer during the five months was greatest in the 20 to 25 km. levels.

The results of some computations of mean meridional winds and the heat balance in stratospheric levels from 250 to 75 mb were next presented (Rubin and Weyant, 1963). These computations, based on data from ten stations near a circle corresponding to the 71 S latitude circle, indicated inflow of air in these stratospheric levels throughout the year. The horizontal eddy transport of heat was also into Antarctica at these levels, but balancing off the heat gain through horizontal transport and through realization of potential heat through vertical sinking (assuming no vertical motion through the 75 mb level) against the actual observed cooling in these layers left as a residual a radiational cooling rate on the order of slightly over 2^{o}C per day. This figure appears too large, probably as the result of the several assumptions made in making the computations. However, about 170 radiometersonde ascents made during 1962 at five Antarctic stations yielded cooling rates considerably less at these levels. (Table 1). Using these as the actual radiational cooling rates and again striking a balance with the horizontal transport of sensible heat and the actual observed cooling rates the residual heat gained or lost from vertical motions became negative, indicating slight upward vertical motions in these layers.

A very brief description of observations planned and further research work in progress was then given. Among items mentioned were the forthcoming intensive radiometersonde observational programmes scheduled for 1964 and 1965, when radiometersondes will be flown daily during the dark season at both Byrd and Pole Stations. Work will be continued on the transport and heat budget study mentioned earlier· a series of maps of Antarctic climatological parameters is being prepared for the American Geographical Society Map Folio series; a radiation atlas is in process of preparation at the Weather Bureau's Polar Meteorology Research Project.

TABLE 1

Observed mean cooling rates from radiometersonde ascents at 5 Antarctic stations during April -September 1962

Layer (mb)	950-775	775-600	600-400	400-250	250-150	150-75
Cooling Rate (oC/day)	- 1.3	- 1.2	- 0.9	-0.4	- 0.1	-0.6
Number of Measurements	89	135	170	166	156	133

REFERENCES:

Phillpot, H.R. : 'Mean westerly jet streams in the southern hemisphere', Antarctic Res., Geophys. Mono. No. 7, 128 - 148 American Geophysical Union 1962.

Rubin, M.J. and W.S. Weyant : ' The mass and heat balance of the Antarctic atmosphere', submitted for publication to Monthly Weather Review, 1963.

THE MASS AND HEAT BUDGET OF THE ANTARCTIC ATMOSPHERE

M.J. Rubin and W.S. Weyant

Mean meridional wind components and eddy transports of sensible heat across 72 S latitude are computed for each of six atmospheric levels from 850 to 100 mb, using 1958 data from 10 Antarctic stations. Mean vertical motions* are obtained from the meridional wind components; a heat balance is struck for each of the six atmospheric layers, with radiational heat changes obtained as a residual. Results are compared with observed long-wave radiational cooling rates for the dark period (1962), and with results of other investigators.

For the entire Antarctic atmosphere between 950 and 75 mb, results showed downward vertical motions and loss of heat by radiational processes throughout the year. The heat thus lost to space is on the order of 10^{22} cal. Downward motion is at a maximum (about .35 cm/sec) in the middle troposphere; heat is transported into Antarctica by horizontal eddies and by the mean meridional cellular circulation, and the relatively small difference between this heat inflow and the heat lost through radiation produces the observed temperature changes. The heat added to the Antarctic atmosphere from sensible heat transport (including realized potential heat) is one order of magnitude greater than that from condensation processes. The several elements - calving, melting, evaporation, drift - of the water (ice) mass budget were discussed in the second lecture. Despite the possibility of large percentage errors in the determination of the elements, there is reasonable certainty that their role in the heat budget is relatively small. The spring warming of the Antarctic stratosphere appears to result directly from dynamical processes of warm air advection and vertical sinking rather than from a direct gain of heat through radiation absorption, at least in the lower stratospheric levels treated here.

* see figure.

MEAN MASS TRANSPORTS AND VERTICAL MOTIONS IN THE ANTARCTIC ATMOSPHERE-1958

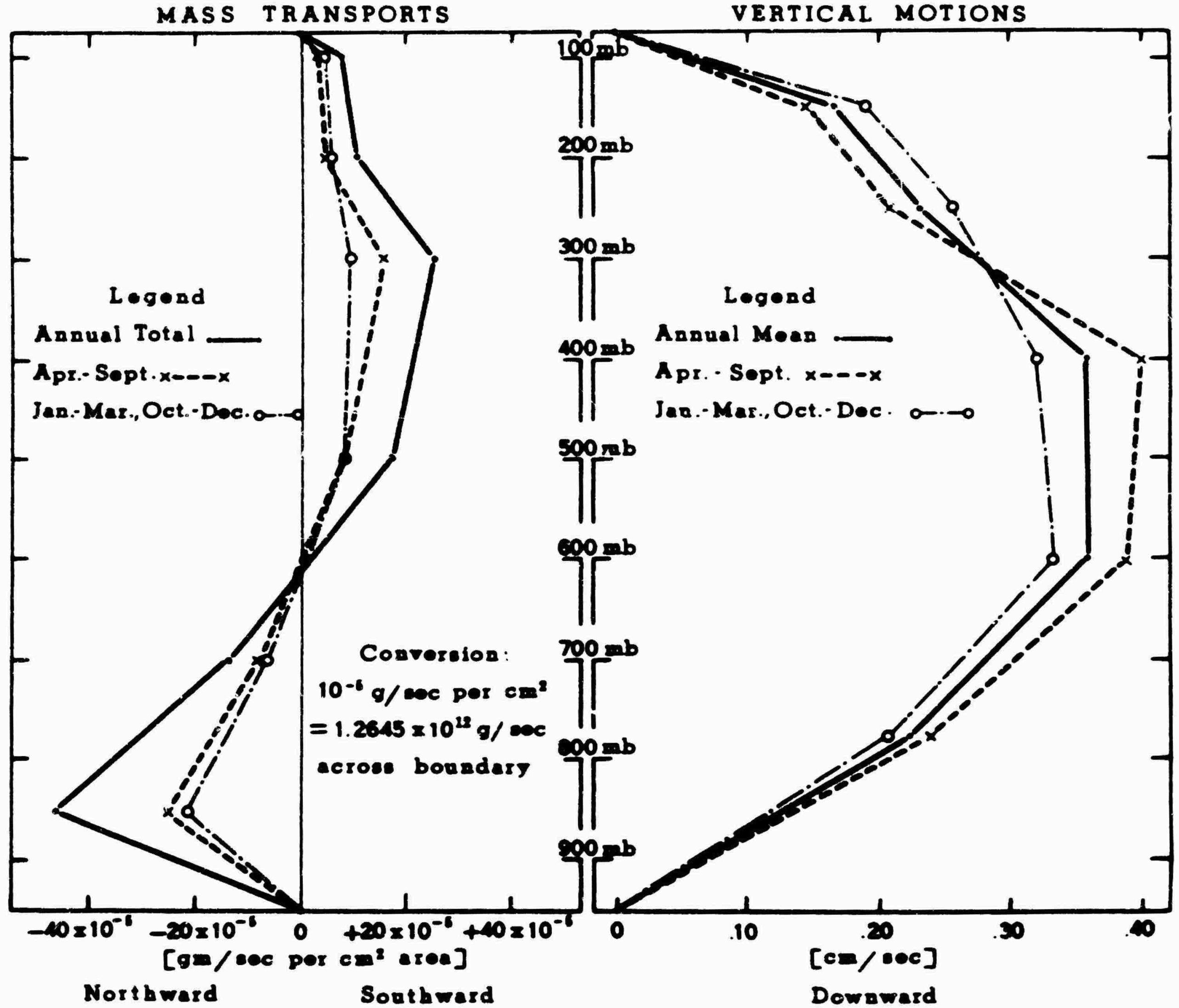

STRATOSPHERIC ENERGY STUDIES

A.A. Barnes, Jr.

Using data from the first six months of the IGY at the 100, 50, 30, and 10 mb levels, terms in the following equations were evaluated.

A. Rate of change of kinetic energy

The time rate of change of kinetic energy may be written as

$$\frac{\partial}{\partial t}\iiint E\frac{dp}{g}\,dxdy = \iint EV\frac{dp}{g}\,dx + \iint \psi V\frac{dp}{g}\,dx$$

$$-\iint\left(\frac{E\omega_c}{g}\right)_L dxdy + \iint\left(\frac{E\omega_c}{g}\right)_u dxdy - \iint\left(\frac{\psi\omega_c}{g}\right)_L dxdy$$

$$+\iint\left(\frac{\psi\omega_c}{g}\right)_u dxdy - \iiint\omega_c\,\alpha\,\frac{dp}{g}\,dxdy - \iint\left(\frac{E\omega_Q}{g}\right)_L dxdy$$

$$+\iint\left(\frac{E\omega_Q}{g}\right)_u dxdy - \iint\left(\frac{\psi\omega_Q}{g}\right)_L dxdy + \iint\left(\frac{\psi\omega_Q}{g}\right)_u dxdy$$

$$-\iiint\omega_Q\,\alpha\,\frac{dp}{g}\,dxdy - \iiint V_p\cdot\mathbf{F}\frac{dp}{g}\,dxdy \qquad (1)$$

The first eight terms have been evaluated from the data. The next five depend on radiation and the last term is the friction term. Since the radiation and friction are not known well enough, these terms could not be evaluated. The radiation terms do not cancel out as they do in the equation for the time rate of change of potential plus internal energy.

The individual integrals of (1) are listed below along with our findings.

1. $\frac{\partial}{\partial t}\iiint E\frac{dp}{g}\,dxdy$ For all three layers there was a slight decrease from July through September and a net increase of kinetic energy from then to the end of December.

2. $\iint EV \frac{dp}{g} dx$ The mean seasonal advection of kinetic energy across the equator in the lower stratosphere was small when compared with the mean seasonal time rate of change of kinetic energy in the stratosphere over the northern hemisphere. This integral is not important and vanishes when the whole sphere is considered.

3. $\iint \psi V \frac{dp}{g} dx$ The eddy terms are not important but the mean term may be .

4. $\iint \left(\frac{E\,\omega_c}{g}\right) dx\,dy$ and $\iint \left(\frac{E\,\omega_Q}{g}\right) dxdy$ The vertical advection of kinetic energy could account for the decrease of total kinetic energy from July through September as computed using the adiabatic vertical motion, but the October through December increase of kinetic energy of the stratosphere must have been due to some other process. Since ω_c is a function of the wind (through $\mathbf{V}_p \cdot \nabla_p T$) and ω_Q is not, one might expect the diabatic integral to be of less importance than the adiabatic one.

5. $\iint \frac{\psi \omega_c}{g} dxdy$ and $\iint \frac{\omega_Q}{g} dxdy$ There were difficulties in evaluating the adiabatic integral, but undoubtedly these terms are very important and cannot be disregarded.

6. $\iint V_p \cdot F \frac{dp}{g} dxdy$ At the present time this term cannot be evaluated, but it probably acts to decrease the kinetic energy of the stratosphere.

7. $\iiint \omega_c\, \alpha \frac{dp}{g}$ dxdy and $\iiint \omega_Q\, \alpha \frac{dp}{g}$ dxdy

Using adiabatic vertical motions, the transient and zonal standing eddies gave a conversion from kinetic energy to potential energy in both summer and winter in the lower stratosphere. Above about

40 mb the net conversion by transient and zonal eddies was in the opposite direction. The diabatic motions are important for the meridional eddy and mean terms, tending to cancel the adiabatic contributions to these terms. Hence we do not know the true role of these terms in the rate of change of kinetic energy.

For the northern hemisphere the seasonal rate of change of total kinetic energy depended almost entirely on the terms in the last three numbered sections. This means that the large hemispheric increase of total kinetic energy observed in the early winter was due to the vertical advection of kinetic energy.

B. Rate of change of potential plus internal energy.

For the time rate of change of potential plus internal energy we have

$$\frac{\partial}{\partial t}\iiint (P + I)\frac{dp}{g}\,dx\,dy = \frac{P_L}{g}\iint \left(\frac{\partial \psi}{\partial t}\right)_L dxdy - \frac{P_u}{g}\iint \left(\frac{\partial \psi}{\partial t}\right)_u dxdy + \iiint c_p \frac{\partial T}{\partial t}\frac{dp}{g}\,dxdy \qquad (2)$$

Using the first law of thermodynamics to obtain $c_p \frac{\partial T}{\partial t}$ we get

$$\frac{\partial}{\partial t}\iiint (P + I)\frac{dp}{g}\,dxdy = \frac{P_L}{g}\iint \left(\frac{\partial \psi}{\partial t}\right)_L dxdy - \frac{P_u}{g}\iint \left(\frac{\partial \psi}{\partial t}\right)_u dxdy$$

$$+\iint \frac{c_p TV}{g}\,dpdx - \iint \left(\frac{c_p T\omega}{g}\right)_L dxdy + \iint \left(\frac{c_p T\omega}{g}\right)_u dxdy$$

$$\iiint \omega\, a\,\frac{dp}{g}\,dxdy \quad \iiint \frac{dQ}{dt}\,\frac{dp}{g}\,dxdy \qquad (3)$$

Since we have calculated the adiabatic vertical motion we have that

$$C_p\,\frac{\partial T}{\partial t} = -C_p\,\mathbb{V}_p \cdot \nabla_p T + C_p\,\omega_c\left(a - \frac{\partial T}{\partial p}\right) \qquad (4)$$

Substituting in (2) we find that all terms on the right hand side can be evaluated with our data.

$$\frac{\partial}{\partial t}\iiint (P+I)\ \frac{dp}{g}\ dx\,dy = \frac{P_L}{g}\iint \left(\frac{\partial \Psi}{\partial t}\right)_L dxdy$$

$$- \frac{P_u}{g}\iint \left(\frac{\partial \Psi}{\partial t}\right)_u dxdy \ + \iint \left(\frac{C_p T V}{g}\right) dpdx \ - \iint \left(\frac{C_p T \omega_c}{g}\right)_L dxdy$$

$$+ \iint \left(\frac{C_p T\omega_c}{g}\right)_u dxdy + \iiint \omega_c\ \alpha\ \frac{dp}{g}\ dxdy \qquad (5)$$

Notice that no diabatic terms (i.e. containing ω_a or $\frac{dQ}{dt}$) appear in (5). The $[V]$ and $[\overline{\omega}_c]$ values will not satisfy the continuity equation unless $[\overline{\omega}] = [\overline{\omega}_c]$ for all latitudes which means that the $[\overline{\omega}_Q]$ values must be at least an order of magnitude smaller than the $[\overline{\omega}_c]$ values, which our data shows not to be true.

Since the radiation terms cancel one another, we do not expect to learn much about radiation in the stratosphere using the equation for the rate of change of potential plus internal energy and adiabatic vertical motions.

Listed below are the various terms of (5) along with conclusions from our data.

1. $\frac{\partial}{\partial t}\iiint (P+I)\ \frac{dp}{g}\ dxdy$ There is a net decrease of potential internal energy at all levels in the northern hemisphere stratosphere during both periods. This is due to a net lowering of the pressure surfaces and decrease of the mean temperature.

2. $\iint \left(\frac{C_p TV}{g}\right) dpdx$ This boundary term is evaluated at the equator. The eddy terms are not important contributors to the time rate of change but the mean term is. Unfortunately, evaluation of the mean term was not considered reliable with our data.

This integral does not appear if we integrate over the entire sphere.

3. $\iint \left(-\frac{C_p \, T\omega_t}{g} \right)$ dxdy The meridional eddy term and mean term are important but the other eddy terms do not contribute significantly .

4. $\frac{P}{g} \iint \frac{\partial \psi}{\partial t}$ dxdy This is a very important term.

The major change of potential energy was due to the change of the mean height of the lower stratosphere rather than redistribution of mass within the lower stratosphere.

5. $\iiint \omega_c \; \alpha \frac{dp}{g}$ dxdy Except for the layer from 30 to 10 mb, the eddy terms did not contribute significantly. On the other hand, the mean terms were very important and cannot be disregarded in our equation for the rate of change of potential plus internal energy.

The remaining three terms are all functions of $\frac{dQ}{dt}$ and are all zero under the adiabatic assumption. However, as indicated above, this does not mean that one is measuring the rate of change of potential plus internal energy in an adiabatic atmosphere. In an adiabatic atmosphere, $\frac{dQ}{dt} = 0$, and the kinetic energy goes to zero with time. This does not happen in the real atmosphere from which we are taking measurements.

Using adiabatic vertical motions, the rate of change of potential plus internal energy appears to be a small difference among large terms. These large terms all stem from the integral

$\iiint c_p \frac{\partial T}{\partial t} \quad \frac{dp}{g}$ dxdy. Thus this method of separating $C_p \frac{\partial T}{\partial t}$, as in equation (4) , does not seem to be a good way of evaluating this term.

C. Rate of change of the zonal kinetic energy.

The eddy kinetic energy is one of the major sources of zonal kinetic energy, but another source must exist. The evidence points to potential energy as the other source. Thus it appears to us that the meridional circulation plays a more important role in the energy balance of the stratosphere than it does in the energy balance of the troposphere where the eddy kinetic energy is more nearly the sole source of zonal kinetic energy.

D. The importance of eddy transports in the stratosphere.

Eddy transport of various quantities in the stratosphere can not be disregarded. Historically one finds a similarity between the sequences of concepts concerning the transport processes in the stratosphere and in the troposphere. Models using only meridional circulations still are being discussed in the literature, but theoretical and observational investigations indicate that eddy transports are important and that the actual atmosphere is a combination of the symmetric and eddy regimes.

In the troposphere the measured eddy transports are capable of providing almost all the necessary transports, and the transports by the mean meridional circulation pattern seem to be of secondary importance. This paper provides empirical evidence that both the mean meridional circulation pattern and the horizontal eddies are necessary for a description of the energy balance of the stratosphere.

REFERENCE :

Barnes, A.A. , Jr . 'Kinetic and potential energy between 100 mb and 10 mb during the first six months of the IGY ', Studies of the Stratospheric General Circulation, Final Report, M.I.T., 8-131, 1962.

INSTABILITY IN THE MIDDLE STRATOSPHERE

B.E. O'Reilly

The faithfulness with which barotropic numerical models can duplicate evolution of large regions of the atmosphere over time periods of a few days is not a completely accurate measure of the amount of physical understanding which has gone into their conception. Multi-level baroclinic models, while they extend reproducibility of atmospheric motions through thicker layers, and incorporate some of the energy - converting features of the real atmosphere, still leave much to be desired in their vertical resolution, and in the manner with which they treat of the linkages between the atmospheric fluid , and energy sources and sinks at its boundaries.

In the particular province of stratospheric studies these problems are acute. Difficulties in allowing any appreciable independence to activities of such a small region, in a model encompassing the whole atmosphere, are large (Figure 1); a four-level model using equal-mass layers will have its uppermost effective level at 125 mb and can thus hardly accommodate complexities which only begin at higher levels. Even a model in which the vertical coordinate is a fractional power of the pressure, such as Murray's (1960) , can lead to inconclusive results unless the number of levels is considerably extended. Charney and Stern (1962) demonstrated that Murray's tropospheric boundary conditions were sufficient to guarantee stability in his stratospheric levels, even though vertical wind shears greater than those normally considered critical for baroclinic instability were postulated. It would appear that merely increasing the number of levels in a model is inadequate , and that a relaxation of restrictions at boundaries is probably necessary before such models can demonstrate stratospheric instability after the manner of the real atmosphere.

We do not as yet have adequate knowledge of appropriate boundary conditions nor are we prepared to handle the mechanisms of vertical propagation of energy. In an effort to circumvent these difficulties, those who have been concerned with energy studies in the middle stratosphere have sometimes turned to conceptually simpler models, those which have internal rather than external boundary conditions, and which are applicable at a single level. Specifically, through successive application at a number of levels , these models can probably set an upper limit to the degree of energy conversion which may be present, and lay the ground work for a study to determine how much is actually present when levels are considered jointly.

One such model is that of Fleagle (1958). In order to assess the model for stratospheric use I have been reviewing it in some detail.

Fundamental to development of Fleagle's model is postulation of a stream-surface of maximum slope along the vertical, to which the large - scale flow must adhere. (Figure 2). The uniqueness and continuity of such a surface are matters of specification, but so long as the slope of the surface is small, as will be demonstrated, the accuracy with which its location in the vertical can be specified is not critical over fairly deep layers. Thus as a diagnostic parameter its height can be specified arbitrarily, so long as terms relevant to its expression at that level are retained. The advantage of such an internal boundary is that , in a coordinate system oriented with respect to this stream-surface of maximum slope, the velocity normal to the surface , and the normal derivatives of that velocity , vanish, achieving a considerable simplification in the equations of motion. The dominant slope of these postulated stream-surfaces is given by $\delta \doteq w/v$, w being the vertical and v the meridional wind. An accurate expression for , δ , and measured meridional wind components, should enable us to compute w . The value which we shall obtain will undoubtedly be a maximum , since boundary constraints, frictional influences, and diabatic heating all normally act as inhibiting factors for large-scale vertical motion.

The basic current postulated for the model has a non-uniform meridional temperature gradient, leading to both vertical and horizontal shears. Ostensibly the model should be capable of demonstrating instability in two forms : baroclinic instability of the normal form, dependent on the vertical shear and corresponding to conversions from internal and potential to kinetic energy, and also linear current instability, or baroclinic instability of the second kind, dependent on the horizontal shear and corresponding to conversion of kinetic energy of the basic current into kinetic energy of disturbances. In actual fact , however, the horizontal shear is specified as a sinusoidal function of latitude, and through this conformity is restricted to subcritical values, so that only one form of instability is revealed.

To derive an adequate expression for the slope of the stream-surfaces suitable for the middle stratosphere, all scaling assumptions used by Fleagle in his troposphere-oriented derivation must be critically reviewed. Most corrections arise from the fact that static stability is about three times as high in the stratosphere as in the troposphere. Other minor changes result from the fact that the angular velocity of the basic current in the polar-night jet surpasses in mid-winter 20% of the angular velocity of the earth, so that inertial terms are no longer negligible. When corrections are made for these features, the equation for maximum stream-surface slope reduces to :

$$\delta_{max} = \left(\frac{\partial Z}{\partial y}\right)_{\theta} - \frac{B}{b}\,\frac{\beta l}{a^2 + B l^2}$$

$$= \left(\frac{\partial Z}{\partial y}\right)_{\theta} - \frac{\gamma f}{R\,(\gamma_D - \gamma_T)}\left(\frac{\beta L^2/4\pi^2}{1 + L^2/d^2}\right)$$

$$B = \frac{d\rho}{dp} \text{ (parcel)} \quad , \quad b = \frac{\delta \rho}{\delta p} \text{ (environment)}$$

$$l = 2(\Omega + K)\sin\phi = f \quad , \quad K = U/a\cos\phi$$

$$\gamma = c_v / c_p \qquad \gamma_T = -\frac{\partial T}{\partial Z}$$

$$\gamma_D = \frac{g}{c_p} \qquad \alpha^2 = \frac{1}{a^2}\left[\frac{m^2 - \sin^2\phi}{\cos^2\phi} + \nu^2\right]$$

The first form is the most complete form, which differs from Fleagle's in several respects. In the second form, for descriptive purposes only, the term Bf^2 which incorporates some of the inertial effects mentioned has been dropped and the symbol α^2, which represents a composite zonal - meridional wave number, is converted to its more familiar rectilinear form, so that L represents zonal wavelength and d the meridional half-width of the perturbation. The factor in parentheses, then, is the familiar term in the equation for the speed of Rossby waves of finite width, as given by Haurwitz, and represents the phase speed of barotropic waves relative to the basic current.

The first term is merely the slope of isentropic surfaces toward the pole, which in the basic flow is the only slope they have. For waves of very small dimensions the second term vanishes; the stream-surfaces will have maximum slppe equal to the slope of the isentropic surfaces, so that such waves will be stable, in accordance with Eady's (1949) analysis. This will only be exceeded if lapse rates are superadiabatic, in which case s_z, the static stability parameter in the second term, is negative. Under all other conditions the second term is positive, and the minus sign indicates that the stream=surface will have slope less than isentropic, so that the second term represents a destabilizing factor. The presence of the Coriolis parameter and its derivative stress the fact that rotation of the earth has a strong stabilizing effect on perturbations of an axially symmetric vortex. The factor $\frac{B}{b}$ incorporates the ratio of the individual change of density with pressure to the environmental change, assuming the parcel to undergo adiabatic change of state, and is thus a buoyancy factor. The last influence , represented by the term in parentheses, brings in the dimensions of the perturbation.

In the stratosphere, isentropic slopes are small , in fact are usually negative south of 35-40 N When the stream-surfaces have a slope less than that of isobaric surfaces (about 1/10,000) disturbances are damped, as Eady also showed, so that it is only in more northerly latitudes of the middle stratosphere that any baroclinic instability can be manifested. Fleagle's original formula gives slopes much too small (Figure 3), and suggests that practically nothing can develop except in extremely high latitude. When the equation is properly adapted to stratospheric conditions, however, the region of potential development is more extensive (Figure 4).

This is illustrated by some sample calculations of the stream-surface slopes using 25 mb data. (Figure 5). The maximum stream-surface slopes occur between 65 -70 N , the region known from observation to exhibit most rapid growth of systems. Wave number 10 has within a very small fraction, the isentropic slope so that waves smaller than 6 or 7 are quite stable. Half-isentropic slope is given by the heavy line, so that in each latitude the wave exhibiting this slope should be the most favoured for growth. This would be wave number 1, north of 65, wave number 2 between 53 and 65, waves number 3 and 4 south to 45 . At the same time the stream-surface slope is decreasing rapidly in magnitude toward these southern latitudes, so that although 3 and 4 are the favoured waves, their development should be weak. South of 35- 40 , nothing can grow at all. All these features are in good agreement with observation.

DATA INPUT, MULTILEVEL MODELS.

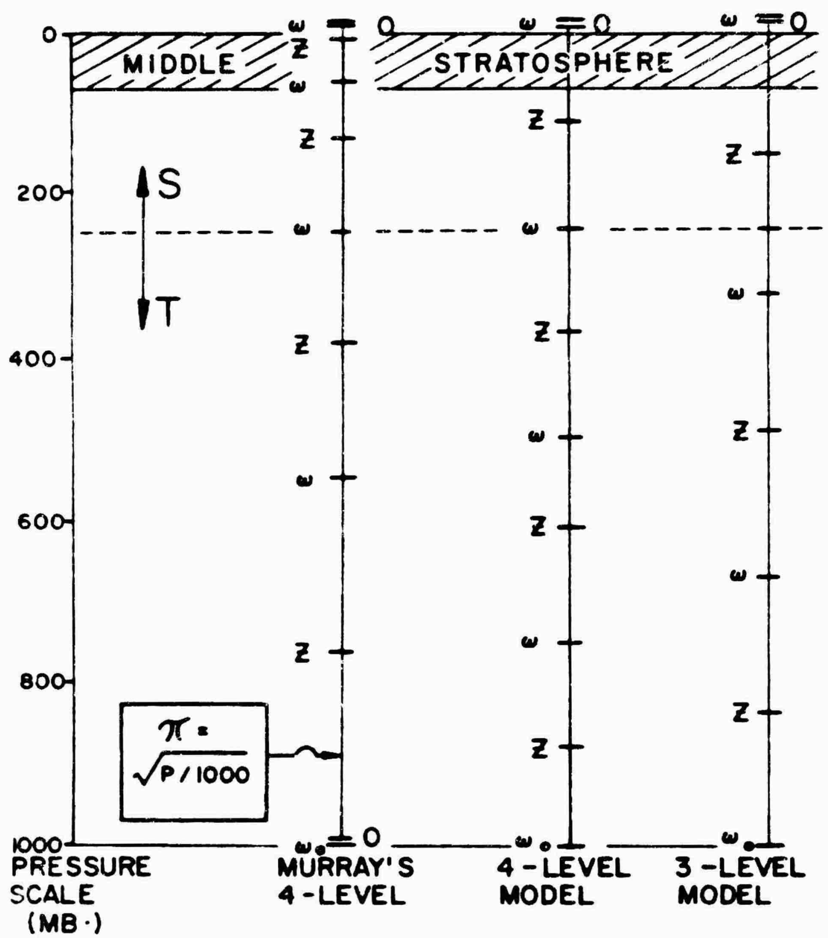

Fig. 1

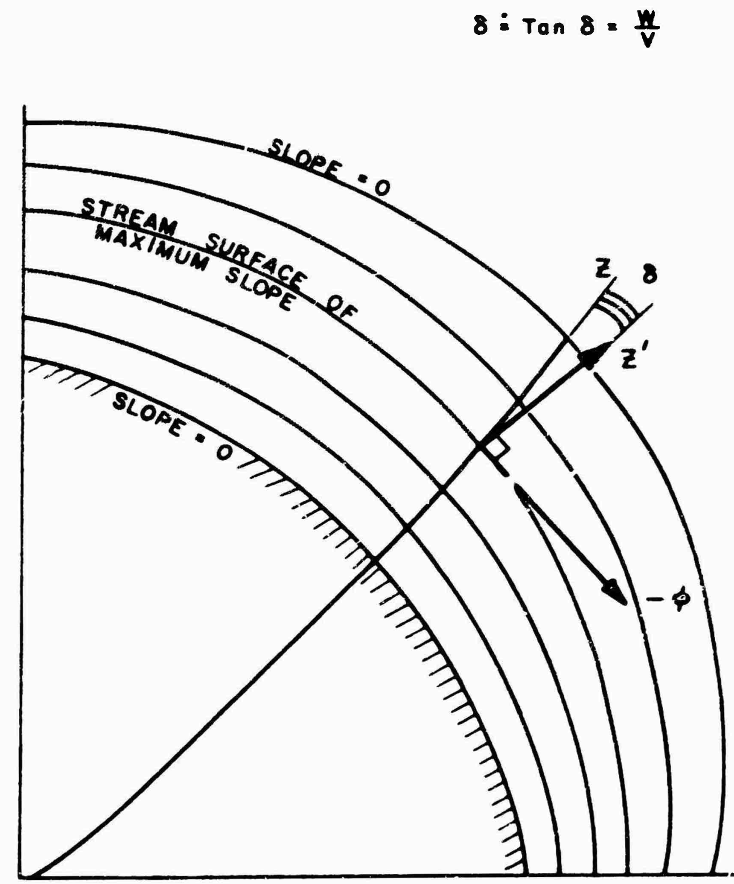

Fig. 2

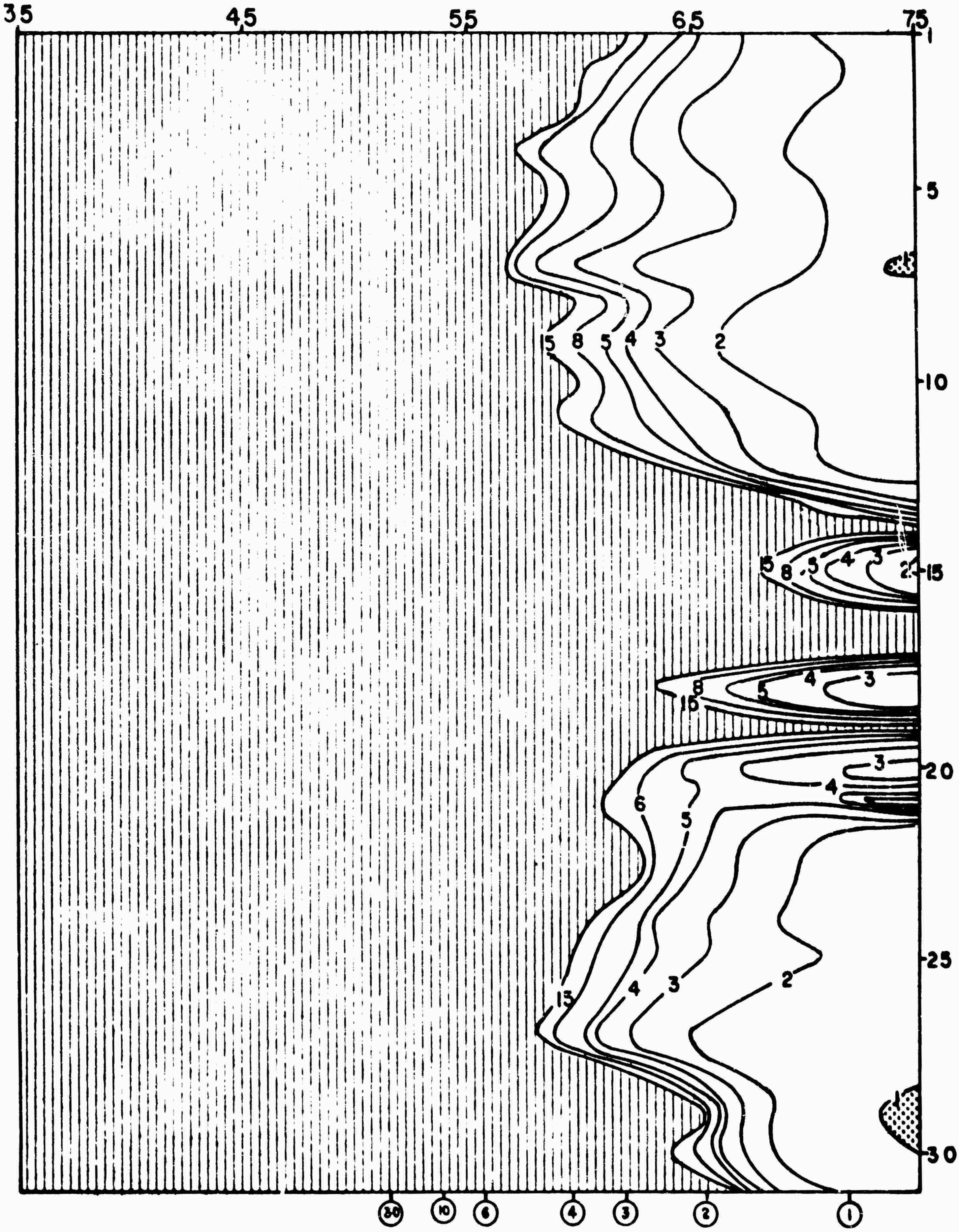

Figure 3. **Fleagle's instability criterion** Within the shaded area all waves are unstable, within the hatched area all are damped. A given wave is stable to the left of the labelled line. January 1959. 25 mb parameters. ([illegible] 4)

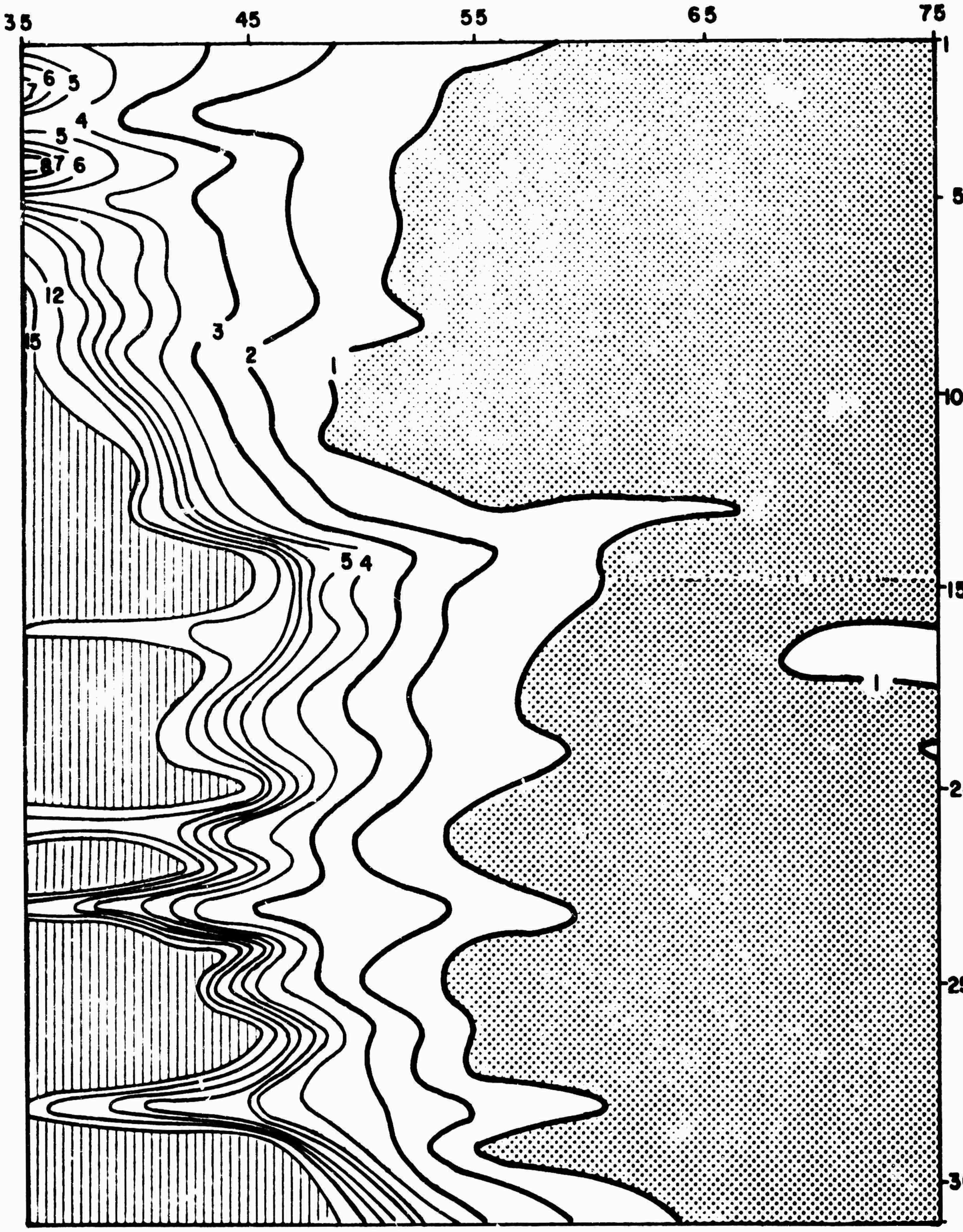

Figure 4. Eady's criterion applied to Fleagle's streamsurface of maximum slope. Within the shaded area all waves are unstable, within the hatched area all are damped. A given wave is stable to the left of the labelled line January 1959, 25 mb parameters, ($\nu = 4$).

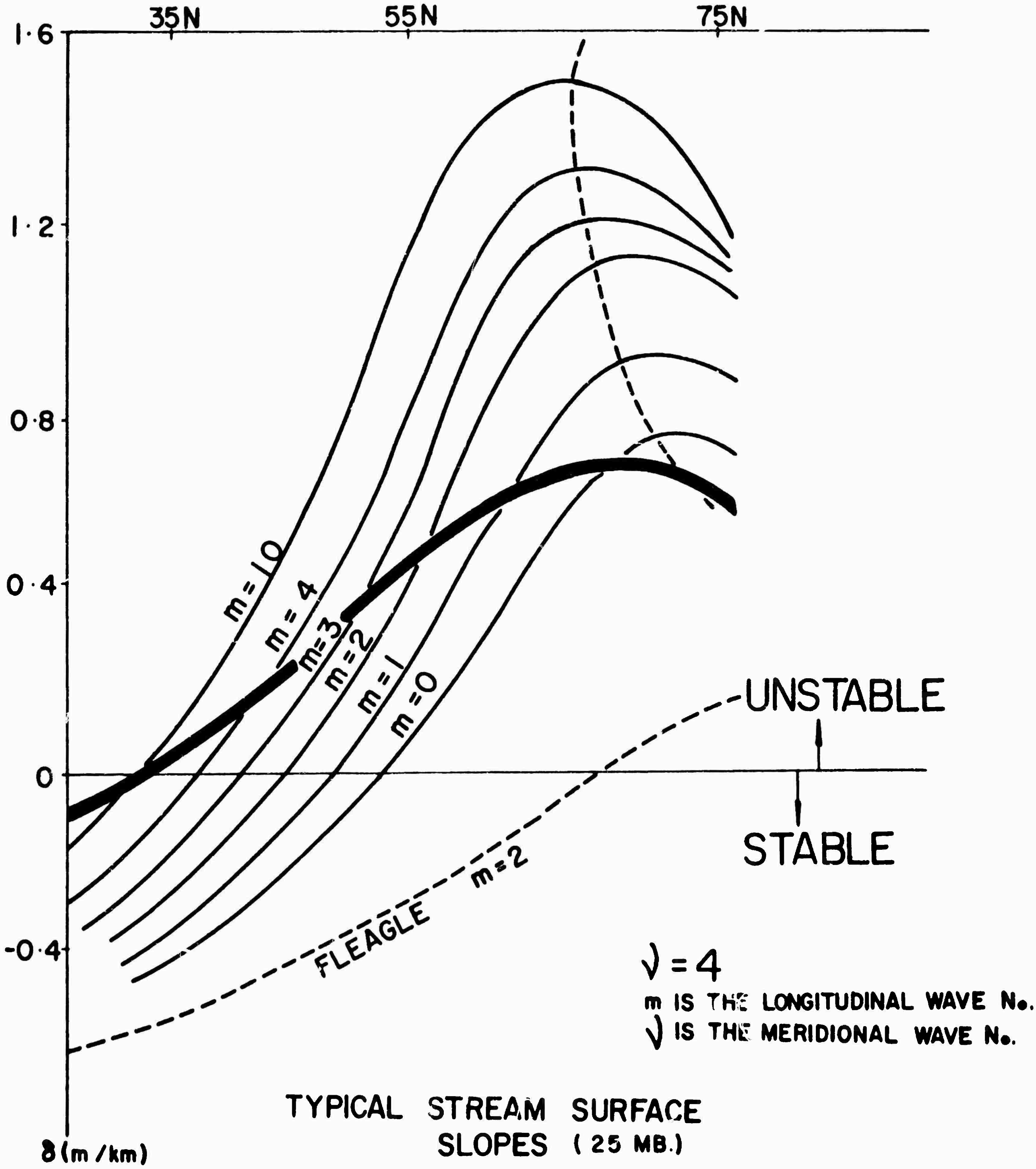

TYPICAL STREAM SURFACE
SLOPES (25 MB.)

Fig.5

Ignoring sphericity considerations for an adiabatic frictionless model in which the basic flow is zonal, the rate of change of kinetic energy within a closed volume can be shown to be proportional to :

$$\frac{\partial}{\partial t}\int E \, d\mathcal{V} = K \int V \left(\delta - \frac{\partial Z_p}{\partial y} \right) dm$$

where the integration is over mass. The factors involved then, are the departure of the stream-surface slope from isobaric, and the magnitude of the perturbations, represented here by the meridional component of the wind ; the production rate varies directly as each factor.

The revised equation for phase speeds of disturbances also shows some features of interest, and is applicable to the troposphere as well as the stratosphere :

$$\sigma_R - m K = \frac{-m\left[\beta (s_Z + B) + \frac{\partial U}{\partial Z} B f^2\right]}{2 a s_Z (\alpha^2 + B f^2) \cos \phi}$$

or

$$C_R = U - k \frac{B}{b} \left(\frac{\beta L^2/4\pi^2}{1 + L^2/d^2} \right) + k \frac{f^2}{\beta(\gamma_D - \gamma_T)} \left(\frac{\beta L^2/4\pi^2}{1+L^2/d^2} \right) \frac{\partial U}{\partial Z}$$

Thompson :

$$C_R = U - \left(\frac{\beta L^2 / 4\pi^2}{1 + L^2/d^2} \right) + \frac{1}{\beta} \left(\frac{\beta L^2/4\pi^2}{1 + L^2/d^2} \right) \cdot \frac{\partial^2 U}{\partial y^2}$$

The factor of 1/2 may be an extraneous algebraic error on my part, since from comparison it should be 1, but I have not yet located the error. The term Bf^2 in the denominator is unimportant for short or medium waves, but has increasing importance for very long waves and also for high static stability, such as occurs in the stratosphere. Because of it, the factor k has a value of about 3/4 for wave number 2 increasing to 1 for shorter waves and thus represents a stabilizing factor for planetary waves. The second form represents the same equation as it would have appeared if derived in rectangular coordinates and converted to classical symbols.

In an autobarotropic atmosphere, changes of density with pressure of an individual parcel follow exactly the changes of density with pressure in the environment ; that is, the coefficients of piezotropy and barotropy are identical. Their ratio would then be 1. Also in such an atmosphere there is no vertical wind shear U_z , so that the second term disappears completely. Under these conditions the baroclinic wave-speed formula reduced to that of Haurwitz, apart from the long wave stabilizing feature previously mentioned.

The second term in Thompson's formula depends on the fact that he allowed horizontal shear, but no vertical shear in his model. This is not very realistic in the atmosphere; when the wind is dominantly geostrophic, the vertical wind shear is given by the first meridional derivative of the temperature field, while the horizontal shear is given by the second. Thompson's model is more properly to be considered a degenerate baroclinic model than a pure barotropic. The last term in my formulation has an order of magnitude one greater than the last term in Thompson's. The most general formula would contain terms of both types. In agreement with numerical results discussed by Kuo, the baroclinic formula also shows that phase speed increases with increasing vertical wind shear and with increasing lapse rate.

Throughout the analysis, the central position occupied by the slope of stream-surfaces in baroclinic systems and their relation to kinetic energy production is stressed. It is hoped from these to develop good working vertical motion formulae for these upper levels.

ENERGY TRANSFORMATIONS IN THE ATMOSPHERE

A. Wiin- Nielsen

My lectures were to a large extent based on already published material which is listed in the references. In view of the fact that the last of these papers is unpublished at present, we include a brief summary of the procedure and main conclusions.

Energy transformations between the zonal mean flow and eddies have been computed from observed data for a single winter month, January 1962. Available data were height fields of the 850, 700, 500, 300 and 200 mb surfaces, and our calculations are therefore based on geostrophic approximations. The horizontal fields of stream-function and thickness are written as one-dimensional Fourier series, and energy transformations between the zonal mean and different longitudinal wave numbers are evaluated. In order to evaluate energy transformations in the wave number regime, it is necessary to compute meridional transports of momentum and heat as a function of wave number. These results appear, therefore, as useful by-products of the calculations.

The main conclusions which can be made on the basis of these calculations are :

1. Maximum transport of sensible heat occurs in middle latitudes and at lower elevations. More than 50% of the transport of sensible heat is carried out by wave numbers 1 to 4, while the next four wave numbers (5 to 8) transport half this amount.

2. Transport of momentum is northward south of about 55 N and southward north of this latitude . Maximum northward transport of momentum occurs at 35 N at higher elevations, while maximum southward transport takes place at 65 N, also at higher elevations. About 50% of the northward transport of momentum

is carried out by wave numbers 1 to 4, and about 30% by the next four wave numbers (5 to 8).

3. Conversion of zonal available potential energy to eddy available potential energy is found to be positive for almost all wave numbers with a single maximum around wave numbers 2 and 3.

4. Conversion of eddy kinetic energy to zonal kinetic energy is found to be positive when summed over all wave numbers. This conversion is much smaller than the conversion mentioned in 3. The spectrum is very irregular, showing positive conversions for small wave numbers, but negative conversions for some of the larger wave numbers.

The above conclusions are tentative since they are based on data from a single winter month; computations for other winter months and for other seasons are being planned.

Due to the great seasonal variation in atmospheric flow patterns, temperature fields and heat sources, as well as marked differences from one year to another, it is clearly desirable to extend these studies to include different seasons and years. Some preliminary results of research toward this goal were presented. Generation of zonal and eddy available potential energy has been computed for eight additional months. Results of these calculations are summarized in Table 1: the first column shows the mean rate of generation of zonal available potential energy, G (P), (watts m^{-2}) for the different months, while the second column shows generation of eddy available potential energy for the same months and in the same unit.

Results in Table 1 show a marked variation of the generation of the two forms of available potential energy. It is especially interesting to note the reversal of sign of G(P) in July, which agrees with the marked changes in atmospheric heat sources from winter to summer. The table shows further that there exists some variation in the results obtained for the same month in different years.

Research which will give results similar to those reproduced in Table 1 for energy conversions between zonal flow and eddies for both potential and kinetic energy is in progress at the present time .

Table 1

Month	G (P)	G (P')
January '59	4.3	-3.0
January '62	3.5	-1.8
January '63	3.6	-2.4
April '61	1.4	-0.9
April '62	1.5	-0.8
July '61	0.2	+0.2
July '62	0.5	+0.1
October '61	2.2	-0.5
October '62	2.3	-0.9

REFERENCES :

Wiin-Nielsen, A. : 'A study of energy conversion and meridional circulation for the large-scale motion in the atmosphere', Monthly Wea. Rev., Vol. 87, No. 9, 319-332, 1959.

Wiin-Nielsen, A. : 'On transformation of kinetic energy between the vertical shear flow and the vertical mean flow in the atmosphere,' Monthly Wea. Rev, Vol. 90, No. 9, 311 - 323 , 1962.

Wiin-Nielsen A., and J. A. Brown : ' On diagnostic computations of atmospheric heat sources and sinks and the generation of available potential energy,' Proc. of the Int'l Symp. on numerical weather prediction, Tokyo 1960, 593- 613, 1962.

Wiin-Nielsen, A., J. A. Brown and M. Drake : ' On atmospheric energy conversions between the zonal flow and the eddies,' to be published in Tellus, Vol, 15 No. 3, 34 p. 1963.

KINEMATIC DIVERGENCE AND LARGE-SCALE ENERGY CONVERSION

A. Eddy

Transformations from potential to kinetic energy within a particular storm present as interesting a problem now as they did in the time of Margules. Just where, relative to the storm centre one can find this transformation taking place, and what quantity of kinetic energy production is involved are two questions vital to weather prediction. Another question which hangs in the background, but is none the less equally as important is : on what scale are the transformations occurring ?

An attempt has been made to answer these questions with respect to a storm which developed in the southern U. S. A. on January 21, 1959 and moved northeastward through the Great Lakes area into Hudson Bay by January 23, 1959. The vertical motion fields needed in finding the $\overline{\omega T}$ correlation (which shows the change from available potential to kinetic energy) were produced by the kinematic technique. This involved the mapping of divergence patterns for several pressure levels and an estimation of the degree to which the rather high random noise level had been reduced. Space correlation of divergence values on a given pressure surface led to the average tropospheric correlation curve shown in Figure 1.

From this curve one can see that the main wavelength present in the divergence field (and hence in the vertical motion field) is of the order of 1,700 nautical miles. This derives from the fact that if the curve were a pure cosine, then the quarter wavelength would be given by separating distance at the point where the curve cuts the zero value for correlation. Another piece of information obtainable from Figure 1 is the percentage of the variance in the divergence data which is the result of noise (random error and high frequency effects). This is clearly given by

$$\sigma_{\Sigma}^{2} = (1 - r_{o}) \ \sigma_{o}^{2} = .53 \ \sigma_{o}^{2}$$

where σ_{Σ}^{2} = variance of noise

σ_{o}^{2} = variance of data

r_{o} = point where curve cuts 'y' axis.

Figure 1 can be used in determining a weight curve for the purpose of making an objective analysis of the divergence fields in the following manner. Suppose grid point values of the objective analysis were produced by means of a linear multiple regression equation of the form

$$Z_{G} = a Z_{1} + b Z_{2} + C Z_{3} \ldots\ldots\ldots$$

where Z_{G} = analysed grid point value

Z_{i} = data values

a, b, c, = coefficients.

The coefficients a, b, c, are determined from intercorrelation involving the data. Now if one assumes that these intercorrelations are a function of separation distance only, and not of any particular pairs, then a, b, and c can be found directly from Figure 1. In practice, one more approximation is made, i. e., that the intercorrelation between the data going into the analysis of a grid point can be ignored. Clearly, this approximation is good for small data density and for large data density, but not particularly good for cases of moderate data density.

However, using the above mentioned approximations , one can produce a weight curve which leads directly to the objective analysis of divergence fields. An example is shown in Figure 2.

Figure 2 shows the evolution of the 850 mb divergence and vertical motion fields for the case history mentioned above. To indicate the vertical distribution of divergence, vertical profiles of this parameter through the center of the low each day were plotted in Figure 3. The low was developing most rapidly on January 21 and by January 23 was occluding.

Since the scale indicated by Figure 1 was about 1,700 nautical miles ωT correlations were made over this area. Maps of this correlation show the production of kinetic energy from available potential energy on the 1700 mile scale. An example is shown in Figure 4.

Kinetic energy production was most pronounced ahead of the moving surface cyclone. The pattern resupports the precept that a weather system need be thought of as the combination of the high pressure and low pressure areas (or of the warm air and the cold air) and NOT as just the low itself.

Figure 5 shows the vertical profile of the average of this transformation process on the 1700 mile scale over North America for the time period indicated.

The maximum conversion seems to be taking place around the 450 mb level, even though the potential energy available seems to be greatest at about 850 mb. This is clearly the result of a combination of high magnitudes in the vertical motion fields and a more propitious phasing between the ω and T fields aloft.

While it is recognised that many more case histories will have to be run to support the technique, it is nonetheless contended that the basic method and general results found in this study are theoretically and experimentally sound.

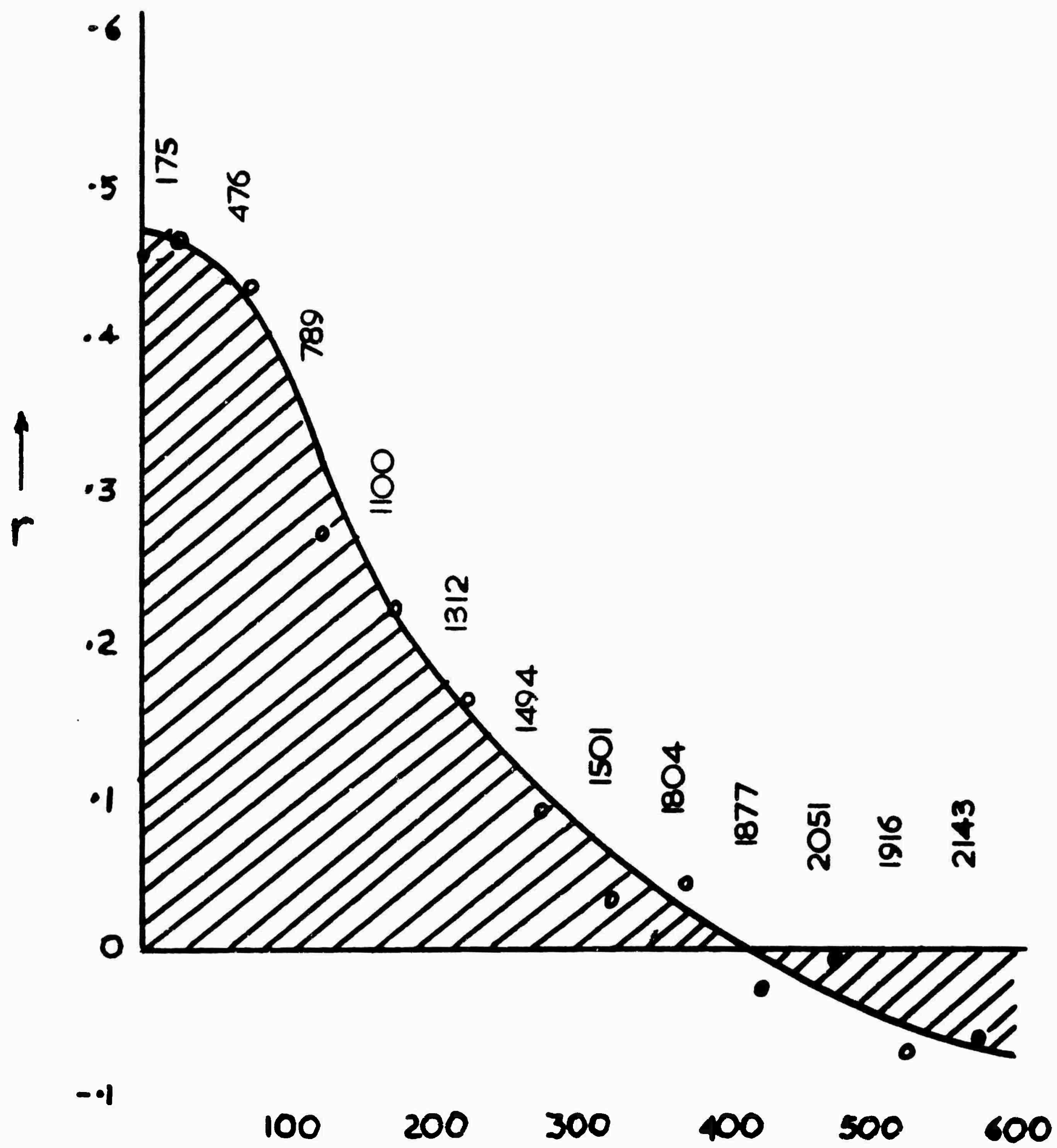

Separation distance in nm.

Figure 1. Horizontal correlation curves for divergence. Mean for 1000, 850, 700, 500, 400, 300 mb for January 21, 22, 23, 1959 0000GMT over North America. Number of pairs in each correlation shown in diagram.

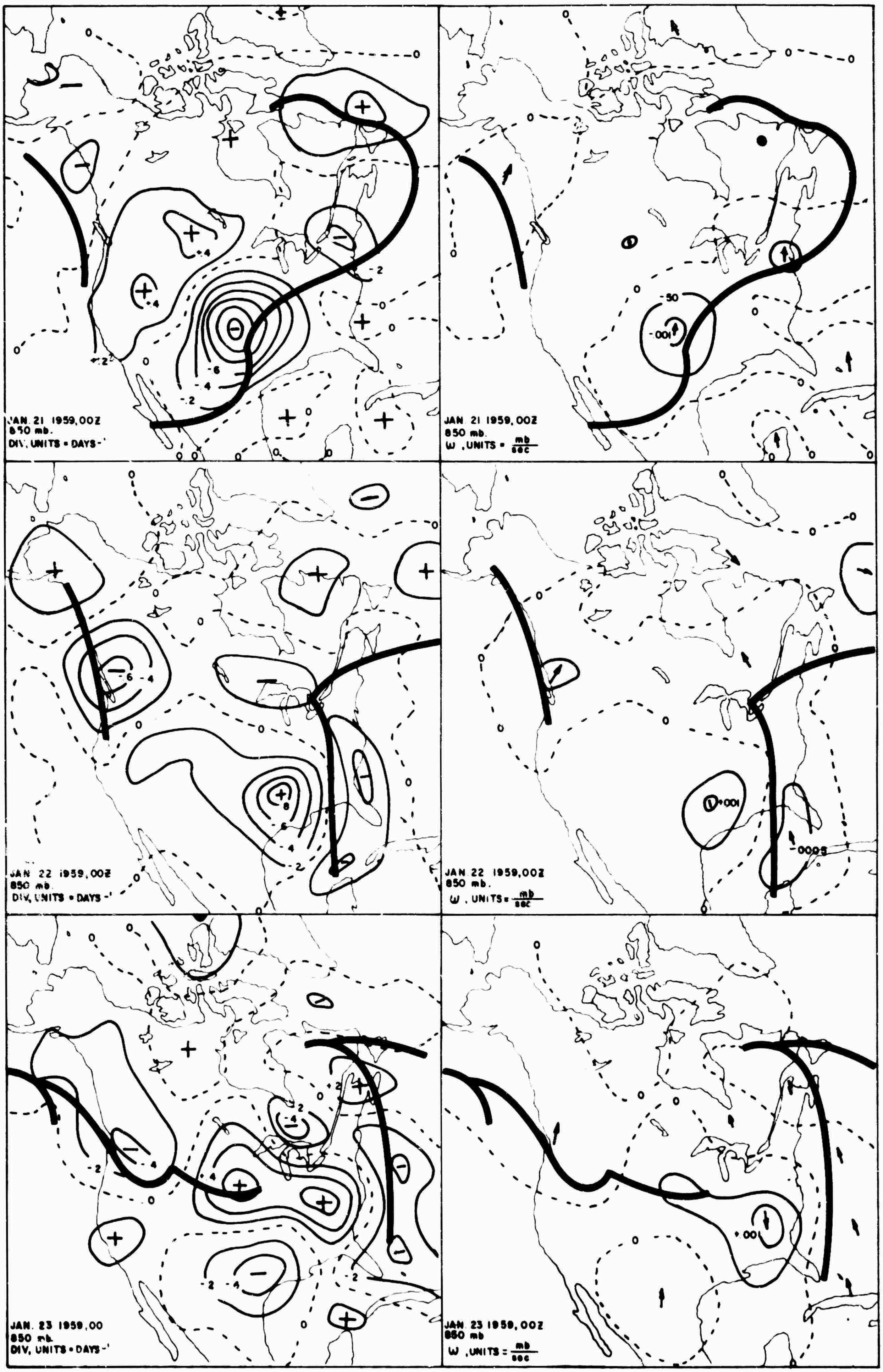
JAN. 21 1959, 00Z
850 mb.
DIV, UNITS = DAYS-1
JAN 21 1959, 00Z
850 mb.
ω , UNITS = mb/sec
JAN 22 1959, 00Z
850 mb.
DIV, UNITS = DAYS-1
JAN 22 1959, 00Z
850 mb.
ω , UNITS = mb/sec
JAN. 23 1959, 00
850 mb.
DIV, UNITS = DAYS-1
JAN 23 1959, 00Z
850 mb
ω , UNITS = mb/sec

Figure 2.

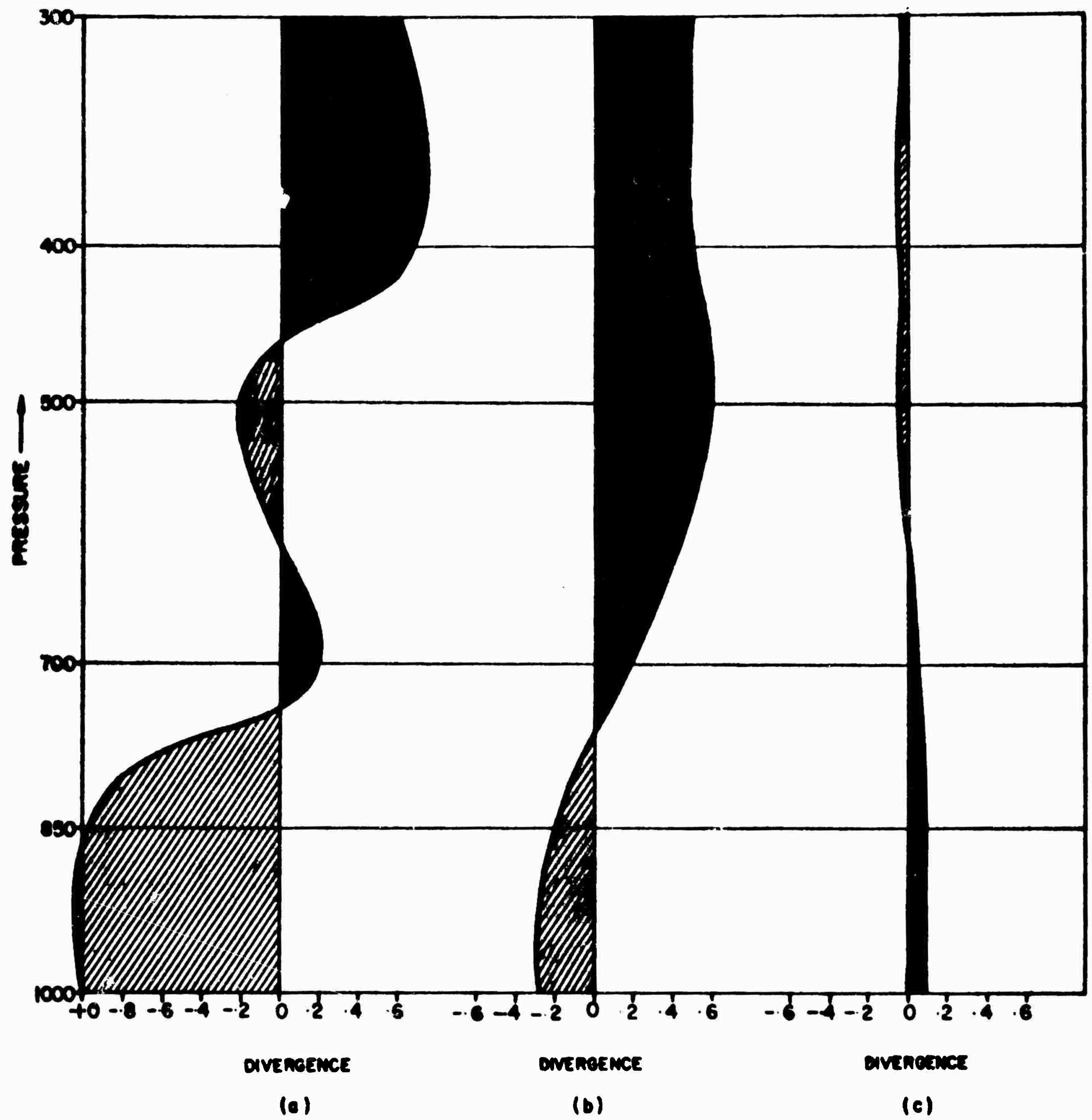

Figure 3. Vertical profiles of divergence through centre of surface low. Units are mb along the ordinate and $days^{-1}$ along the abscissa ($1 day^{-1} = 1.16 \times 10^{-5} sec^{-1}$). (a) January 21, 1959 0000Z, (b) January 22, 1959 0000Z, (c) January 23, 1959 0000Z.

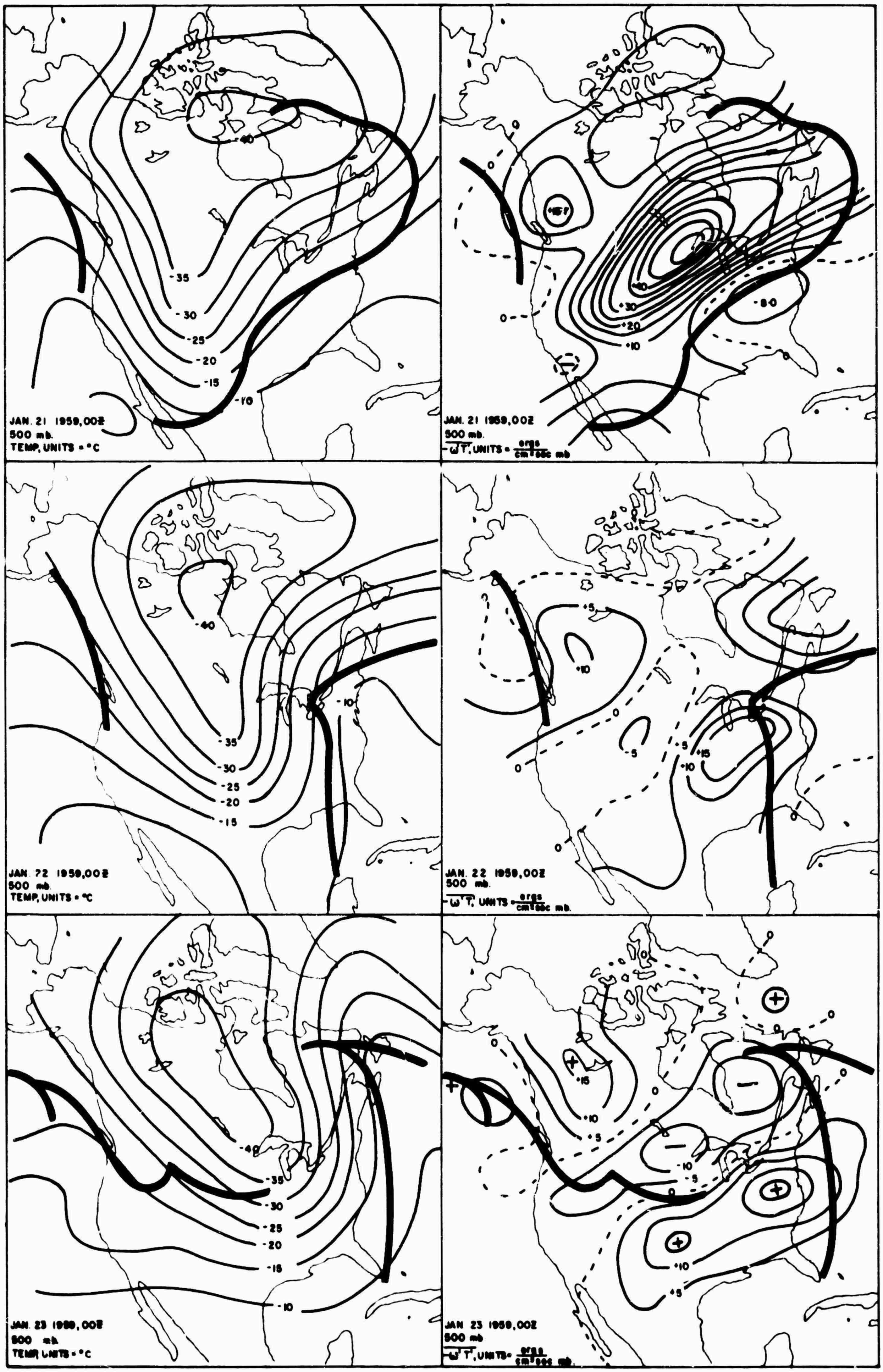
JAN. 21 1959,00Z
500 mb.
TEMP, UNITS = °C
JAN. 21 1959,00Z
500 mb.
$-\overline{\omega' T'}$, UNITS = $\frac{ergs}{cm^2 sec\ mb}$
JAN. 22 1959,00Z
500 mb.
TEMP, UNITS = °C
JAN. 22 1959,00Z
500 mb.
$-\overline{\omega' T'}$, UNITS = $\frac{ergs}{cm^2 sec\ mb}$
JAN. 23 1959,00Z
500 mb.
TEMP, UNITS = °C
JAN 23 1959,00Z
500 mb
$-\overline{\omega' T'}$, UNITS = $\frac{ergs}{cm^2 sec\ mb}$

Figure 4.

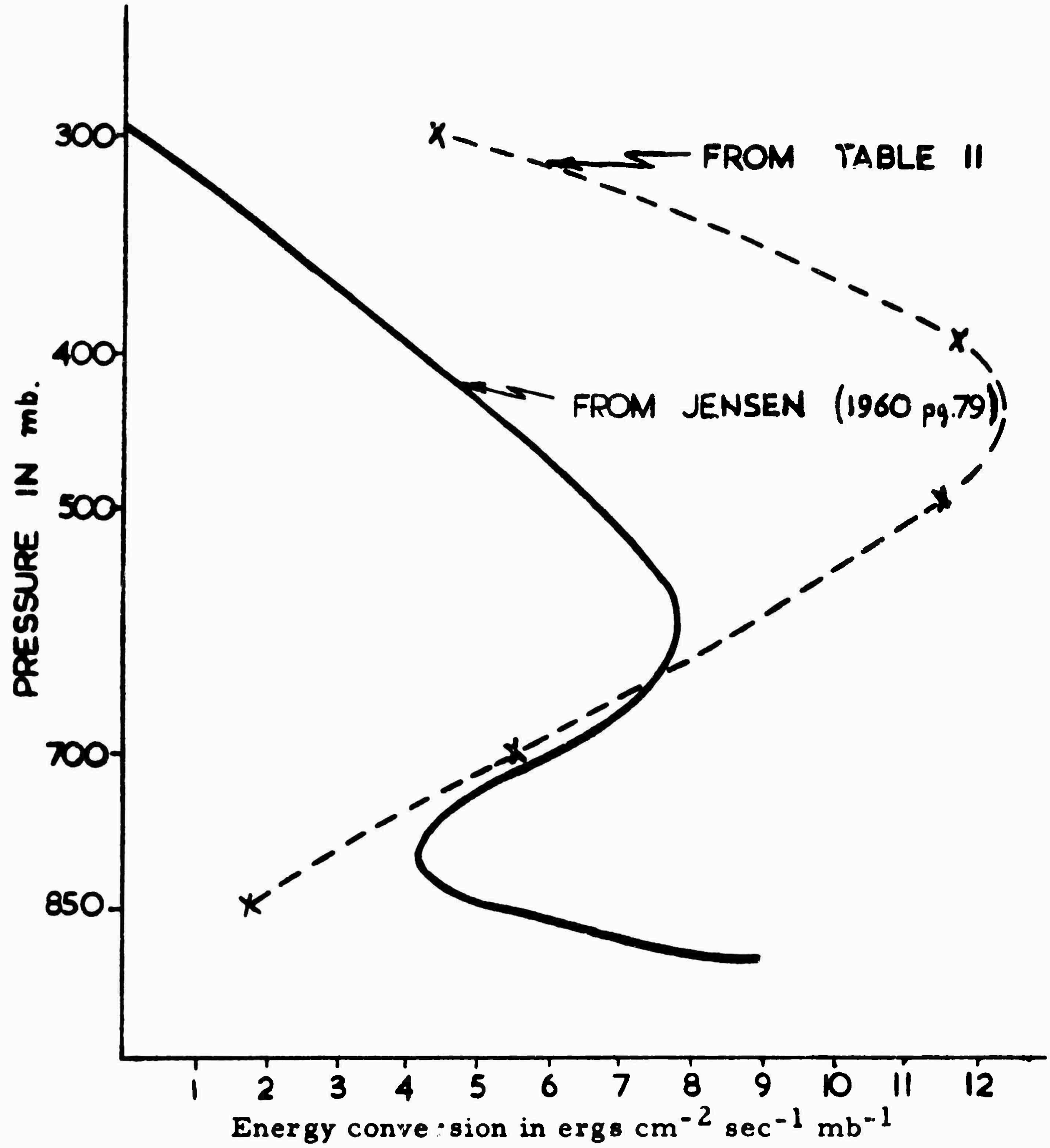

Figure 5. Vertical profiles of conversion from available potential energy to kinetic energy. Solid curve from Jensen (1960) represents the combined effect of transient and standing eddies (zonal) over the Northern Hemisphere for January 1958. Dashed curve represents the combined effect of two space scales of activity over North America for January 21 to 23, 1959

AUTOMATIC PROCESSING OF METEOROLOGICAL DATA

G.P. Cressman

The following will consider the automatic processing of meteorological data required in the operation of a large scale analysis and forecasting center and some new methods of data handling for data exchange among research workers. Many other types of automatic data processing exist, e.g., automatic observing stations, automatic sequencing of communication circuits, and the automatic reduction of special data for research. These will not be discussed here.

The automatic processing of meteorological data from the telecommunications circuits requires the following steps, i.e., collection and introduction into a digital computer, editing, checking, and sorting.

The collection of the incoming data requires the collection of the data on a temporary storage medium due to the relatively long time it takes in arriving as compared to the short time required for editing, etc. Paper tape has been extensively used in the past, but is being replaced by magnetic tape or disc storage as manufacturers make new equipment available. Under the present circumstances it would be a mistake to make the collection online to a general-purpose digital computer.

The editing process is quite difficult as a result of the complexity of the world-wide communications system. It involves :

(a) The recognition of the various types of reports,

(b) The correct identification and locating of the observing station

(c) The extraction of the required meteorological information.

The steps (a) and (b) above are the most difficult. Heading information is helpful, but due to its unreliability, the unique format specifications of each type of report must be checked for a minimum amount of fit to the required pattern. Recent WMO action in improving the code forms will be very helpful with this part of the task. Step (c) is relatively easy and straightforward.

Checking begins during the editing process by the checks on format and by comparison of format fitting with the heading information. The checks on position of movable stations present special problems. These can be partly solved by internal check groups in the code (upper air ships) and by ship position logging (surface ship reports). For upper air data, hydrostatic checks and checks on the vertical consistency of wind reports must be made. Further checking can be done during the sorting process, when duplicate reports arriving on different circuits can be compared to detect communication errors. This does not conclude all checking. Additional checking can be done during the objective analysis.

At this point, before the analysis begins, the data have been collected, edited, checked, and sorted, and can be rewritten in clean format on magnetic tape. This tape of processed data contains the real information from many hours of communication circuit operation, and contains data useful for both meteorological operations and research.

For operational purposes, the data can be repunched on paper tape in approved WMO code form for retransmission in complete form or as selected upper-air levels. Regional centers exchanging hemispheric data of this type could greatly improve the efficiency of the present data exchange system.

These magnetic tapes of clean data have also been found very useful for research. At the U.S. Weather Bureau's National Meteorological Center, they are kept, filed by synoptic times, as a permanent record suitable for rapid recall for research purposes. They can be repunched on paper tape or on punched cards, if required, for use by other organizations.

A WMO working group has recently arranged for the use of a special 8-day test series of data for research purposes. Three national centers were designated as archives for these data, which are now available to any other group upon request. So far, requests for data in all three forms, i. e. magnetic tape, punched cards, and paper tape have been honored. The very small additional effort required to make use of processed data in this form is a significant advantage of this type of exchange.

OBJECTIVE ANALYSIS

G.P. Cressman

We can understand objective analysis to comprise that part of treatment of the data in which we proceed from observations at randomly located points to the required field values at the regularly located points of the grid. Special treatments of these data required for specific forecast models, such as solving the balance equation, will not be considered.

Nearly all forms of objective analysis currently being used consist of either fitting a 2nd degree polynomial to the data or of making successive approximations by correction of errors of a guess field. Essential features of these two methods will be described, with emphasis on experience gained at the Weather Bureau's National Meteorological Center.

To apply quadratic surface fitting, we consider the data locally around each grid point. We wish to fit the surface

$$Z = a_1 + a_2 x + a_3 y + a_4 x^2 + a_5 y^2 + a_6 xy \tag{1}$$

by least squares to the data. Choosing a surface of geopotential, for example, we proceed to minimize the error E by the method of least squares, i.e.,

$$E = \Sigma p \, (Z_c - Z_o)^2 + w \Sigma q \, (\mathbb{V}_c - \mathbb{V}_o)^2 + \Sigma r \, (Z_f - Z_o)^2 + \Sigma s \, (Z_p - Z_o)^2 \tag{2}$$

forming and solving the six linear equations

$$\frac{\partial E}{\partial a_1} = \frac{\partial E}{\partial a_2} = \frac{\partial E}{\partial a_3} = \frac{\partial E}{\partial a_4} = \frac{\partial E}{\partial a_5} = \frac{\partial E}{\partial a_6} = 0 \qquad (3)$$

In the above, Z_c is calculated geopotential, Z_o is observed geopotential, Z_f is first guess geopotential, Z_p is previously calculated geopotential, $V_c = k \times \nabla Z_c$, $V_o = k \times \nabla Z_o$, p, q, r, and s are distance weighting functions, and w is a special weight for winds. If the geostrophic wind approximation is used, V_c and V_o are f/g times the calculated and observed winds, respectively.

The procedure then involves proceeding from grid point to grid point, making a fit at each point by forming and triangularizing a 6 x 7 matrix. Stability of the calculation as well as some smoothing can be promoted by requiring surplus information, e.g., 50 - 75% more than the minimum 6 pieces of information for each grid point.

Better resolution of the field around cyclones has been achieved, by making a second analysis applying the gradient wind approximation and obtaining curvatures from the first pass. Other improvements in the analysis have come from adaptation of special correction features from the second analysis system, following.

Disadvantages of this technique are the numerous multiplications and divisions required, which increased computation time, and the great care required to prevent ill-conditioned matrices from occurring.

The method of successive approximations begins by obtaining the best possible set of first guesses for the fields to be analyzed. The procedure then consists of making successive corrections to the guess field, first on a large scale, and then on smaller and smaller scales until the limits of resolution of the grid are reached. The corrections are made as follows: height only reported, $C_h = WE_o$; height and wind reported, $C_w = W\left[Z_o + \frac{\partial Z_o}{\partial x}\delta x + \frac{\partial Z_o}{\partial y}\delta y - Z_1\right]$

and wind only reported, the same as the latter, except use the previous guess for Z_o . In the above C_h or C_w are the correction for the grid point, E_o is the error of the guess at the observation location, Z_o is the observed height at the observation point, Z_1 is the guess height at the grid point, the horizontal derivatives of Z_o are determined from the wind law used, and W is a weighting function.

When analyzing fields of geopotential it is convenient to use the geostrophic approximation on early scans. Using these as guess fields, a higher order wind approximation can be used on subsequent scans. The distance weighting function can be obtained statistically for each individual station, for each level, or an over-all function can be used.

The correction to be applied at the grid point , C_g is obtained from

$$C_g = \frac{A \Sigma C_h + \Sigma C_w}{A N_h + N_w} \tag{4}$$

where N is the number of heights reported, and A is a weight (generally $A < 1$). Better detail can be obtained on the last scan by more complicated weighting procedures in computing C_g .

The above method can be used for analyzing practically any scalar field. It has been used for geopotential, temperature, static stability, mixing ratio, and wind components. Its advantages include flexibility and very short computation time. As a disadvantage, its success depends on obtaining a good first guess field. Also, systematic errors sometimes creep in around poor-data areas through the guess field. This has necessitated some special treatment of boundaries.

REFERENCES

Corby, G.A. : 'Some experiments in the objective analysis of contour charts,' Q.J.R.M.S. , 34, Jan. 1961.

Cressman, G. P. : 'An operational objective analysis system,' Monthly. Wea. Rev. , 367 - 374, Oct. 1959.

McDonnell, J. E. : 'On the objective analysis system used at the National Meteorological Center,' Ntl. Met. Center, Tech. Memo. No. 23.

COMPUTER APPLICATIONS IN STRATOSPHERIC ANALYSIS AND FORECASTING

F. W. Murray

The particular computer applications I shall describe are those of the Third Weather Wing, Offutt Air Force Base, Nebraska. There are two circumstances that should qualify my remarks. In the first place, I am no longer with the Third Weather Wing, having retired from the Air Force in February. Consequently my remarks may be a bit out of date. However I have remained in touch with my former colleagues, and some of the information I have to impart is quite recent. In the second place, much of what I am to talk about is the work of others, and some of it I am not very familiar with. However, I have consulted the experts on the various phases of the subject, and I hope to be able to transmit the information to you in a relatively ungarbled form.

First, I should give you a little background information on the organization. Third Weather Wing has the responsibility for providing all meteorological and climatological support for the Strategic Air Command plus certain types of support to other Air Force and Army activities. Since the meteorological information is tailored to the customer's requirements, and since the customer is a voracious devourer of all forms of meteorological and climatological information, it has become necessary to centralize and automate to the highest degree possible.

The objective, which has been met rather well, is to have an integrated system which starts with raw data and finishes with a complete set of forecast messages and ready drawn charts, all with an absolute minimum of manual input. The final product must include, among other things, detailed wind and temperature forecasts for a large number of specified routes. To this end a program has been written for each element of the job, and these programs are called in turn by a sort of monitor program. The operator can feed control data to the monitor to determine the sequence of the programs to be run and various options within the programs. For example, there are four standard variations of the automatic data processing run ; namely, surface and preliminary upper-air, operational upper-air, surface and one-time upper-air, and intermediate-hour surface. In addition, non-standard variations may be called for. Between 30 and 40 programs are involved in this.

In the normal course of events the surface and preliminary upper-air ADP is run 4 hours and 20 minutes after the 00Z and 12Z observation times, and it requires 20 minutes to run. Cressman has described some of the things an ADP program must do. This one does all of them plus some others, producing checked and sequenced data tapes for surface and upper-air reports available at that time, operational surface analyses of pressure and temperature, preliminary upper-air analyses, and various displays, including nephanalysis. At 6 hours and 20 minutes after observation time the operational upper-air ADP is run, combining the new data with the previously processed data. This requires 50 minutes. After this, the forecast run is made. It not only produces the dynamical forecasts for several surfaces, but also produces the many specialized types of forecasts, formats the messages for teletype transmission, produces tapes for graphical outputs whether by printer or Dataplotter, and verifies forecasts made previously. It takes 50 minutes. At 4 hours and 20 minutes after the 06Z and 18Z observation times the surface ADP, including nephanalysis, is run, taking 20 minutes.

To get to more specific detail, an ordinary ADP run contains, among others, the following programs :

1. ADX Sequencer. The ADX computer, when last heard from, had not been taught to maintain the integrity of the teletype circuits. This program takes the scattered data and sequences it by circuits.

2. Decoder. This program searches for bulletin headings, determines usable reports by format and discards unusable reports such as forecasts, decodes surface and upper-air reports, and writes them on tape.

3. Surface Sequencer and Upper-Air Output. This program separates surface reports from upper-air reports, sequences the surface reports in order of I - J coordinates, and writes them on a tape. From stored tables it determines for each upper-air report the type of instrument used, the units used, and the station elevation.

4. Upper-Air Sequencer. This program collects all reports from a given station, compares them, combines first and second transmissions, and selects the best and second best RAOBS and the best PIBAL. After doing this for all stations, it writes a tape containing all reccos, combars, roving ships, and aireps in the order decoded and all other reports in ascending numerical order by block and station number.

5. Hydrostatic Check. This program performs a complete hydrostatic and stability check on all RAOBS and a shear check on all winds. If errors can not be corrected, the report is discarded. A list of discards and reasons therefore is printed. Radiation corrections are made for all RAOBS above 100 mb. The program determines whether the instrument is in sunlight or darkness, and applies the correction appropriate for the instrument. In general, these are the corrections that have been suggested by Teweles and Finger. Corrected reports, both mandatory and significant levels, are written on tape.

6. Surface Check. This program converts all surface temperatures to Celsius, winds to knots, and pressures to millibars. It uses a first-guess field to determine whether a given pressure is over or under 1000 mb. It also eliminates all duplicate reports.

7. Upper-Air-Data Plotting. This prints display maps of data at specified surfaces for the use of the monitoring analyst.

8. Weather Chart. This prints maps that simulate hand-plotted maps of certain weather parameters.

9. Weather Depiction. This prints a map giving certain categories of ceiling and visibility.

10. Surface Analysis. Using essentially the procedure developed by Cressman and his colleagues, and described in detail by him at an earlier session, this program uses surface data to modify first guesses of pressure and temperature. Slightly different techniques are used for land and ocean areas. At this time the monitoring analyst may add bogus data if it is required.

11. Skew-T. This program writes a tape which produces on the high-speed printer plotted thermodynamic diagrams, including contrail data, for specified stations. Usually about 100 stations are selected for each run.

12. Tape Convert. This program sorts out upper-air data by standard pressure surfaces and counts the number of reports available. Bogus upper-air reports may be inserted at this point.

13. Guesser. Using the best available height and temperature estimates at grid points, this program produces by least squares a cubic curve of temperature against the logarithm of pressure from 850 mb to 100 mb. This curve is constrained so

that the mean temperature is the average of the top and bottom temperatures rather than the temperature at the mean pressure. The temperatures so produced are used as the first guess in the preliminary analysis. The advantage of this procedure is that hydrostatic consistency is preserved.

14. Multan. By modifying first-guess height and temperature fields this program produces analyses for ten surfaces from 850 mb to 10 mb. I shall discuss this in more detail later.

15. Metwatch. All forecasts made within the past 48 hours and valid at the present time are compared with the present analysis. This information is used by the Current Operations Section.

16. Display. Selected analyses are contoured and printed.

17. Tracer. Selected analyses are contoured and put out by Dataplotter.

18. Nephanalysis. This program analyses total cloud cover using a grid of 1/4 the normal spacing.

19. Neph Contour. This program contours the nephanalysis and puts it out by Dataplotter.

There is an analogous set of programs to produce the forecasts, but I do not plan to go into that here. Instead, I shall discuss in some detail the analysis program. This program is designed to produce grid -point analyses of height and temperature of all standard surfaces from sea-level to 10 mb, making maximum use of all available data and maintaining hydrostatic consistency. It also produces dew-point-depression analyses at 850 , 700, 500 and 400 mb. The basic technique is that of modifying a first guess to fit the observations, as developed at the National Meteorological Center in Suitland. With this technique the choice of a first guess is rather critical so that step is the principal part of this exposition.

Figure 1 shows the flow diagram of the entire process starting with the analyses produced 12 hours previously, and going through the computation of a crude first guess, a hydrostatically consistent temperature-pressure curve, a preliminary analysis, and a final analysis. You will see that in general the procedure is one of working from lower levels to higher , thereby taking full advantage of the greater abundance of data in the lower levels. The S blocks represent specific modules, or repeated sets of operations, as shown in Figure 2.

In Figure 2 the block A represents the entire Cressman method of successive corrections. This involves several scans over the entire grid with varying radii of influence. The relative weights of different types of observations can also be varied. One particular modification that has been found to be useful should be mentioned. The smoothing processes at work tend to degrade the high and low centres. To counteract this, Laplacians for each grid point are computed after the first pass and their magnitude is then increased by a small percentage. Relaxation then yields a field in which some of the vorticity lost by smoothing is restored. The program is constrained to avoid a net change in mean height for the entire grid.

The Block B represents the blending of two fields by averaging their values at each grid point. The fields may be given equal or different weights. The Block D represents constant difference. For example, at a lower level a crude guess T and a refined value T^P of temperature may be available. Then at the higher level the difference TP - T is added to the crude guess of temperature to produce a first guess T', which is then analysed to produce T^P . The Block F represents linear extrapolation, the Block H a hydrostatic build-up, and the Block R a computation by regression. There are three forecast blocks. F 1 is a sea-level forecast by the method proposed by Reed . F 2 was originally a single-parameter forecast

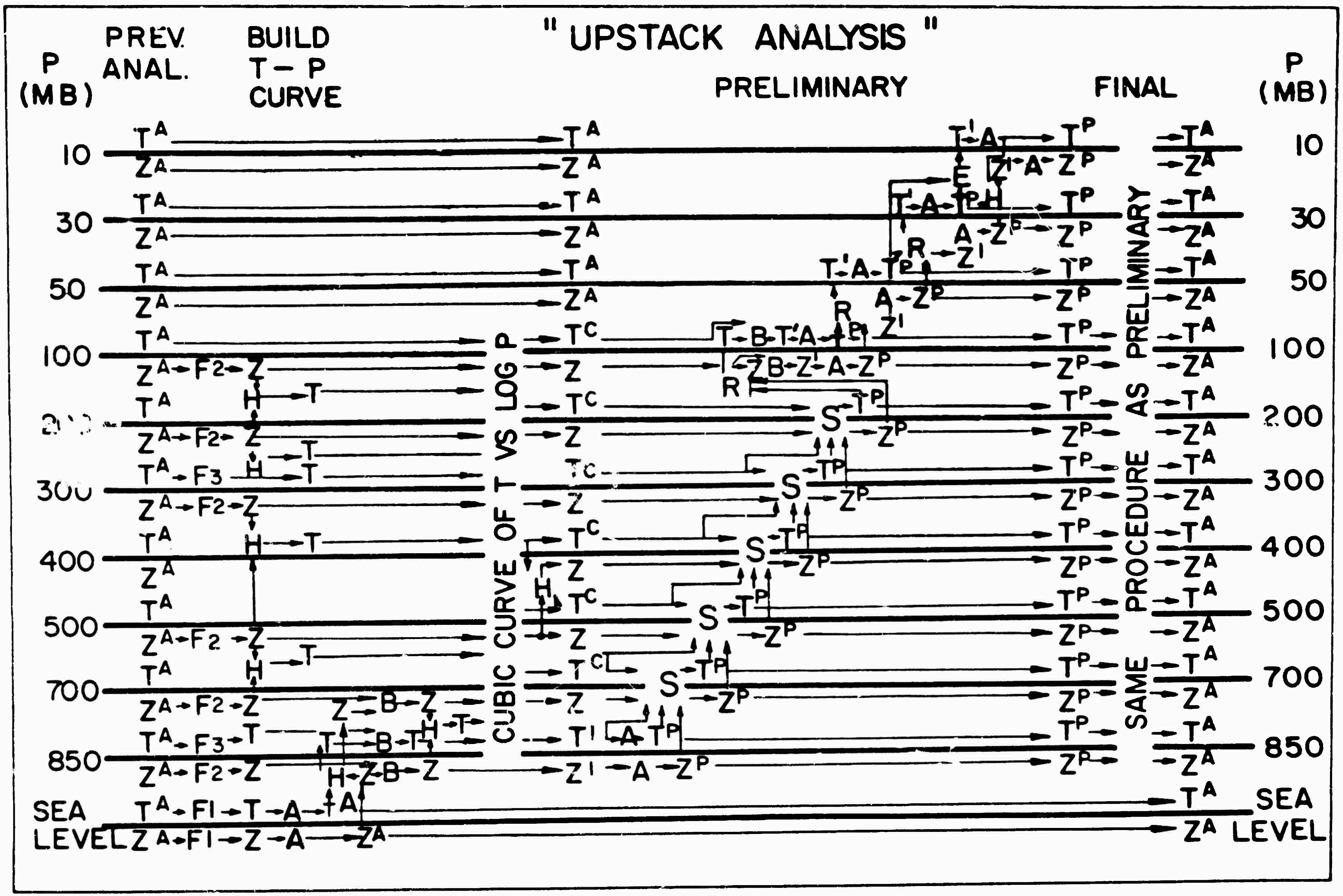
"UPSTACK ANALYSIS"
P (MB)
PREV. ANAL.
BUILD T – P CURVE
PRELIMINARY
FINAL
CUBIC CURVE OF T VS LOG P
SAME PROCEDURE AS PRELIMINARY
10
30
50
100
200
300
400
500
700
850
SEA LEVEL

FIGURE 1

"S" MODULE

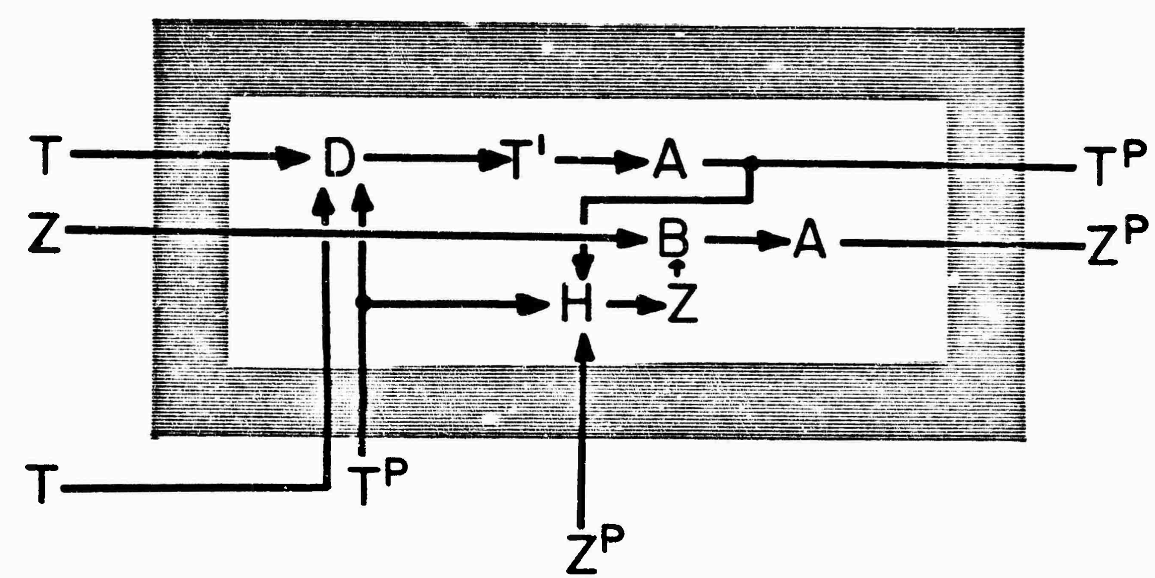

OTHER MODULES

A ANALYSIS
B BLEND
D CONSTANT DIFF.

E EXTRAPOLATION
H HYDROSTATIC BUILD-UP
R REGRESSION

F_1 REED FCST
F_2 FJØRTOFT FCST
F_3 ADVECTION FCST

FIGURE 2

following the method of Fjørtoft, but is now in most cases the operational baroclinic forecast. F3 is a simple advection forecast utilizing the successive time steps of F2.

The Block S represents the heart of the "upstack" procedure. Its inputs are crude and analysed temperatures and analysed heights of a lower surface and crude temperatures and heights of the surface being analysed. The lower -level temperatures are differenced, and the difference applied to the upper -level temperature to get a first guess. This is analysed, producing T^P. The analysed temperatures of the two surfaces and the analysed height of the lower surface are used in the hydrostatic equation to get a height for the upper surface. This is then blended with the crude height already available to produce a first guess for the analysis procedure. The analysed height Z^P is then produced.

Now let us look at the flow diagram in some detail. Starting from the left-hand side, the first column represents analysed temperature T^A and Heights Z^A of all the standard surfaces for 12 hours previous. Twelve-hour forecasts are available for Z at 100, 200, 300, 500, 700 and 850 mb and sea level and for T at 300 and 850 mb and sea level. These forecasts at sea level are used for the first guess, and a two-pass analysis program produces the final analyses.

These analyses are built up hydrostatically to 850 and 700 mb , and the heights and temperatures so produced are blended with the forecasts. Next, thicknesses of the layers 850-700, 700-500, 500-300, 300-200 and 200-100 are used to get mean temperatures. These five temperatures, forecast temperatures at 850 and 300 mb, and the persistent temperature at 100 mb are then fitted by least squares to a cubic curve of temperature against logarithm of pressure, represented by the second column. Temperatures from this curve are used as the first guess at 850 mb and one of the inputs to the first guess at other surfaces up to 100 mb. They are also used to produce hydrostatically a first-guess height at 400 mb. Other heights are carried across from previous computations, and heights and temperatures now available are shown in the next column.

Now with the use of preliminary data (early cut-off), the analysis of the 850-mb surface is made. These values of T^P and Z^P are used to build up to 700 mb and combined by the S module with guessed values available there, and an analysis is made at 700 mb. This procedure continues surface by surface, to 200 mb.

To build up from 200 to 100 mb a regression formula is used. The coefficients used are those developed by Duane Lea of the U.S. Navy at Norfolk. The first guess T and Z are blends of regression values with T from the curve and forecast Z respectively. In going from 100 to 50 mb and from 50 to 30 mb, the same regression technique is used except that here the computed T and Z values are used directly as the first guess without any influence from the analysis of the previous twelve hours. This lack of a direct continuity control may be considered a weakness of the system, but with observations above 100 mb being what they are, it seems better to carry the continuity at lower levels, and then achieve vertical consistency. For the last step, from 30 mb to 10 mb, we do not even have regressions available. Instead, we take a direct linear extrapolation of the 50-mb and 30-mb temperatures to 10 mb, and use this as a first guess. The analysed temperature resulting therefrom and the analysed temperature and height at 30 mb are combined hydrostatically to produce a first guess of height at 10 mb, and this is analysed.

On the basis of early cut-off of data we now have preliminary values of temperature and height (T^P and Z^P) at all standard surfaces from sea level to 10 mb. One of the principal uses of these preliminary analyses is to enable the monitoring analyst to determine what bogus data are necessary for the operational analysis. After the later data are in, the entire "upstack" procedure is repeated. The only difference is that the preliminary analyses form the first-guess input. There finally results the operational analyses indicated by T^A and Z^A in the column on the right.

SURFACE	JANUARY	MAY
300 mb	576	726
100 mb	356	410
50 mb	141	180
30 mb	111	150
10 mb	61	90

Table 1. Average number of usable reports

Table 1 shows the number of usable reports available this year for several pressure surfaces. There is an encouraging increase between January and May. The program is designed to handle a maximum of 900 reports . At 10 mb there has been a 50 per cent increase this year, and there are now enough reports to lend some credence to the daily analysis, especially in view of the forced hydrostatic coupling with the lower surfaces. The contours that are determined by the computer appear to match the reports , particularly the winds, very well.

In considering the series of analyses that are the fully automated product, the synoptician following the maps on a current basis must be prepared to evaluate questionable reports, and if need be , supplement or replace them. In this sense, then , we cannot claim complete automation. However, the high degree of automation leaves the analyst free to concentrate on critical areas and questionable reports.

In addition to analysis and data processing we have also worked on forecasting , but our accomplishments have been slight.

Operationally, we have developed a model which has given us useful forecasts for 500, 300, 200, and 100 mb. It has been reported on at an AMS meeting, so I will not go into detail about it. Suffice it to say that it is a four-level geostrophic model of the type originally developed by Charney and Phillips. It has no mountain or frictional effects in it, and it assumes constant static stability in each layer. After comparison of results we have come to the conclusion that the four-level model yields forecasts that are comparable in accuracy to those of the NMC three-level model.

Above 100 mb I have but one slight experiment to report. Since the equivalent-barotropic model is cheap to run and has shown considerable success at a variety of levels other than that for which it was designed, we decided to try it out at 50 mb. Our experiment was made in the difficult month of April, but the polar vortex still dominated the circulation. For a two week period in April the root mean square height error for the entire grid was compared for the barotropic, persistence, and a regression upward from the four-level model. The first two are quite comparable, with persistence winning at 24 hours and the barotropic having a slight edge at 36 and 48 hours. The regression result shows much larger errors than the other two. When only the gross errors at the grid points north of 25N are considered, the barotropic shows definite superiority over persistence. The root mean square errors for both the barotropic and persistence are between 150 and 300 feet, and I am not prepared to assert that the analysis at 50 mb is that good. It was because of this question as to the significance of our results that we abandoned the experiment.

In addition to current analyses and forecasts, an important part of the computer use at Offutt is in climatology. One of the products that is likely to be of general interest is a set of monthly mean maps produced by computer averaging of all the analyses at grid points.

As technology advances, the users of meteorological information require more and more from higher and higher levels. It is no longer possible to keep up with the demands of a large agency such as the Strategic Air Command, let alone a national meteorological service , without some degree of automation. Experience at Offutt Air Force Base shows that given proper machines and an adequate programming staff most of the problems of data processing and analysis can be handled, even when we are working near the limits of present observational techniques. There has already been some effort at the introduction of satellite observations into the operational system (use of TIROS data in nephanalysis), and in the future there is sure to be more of this. Also, rocketsonde observations may later find their way into the system. The computer is capable of treating them all impartially (or with prejudice, if we so desire).

Automatic analysis is limited only by the density of the data, and we have demonstrated that it can now be done with some degree of success up to 10 mb. No doubt our stratospheric analyses will continue to improve, especially as observations become better and more plentiful. And this, I believe, is our real limitation on numerical forecasting. While there have been no dramatic break-throughs lately, we have a solid body of techniques that have been successful in the lower atmosphere and that can be made applicable to the upper atmosphere. More elaborate baroclinic models and usable primitive-equation models will come along as computers adequate to handle them become available.

There is one aspect of stratospheric numerical forecasting that still needs a good deal of theoretical attention: the peculiar dynamics of the polar vortex and its break-down. The exchanges of energy involved are not fully understood, and are probably not adequately handled by our existing forecast models. It may well be necessary to introduce into our models some effect of diabatic heat transfer, particularly in the ozonosphere. Until we understand more fully the processes involved and until we get more and better observations, we will be fighting with only marginal success to improve on persistence.

A BAROCLINIC MODEL FOR THE CANADIAN NUMERICAL WEATHER PREDICTION PROGRAM

A. Robert

Early in 1959 a small group of meteorologists located at the Central Analysis Office in Montreal and working under the direction of M. Kwizak, started testing models of the atmosphere in preparation for an operational numerical weather prediction program. In a period of three years, seven numerical models of the atmosphere were tested on an IBM 650 computer located at McGill University. About 135 cases altogether were integrated up to 48 hours for an 896-point grid network. In September 1962, a Bendix G-20 computer was installed at the Central Analysis Office , most programs have been translated, a 1709-point grid network has been adopted and the operational production of forecasts is expected to start early in September. Initially, a barotropic model will be used and it is hoped that during the winter a change over to a four-level model will take place.

Now that Canada is irreversibly involved in the field of numerical weather prediction, a developmental research program should be established and discussed with meteorologists of other countries in order to ensure that useless duplication will be avoided. In such an exchange of ideas, it is reasonable to expect that meteorologists with a considerable amount of experience in this field will provide our group with constructive suggestions for future research. These suggestions, even if they are not followed literally, will at least have a considerable influence on our methods of attacking the prediction problem.

The Canadian N.W.P. group is presently preparing for operational production and a clear, concise statement of future plans is not practical. Instead , modelling experiments carried out in the past four years will be reviewed briefly, and extrapolated into the immediate future.

When the unit was originally formed, few members had experience in the field of numerical weather prediction, and it was decided to duplicate some of the models used in other countries. In a period of two years, four different barotropic models were programmed and tested. Each model has been integrated up to 48 hours for 26 selected cases.

Subsequently, experiments were performed with two baroclinic models. The first one is a slightly simplified version of the three-level model used by Cressman's group, and the second one is a model which was proposed by Dr. Godson a few years ago. A brief description of both these models will be given, followed by a comparison. The differentiated approach is used in both cases. The two equations for horizontal motion are transformed into the vorticity equation and the balance equation. The first law of thermodynamics is also used with the assumption of adiabatic motion.

$$\frac{DQ}{Dt} = f_o \frac{\partial \omega}{\partial p}$$

$$\nabla \cdot (+\nabla \psi) + 2J(u,v) = g \nabla^2 Z$$

$$\frac{D}{Dt}\left(\frac{\partial \psi}{\partial p}\right) + \sigma \omega = 0$$

$$\frac{D}{Dt} = \frac{\partial}{\partial t} + u \frac{\partial}{\partial x} + v \frac{\partial}{\partial y} \qquad \sigma = \frac{1}{\rho + \theta} \frac{\partial \theta}{\partial p}$$

The vorticity equation is written in a greatly simplified form where Q represents the absolute vorticity and f_o is the value of the Coriolis parameter at 45 N. The wind field is assumed to be non-divergent and the corresponding balance equation is derived. The non-linear Jacobian term appearing in the balance equation was not used. The stream field has been substituted for the height field which normally appears in the first law of thermodynamics.

The vertical velocity is eliminated between the equations of vorticity and the first law of thermo-dynamics, giving the so-called potential vorticity equation. Elimination of the time tendencies between the same two equations gives a diagnostic equation relating the vertical velocity to the horizontal wind.

$$\frac{D}{Dt}\left[Q + \frac{\partial}{\partial p}\left(\frac{fo}{\sigma}\frac{\partial \psi}{\partial p}\right)\right] = 0$$

$$\sigma \nabla^2 \omega + fo \frac{\partial^2 \omega}{\partial p^2} = \frac{\partial}{\partial p}\left(\mathbf{V} \cdot \nabla Q \right) - \nabla^2 \left(\mathbf{V} \cdot \nabla \frac{\partial \psi}{\partial p}\right)$$

In both equations, the stability parameter has been assumed to depend only on pressure. It should be noted that the two equations given above are not new and different, they are simply the two basic equations presented in a different form. There are two ways in which a model may be constructed from the above equations. The first method uses the following set of equations :

$$\frac{D_2}{Dt}(\psi_3 - \psi_1) + \sigma_2 P \omega_2 = 0$$

$$\sigma_2 P \nabla^2 \omega_2 + \frac{fo}{P}(\omega_4 - 2\omega_2) = \mathbf{V}_3 \cdot \nabla Q_3$$

$$- \nabla^2 \left[\mathbf{V}_2 \cdot \nabla (\psi_3 - \psi_1) \right]$$

$$\frac{D_3}{Dt} Q_3 = \frac{fo}{P}(\omega_4 - \omega_2)$$

$$\sigma_4 P \nabla^2 \omega_4 + \frac{fo}{P}(\omega_2 - 2\omega_4) = \mathbf{V}_5 \cdot \nabla Q_5 - \mathbf{V}_3 \cdot \nabla Q_3$$

$$- \nabla^2 \left[\mathbf{V}_4 \cdot \nabla (\psi_5 - \psi_3) \right]$$

$$\frac{D_4}{Dt}(\psi_5 - \psi_3) + \sigma_4 F \omega_4 = 0$$

In these equations σ_2 and σ_4 are determined from climatology, $\mathbf{V}_2$ and $\mathbf{V}_4$ are replaced by the average of the wind above and below each level. This model requires only three levels of information, but it essentially contains five equations and five unknowns. The second method is based entirely on the potential vorticity equation.

$$\frac{D_1}{Dt} \quad Q_1 + \frac{fo}{\sigma_2 P^2}(\psi_3 - \psi_1) \qquad = 0$$

$$\frac{D_3}{Dt} \quad Q_3 + \frac{fo}{\sigma_4 P^2}(\psi_5 - \psi_3) - \frac{fo}{\sigma_2 P^2}(\psi_3 - \psi_1) = 0$$

$$\frac{D_5}{Dt} \quad Q_5 - \frac{fo}{\sigma_4 P^2}(\psi_5 - \psi_3) \qquad = 0$$

In this case vertical motion does not appear in the equations. The two models described here are exactly the same because they are both based on the same two equations and they both use the same finite difference approximations. Both of them were integrated for the same test case and the forecasts were identical.

The choice of a baroclinic model was based on a double criterion. First, it was considered desirable that for certain values of its coefficients, the model should degenerate into a barotropic model. Secondly, it was considered necessary that the model must be stable in the short waves. This condition is easily examined if the analysis of the predictive equations is restricted to the shortest waves. These two conditions are fulfilled in the present case. When both σ_2 and σ_4 are made very large, the model produces barotropic forecasts. The fact that the model can produce barotropic forecasts is an asset. If the values of the stability parameter capable of giving the best forecasts are selected, then one is sure even before the model is programmed that it will produce forecasts at least as good as, if not better than, the barotropic model.

The climatological values of the stability parameter have been found to produce the best forecasts even though the improvement over barotropic forecasts is not very significant. Experiments were performed with intermediate values and have shown no advantage over climatological values.

The model based on the potential vorticity equation was programmed for four levels while the other method was programmed for three levels. The three-level model required 26 hours of computing time on the IBM 650 to produce a 48-hour forecast while the four-level model required only 16 hours. Because of the considerable economy in computing time, the approach based on the potential vorticity equation was adopted.

As suggested by Dr. Godson, potential vorticity is evaluated from a linear regression equation :

$$Q + \frac{\partial}{\partial p}\left(\frac{fo}{\sigma}\frac{\partial \psi}{\partial p}\right)_i = Q_i + \sum_{k=i}^{N} C_k \psi_k$$

The coefficients of the regression equation have to be evaluated in some fashion. Four methods have been considered and three of them have already been worked out. The four level model has been reprogrammed for the Bendix G-20 computer. A 48-hour integration requires 25 minutes. The integration of test cases has been started and results are expected to come out during the winter. At present, the model contains no mountains or other influences of a geographical nature. A considerable amount of experimentation will be performed during the next two years with frictional and non-adiabatic effects, the evaluation of vertical motion and the divergent part of the wind, and the approximations on which the model is based. In the long run the model will gradually evolve towards the primitive equations approach. It is believed that with the addition of some refinements, this model will eventually result in a considerable improvement over barotropic forecasts.

ON OBJECTIVE ANALYSIS OF STRATOSPHERIC DATA BY SASAKI'S METHOD

W. M. Washington and R. T. Duquet

PART 1 - THEORETICAL CONSIDERATIONS

DERIVATION OF THE ANALYSIS EQUATION

We begin by considering the problem of constructing a single, internally consistent, analysis of atmospheric conditions from wind, height and temperature fields, each derived independently from observations. In practice the values of these three quantities must be determined at a regular network of points from data given at irregularly spaced stations by some interpolation and/or extrapolation scheme which is not our present concern. We assume that the data fields are to be considered interdependent and that they are to satisfy certain functional relationships such as the hydrostatic and geostrophic equations, the balance equation or some other counterpart equation.

We now set as the objective of our analyses the reconciliation of the independent fields which is achieved when the volume integral of some quantity "E" is reduced to a minimum. Following Sasaki, we choose an "E" defined as

$$E = \alpha_1^2 (u - u_o)^2 + \alpha_1^2 (v - v_o)^2 + \alpha_2^2 (Z - Z_o)^2 + \alpha_3^2 (T - T_o)^2 \qquad 1.1$$

Other possible choices of "E" will be discussed later. In (1.1) the variables subscripted with zero are observed at a given pressure level (or within a layer in the case of T_o) whereas unsubscripted quantities are the final analysed values. The alpha's are weights and may be defined by

α_1	$1/\sigma_{o_v}$	the inverse of the standard deviation of observed winds about the "true" wind.
α_2	$1/\sigma_{oz}$	the inverse of the standard deviation of observed heights about the "true" heights.
α_3	$1/\sigma_{o_T}$	the inverse of the standard deviation of observed mean temperature about the "true" mean temperatures.

A discussion of the derivation of these three quantities has been given by Hovermale (1962).

In order to proceed we must select the relationship between winds, heights and temperatures which will be valid in the analysis. Let us say the choice is the geostrophic and the hydrostatic equations :

$$\mathbf{V} = g/f \; \mathbf{k} \times \nabla Z \tag{1.2}$$

$$\partial Z/\partial p = RT/gp \tag{1.3}$$

where $\mathbf{V} = iu + jv$, is the horizontal wind.

g	=	acceleration of gravity	R	=	gas constant
∇	=	$i\dfrac{\partial}{\partial x} + j\dfrac{\partial}{\partial y}$	f	=	coriolis parameter
Z	=	height of an isobaric surface	ϕ	=	latitude
T	=	absolute temperature	Ω	=	angular speed of the earth's rotation

For convenience we may follow Sasaki (1958) and rewrite equation (1.3) as

$$T = \partial z/\partial p^* \tag{1.4}$$

where $p^* \equiv -\dfrac{R}{g} \ln \dfrac{p}{\pi}$ and π is some reference level .

If the functional relationships (1.2) and (1.4) are substituted into (1.1), the quantity "E" is given by

$$E = \alpha_1^2 \left(g/f \frac{\partial Z}{\partial y} + u_o \right)^2 + \alpha_1^2 \left(g/f \frac{\partial Z}{\partial x} - v_o \right)^2 + \alpha_2^2 (Z - Z_o)^2 + \alpha_3^2 \left(\frac{\partial Z}{\partial p^*} - T_o \right)^2 \tag{1.5}$$

The minimum in the volume integral, I, ($\equiv \int_V E \; dV$) where V is the volume being analyzed, is achieved by satisfying the usual " Euler Equation" which is derived in standard texts on calculus of variation (Morse and Feshbach, 1958). For problems involving only first order derivatives, this equation is :

$$\frac{\partial E}{\partial Z} - \frac{\partial}{\partial x}\left(\frac{\partial E}{\partial Z_x}\right) - \frac{\partial}{\partial y}\left(\frac{\partial E}{\partial Z_y}\right) - \frac{\partial}{\partial p^*}\left(\frac{\partial E}{\partial Z_{p^*}}\right) = 0 \qquad (1.6A)$$

where Z subscripted x, y and p^* refer to the derivatives of Z with respect to these three independent variables. The corresponding boundary conditions are :

$$\left[\frac{\partial E}{\partial Z_y}\,\delta Z\right]_{Y_1}^{Y_2} = \left[\frac{\partial E}{\partial Z_{p^*}}\,\delta Z\right]_{p_1^*}^{p^*_2} = \left[\frac{\partial E}{\partial Z_x}\,\delta Z\right]_{x_1}^{x_2} = 0 \qquad (1.6B)$$

where δZ is the change in the function describing the field Z and the subscripts 1 and 2 refer to end point values. The problem of boundary conditions becomes particularly important when it is desirable (or necessary) to restrict the analysis area. In the stratosphere, data density varies to such an extent from one sector of the world to another that analysis of limited areas only may be unavoidable in many instances. In his initial paper, Sasaki assumed that δZ was zero along the boundary but this is not necessarily the optimum boundary condition as will be discussed later.

Substituting equation (1.5) into 1.6A) gives

$$\alpha_2^2\,(Z - Z_0) - \alpha_1^2\,(g/f)(\nabla^2 Z - \zeta_0) - \alpha_3^2\left(\frac{\partial^2 Z}{\partial p^{*2}} - \frac{\partial T\varrho}{\partial p^*}\right) = 0 \qquad (1.7)$$

where $\nabla^2 \equiv \partial^2/\partial x^2 + \partial^2/\partial y^2$, the Laplacian Operator

and $\zeta_0 = \frac{\partial vo}{\partial x} - \frac{\partial uo}{\partial y}$, the observed vorticity. In deriving this equation (1.7) the horizontal variation of the coriolis parameter has been neglected. Rewriting (1.7) to collect known and unknown terms we have

$$\nabla^2 Z + \left(\frac{a_3}{a_1}\frac{f}{g}\right)^2 \frac{\partial^2 Z}{\partial p^{*2}} - \left(\frac{a_2}{a_1}\frac{f}{g}\right)^2 Z = \frac{f}{g}\zeta + \left(\frac{a_3}{a_1}\frac{f}{g}\right)^2 \frac{\partial T_o}{\partial p^*} - \left(\frac{a_2}{a_1}\frac{f}{g}\right)^2 Z_o \tag{1.8}$$

If the boundary conditions (1.6) are satisfied by taking $Z = 0$, they and equation (1.8) represent a Dirichlet boundary problem (boundary conditions of the first kind); if the boundary conditions are chosen so that $\frac{\partial E}{\partial Z_x}$, $\frac{\partial E}{\partial Z_y}$ and $\frac{\partial E}{\partial Z_{p^*}}$ are set equal to zero, we have a Neumann boundary problem (boundary condition of the second kind). Equation (1.8) by itself is referred to, in mathematical literature, as a " Helmholtz" type equation.

By placing a_3 equal to zero (no weight given to temperatures) the analysis equation is reduced to

$$\nabla^2 Z - \left(\frac{a_2}{a_1}\frac{f}{g}\right)^2 Z = \frac{f}{g}\zeta - \left(\frac{a_2}{a_1}\frac{f}{g}\right)^2 Z_o \tag{1.9}$$

This same equation is derived if we require that the surface integral of E be a minimum and define E as in (1.1) but without the last term.

The extreme in simplification is reached if we further set a_2 equal to zero, for then we have merely

$$\nabla^2 Z = \frac{f}{g}\zeta_o \tag{1.10}$$

which states that the analysed heights are to be determined entirely by the vorticity of the observed winds (with no consideration given to observed heights except possibly as boundary conditions for the Dirichlet case.)

The following material will deal with the two dimensional equation (1.9) rather than the three dimensional one (1.8) for several reasons. First, since heights and temperatures are not observed independently but are, instead, found one from the other through the hypsometric equation, we are not completely justified in treating these two fields as independent data. Further as we noted above, the observed temperature (T_o) in equation (1.7) must be the mean temperature of a layer; this is inconvenient to obtain, particularly where the lapse rate is irregular. Finally, the need for specifying vertical boundary conditions (which again poses a small practical problem) is avoided when the analysis is made in two dimensions only.

WAVELENGTH CHARACTERISTICS OF THE ANALYSIS EQUATION

An analysis based on the equations presented above has properties not found in other methods of objective analysis. One important property is the manner in which the equation incorporates different information into the analysis at different scales. This property has been demonstrated by Sasaki (1958) and is shown again here in order to demonstrate the significance of the weighting factor ratio.

Assume that the observations used in equation (1.9) define a simple wave

$$u_o = iU_o \exp\left[i(kx + ny)\right] \tag{2.1}$$

$$v_o = iV_o \exp\left[i(kx + ny)\right] \tag{2.2}$$

$$Z_o = Z_o \exp\left[i(kx + ny)\right] \tag{2.3}$$

and that the solution is also a wave given by

$$Z = Z \exp\left[i(kx + ny)\right] \tag{2.4}$$

where $k = 2\pi/\lambda_x$, λ_x = wavelength in the x direction

and $n = 2\pi/\lambda_y$, λ_y = wavelength in the y direction

By substituting equations (2.1 to 2.4) into (1.9) we obtain

$$Z = \frac{\frac{f}{g}(k V_o - n U_o) + \left(\frac{\alpha_2}{\alpha_1}\frac{f}{g}\right)^2 Z_o}{\left[(k^2 + n^2) + \left(\frac{\alpha_2}{\alpha_1}\frac{f}{g}\right)^2\right]} \tag{2.5}$$

If we define a critical wave length L_c :

$$4\pi^2 L_c^{-2} \equiv \left(\frac{\alpha_2}{\alpha_1}\frac{f}{g}\right)^2 \tag{2.6}$$

we can distinguish two limiting situations :

the first where $(k^2 + n^2) >> 4\pi^2 L_c^{-2}$

and $$Z \approx \frac{f}{g}\frac{(k V_o - n U_o)}{k^2 + n^2} \tag{2.7}$$

and the second where $(k^2 + n^2) << 4\pi^2 L_c^{-2}$

and $$Z \approx Z_o \tag{2.8}$$

It is apparent from (2.7) that the analysis of waves shorter than some critical wavelength (which corresponds to a certain ratio in the weights assigned to winds and to height information) is derived primarily from observed winds; from (2.8) it is apparent that the long wave analysis is based on observed heights. If we choose α_2 and α_1 so that equal weight is given to an error of 1 m /sec in the wind field and to an error of 1 m in the height field, the critical wavelength is close to 600 km. Figure 1 shows the variation of the ratio α_2 / α_1 (and of the implied L_c) with height that was found by Hovermale (1962) . It is apparent that the weighting factor ratio which was found to be appropriate for use with stratospheric data (as a

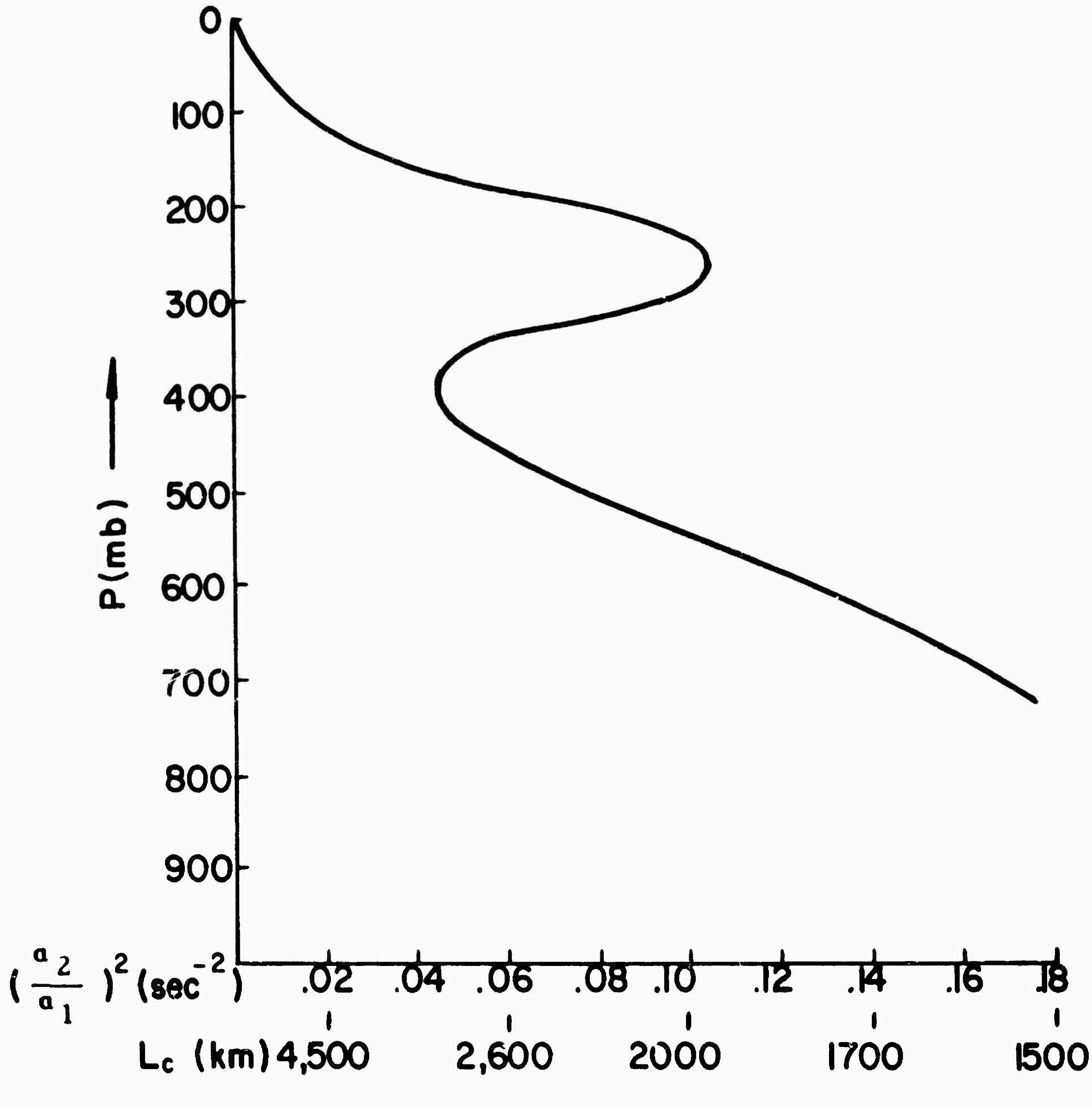

Figure 1. The distribution of the ratio of weighting factors a_2/a_1 for wind vs height observations as a function of pressure (after Hovermale, 1962). A ratio of unity corresponds to equal weight assigned to an error of 1m/sec in winds and 1 m in heights. The weights are inversely proportional to standard error of observations found by technique using spectrum analysis. The lower line gives values of the critical wavelength, L_c ($= 2\pi \frac{a_1}{a_2} \frac{g}{f}$) as discussed in the text.

result of uncertainty in the observations) causes the analysis to be derived almost entirely from winds data.

INFLUENCE FUNCTION OF THE ANALYSIS EQUATION

The difference between the role of the observed vorticity of the wind and the role of the observed heights in determining the final analysis can also be seen from the influence function (i.e. Green's function) solution of the analysis equation. On physical grounds it is obvious that this influence function must have certain properties; it must be a function of distance only; it should approach zero as distance increases, it must remain real for real arguments; it may have a singularity at "zero" distance. For a Helmholtz equation such as equation (1.9) an influence function which has the above properties is given from classical theory (c.f. Morse and Feshback, 1953) : it is a zero order Bessel function of the second kind with imaginary argument : $K_o (R/2 \pi L_c)$. In this function the parameter R is defined as

$$\left[(x - x^1)^2 + (y - y^1)^2 \right]^{1/2}$$

the distance between a point (x^1 , y^1) at which the analysis is made and any other points (x, y) at which data is supplied.

For large values of R, the asumptotic expansion of $K_o (R/ 2 \pi L_c)$ is

$$G \approx \left(\frac{\pi^2 L_c}{R} \right)^{1/2} e^{- (R / 2 \pi L_c)} \tag{3.1}$$

A plot of influence versus the argument $R / 2 \pi L_c$ is shown in Figure 2.

It should be noted at this point that the influence function involves the ratio of weights α_2/α_1, (through the parameter Lc) in such a way that the ratio effectively modifies the distance between the analysis point and the data points.

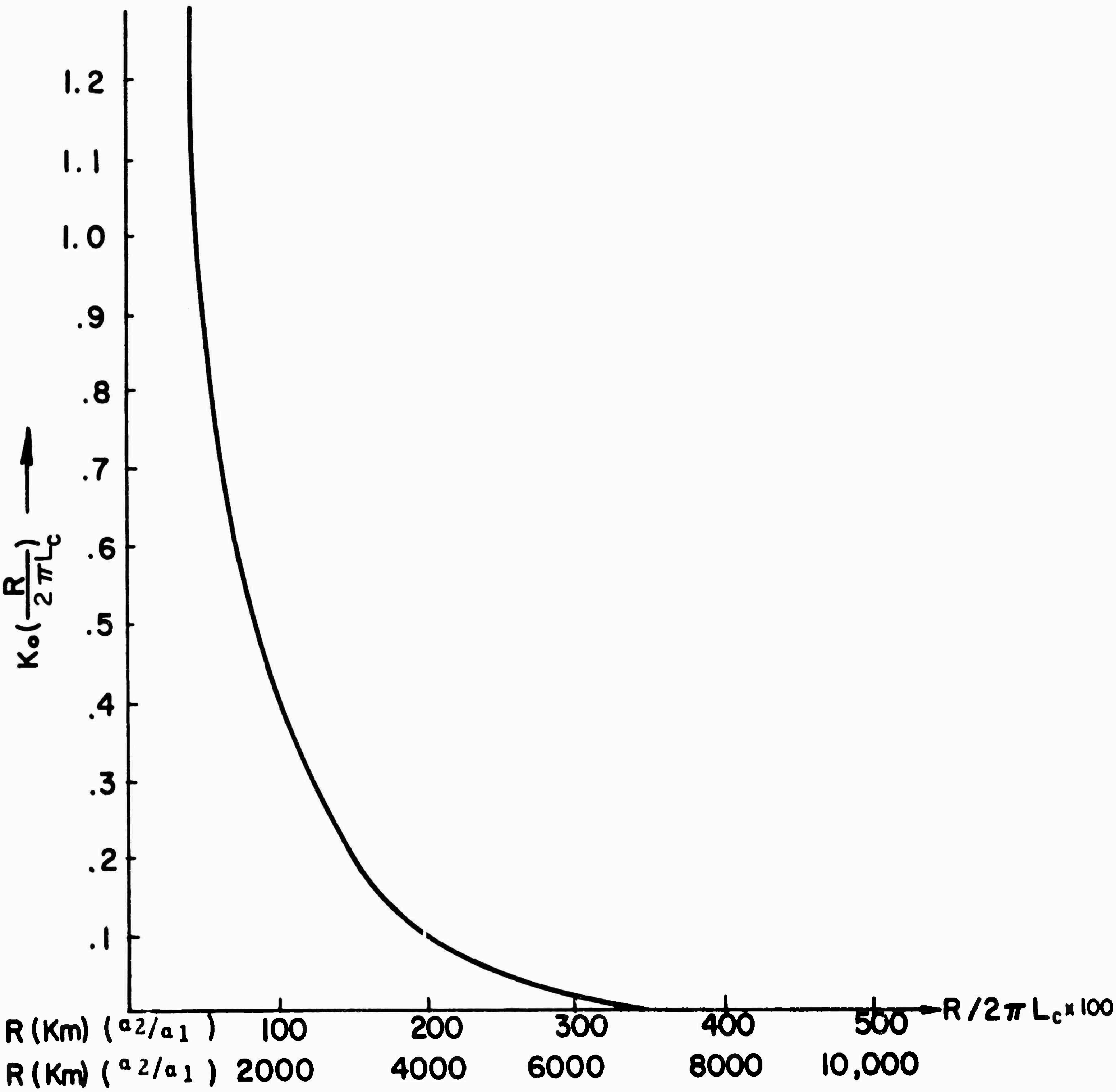

Figure 2. **The zero order Bessel function of the second king versus its argument. The lower scales refer to values of L_c corresponding to ratios a_2/a_1 equal to 1 and to 1/20 and a latitude of approximately 45^o.**

Aside from constraints due to boundaries (they may be assumed to lie at infinity), the integral solution of the analysis equation (1.9) is simply

$$Z = \iint G \left(\frac{f}{g} \zeta_o - \left(\frac{\alpha_2}{\alpha_1} \frac{f}{g} \right)^2 Z_o \right) dx\, dy \qquad (3.2)$$

From (3.1) and (3.2) it is apparent then, that as less weight is given to height data (α_2 becoming small) the analysis not only is based more heavily on the vorticity of the observed wind, ζ_o , but is simultaneously made more heavily dependent upon observations at distant points.

It follows from this and from the previous section that analysis in the stratosphere involves something of a paradox. Wind data is most suitable for definition of the smaller features in a flow pattern , yet in the stratosphere, where the smaller perturbations are less pronounced than in the lower levels of the atmosphere, the relative accuracy of available information forces a wind-dependent analysis. The extent of this dependency may be realized when it is noted that a relative weight of the order of 20 : 1 is appropriate for stratospheric wind and height data; this corresponds to a critical wavelength of about 12,000 km.

OTHER ANALYSIS EQUATIONS

Equation (1.9) was derived on the basis of a particular choice of "E" , the quantity to be minimized over a given volume (or area in the 2-dimensional case). Other choices of "E" lead to different analysis equations with different Green's functions and different scale properties.

As an example of other possibilities, consider the choice (for a two dimensional analysis) :

$$E = \alpha_1^2 (V - V_o)^2 + \alpha_2^2 (\nabla \psi - \nabla \psi_o)^2 \qquad (4.1)$$

where ψ is a stream function. (Of course, ψ_o is not observed as directly as V_o (and T_o) . The " o" subscript, in this case, refers to a field derived from observations and from some definition which does not involve the distribution of other observed quantities. A simple example would be the quasi-geostrophic stream function $\psi_o = g/f\ Z_o$). The relationship between $\mathbb{V}$ and ψ in the final analysis may be taken as

$$\mathbb{V} = k \times \nabla \psi \qquad (4.2)$$

Following the same procedure as before, but retaining vector notation, we minimize the area integral

$$\iint I\,dA \equiv \iint \Big\{ (a_1^2 + a_2^2)(\nabla\psi)^2 + 2\nabla\psi \cdot (a_1^2\, \mathbb{k} \times \mathbb{V}_o - a_2^2 \nabla\psi_o) + a_1^2 \mathbb{V}_o^2 + a_2^2 (\nabla\psi_o)^2 \Big\}\, dA$$

which is accomplished by setting

$$\iint \Big\{ \frac{\partial I}{\partial(\nabla\psi)} \cdot \nabla \delta \Big\}\, dA$$ equal to zero, that is , by satisfying

$$\iint \Big\{ \big[(a_2^2 + a_1^2) \nabla\psi + a_1^2\, \mathbb{k} \times \mathbb{V}_o - a_2^2 \nabla\psi_o \big] \cdot \nabla\delta \Big\}\, dA = 0 \qquad (4.3)$$

This can be transformed by means of the identity

$$\nabla A \cdot \nabla B \quad \nabla \cdot A \nabla B \;-\; A \nabla^2 B$$

and by applying Gauss' theorem so that it becomes

$$\oint \delta \cdot \Big\{ (a_1^2 + a_2^2)\nabla\psi + a_1^2\, \mathbb{k} \times \mathbb{V} - a_2^2 \nabla\psi_o \Big\}_n\, dS \;-$$

$$\iint \delta \Big\{ (a_1^2 + a_2^2) \nabla^2\psi - a_2^2 \nabla^2\psi_o + a_1^2 \nabla \cdot \mathbb{k} \times \mathbb{V} \Big\}\, dA$$

$$= 0 \qquad (4.4)$$

The minimum E is achieved then by satisfying

$$\nabla^2\psi = \Big(\frac{a_2^2}{a_1^2 + a_2^2} \Big) \nabla^2\psi_o + \Big(\frac{a_1^2}{a_1^2 + a_2^2} \Big)\, \mathbb{k} \cdot \nabla \times \mathbb{V}_o \qquad (4.5A)$$

in the interior of the region in question, and

$$\nabla\psi = \left(\frac{a_2^2}{a_1^2 + a_2^2}\right)\nabla\psi_o + \left(\frac{a_1^2}{a_1^2 + a_2^2}\right) V_o \times 1k \qquad (4.5B)$$

on its boundaries.

Equations (4.5) are, therefore, the analysis equations under the requirement of a minimum "E" defined by (4.1). It is easily demonstrated by the method of Section 2 that equations (4.5) are insensitive to wavelength; i.e., that, in this case, the final analysis is based on the observed stream function field and on the observed wind field in the same proportion (determined by the weighting factors) for all scales of motion.

Equations such as (4.5A) are known as "Poisson" equations and the Green's function for this type (again under the assumption of boundaries at infinity) is given in classical theory (c.f. Morse and Feshback, 1953) as

$$G = -2 \ln R \qquad (4.6)$$

Unlike the Green's function for analysis equation (1.9), this function does not approach zero as R increases indefinitely. An intuitive understanding of the reason for this difference between the Green's functions for the two analysis equations may be gained by noting that the first contains a term wherein the dependent variable appears undifferentiated whereas the second does not. Analysis equations (4.5) therefore specify the stream function only within an arbitrary constant. When the Green's function is applied over any finite area the value of the function at that range can be used to determine this constant.

If we assign a value of zero to a_2 and define the stream function as $g/f\ Z_o$ (with f considered constant), the difference between the "E's" specified in Section 1 and in this section disappear; so does the difference between the two analysis equations, and the boundary condition (4.5 B) corresponds to the choice of boundary conditions of the second kind in Section 1.

The problem of the additive constant in the height or in the stream function field may be met by any number of simple means such as by adopting the mean value of the observed height field as the mean value of heights in the final analyses. The use of this mean value will be acceptable to the extent that the error in height observations in the stratosphere is random.

If the analysis is performed in three dimensions the hydrostatic assumption which gives rise to the additional terms in analysis equation (1.6), also provides a means of determining the mean height value of the entire field.

Both choices of "E" discussed so far have involved two differences (squared), one for each of two observed variables. It is possible, however, to impose on an analysis the requirement that a minimum be achieved in the integral of a quantity involving more differences that there are observed variables. For some purposes it might be desirable to minimize a quantity which includes the difference between the vorticity implied by the analyzed stream function and that implied by an " observed " stream function. To accomplish this one might choose

$$E = a_1^2 \, (\nabla^2\psi - \nabla^2\psi_o)^2 + a_2^2 (\nabla\psi - \nabla\psi_o)^2 + a_3^2 (\psi - \psi_o)^2 \quad (4.6)$$

It can be shown that a minimum in the area integral of this "E" is attained if ψ satifies

$$\nabla^4\psi - \left(\frac{a_2}{a_1}\right)^2 \nabla^2\psi + \left(\frac{a_3}{a_1}\right)^2 \psi = \nabla^4\psi_o - \left(\frac{a_2}{a_1}\right)^2 \nabla^2\psi_o + \left(\frac{a_3}{a_1}\right)^2 \psi_o \quad (4.7)$$

where $\nabla^4 \equiv \nabla^2 \cdot \nabla^2 \equiv \dfrac{\partial^4}{\partial x^4} + 2\dfrac{\partial^4}{\partial x^2 \partial y^2} + \dfrac{\partial^4}{\partial y^4}$

The fact that this analysis equation is sensitive to wavelength leads to the possibility of incorporating into the end product three different stream functions where each has been determined from the observations on the basis of a relationship most appropriate for one of three ranges of wavelengths. As an example, the observed stream function in the first terms on the right hand side of equation (4.6) might be based on wind data only ($\nabla^2 \psi_o \equiv \nabla \times V_o$), that in the second term from heights through a balance equation and that in the third term from heights through the quasi-geostrophic approximation $\nabla^2 \psi_o \equiv g/f\,(\nabla^2 Z_o - \frac{1}{f} \nabla Z_o \cdot \nabla f)$.

SHEAR AND CURVATURE

Returning to the analysis equation (1.9) discussed in the first section

$$\nabla^2 Z - \left(\frac{\alpha_2}{\alpha_1} \frac{f}{g}\right)^2 Z = \frac{f}{g} (\nabla \times V_o) - \left(\frac{\alpha_2}{\alpha_1} \frac{f}{g}\right)^2 Z_o$$

we note once more that it is the vorticity of the observed wind, rather than the wind speed or direction, that influences the analysis of the height field Z and, implicitly, the analysis of the wind field (since the two fields were assumed to be geostrophically related). Vorticity, of course, may be due either to shear or to curvature in a flow pattern but nothing in the analysis equation (1.9) distinguishes between the two forms. As a consequence, the final analysis is subject to a certain ambiguity.

The results of a simple experiment illustrate this point. A fictitious (and unrealistically extreme) set of height and wind values were specified at points in a small (11 x 17) network. The given "data" was in geostrophic balance except at one row of points along which wind speeds were increased by a factor of 100. Equation (1.9) was solved numerically with boundary conditions of the first kind(heights held constant or "true" along the boundaries) but with α_2 set equal to zero i.e. no weight given to heights in the interior of the network.

Despite the obvious contradiction between boundary conditions and weighting factor, it was possible to get a "solution" to the analysis equation which simply set the Laplacian of heights equal to the curl of the wind field times f/g. Table 1 shows the initial winds (which were entirely "zonal " and constant along each row), the wind implied by the analysis along a column where the wind remained "zonal", the initial and the final shears. It is quite obvious that the analysis implied wind speeds which were outrageously incorrect at most points in this column but the implied wind shear (and vorticity) were correct to within the tolerance limits accepted in the computation. At the lateral boundaries, where the "jet" should have entered and left the network, the inconsistent boundary conditions turned the wind in the analysis to produce the "meridional" components shown in Table 1. Near these boundaries both curvature and shear components of vorticity were present but the total closely matched the vorticity of the initial "observed" wind which was due entirely to shear.

TABLE 1

Initial winds and analyzed winds along a column of points in a grid of "data" used with analysis equation (1.9) and the conflicting conditions and Z held constant on the boundary. Both initial and analyzed winds were "zonal" at all points in the column.

Grid Point	1	2	3	4	5	6	7	8	9	10	11
Initial Speed (m/sec)		.2	.4	.8	1.6	320.0	6.4	12.8	25.6	51.2	102.4
Analyzed Speed (m/sec)		-28.4	-28.8	-29.2	-29.2	295.2	-24.0	-16.8	-3.0	24.0	72.6
Initial Shear (m/sec/ y)	0	.2	.4	.8	318.4	-313.6	6.4	12.8	25.6	51.2	
Analyzed Shear	-.6	-.4	-.4	.2	324.2	-319.2	7.2	13.8	27.0	48.6	

TABLE 2

Analyzed "meridional" winds along two rows of points bounding the "jet" in Table 2. The values are symmetrical about Grid Point 9.

Grid Point	1	2	3	4	5	6	7	8	9	10	11
"North" Row Speeds (m/sec)		-104.6	-28.2	-9.6	-4.0	-1.8	-.8	-.4	0	0	+.4
"South" Row Speeds (m/sec)		95.0	28.2	9.4	3.8	1.6	1.0	.4	0	0	-.4

PART II - PRACTICAL CONSIDERATIONS AND A SAMPLE ANALYSIS

PREPARATION OF INITIAL DATA FIELDS

The "Sasaki" technique of analysis separates into two distinct operations the tasks of interpolating and interrelating the data. The discussion presented above has dealt with the second problem only and has assumed that the observed data had been defined at points in a regular grid. With respect to the first problem, the "Sasaki" technique involves all of the difficulties encountered in "conventional " objective analysis schemes and, in fact, exacerbates many of the difficulties if complete independence of the initial fields is to be maintained.

After a few test runs, with various methods of preparing the initial data fields, failed to show any obvious superiority of one over another , the standard procedure used in the N.W.P. Branch of the National Meteorological Center, (described by Cressman, 1959) was adopted for experimental analysis of real observations by Sasaki's technique. Treating winds and heights independently involved a modification to this standard procedure which had been used by Brown and Neilon (1961).

The first phase of the analysis then consists of repeated modifications of a "first guess" field, which is corrected in proportion to the difference between station observations and interpolated values of the latest "guess" at the same locations. In a succession of scans over the entire field, values at each point are modified according to a weighted sum of those differences which occur in progressively smaller areas around the point in question. Small discontinuities may be eliminated by the application of a smoothing operator after each scan. The smoothing undoubtedly alters the small scale features but this effect is believed to be relatively unimportant especially in analyses of stratospheric conditions since data over wide areas are used by the analysis equation in the second phase.

In the examples that will be shown later, the "first guess" fields were taken from subjective analyses of the previous day's observations rather than from forecast maps which are used in operational applications of the above method. The zonal and meridional components of the wind were analyzed separately. Components of the observed winds were provided to the machine from hand calculations.

NUMERICAL SOLUTION OF THE ANALYSIS EQUATION

There are well known methods (e.g. relaxation) of obtaining numerical solutions of elliptic second-order partial differential equations with Dirichlet boundary conditions. Comparatively little is known about the corresponding Neumann problem. Truncation error at the boundary which is non-existent for Dirichlet problems can be significant with Neumann conditions. In fact, the truncation error at the boundary may become sufficiently large in the latter case to prevent convergence to a numerical solution. This occurs mostly where the gradients along the boundary are large. Giese (1958) has published a mathematical discussion of the effect on the convergence of the Neumann problem which follows from a given approximation to a normal derivative.

The finite difference forms of the analysis equation and of the boundary conditions should have approximately the same truncation error. The truncation error of the usual five point approximation to the Laplacian is of the order of (Δ^2) where Δ is the grid interval. Giese showed that if a non-centered difference were used to approximate a derivative on the boundary, the error would be of the order of (Δ); if a centered difference were used, the error would of the order ($\Delta^2 \log \Delta$) which is approximately (Δ^2).

The finite difference approximation to the analysis equation (1.9) was taken to be

$$Z_{i+1,j} + Z_{i-1,j} + Z_{i,j+1} + Z_{i,j-1} - (4 + W_{i,j}) Z_{i,j} =$$

$$= \frac{\Delta f_{i,j}}{2 m_{i,j} g} \left((v_o)_{i+1,j} - (v_o)_{i-1,j} - (u_o)_{i,j+1} + (u_o)_{i,j-1} \right) - W_{i,j} (Z_o)_{i,j}$$

where $A_{i,j}$ is the value of A at $x = i\Delta$, $y = j\Delta$

m is the map scale factor and $W_{i,j} \equiv \left(\frac{a_2}{a_1} \frac{f \Delta}{g \ m} \right)^2_{i,j}$

For Dirichlet case $Z_{i,j} = (Z_o)_{i,j}$ was used as the boundary condition and for the Neumann case

$$(Z_{i,j+1} - Z_{i,j-1}) = -2\Delta f_{i,j} (u_o)_{i,j} / m_{i,j}$$

$$(Z_{i+1,j} - Z_{i-1,j}) = 2 \Delta f_{i,j} (v_o)_{i,j} / m_{i,j}$$

were the boundary conditions along the horizontal and lateral boundaries respectively.

Since Neumann boundary problems have a unique solution within an additive constant only, the mean height of the pressure surface at observation points was specified as the mean height of the entire analyzed surface.

The accelerated Leibmann method of relaxation was used to solve the above system of equations. Proof of the numerical convergence of Neumann problems has generally been limited to the trivial case of zero mean normal derivative on the boundary and zero mean Laplacian in the interior of a region. These hypothetical conditions are not usually present in the case of analysis of atmospheric fields except, perhaps, if the analysis area is hemispheric. Numerical convergence of the analysis equation (1.9) with Neumann conditions is therefore dependent upon the size of the analysis area, the mean vorticity within the area (or, equivalently, the mean circulation around the area) and the truncation errors in the finite difference approximations. The criterion for convergence that was used in the examples to be shown was $\pm$ 50 m. Efforts to reduce this criterion delayed convergence beyond reasonable time limits and in some examples resulted in no convergence at all.

It follows from Stoke's theorem $\oint V.\ dl = \iint \nabla x\ \ V.dS$ that Neumann boundary conditions specify the mean relative vorticity in an analysis. Some attempts were made to use this as an integral constraint on the numerical calculations but it did not appear to improve the results of the analysis.

RESULTS OF SOME ANALYSES

Two pairs of analyses of conditions over North America and vicinity at 50 mb on January 2, 1959 and July 2, 1959 will illustrate results obtained with the analysis equation (1.9) and the two types of boundary conditions.

The data were obtained as part of a file prepared by the Travelers Research Center for the 433L Project and had been corrected for gross errors and radiation effects. For the January case there was a total of 75 reports at 50 mb over the area of interest but only 27 of these reports included wind observations. Roughly the same proportion between the number of wind and height reports existed in the July data.

All analyses were performed both with a zero weight given to the observed height field and again with a small weight ($\alpha_2 / \alpha_1 \approx 1/15$) given to observed heights. The differences between the two sets were quite small and affected only the longest wavelength represented in the analysis area as the foregoing theory had predicted. Only those analyses made with α_2 equal to zero are presented below.

Figure 3 shows the analyzed height fields for January 2, 1959. (The contours were produced by an adoption of an Air Weather Service Program. The somewhat irregular "frame" into which the contours appear to merge was produced by this contouring program and is not due to the analysis procedure.) The closed circulation near the North Pole in the analysis performed with Dirichlet boundary conditions is fictitious -- no justification for such a system appears in the original data and subjective analyses of the same data (e.g. Teweles, 1960) do not indicate a closed circulation in this region. The analysis that employed Neumann conditions is much more satisfactory in this respect. The difference between the two January analyses is shown in Figure 4. It is apparent from this difference that the boundary effects were largest along boundary segments where strong gradients existed independently of the direction of the flow with respect to the boundary. Since the analysis equation (1.9) was derived on the simplifying (but unnecessary) assumption that the Coriolis parameter was constant, a further analysis of the January data was made with this same condition ($f = 2\ \Omega \sin 60^{o}$) applied to the finite difference form of equation (1.9) given in the previous section. The result also appears in Figure 4. The weakened gradient that appears at high latitudes as a result of this approximation is not realistic and the simplification permitted no significant saving of machine time.

The analysis of the June data are shown in Figure 5. Since height gradients were uniformly weak at this time (Note that the contour interval in this figure is only half of that in Figure 3.) no large differences were produced by the different boundary conditions. The January analysis is in substantial agreement with subjective analyses (Teweles, 1960).

REFERENCES

Brown, J.A. and J.R. Neilon : ' Case studies of numerical wind analyses', Mon. Wea. Rev., 89, 83 - 90, 1961.

Cressman, G.P. : ' An operational objective analysis system', Mon. Wea. Rev., 87, 367 -374, 1959.

Giese, J.H. : 'On the truncation error in a numerical solution of the Neumann problem for a rectangle ', J. Math. Phys., 37, 169 - 177 , 1958.

Hovermale, J. B. : ' A comparison of data accuracy in the troposphere and in the stratosphere ', The Penna. State Univ. , Dept. of Met. Sci. Rpt. No. 2 1962.

Morse, P.M. and H. Feshback : ' Methods of theoretical physics - part I ', 277- 280 and 791 - 890 , McGraw-Hill, 1953.

Sasaki, Y. : ' On objective analysis based on the variational method', J. Meteor. Soc., Japan, 36, 77 - 88 1958.

U.S. Weather Bureau : ' Daily 100-mb and 50 mb and three times monthly 30-mb synoptic weather maps', Washington, D.C ., 1960.

Figure 3. The figures show the analyses for cases where no weight was given for heights for the two different conditions on January 2,1959 at 50 mb using a 200 m contour interval.

Figure 4. The left figure shows a difference contour map of Figures 3a and 3b. The contour interval is 200 m. The right hand figure shows the same Neumann case as Figure 3 except f is a constant.

Figure 5. The figures show the analyses for cases where no weight was given to heights for the two boundary conditions on July 2,1958 at 50 mb using a 100 m contour interval.

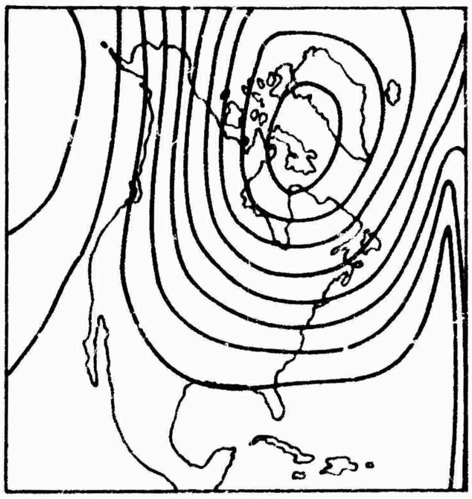

3(a) DIRICHLET

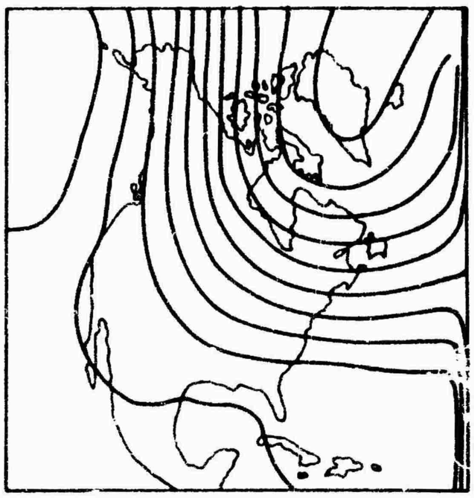

3(b) NEUMANN

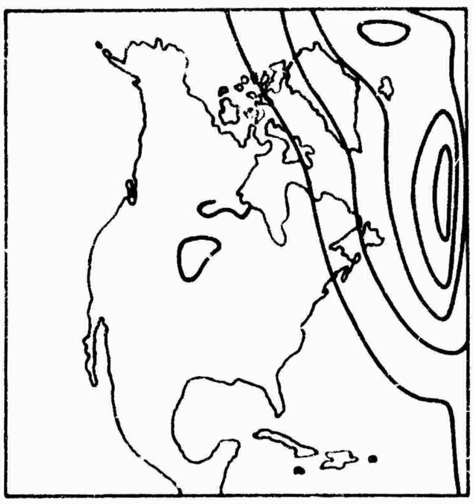

4(a) DIFFERENCE BETWEEN 3a & 3b

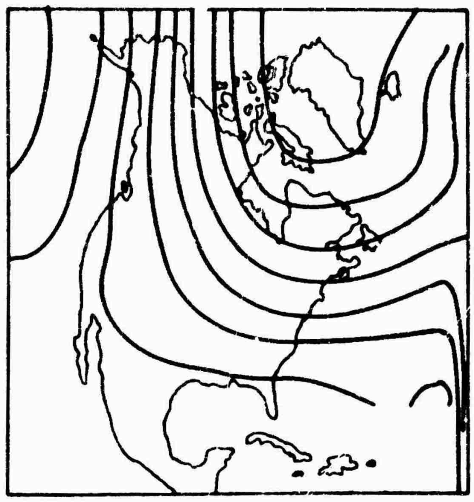

4(b) NEUMANN

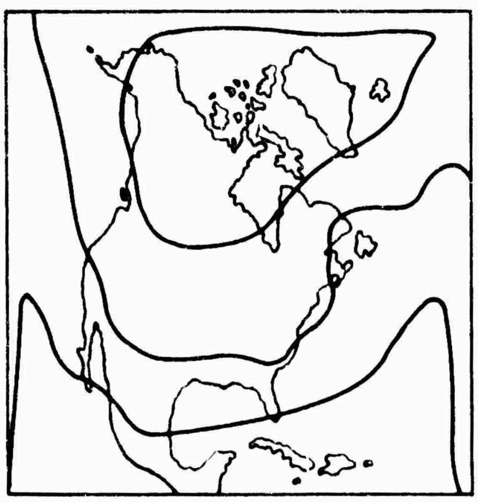

5(a) DIRICHLET

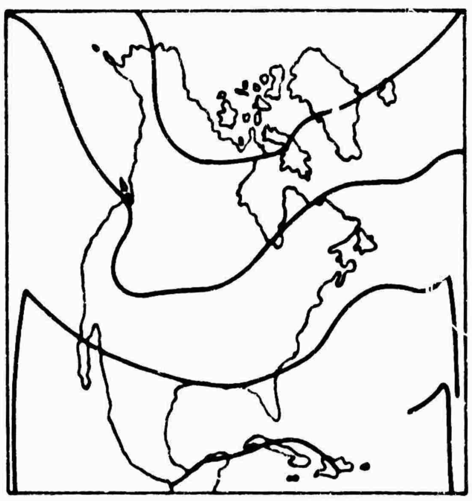

5(b) NEUMANN

TWENTY-SIX-MONTH OSCILLATIONS IN GEOPHYSICAL PHENOMENA

W. L. Godson

ANCIENT HISTORY

On August 27, 1883, the Krakatoa volcano erupted (near 6° S) and sent debris well into the stratosphere, which remained visible while it circled the globe at least three times, from east to west. Stratospheric winds in the equatorial region were presumed predominantly easterly thereafter (Krakatoa easterlies). On October 17, 1908, at Dar-es-Salaam in central east Africa, Von Berson obtained a pibal ascent showing westerlies to 20 km and easterlies immediately above. Subsequent pibals in Batavia (Van Bemmelen) from 1911 - 1913, reaching high levels, also showed a limited band (in the vertical, and in time) of such westerlies (Berson westerlies). Palmer in 1954 assigned them to a narrow belt near the equator, in the lower stratosphere, with a variable upper limit.

MODERN HISTORY

By 1959 it had become apparent that Berson westerlies underwent periodic fluctuations and by 1960 it was realized that "relative" westerlies also had this behaviour and propagated in the vertical toward the tropopause, being replaced by "relative" easterlies aloft, which also subsequently descended in time. A period of about twenty six months was observed at any stratospheric level near the equator, relative to the periodic fluctuation of mean zonal velocities about seasonal means.

A number of papers have been published since 1960 (principally by Ebdon and by Reed, with various co-authors) and these have suggested the following behaviour for this atmospheric oscillation :

(a) Equatorial stratospheric zonal winds exhibit a relatively large oscillation of about a twenty six month period, and have apparently been doing so for at least the last fifty years. Near the equator the mean winds are light, so that westerlies and easterlies alternate; further from the equator mean winds are stronger from the east and only relative westerlies are observed; at even higher latitudes the seasonal variations (westerlies in winter and easterlies in summer) must be subtracted before the oscillation is apparent.

(b) The amplitude is a maximum at the equator (50 kt at 30 mb, for example) and decreases rapidly with latitude, becoming insignificant near 30 N and S.

(c) The amplitude is very small near the tropopause and increases upwards at least to 30 mb and possibly to 10 mb or even higher. Zonal wind oscillations in the equatorial troposphere are apparently insignificant.

(d) Poleward of 30^{o}, the amplitude appears to increase again and may still be present in polar latitudes. The data suggest a secondary maximum near 40-50 N, but with an amplitude decrease upwards from 100 to 50 mb.

(e) Amplitudes appear to have decreased slowly over the last eight years or so.

(f) The phase of the zonal velocity oscillation in the tropical stratosphere is virtually independent of longitude, and is approximately independent of north or south latitude in the equatorial belt. Poleward of about 20^{o} the maximum relative westerlies are observed to occur earlier than near the equator and this effect is very apparent by 30^{o}, and especially so at the secondary maximum near 40 - 50 N.

(g) The phase is definitely earlier with increasing height, with a downward phase velocity of about 1 km per month.

(h) No evident wave is visible for the meridional winds in troposphere or stratosphere in tropical regions.

(i) Since accelerations are trivial, winds are geostrophic to within a few kilometers of the equator; as a result, temperature waves can be detected in the tropical stratosphere. Their variations of amplitude and phase with latitude and height are rather complex. Within ten degrees of the equator, the temperature maximum leads the west wind maximum by about three months; further north the 100-mb temperature comes into phase with the west wind but at 50 and 25 mb the temperature maximum becomes, by 30 N, almost 180° out of phase with the west wind maximum. Temperature amplitudes increase with height, except near the equator.

(j) Approximately twenty-six month waves have been detected in many areas in surface weather phenomena (temperature, pressure, precipitation) and seem to have been the most obvious and coherent periodic phenomena over many centuries. It was first demonstrated by Clayton 1884, for U.S. temperatures, and may be related to Sir Gilbert Walker's "southern oscillation".

(k) The twenty-six month period (somewhat variable from parameter to parameter, station to station and with length of record, varying between twenty-four - twenty-eight months in length) is not apparent on solar parameters but has been suggested by spectra of geomagnetic parameters (lower harmonics of the eleven year solar cycle - twenty-six months would be the fifth - do, however, appear on solar parameter spectra).

(l) No rational explanation has so far been published.

BASIC PROBLEMS

The fundamental problem is of course the full explanation of the phenomenon. Such an explanation could, quite reasonably, have ramifications far beyond the equatorial stratosphere particularly if, as seems likely, large-scale atmospheric feedback mechanisms are involved. It is therefore important that one be in a position to define the oscillation, and its temporal variabilities (if significant) as a function of the various dynamic and thermodynamic parameters, latitude (possibly even longitude in middle latitudes) and pressure, even for parameters and/or for levels for which amplitudes are weak.

The above requirement implies the need for a sensitive form of harmonic analysis (or spectral analysis). Since the evidence points to a relatively coherent wave in time, one is justified in preferring the more-sensitive alternative-harmonic analysis, the main problem being to reduce the noise level without averaging over such a long period (seldom available, at any rate) that real fluctuations in period reduce the signal level. The band pass is not infinitely narrow and both pure noise and other periodicities affect a given response in a largely unpredictable manner. One important consideration is the necessity to take care of long period trends in a sophisticated manner to avoid unwanted contamination of signal levels. If amplitudes and periods vary in time, any clear resolution by harmonic analysis becomes difficult. Both these possibilities seem very likely, since no "balance wheel" is apparent on physical grounds, and since fluctuations on other time scales are bound to produce non-linear interactions, affecting both period and amplitude.

For a full theoretical explanation, one must specify the basic (or mean) properties of the atmosphere to great heights, especially over equatorial areas in the northern and southern hemispheres; it is highly doubtful if adequate data are at present available.

The question of a possible solar role is still very much an open one but if we admit this as a possibility then we cannot avoid looking at other smaller harmonics of the eleven year sunspot cycle, particularly since we know that certain atmospheric parameters, especially in tropical regions, do appear to be related to sunspots (by the work of Willett, Wexler and others), and since some low order harmonics do appear on power spectra of solar parameters. Even if the sun is not involved, the clear demonstration that a period of the order of twenty-six months does exist in the atmosphere suggests that this may well be true for other periods as well, perhaps in other parameters and/or other regions. Even if the variance explained by such periods is not large, the physical explanation of all such periods should lead to an enhanced understanding of the general circulation on various extended scales of time and space. Finally, one could well imagine that a combination of persistence and a few dominant waves might account for an appreciable fraction of the predictable variance, even if not of the observed variance.

HARMONIC ANALYSIS

The classical technique in this field is Fourier analysis in which a sum of sine and cosine waves with period of T, T/2 , T/3 ... (T = period of record) are fitted, indirectly by least squares to a sequential array of data. This does not necessarily produce the least bias estimate for an arbitrary wave of period $\approx$ (τ = $T\text{-}a/_n$, where a is the minimum number of pieces of data that must be discarded, n is a positive integer). The Fourier filter has moderate response in side lobes adjacent to the main pass band and a finite response to a linear trend. The latter can be corrected by removing a linear (or other) trend by least squares in advance, and this should always be done. When the period is short relative to the periods of interest some discontinuity is introduced as "n" changes by integral decrements. On the other hand, separate but not independent estimates of amplitude and phase are available for period increments equal to the data interval.

An alternative technique can be developed based on a procedure suggested by Labrouste and Labrouste. Essentially the procedure is to divide the data up into half-waves of a desired period and average these, reversing the sign for each even half-wave. At the same time a simple numerical correction for trend can be introduced to minimize the effect of long-period changes. Subsequently the mean half wave is folded over in time and smoothed by two term-averaging operations (to remove odd harmonics of T ; even harmonics only are removed by the initial wave-averaging). Amplitude and phase follow from the final wave, with correction for the smoothing performed . This technique gives a slightly broader half-width than the Fourier technique, but compensates by reason of a reduced response away from the main band and by using an odd number of half-waves (i.e. , more data) one-half of the time. Thus the discontinuity on changing n (by 0.5 , in this case) is reduced, but estimates are only available for period increments of twice the data interval. On the other hand, this technique is very suitable for hand calculations without desk computers, since virtually all operations can be performed mentally if one uses departures from means, which are a great advantage in any case to remove annual periods in advance. Nearby periods always produce contamination for restricted data records, and their successive removal, once they have been proven real, will invariably improve the remaining spectrum.

EQUATORIAL STRATOSPHERIC OSCILLATIONS (data provided by U.S.N. Weather Research Facility and by Ebdon, U.K. Meteorological Office).

(a) 50-mb U at Canton I. (2.8 S), Balboa (9.0N) and San Juan (18.5 N). - The amplitude versus period plots show the major wave to have a twenty-six month period, with an amplitude of about 30 kt near the equator.

(b) 30-mb U at three stations as in (a). - The maximum amplitude is still for a twenty-six month period, and reaches about 45 kt near the equator. As at 50 mb , secondary peaks are almost completely "submerged ".

(c) 50-mb V at same three stations. - Balboa clearly shows a twenty-seven-month wave (10% of amplitude of U-wave); the San Juan maximum is only 3% of that of the U-wave and for Canton I. it is undiscernible ($<$ 0.3% of U-amplitude). At Canton I. a peak at thirty-two months is evident, corresponding to a secondary peak for U, but the other two stations do not show this.

(d) 30-mb V at same three stations. - Waves with a thirty-two to thirty-four month period appear to interfere with the twenty-six-month wave, giving an apparent broad peak for intermediate periods. At twenty-six months the amplitudes are 8% relative to U at Balboa, 5% at San Juan and 2.5% at Canton I.

(e) Variation of amplitude and phase with latitude for 50-mb U and 30-mb U. - The two stations at about 9 N are over 110 degrees of longitude apart, yet differ in phase by only three degrees for the average of 30 and 50 mb (about one week in time.) The phase shifts from 30 to 50 mb indicate that wave phase is propagated downwards at an approximately constant speed at all latitudes of 0.9 km/month. The variation of phase with latitude at each level suggests there is little if any phase shift from the equator to about 15N, but earlier maxima farther north. Using weighted means to smooth the data, the phase is about 12.5° earlier at 18.5N than at the equator (i.e., about four weeks earlier). Wave data at 22N, although noisy and of weak amplitude, suggest a phase shift of 29° or nine weeks earlier than at the equatc . The amplitude ratio at 30 mb relative to 50 mb is about 1.43, with a suggestion that it may be increasing at the higher latitudes (beyond 20N).

(f) Variation of amplitude and phase with latitude for 30-mb V and 50-mb V. - The data for meridional wind components are very noisy but the picture is clarified when stations are averaged in groups (of 4). Then we find that the ratio of amplitudes

(V_{30}/V_{50}) increases from 1.2 at 9 N to 2.2 at 18.5 N (for U_{30}/U_{50} the increase is from 1.3 to 1.6). U/V has an average value of about 30 but is highly variable. The downward phase velocity for V at 9 N and 14 N is almost exactly one-half of that for U (i.e. , about 0.45 km/month), but at 18.5 °N it is much faster (2.4 km/month, although the data are more doubtful here).

At 30 and at 50 mb, U and V waves are roughly out of phase; in other words, at these levels maximum westerlies approximately coincide with maximum northerlies, and easterlies with southerlies , and there is southward transport of westerly momentum from the equator to at least 18.5 N. The phase shift is slightly variable with latitude and height, apparently increasing with both except at 18.5 N at 30 mb. At 14N , the V-wave occurs roughly six months earlier than at the equator. Amplitudes appear to have a maximum away from the equator at 30 and 50 mb, in excess of 1 kt in both cases, but to decrease from 9 N to higher latitudes.

(g) Variation of amplitudes and phases with pressure at Canton I. - For the layer from 30 to 80 mb, the average vertical phase velocities (downward) are: for U, 0.81 km/month; for V, 0.39 km/month; for T, 0.48 km/month. The amplitude for U decreases from 45 kt at 30 mb to 13 kt at 80 mb (and is less than 3 kt at 200 and 500 mb) ; the amplitude for V decreases from 1.2 kt at 30 mb to near zero at 50 mb, then increases to 0.7 kt at 80 mb; the amplitude for T increases slightly from 1.2°C at 30 mb to 2.2°C at 80 mb. There is a suggestion that the waves in zonal (W) and meridional (S) velocity and in temperature might come into phase at or near the tropopause level; at 30 mb, on the other hand, the S-wind maximum is 145° in advance of the W-wind maximum, and the T maximum 96° (10.5 and 7 months , respectively). Thus, westerly momentum is transported southward from 30 to 50 mb and northward from 50 to 80 mb, whereas sensible heat is transported northwards for the entire layer from 30 to 80 mb (10^{13} cal/sec).

(h) Variation of amplitudes and phases with pressure at San Juan. - The average downward phase velocities here are 1.04 km/month for U (30 to 80 mb) and 0.42 km/month for T (40-60 mb). The data for V are too noisy to deduce such values, or even to be sure of relative amplitude variations in the vertical. For U, the amplitude decreases from 8 kt at 30 mb to 3 kt at 100 mb, and then slowly to 2 kt at 500 mb. For V, the data suggest a decrease from 0.4 kt at 30 mb to 50 mb, and an increase from 50 to 200 mb (in excess of 1 kt), becoming quite insignificant (0.2kt) at 500 mb. For temperature, the amplitude increases slightly from 40 to 60 mb, averaging slightly over 0.5°C; at 200 and 500 mb the values are much smaller ($<$ 0.2°C). The U-waves at San Juan occur slightly earlier than at Canton I., by 0.9 month at 30 mb, 1.0 month at 40 mb, 1.2 months at 50 mb, 1.7 months at 60 mb and 2.5 months at 80 mb. The temperature waves are earlier by about 13 months more than the above shifts (i.e., they are essentially out of phase with those at the equator).

(i) Amplitude versus period at San Juan, 60 mb. - The plots for U and T show good peaks near twenty-six months, with complex wings suggestive of a wave near thirty-two and thirty four months. Even the V-plot shows the twenty six month peak, and all three curves are in agreement on a peak near fifty-two months.

Despite the small amplitudes at 18.5 N, there seems no longer any reason to doubt the presence of twenty-six month waves in the meridional velocity in the tropical stratosphere. Particularly in the zone between the equator and 10°, with V - amplitudes around 1 kt, the twenty-six month wave could be effective in certain transport phenomena, especially if the linked wave in vertical velocity operated to transport a given property with convergence in the same (or complementary) manner. Since $dp/_{dt}$ will depend on $\partial v/\partial y$, it is interesting to note that at both 30 and 50 mb the latitudinal change of the twenty-six month V wave from the equator to 18.5 N is such that the phase change is small when the amplitude change is relatively rapid and vice versa, so that $\partial v/\partial y$ always has moderately large values, but a rather complex structure for $dp/_{dt}$ would be expected. Horizontal heat transport northward converges at a rate equivalent to about $0.05^{\circ}C$/day from 30 to 80 mb between 0 and 18.5 N.

TROPOSPHERIC OSCILLATIONS, AND STRATOSPHERIC OSCILLATIONS IN MIDDLE AND HIGH LATITUDES.

(a) Amplitude versus period at San Juan, 200 mb - The U wave is still evident at 200 mb for a twenty-six month period, and a weak temperature wave and possibly a V-wave as well. A relatively strong T-wave shows for a period of forty months with a fair U wave, although neither appeared at stratospheric levels. On the other hand, the secondary maxima for thirty-two to thirty-four months seen in the stratosphere do not appear in the troposphere.

(b) Amplitude versus period at San Juan, 500 mb - At this level a relatively strong U-wave appears at a 28-month period with relatively weaker response on the V and T fields. Once again, forty month waves appear for U and T, although not for V (as at 200 mb). We may conclude that tropospheric waves of approximately a period of twenty-six months do occur in the troposphere at tropical latitudes, although they appear weak on the wind field near the equator, but somewhat stronger on the temperature field, especially in the upper troposphere, consistent with an amplitude decrease upward from 80 mb.

(c) Amplitude versus period for msl and 700-mb zonal indices (20 - 35 N). - Very clear peaks appear (for an 18 - year record) at about twenty-six months, with amplitudes of 0.7 kt at 700 mb and 0.45 kt at msl for mean zonal velocity, even after averaging over 15 degrees of latitude and 180 degrees of longitude in a belt where appreciable variations in amplitude and phase might be expected. Other peaks appear at 22, 32, 40 -44, 56, 68 and 84 months, on both records, and these persist when slightly different record lengths are chosen. These curves verify the existence of the twenty-six month oscillation in the troposphere, over a latitude belt where the stratospheric wave is rather weak,

(d) Global distribution of amplitude of twenty-six-month wave in 500-mb temperature. - The amplitude is certainly a function of longitude as well as of latitude. The network was inadequate to define real patterns except over North America but the main features are probably real. There is no apparent symmetry between the northern and southern hemispheres, and undoubtedly geography is involved (oceans and topography). Insufficient data are available to define the dominant scales of the systems but it appears that small hemispheric wave numbers are involved. The amplitude exceeds 1.0°C over northern Quebec, in the vicinity of a permanent 500-mb trough.

(e) Global distribution of phase of twenty-six-month wave in 500-mb temperatures. - Interpretation of such data is difficult due to the circular nature of phase angle (gradient ambiguity) and sparsity of stations analysed. There are marked variations with longitude, however, somewhat greater in high latitudes than in tropical latitudes.

(f) Global distribution of amplitude of twenty-six-month wave in 200-mb temperatures. - In temperate latitudes this level is in the lower stratosphere and the wave continues to show higher amplitudes outside of tropical regions, although over central Africa the amplitude is of the order of 0.5°C. Over eastern Canada the maximum (in excess of 1.0°C) has shifted to the north and a second maximum is suggested over northern Scandinavia, with a marked minimum over Kamchatka (as at 500 mb).

(g) Global distribution of phase of twenty-six-month wave in the 200-mb temperatures. - Longitudinal gradients of phase are relatively small at high northern latitudes with much longer north-south gradients near the mean 200-mb tropopause, corresponding to an 180° phase shift from troposphere to stratosphere. In the tropics, also, east-west gradients of phase angle are relatively small.

Very few analyses were performed with 100-mb temperature but over Canada the maximum, still in excess of 1.0°C, shifted further north again into the Arctic archipelago, with a phase advancement of about one month relative to 200 mb.

(h) Temperature amplitude versus period for Nitchequon, 700 to 200 mb. - The dominant wave here is of 26-27 months period, and is very strong in the troposphere, of minimum amplitude at 300 mb and stronger again at 200 mb. There is some evidence for a 36 - 40 month wave in the stratosphere and a roughly 68-month wave in the troposphere.

(i) Temperature amplitude versus period for Eureka, 700 to 100 mb. - Here the twenty-six month wave is weak in the troposphere but increases in amplitude with height up to 100 mb. There is a suggestion of other waves with vertical coherence, and periods of the order of 32, 36 and 68 months.

(j) Amplitude and phase variations in the vertical for twenty-six-month wave. - At Nitchequon and Churchill a phase shift of 180° occurs near the tropopause. 100-mb waves seem to be about one and a half months earlier than those at 200 mb.

(k) Amplitude-period relations for long record stations in eastern

Canada at 500 mb. - The predominant characteristic here is the twenty-six month wave, with lesser peaks at 22 and 32 months, and possibly in the vicinity of 40 months.

(l) Amplitude-period relations for ozone at three Indian stations (34, 23 and 10 N). - These suggest a 24-26 month period becoming weak at 34 N.

(m) Amplitude-period relations at New Delhi (29N) (ozone and 500 -mb and 200-mb T).

The twenty-six month peak on ozone does not appear related to tropospheric phenomena, although some correspondence appears for other peaks (36 - 40 and 18 months). For a longer period of record, the 200-mb temperature did show a minor peak at twenty-six months.

(n) Amplitude - period relations at Brisbane (28 S) (ozone and 500-mb and 200-mb T). Maxima near twenty-six months show up here on temperature and on ozone, the latter with greater amplitude than at New Delhi at the same latitude in the northern hemisphere. The secondary maximum for ozone near 32 months also shows on the temperature data.

(o) Amplitude - period relations at Melbourne (38 S) (curves as above). All three curves are very similar with marked waves of 24 - 26 month period, suggesting that the Reed-Normand mechanism may be in operation for extremely long as well as short periods - although this is not borne out by a study of phase angles.

(p) Amplitude and phase for total ozone at 24 and 26-month periods. - Ozone phases do not agree well with those of 500 and 200 -mb temperatures, even when amplitudes all seem significant. While this may be due to relatively strong vertical - motion waves (not in phase with temperatures), it is significant to note that the 100 - mb temperature wave at Hobart (43 S) has exactly the same phase as ozone at both Melbourne and Brisbane (38 and 28 S), suggesting the importance of sub-Antarctic middle stratosphere events on longer period variations. The two hemispheres are about 100 - 120° out of phase, with the equatorial station (Kodaikanal) showing an intermediate behaviour. Presumably the ozone waves where strongest (Australia, in this case) are related to stratospheric waves of an extra-equatorial nature. One might therefore expect significant waves in at least certain regions of the stratosphere of middle and high latitudes for meridional and vertical velocities. 26 - 27 month waves in precipitation, observed at many stations at all latitudes , suggest these V and dp/dt waves may also be significant in the troposphere.

HARMONIC ANALYSES OF SOLAR AND RELATED PARAMETERS.

(a) Sunspot number -amplitude versus period for three data sets . - The period 1948-61 seems to have been the most active re sunspots of the three periods shown here, with this period and the 1922 - 38 period suggesting a peak near 27 months. If one assumes the many peaks shown are real, one would conclude that the periods for a given harmonic are variable in time - and this is certainly true for the roughly eleven-year solar cycle itself.

(b) Magnetic planetary amplitude figure - amplitude versus period for three sets . - Only the 1948 - 61 period suggests a wave of about twenty seven months but it is even weaker than for sunspot number. A number of different periods of data for various solar and geomagnetic parameters have been examined in this way and a semi-normalized frequency of peaks (i.e., of maxima) has been claculated. These show a maximum number of peaks at about 25 and 34 months, with lesser maxima at 40, 54 and 64 months, corresponding roughly to harmonics of a fundamental of 124 months.

(c) Frequency of harmonic-analysis peaks for miscellaneous data. - As in the data quoted above, numbers of maxima have been semi-normalized but not corrected for variations in record length. A number of equatorial sets are included which partly explain the major modal peak at 26 months; however, many other data sets were used, of tropospheric and stratospheric temperatures and oceanic cloudiness and water temperatures, etc. The other peaks suggested, which appear on virtually all sub-sets of the several hundred series analysed, correspond to 36, 54, and 64 months - a rather similar set to the sub-set for solar and geomagnetic parameters. We may conclude that the solar question is still an open one, and that a good physical explanation for atmospheric waves of these periods will be required, which should include both dynamic and diabatic considerations.

ATMOSPHERIC TIDES

B. Haurwitz

Of the oscillations referred to as atmospheric tides the most important are those with a twelve-hourly period (S_2), a twenty four - hourly period (S_1), and with a period of twelve lunar hours (L_2). At the earth's surface these oscillations are most readily found in the air pressure, although statistical procedures are required to separate them from the meteorological noise. S_2 is distributed most regularly and has the largest amplitude, about 1 mb in tropical regions, S_1 is about half as large and much more irregularly distributed. The lunar oscillation, L_2 has an amplitude less than one-tenth of S_2. It is to be expected on theoretical grounds that these oscillations increase with elevation. Such as increase has actually been observed at levels between 80 and 100 km where drifts of ionized meteor trails provide means of determining winds sufficiently frequently so that the periodic variations can be obtained. The tidal oscillations are here two orders of magnitude larger that at the ground. Thus tne atmosphere at these levels is subjected to periodic variations whose relative magnitudes are comparable to changes occurring during cyclone passages in the low atmosphere.

The lunar gravitational tidal force is more than two times larger than that of the sun. Nevertheless S_2 is much larger than L_2. To expiain this discrepancy it was already suggested by Laplace that S_2 is largely produced by the thermal action of the sun. Since the diurnal temperature oscillation has a larger amplitude (3 times or more) than the semidiurnal temperature oscillation Kelvin suggested that the atmosphere may have a free period in close proximity to 12 hours, in which case S_2 would be greatly magnified by resonance. Theoretical studies have shown that this "resonance theory" requires a much warmer stratopause than does exis so that actually the resonance magnification is only about three-fold rather than 60 times or more, as postulated by the resonance theory. The surface pressure amplitude for S_2 is about twice of that for S_1, while the surface temperature amplitude for S_2 is about one third of that for S_1. Hence a six-fold magnification would account for the observations while only a three-fold magnification occurs according to the theory. On the other hand, it appears from theoretical considerations that a thermally caused S_1 would be suppressed in the atmosphere, thus removing the remaining discrepancy in the relative magnitudes of S_1 and S_2.

The heating causing these oscillations is only in part due to the daily heating of the lowest atmosphere by turbulent and radiative transfer upwards from the earth's surface. Much of it is due to direct absorption of solar radiation which extends throughout the whole atmosphere. If there are regions such as the ozonosphere where the temperature variations are particularly large S_2 should show a nodal surface below this region. But the observations of S_2 obtained so far above the earth's surface do not yet allow a decision whether or not such a node exists.

INTERNAL ATMOSPHERIC GRAVITY WAVES

C. O. Hines

Internal atmospheric gravity waves are the low-frequency equivalents of ordinary acoustic waves, which they supplant at periods exceeding the Brunt-Vaisalla period of the atmosphere. Their characteristics are quite different from those of sound waves, as a result of the anisotropic influence of gravity. They are, for example, virtually shear waves - parcels of the atmosphere oscillate in a direction nearly perpendicular to the direction of phase propagation - and , in most modes of interest, it is the direction of propagation rather than the wavelength that is determined by the frequency. They share with sound waves the property of amplifying as the height is increased, the amplification being a consequence of the decrease of gas density and a requirement to maintain energy flux more or less constant.

The amplification feature results in these waves becoming strong oscillations in the upper atmosphere, at heights of 80 km and above, say; they lead to winds of 30 m/s and more, associated temperature fluctuations (due to adiabatic compression) of 20°K and more, and pressure and density fluctuations of several percent. They are revealed by vertical (rocket -borne) soundings of the temperature, by the distortion of long-enduring meteor trails and rocket-released vapour trails, and by perturbations produced in the distribution of ionization (culminating, in extreme cases, with the production of a "sporadic E layer"). Waves observed in noctilucent clouds may also be of this type, though the relevant quantitative data in this case are too meager to judge.

The waves are subject to dissipation through the effects of viscosity and thermal conduction. As a result, more and more of the wave spectrum is damped out as the wave energy progresses upwards. In the end, at levels of 200-300 km, only a relatively confined spectrum remains and the noise-like appearance of the wind systems gives way to quasi-sinusoidal oscillations in "travelling ionospheric disturbances".

Refraction and reflection occur in the mesosphere, and can result in a ducting of some internal gravity wave modes below the mesopause. The energy in these modes can be carried to great distances without severe attenuation, while a small leakage of energy into the regions above can still lead to large-amplitude oscillations at much greater heights. Here again, the travelling inonospheric disturbances appear to be a manifestation of the process at the higher levels.

The sources of the wave energy lie primarily in and below the mesosphere, in various weather systems, jet streams, instabilities, and irregular flows over surface features: the specific origins have yet to be determined.

REFERENCES:

Hines, C.O. Can. J. Phys. 38, p. 1441, 1961.

TURBULENCE IN THE UPPER ATMOSPHERE

C. O. Hines

Long-enduring meteor trails appear to expand at rates too fast to be explained by molecular diffusion alone, as do rocket-released vapour trails at heights below 100-110 km. This behaviour is attributed to turbulent diffusion, and there is some support for the belief that the turbulence in question represents the ambient turbulence of the atmosphere rather than some transient turbulence generated with the formation of the trail. Estimates of a turbulent dissipation at a rate of 10^{-1} or 10^{-2} watts/kg are currently made. The molecular kinematic viscosity is of the order $10\ m^2/s$ at 95 km, from which the smallest scales of the turbulence spectrum may be inferred to be of the order 15 meters and 20 seconds. The largest spacial scales as seen visually are about 500 m, and associated with these are time scales of about 300 s. These latter values combine to yield an eddy kinematic viscosity of about $100\ m^2/s$.

The turbulence appears to be generated as a consequence of shear, the atmosphere being statically stable. The Richardson criterion for the establishment of turbulence is not satisfied, however, and some explanation must be found . Two possibilities emerge if it is accepted that the shearing winds are due to internal atmospheric gravity waves, for it may then be inferred that (a) the smaller-scale shears, which are the most effective in the production of turbulence, are oblique shears in oblique winds - not vertical shears in horizontal winds - and a criterion less stringent that Richardson's may then apply ; (b) the density and temperature fluctuations within the shearing system are such as to decrease the (quasi) static stability of the atmosphere over half-wavelength height intervals and may even reduce the stability to the vanishing point.

The termination of turbulence near 105 km appears to be related to the removal of the small-scale wind shears, which in turn is caused by the dissipation of the internal gravity wave energy. (The energy lost by the gravity waves to the turbulence may be estimated, and it equals the rate at which the turbulence loses energy to the atmosphere, within the uncertainties of the estimates.)

The energy of the turbulence goes eventually to heat the atmosphere at a rate of a few ^{o}K per day at 100 km. It therefore compliments direct radiative input of solar energy. With a modest increase, it can exceed the radiative heating and may then account for abnormal increases of temperature (as exemplified by the high temperatures found over the winter poles - in a region where enhanced turbulence may be expected for other reasons).

The observed turbulence appears to be adequate, but only just, to maintain the atmosphere in a chemically mixed state up to its level of termination.

REFERENCES :

Hines, C . O. : Quart. J. Roy. Met. Soc. , 89, p. 1, 1963.

RADAR METEOR TRAIL SETS

A.A. Barnes Jr.

When a meteor plunges through the earth's atmosphere, it leaves an ionized trail behind in the atmosphere. Radar reflections from these trails can be used to obtain wind and density information about the atmosphere in the region 80 to 120 km. AFCRL is procuring a radar set operating on wave lengths of 4 and 8 meters to investigate this part of the atmosphere.

A single station will give information about atmospheric tides and gravity waves at these levels, but a network of stations is needed to study the synoptic features. The accompanying figure shows 14 locations which are believed to have radar equipment capable of obtaining either wind or density measurements, or both. The simultaneous operation of these sets as a network would allow us to have our first picture of the synoptic patterns in the region of the lower thermosphere.

REFERENCE :

McKinley, D.W.R. 'Meteor Science and Engineering,' McGraw Hill Book Co. Inc., New York Toronto, London, 1 x + 309 , 1961

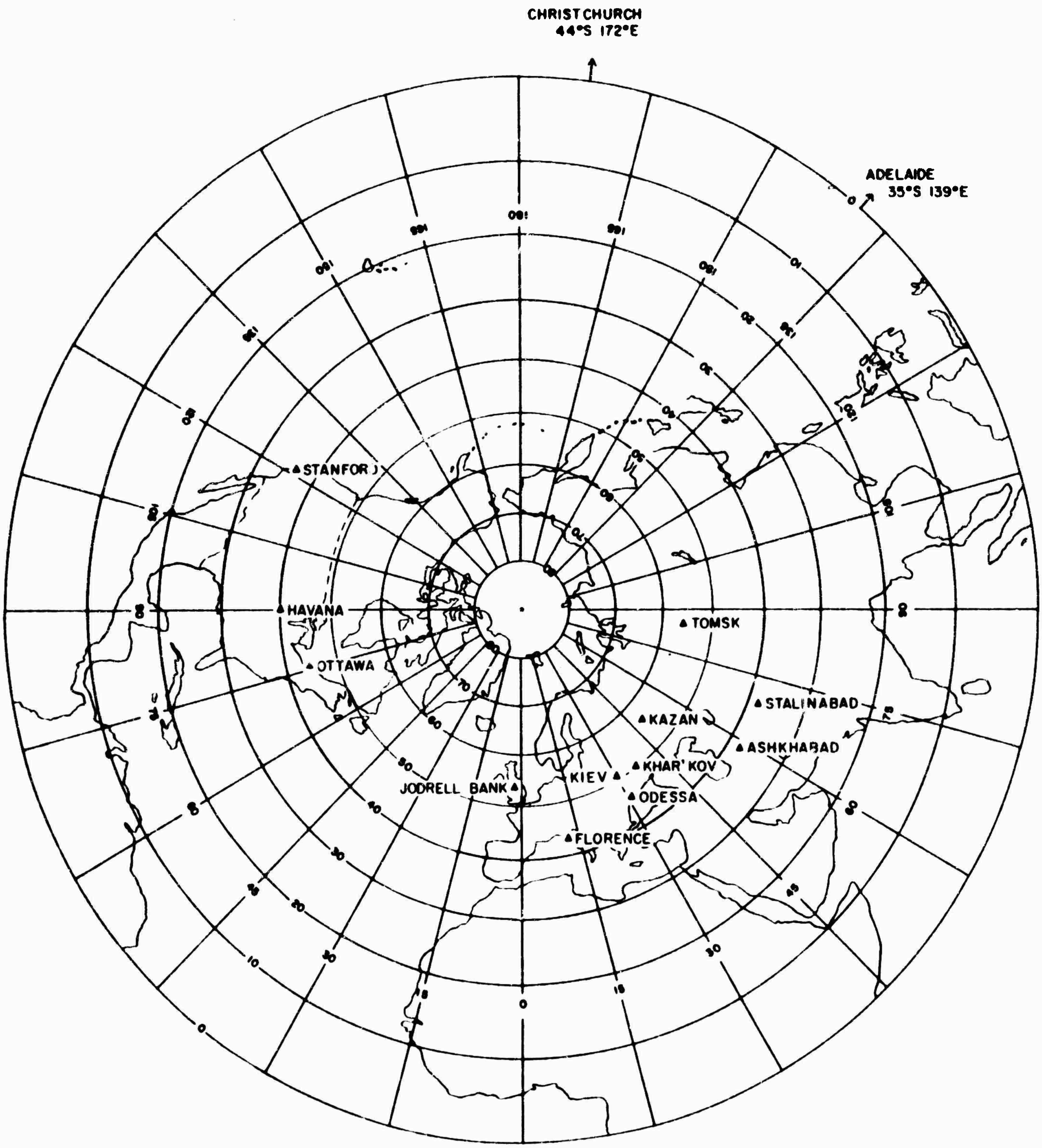

RADAR METEOR TRAIL SETS CAPABLE
OF MEASURING WIND AND DENSITY IN
THE UPPER ATMOSPHERE

JUNE 1963

AIRGLOW STUDIES AT CARDE

J. Hampson

Measurements of night hydroxyl radiation (1) suggest knowledge of the temporal behaviour would assist interpretation of the responsible mechanisms. A dayglow spectrum obtained in 1962 is compared with an earlier nightglow spectrum in Figure (1) and appears of comparable intensity. Nightglow occurs at 85 kilometers. Equilibrium ozone at this altitude decreases by a factor of 10^4 from night to day (2), and since the hydrogen concentration cannot increase by this factor, the reaction between atomic hydrogen and ozone can be the source of dayglow hydroxyl radiation only if the emission occurs at a low altitude.

Assuming atomic hydrogen can be produced at low altitudes during the day, for example by photolysis of perhydroxyl radicals, analysis of the chemical kinetics shows that during a solar eclipse the airglow signal could be substantially reduced if the dominant control on hydrogen concentration is the reaction :

$$H + O_2 + M \rightarrow HO_2 + M ,$$

the latter removing hydrogen so fast in comparison with the rate of formation of ozone as to reduce the product of hydrogen , ozone concentrations. CARDE observations from Grand'Mere , Quebec during the recent eclipse are being analysed. The latter observations serve the additional purpose of studying emission from the $'\Delta_g$ state of oxygen.

Extension of earlier chemical kinetic arguements (3) to assess the significance of wet ozone photolysis in the atmosphere indicates that if the day hydroxyl glow occurs at low altitudes, dayglow measurements may enable the rate of removal of ozone by water vapour products to be assessed.

Numerical inferences are given in the appendix. Thus the conjecture (3) that water vapour in the stratosphere acts as a thermostatic content on the stratosphere may be subject to experimental verification.

Extensive solar spectroscopic measurements from an altitude of 40,000 feet over the Florida peninsula are in progress. From several hundred spectra obtained with cooled lead sulphide detectors, there are indications the water vapour above 40,000 feet may vary substantially. It is possible the variability has a seasonal characteristic with little variation in the spring and summer but considerable variation in the fall. It is hoped that an improved understanding of water vapour concentrations above the tropopause will emerge when the measurements and analyses are completed. (Stratospheric water vapour content is being assessed from a solar spectrum obtained recently from 100,000 feet.)

Analyses of high altitude atmospheric emission spectra from 4 to 8 microns, and supporting laboratory measurements, continue. Averaged spectra, with improved signal/noise, superseding earlier data (1a) are given in Figure (2). Thermal emission from CO_2, O_3, H_2O, CH_4 and N_2O is evident. Recent laboratory data indicate the reaction between nitric oxide and ozone produces vibrationally excited NO_2. The inference that emission near 6.2 microns is due to this reaction is being investigated. Experiments to assess the possible sources of features, at 5.25, 5.45, 5.6 and 5.9 microns continue.

Ascent data between 40,000 feet and 60,000 feet are difficult to interpret for changes in the temperature of mirrors in the reference and signals paths in the spectrometer introduce differential grey body signals. The spectra suggest the signals between 5.8 and 6.7 microns do not change between 60,000 feet and 90,000 feet, i.e. emission from water vapour and the unknown features are constant in this altitude range.

Carbon dioxide emission at 4.2 microns may increase by up to a factor of 4 and ozone emission at 4.7 microns by up to a factor of 2 in ascending from 60,000 feet to 90,000 feet.

Seeding experiments with nitric oxide in the E layer have yielded spectral spatial, temporal data which are being analysed. Figure (3) gives a series of photographs of the trail.

Through improvements in resolution, laboratory experiments and further increasingly selective measurements it is hoped to assess further aspects of the chemical and photochemical behaviour of the atmosphere.

ACKNOWLEDGEMENT

Principal additional participants to those given in reference 1(a) include Dr. E.A. Lytle, Dr. M. McKinnon, Dr. D. Pleiter, Mr. G.B. Spindler, and Mr. E. Rance. Permission to publish given by the Chairman, DRB, is gratefully acknowledged.

REFERENCES

Hampson, J. :	'Airglow studies at the Canadian Armament Research and Development Establishement', Seminar on the Stratosphere and Mesosphere, Arct. Met. Res. Gp. Pub. in Met. 47 McGill University, 1962. (1 a)
Lowe, R.P. :	CARDE Report 291/59. (1 b)
Bates, D.R. :	'The Physics of the Upper Atmosphere'.
Hampson, J. :	Third Int'l Congress of the Aeronautical Sciences October, 1962.

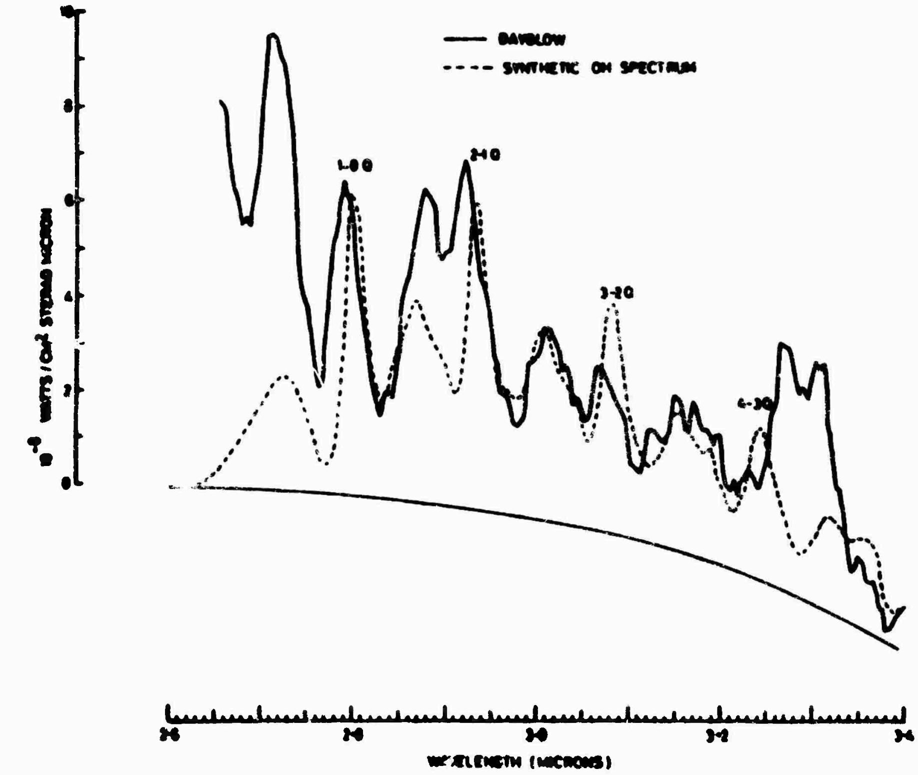

FIGURE 1a

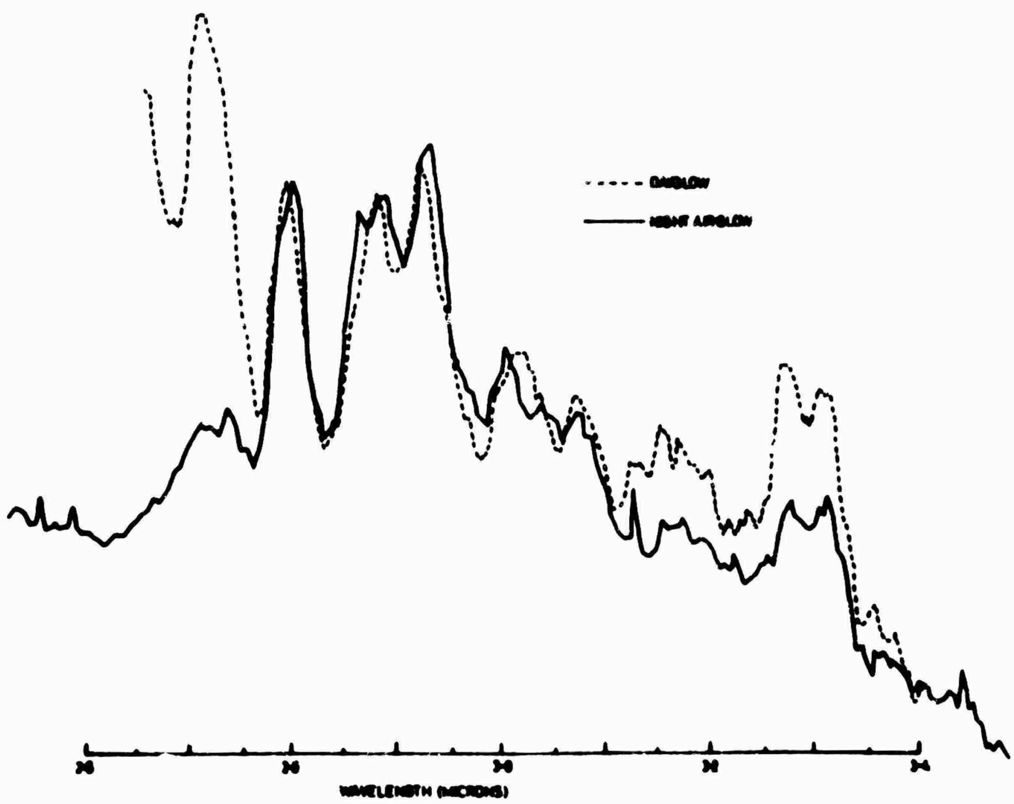

FIGURE 1b

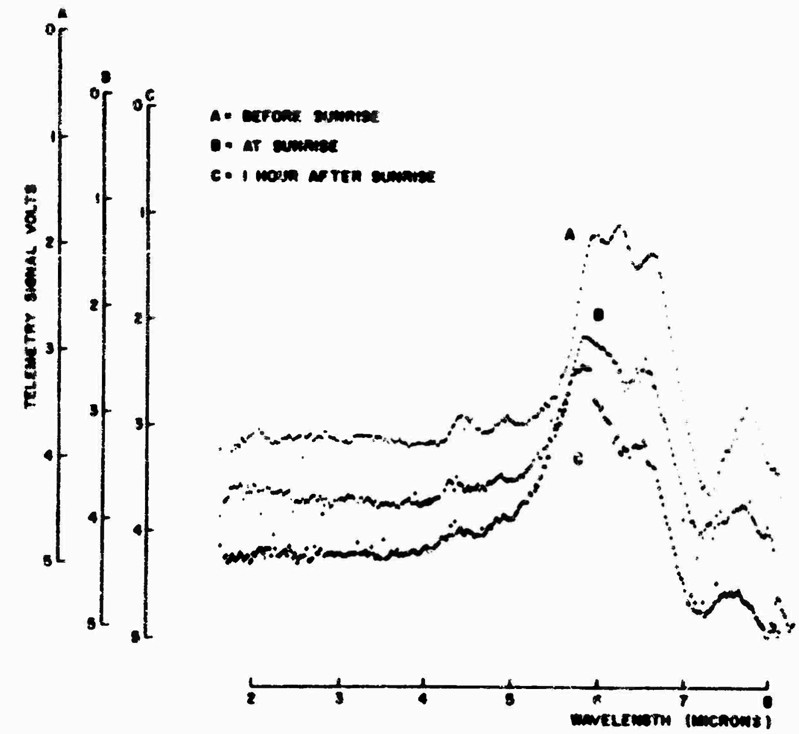

I.R. AIRGLOW FROM 100,000 FEET (Sept. 1959)

FIGURE 2a

UNCLASSIFIED
CARDE

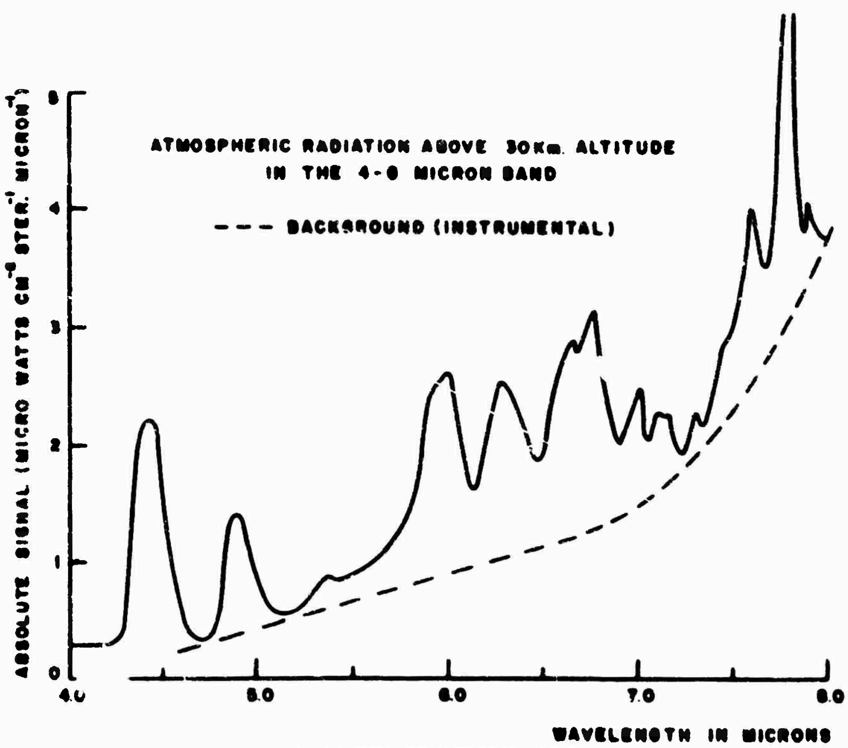

FIGURE 2b -ATMOSPHERIC INFRARED EMISSION SPECTRUM. (REDUCED)

(Sept. 1961)

UNCLASSIFIED
CARDE

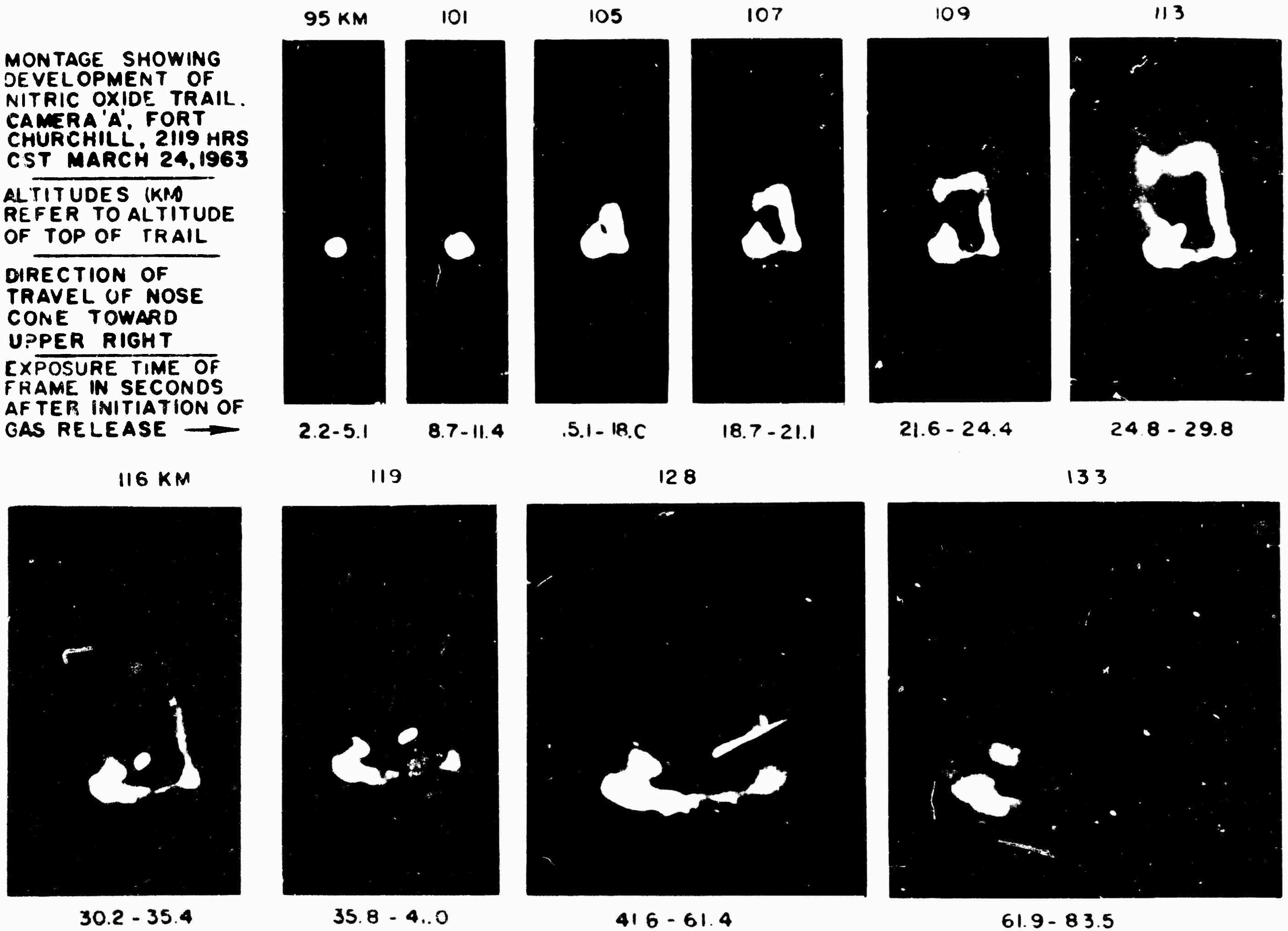
MONTAGE SHOWING DEVELOPMENT OF NITRIC OXIDE TRAIL. CAMERA 'A', FORT CHURCHILL, 2119 HRS CST MARCH 24, 1963
ALTITUDES (KM) REFER TO ALTITUDE OF TOP OF TRAIL
DIRECTION OF TRAVEL OF NOSE CONE TOWARD UPPER RIGHT
EXPOSURE TIME OF FRAME IN SECONDS AFTER INITIATION OF GAS RELEASE
95 KM
101
105
107
109
113
2.2-5.1
8.7-11.4
.5.1-18.C
18.7-21.1
21.6-24.4
24.8-29.8
116 KM
119
128
133
30.2-35.4
35.8-4..0
41 6-61.4
61.9-83.5

FIGURE 3a

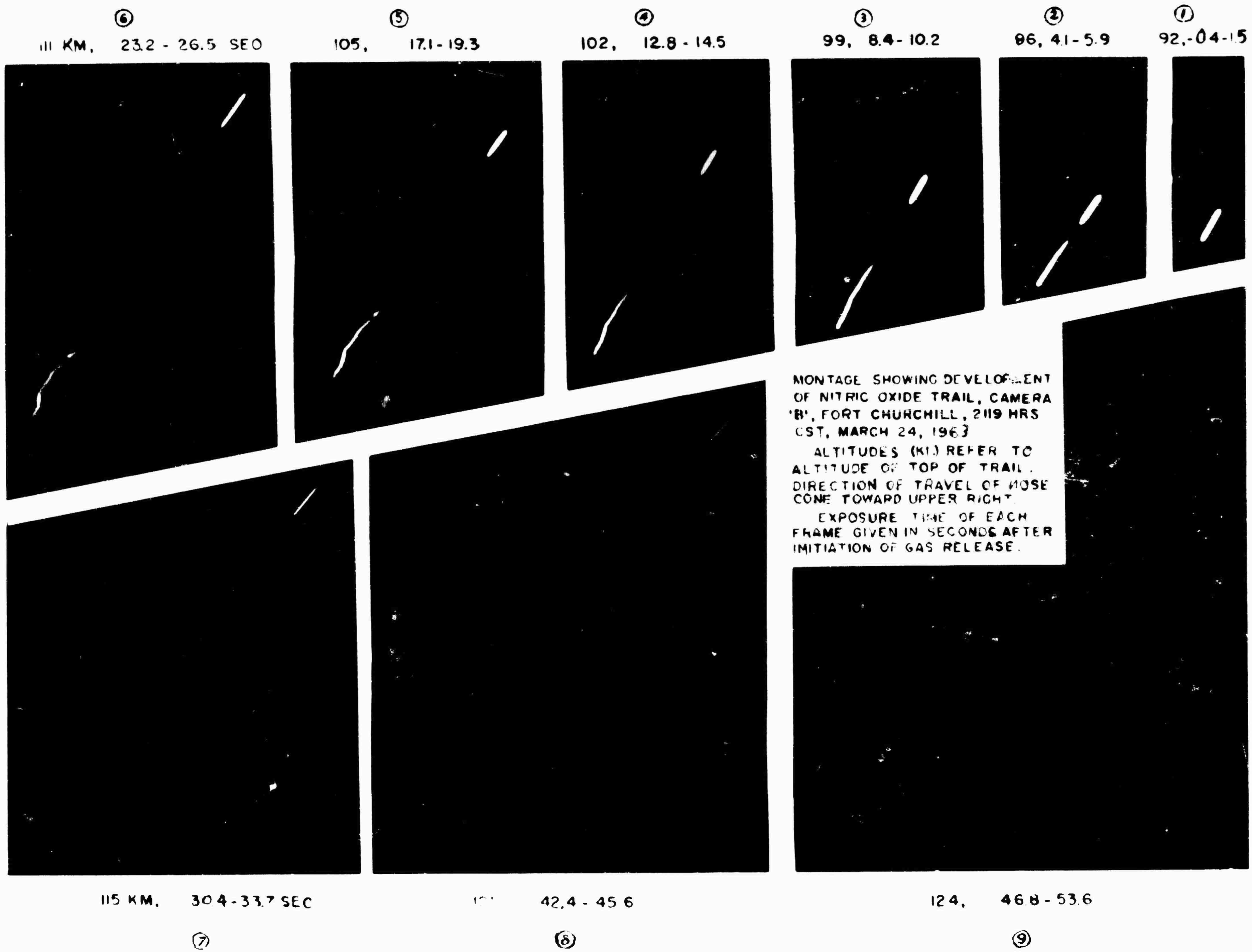
⑥ 111 KM, 23.2 - 26.5 SEO
⑤ 105, 17.1 - 19.3
④ 102, 12.8 - 14.5
③ 99, 8.4 - 10.2
② 96, 4.1 - 5.9
① 92, -0.4 - 1.5
MONTAGE SHOWING DEVELOPMENT OF NITRIC OXIDE TRAIL, CAMERA 'B', FORT CHURCHILL, 2119 HRS CST, MARCH 24, 1963
ALTITUDES (KM) REFER TO ALTITUDE OF TOP OF TRAIL.
DIRECTION OF TRAVEL OF NOSE CONE TOWARD UPPER RIGHT.
EXPOSURE TIME OF EACH FRAME GIVEN IN SECONDS AFTER INITIATION OF GAS RELEASE.
115 KM, 30.4 - 33.7 SEC
⑦
42.4 - 45.6
⑧
124, 46.8 - 53.6
⑨

FIGURE 3b

APPENDIX

Data on the photodissociation of wet ozone (1) , if interpreted as due to the reactions,

Initiation	$O_3 + h\nu \rightarrow O_2 + O\,^{1D}$
	$O\,^{1D} + O_2 \rightarrow O_2^{*} + O^{3P}$
	$O\,^{1D} + H_2O \rightarrow 2OH$
Propagation	$OH + O_3 \rightarrow O_2H + O_2$
	$O_2H + O_3 \rightarrow OH + 2O_2$
Termination	$OH + O_2H \rightarrow H_2O + O_2$,

can be used to derive the relation

$$\frac{\partial [O_3]}{\partial t} \simeq 10^{-9} [O_3] \sqrt{5 Q_3 W}$$

$[O_3]$ is the ozone concentration.

$Q_3 = [O_3]\, a_3 q_3$ is the numb r of quanta absorbed per unit volume per second where a_3 is the molecular absorption coefficient and q_3 the incident lightflux. W is the water vapour mixing ratio.

Assuming the bulk of ozone removal is produced by these reactions,

$$W \geq \frac{1}{5 Q_3} \left(\frac{2Q_2 \times 10^9}{[O_3]} \right)^2$$

where Q_2 is the number of quanta absorped per unit volume per second by oxygen . Using the ozone concentrations given by Craig (2),(Fig. 1) the water vapour mixing ratio required to make the equilibrium ozone concentrations primarily dependent upon water vapour is shown in Fig. 2.

A pronounced effect occurs at altitudes below 30 kilometers. (Craig's estimates of equilibrium tropical atmosphere ozone concentration appear too large at the lower altitudes).

Low altitude polar ozone would not be greatly affected by water vapour since Q_3 , Q_2 are extremely small for large solar zenith angles and the rate of removal of low altitude ozone would be negligibly small.

The rate of removal of ozone at higher altitudes would be somewhat greater than indicated by the foregoing argument.

Direct photodissociation of water vapour by

$$H_2O + h\nu \longrightarrow H + OH$$

and recovery of hydrogen atoms from such perhydroxyl , hydroxyl reactions as

$$O_2H + h\nu \longrightarrow O_2 + H$$

$$O_2H + O \longrightarrow O_2 + OH$$

$$OH + O \longrightarrow O_2 + H$$

further increases the removal of high altitude ozone by providing more reactants and faster reactions with ozone, such as $H + O_3 \quad OH + O_2$.

However, the significant point is that study of ozone reactions with water vapour products in the lower stratosphere may be most rewarding if the reactions taking place in the atmosphere are the same as those present in Forbes and Heidt's measurements .

REFERENCES

Forbes and Heidt : J. Am. Chem Soc. 56, 1934 (1)

Craig, R.A. : Harvard Met. Monographs, Vol. 1, No. 2 September, 1950. (2)

Appendix Fig. 1

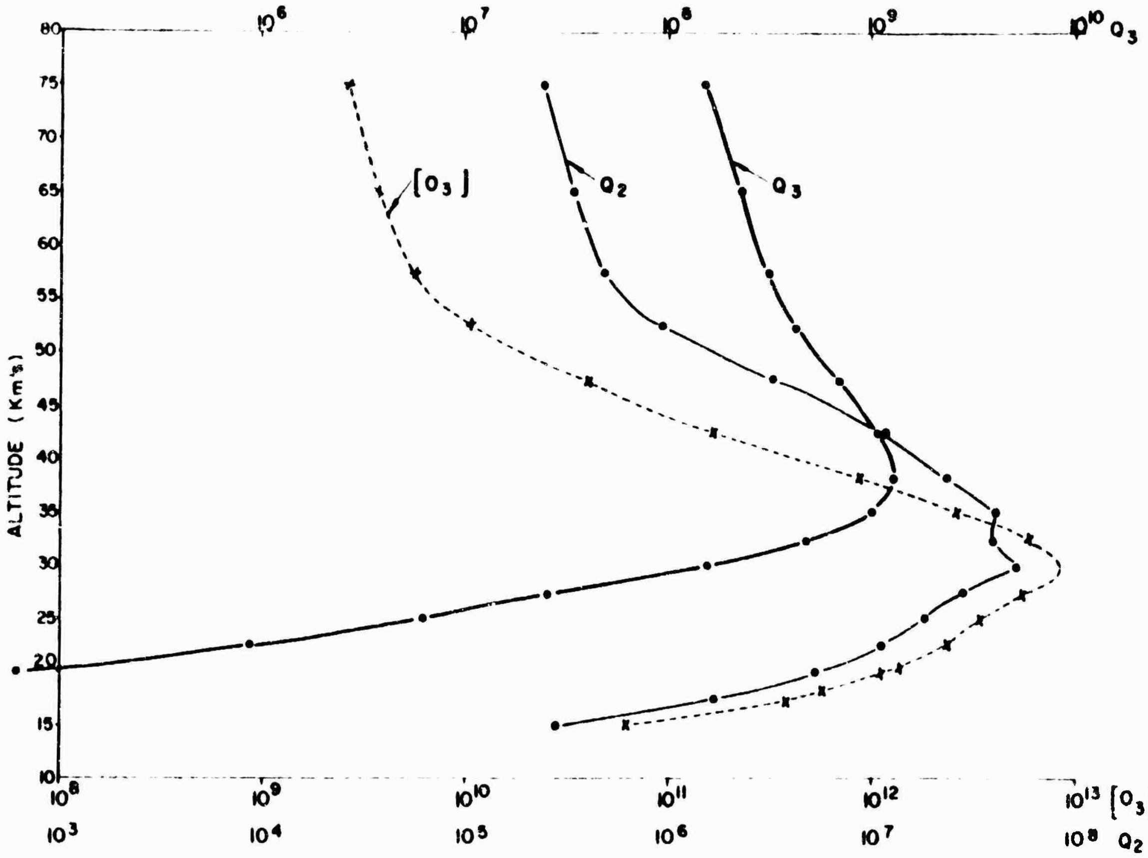

Appendix Fig. 2

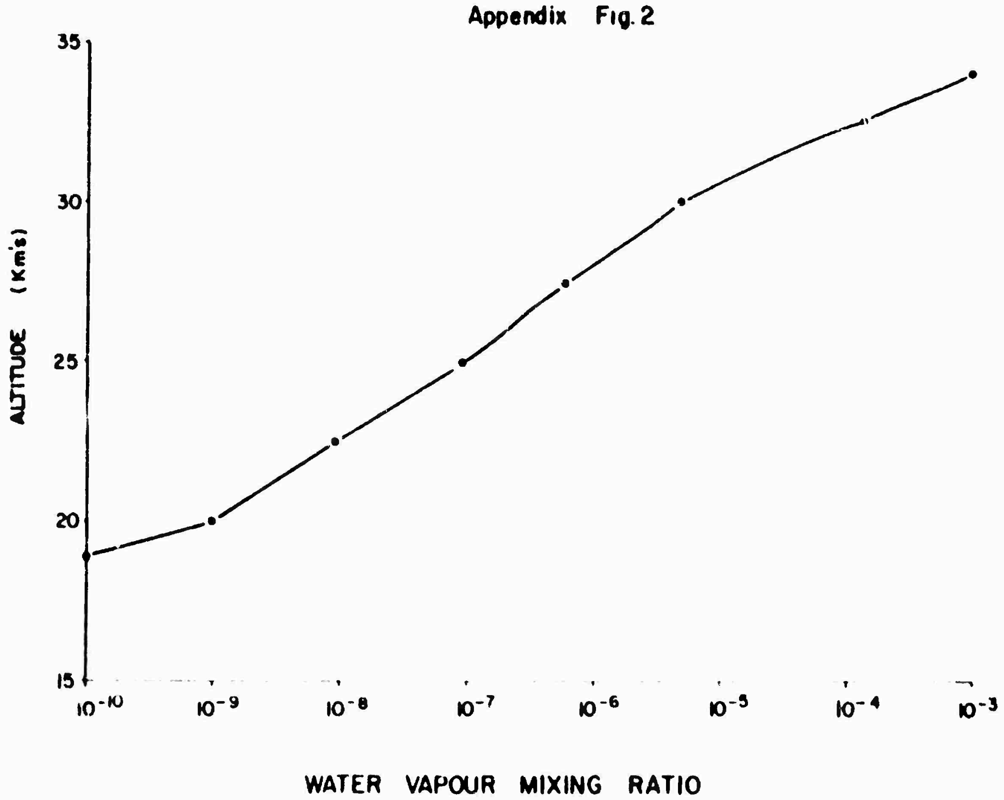

CHEMICAL AERONOMY

H. I. Schiff

Meteorologists have become increasingly interested in the atmosphere between 20 and 120 km, since the chemical processes which can occur in this region play important roles in determining both composition and heat balance.

Atomic oxygen is undoubtedly the most important reactive species in the chemosphere. At altitudes above 70 km, O_2 is dissociated mainly by the strong absorption in the Schumann- Runge continuum

$$O_2 + h\nu (\lambda < 1760\ A^o) \rightarrow O(^3P) + O(^1D)$$

and recombines largely by the three-body process

$$O + O + M \rightarrow O_2 + M \qquad (1)$$

where M is any inert gas molecule . At altitudes of about 30 km , O_2 is dissociated by the relatively weak Herzberg continuum

$$O_2 + h\nu\ (\lambda < 2420\ A^o) \rightarrow O(^3P) + O(^3P)$$

and recombines mainly by the mechanism

$$O + O_2 + M \rightarrow O_3 + M \qquad (2)$$

$$O + O_3 \rightarrow 2\ O_2 \qquad (3)$$

Although these reactions are among the most important aeronomic processes, their rate constants are not known with any degree of unanimity.

The first information on reactions (2) and (3) came from the study of the decomposition of ozone under the influence either of heat or of light. There now seems to be general agreement that the kinetics for the thermal decomposition of ozone can be adequately represented by the reaction

$$O_3 + M \rightarrow O_2 + O + M \qquad (4)$$

followed by (3) and (2). The expression for the rate of decomposition of O_3 is then given by

$$-\frac{d[O_3]}{dt} = \frac{2k_4 \cdot k_3 [O_3]^2 [M]}{k_3 [O_3] + k_2 [O_2][M]}$$

Combination of decomposition rate data with thermodynamic data for the equilibrium constant for reaction (2) and (4) permits evaluation of all the rate constants.

All the data obtained in this way has recently been analysed and shown to best fit the expressions

$$k_2 = 5 \times 10^{-34} \exp(300/RT)$$

$$k_3 = 9 \times 10^{-12} \exp\left[-4300 \pm 1000/RT\right]$$

$$k_4 = 4 \times 10^{-32} \exp\left[24,800/RT\right] \text{ when } M = O_3$$

(all expressed in cm^3, molecule, second units).

There are two main criticisms of this method of obtaining these rate constants. One is the extreme sensitivity of O_3 towards catalytic decomposition by trace impurities which makes reproducibility difficult. The other is that the values depend on the mechanism and considerable uncertainty results from trying to obtain three separate rate constants from essentially one type of measurement.

The converse approach can also be used by starting with a system containing O and O_2. If sufficient time is allowed for the reactions (2) and (3) to reach a steady state with respect to $[O_3]$ then

$$[O_3]_{ss} = \frac{k_2}{k_3} [O_2][M]$$

and a measurement of this steady state gives the ratio of k_2/k_3.

This approach was first used by Patat and Euchen who produced O atoms by photolysis of O_2. There were, however, a number of serious errors in this work. The wavelength of the light used was such that half the O atoms would have been formed in the first excited O (^1D) metastable state. Such atoms are incapable of forming O_3 but are capable of causing a chain decomposition of O_3. Also, no account was taken of the possible formation of O_3 in the liquid air traps, a process which is known to occur readily.

Several other attempts to use this method have been made using electrically discharged O_2 as a source of O atoms. However, recent work in our laboratory has shown that irreproducible results are obtained unless the gases have been scrupulously dried. An explanation for this is obtained when one realizes that H_2O is efficiently converted to H atoms in an electrical discharge. The reaction

$$H + O_3 \rightarrow OH + O_2 \tag{5}$$

is 1000 times more rapid than reaction (3). Moreover, it will be followed by the equally rapid reaction

$$O + OH \rightarrow O_2 + H \tag{6}$$

The H atoms will be regenerated and the chain will simply represent an H atom catalysed decomposition of O_3. This chain can play an important role in the atmosphere in determining the O_3 concentration. Not only can O_3 be destroyed by H atoms but also by the OH formed by (5) (or in the atmosphere by photolysis of H_2O)

$$OH + O_3 \rightarrow HO_2 + O_2 \tag{7}$$

$$HO_2 + O_3 \rightarrow OH + O_2 + O_2 \tag{8}$$

although very little is known about these reactions.

Many studies have been made of reaction (2) using discharged O_2 as the source of O atoms. However, recent results have indicated that such discharges also produce large quantities of electrically excited O_2 molecules which are capable of destroying O_3. Thus the best data to date for k_2 appears to be that given above.

A direct study of reaction (3) has been made in our laboratory using a mass spectrometric technique, and a value of $k_2 = 2.5 \times 10^{-14}$ was obtained at 25°C. At that time, however, the effect of H atoms and excited O_2 molecules was not known, and it is possible that this result is somewhat too high.

In order to study the direct recombination of O atoms in the laboratory by the process

$$O + O + M \rightarrow O_2 + M \tag{1}$$

it would be necessary to have a source of atoms in the absence of molecular O_2. Otherwise the recombination would also occur via reactions (2) and (3). This can be achieved by mixing equal proportions of NO and N atoms produced by subjecting N_2 to electrical discharge. Under these conditions the rapid reaction

$$N + NO \rightarrow N_2 + O \tag{8}$$

occurs and the system contains only O atoms and inert N_2 molecules. Using this method we have been able to obtain a value for the rate constant of reaction (1) of $k_1 = 2.8 \times 10^{-33}$ cm^6 molecule^{-2} sec^{-1} at 25°C with a negligible temperature coefficient. The relative efficiencies of other third bodies M, have also been measured and these have been found to be in the ratio He : Ar: N_2 : N_2O : CO_2: SF_6 = 0.3 : 0.3 : 1 : 1.5 : 3.0 : 3.0 .

Thus it appears that at present the value of k_1 is known with satisfactory accuracy, but still more work is required to obtain unequivocal values for the rate constants of reactions (2) and (3).

ABSORPTION PROCESSES IN THE UPPER ATMOSPHERE

J. London

The major diabatic energy source for the region of the atmosphere between 30 and 70 km is that due to the absorption of solar ultraviolet radiation by ozone. The net result of this absorption of solar energy is first to produce a photochemical equilibrium distribution of ozone (above about 35 km) and then, through absorption in the strong Hartley bands ($2200 < \lambda < 3200$ Å), to produce the observed temperature maximum at about 50 km. Above 70 km the absorption by molecular oxygen particularly in the Schumann-Runge continuum ($\lambda < 1750$ Å) becomes dominant. Calculations of energy absorption in the stratosphere and mesosphere depend, in part, on the vertical distribution of molecular oxygen and ozone. In what follows it is assumed that the atmosphere is well mixed up to 90 km and that molecular oxygen represents a fixed reservoir for the formation of ozone, and for heating the upper layers. The vertical distribution of ozone was calculated from photochemical equilibrium theory for various latitudes and for various seasons.

THE PHOTOCHEMICAL DISTRIBUTION

Under the assumption that atomic oxygen and ozone are in photochemical equilibrium and assuming only oxygen reactions , it is possible to write a closely approximate expression for the ozone density as a function of height and solar zenith angle (see, for instance London et la, 1962)

$$n_3 \approx 2.18\, n_2^{\,2} \left[\frac{(f_2/f_3)\cdot k_1/k_3}{f_3 \dfrac{k_1}{k_2 k_3} + n_2} \right]^{1/2}$$

where n_2 and n_3 are the number densities of molecular oxygen and ozone ;

f_2 and f_3 are the number of quanta of solar radiation absorbed per molecule of oxygen or ozone per unit time.

k_1 , k_2 and k_3 are the rate reaction coefficients that enter into the various recombination reactions involving atomic and molecular oxygen, and ozone.

Calculations of the ozone distribution using the expression given above and the most recent available data of the solar spectrum, absorption cross-sections for O_2 and O_3 and the rate reaction coefficients, give vertical ozone distributions for various latitudes and seasons as shown in figures 1 and 2. The computed equilibrium distribution for winter and summer show the expected overall features and need little comment here. Three features of these results, however, are noteworthy:

1) The level of maximum ozone density increases with increasing average solar zenith angle in a fashion rather typical of a 'Chapman distribution.'

2) Above 35 km there is little latitudinal variation in the equilibrium ozone amount during the summer but a significant latitudinal variation above 50 km during the winter.

3) Above about 55 km there seems to be an unusually large equilibrium amount of ozone during all seasons. This will be commented on below.

The height in the atmosphere above which a fixed percentage of the solar beam is absorbed by oxygen and ozone can be calculated as a function of wavelength and the mass depth of the absorbing gas (i. e. solar zenith angle). The following table gives the spectral distribution of the depth of penetration of solar radiation assuming an atmospheric transmissivity of 5 percent. It should be pointed out that the little solar radiation that does penetrate below 35 km in the region 2100-2200 Å is extremely important in producing the maximum ozone amounts found at 25 -30 km.

Table I

Depth of penetration for 5 percent transmission of solar radiation

λ Å	h, km
1700	90
1800	85
1900	70
2000	50
2100	35
2250	37
2500	48
2750	45
3000	20

Local heating in the upper atmosphere, in the absence of condensation or non-balanced photochemical effects, results from the direct absorption per unit mass of solar energy by oxygen and ozone. The heating due to molecular oxygen varies somewhat with latitude but is found to be generally negligible below 50 km (less than 0.1°C/day) increasing to about 1/2°C/day at 60 km, 1 1/2 °C/day at 70 km,and about 4-5°C/day at 80 km .

In the stratosphere heating is due to the absorption of solar radiation by ozone. The level of maximum stratospheric heating is found at about 45 km near the equator and, at high latitudes, varies from about 50 km during the summer to about 55 km during the winter. The heating rate due to ozone at the maximum is about 10-12°C/day near the equator decreasing to zero near the winter pole and, because of the increased length of the sunlight day, to about 16°C/day near the summer pole.

The calculations also show a strong heating due to ozone absorption at about 70-80 km. This results from the anomalously high ozone values calculated for this regi n as already noted above. Two effects have been neglected in the calculations above which would noticeably reduce the con.puted ozone amounts ;

a) The night-time destruction of ozone.

b) The destruction of ozone that takes place in the presence of hydrogen atoms.

Both of these effects could reduce the amount of ozone computed for levels above 65 km by one order of magnitude and lower the fictitious heating rate found at these levels by about the same amount. Certainly the absorption processes and subsequent heating effects at levels of 60 - 90 km depend rather critically on a correct evaluation of the ozone distribution in this region.

REFERENCE

London, J., K. Ooyama, and C. Prabhakara : 'Mesosphere Dynamics". Final Rpt. Contract AF 19(604)-5492. College of Engineering, New York University, 1962.

OZONE AND THE CURTIS- GODSON APPROXIMATION

W. Hitschfeld

TRANSFER THEORY

The greenhouse properties of the atmosphere derive chiefly from three of its trace constituents : water vapour, carbon dioxide and ozone. The contribution of ozone is generally small, but in the stratosphere ozone is the only active radiator with a widely variable concentration, so that through its 9.6-micron absorption band, ozone may play an occasionally decisive role. To study this effect adequately, reliable and readily usable methods for assessing its heating effect are needed.

A few words will suffice to describe the general problem of radiative energy transfer. The radiation flux can be stated precisely and simply by the Schwarzschild quadruple integral. Usually, a somewhat simplified form (a triple integral) which can be readily visualized is adequate. Thus the upward flux at a reference level z_o can be written as :

$$F\uparrow = \int_{\lambda} \Sigma (B_{\lambda} \Delta \tau_{\lambda}) \, d\lambda \quad , \qquad (1)$$

where B_{λ} is the monochromatic black-body flux intensity at level $z + \Delta z/2$, and $\Delta \tau_{\lambda}$ is the difference in the monochromatic transmissions of the layers extending from z_o to $z + \Delta z$ and from z_o to z.

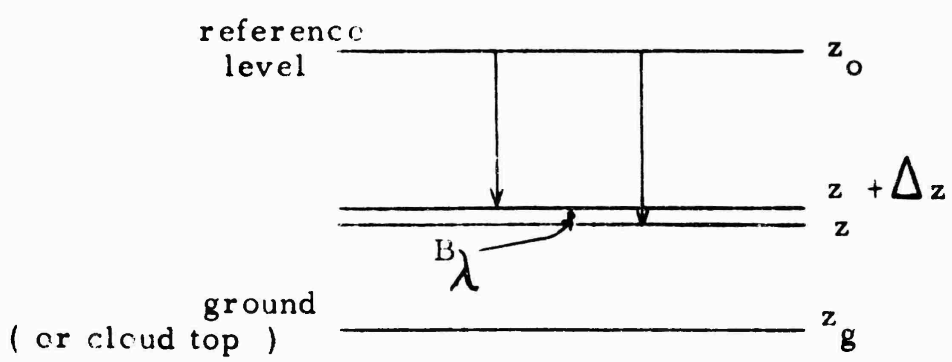

In general, each such transmission is a function of the distribution of pressure and absorber concentration throughout the layer. The integration over wavelength λ in equation (1) should extend over the entire spectrum of the absorption band, while the summation Σ needs to be carried through the range of heights z_g to z_o. (Note that z_g is the height of the ground or of the top of a cloud undercast, and in either case is the level of the nearest effectively black surface below z_o.) In spite of its compact appearance, equation (1) is complex ; a direct numerical integration is probably too demanding of computer time in routine applications, though in special cases such computations may be justified (Houghton and the author (1961) made such an attempt to obtain precise heating rates for the 9.6-micron band).

A real simplification can result only if the integration over wavelength can be carried out once and for all. This is the purpose of "spectral models", by which the line spectrum of the absorption band is smoothed in a variety of reasonable ways. Such models were designed by Elsasser (1942) and Goody (1952). The result is an effective τ^*, to be substituted for τ_λ in equation (1). The new τ^* is as smooth a function of λ as B_λ, and depends on absorber concentration and total pressure and on one or two parameters characteristic of the band. The resulting simplification is enormous, since for a typical band it may reduce the number of integrals to be computed for the numerical integration from, say 10^6 to 10; for narrow bands it may eliminate the integration over wavelength entirely.

THE CURTIS-GODSON APPROXIMATION

But an important problem remains : the evaluation of the effective τ^* for layers with pressure and absorber gradients. No exact method is available, except in special cases. Elsasser used "pressure scaling" which amounts to using an effective absorber mass, which is a pressure-weighted average concentration. An alternative procedure, suggested by Curtis (1952) and examined in detail by

Godson (1955), consists in using the total mass of absorber and an effective pressure, which is the mean of the actual pressure, weighted according to the absorber mass. Thus

$$\bar{p} = \int_{z}^{z_o} p\, du \Big/ \int_{z}^{z_o} du \,, \qquad (2)$$

where u is the absorber concentration in some suitable units.

Equation (2) is obviously an intuitively reasonable form. It can moreover be shown to be exactly applicable when the lines are either very weak or very strong. In the former case, the pressure does not enter the form of τ^* at all; hence any effective value of p can be used. In the case of strong lines, a simple intuitive argument for the validity of equation(2) can be put forth on the basis of the equation for the line shape.

Godson, and Kaplan and Eggers (1956) have examined the applicability of the C-G approximation for water vapour and carbon dioxide, respectively, and conclude that it provides adequate precision in most cases. Kaplan's (1959) arguments for its applicability for ozone are not so convincing, since the band involved is neither weak nor strong enough, and since moreover the ozone concentration often shows steep vertical gradients. Plass (1960) developed easily-used theoretical criteria from which we prepared Figure 1. This diagram permits a judgement whether the effective transmission τ^* may be expressed as a function of p. But useful as such an analysis is, the applicability of the approximation can be decided only on the basis of actual trials.

John Clark and I therefore undertook a direct test by using the C-G approximation to work out heating rates for a few real ozone soundings, for which earlier model-free calculations were available (Hitschfeld and Houghton, 1961). One typical example of our comparisons is shown in Figure 2 a. Computations were made using equations (1) and (2), and assuming ground or cloud top temperatures

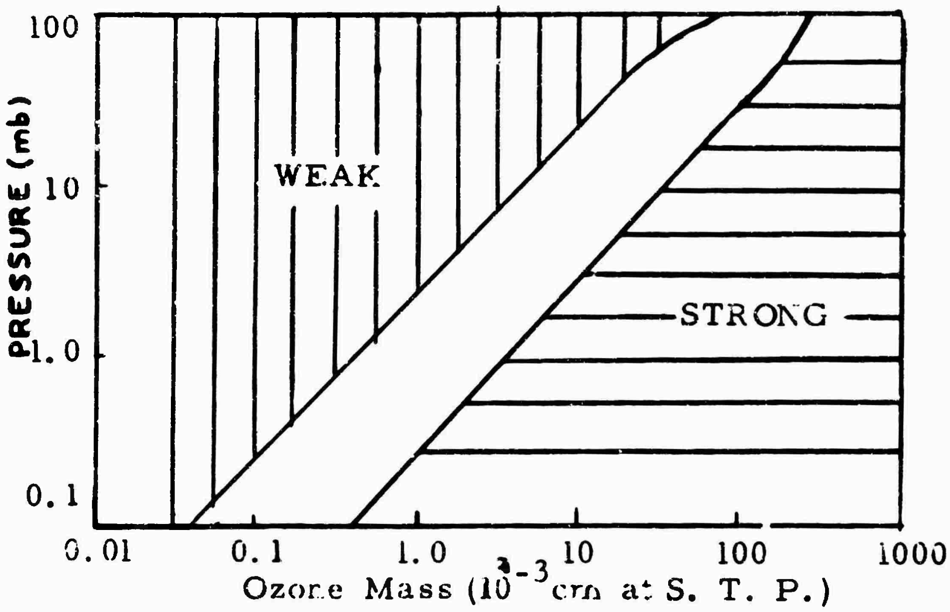

Figure 1

Regions of validity of strong and weak-line approximations for 9.6-micron band of ozone, according to Plass. Approximations give absorptivities (i. e. $1 - t^*$) with less than 10% error within shaded areas.

of 283 and 223 K. Results are presented in Figure 2 b in terms of the temperature tendency , which is proportional to the vertical divergence of the net flux ($dT/dt = -\frac{1}{\rho c_p} \frac{\partial}{\partial z} \left[F\uparrow - F\downarrow \right]$). Also presented in Figure 2 b are the results of the earlier computations which did not of course involve equation (2). The great importance of the base temperature, and hence of the cloudiness, was already pointed out in the earlier study, but may be worth repeating here. The dependence on this temperature is of course a consequence of the transparency of a cloud-free troposphere to 9.6μ radiation. It is clear that the agreement of the calculations by the two methods is quite good near the bottom and top of the ozone layer, but is poor between about 15 to 23 km, in the very region where the heating effect is really important. It is probably fair to say that in this important height interval, the C -G approximation is merely a qualitative guide. This is a matter of considerable interest and should be viewed in the light of the rather harsh fact that at present no promising alternative exists to the approximation.

The use of Plass' criteria, summarized in Figure 1, permits us to decide whether it is indeed specifically the C-G approximation of equation (2) which is to blame for the difference. For this purpose we have plotted in Figure 2c the difference in net flux (as function of height) obtained by the two methods; and right next to it (dashed) a score of validity, obtained by counting the layers which enter into the calculations for any height and for which the lines were neither "strong" nor "weak" in the sense of Figure 1. This procedure is of course somewhat arbitrary, and it is quite possible that a different method of scoring would be more significant. We feel nevertheless that the two curves of Figure 2c demonstrate our contention that the most important cause of the difference between the two sets of results lies in the C-G approximation.

Earlier this year, Walshaw and Rogers (1963) reported tests of the C-G approximation for the three active radiators in the atmosphere. They examined fairly typical absorber distributions, but, unlike us, employed spectral models for smoothing τ_λ over wavelength. Their conclusions for water vapour and carbon dioxide agree substantially with the earlier studies mentioned above. Regarding ozone, their conclusions and ours are also in qualitative agreement, though we find the C-G method somewhat less suitable than they. We consider our tests to be more incisive, since spectral models, as employed by Walshaw and Rogers, are believed to be more tolerant of the C-G approximation than the model-free standards we employed.

A RADIATION CHART

Though our conclusions are that the approximation under test permits results of only limited precision, there can be no doubt as to its convenience. To illustrate this, we have prepared a radiation diagram (more for the purpose of lucidity than of speed), reproduced in Figure 3. This chart is a plot of black-body flux versus layer absorptivity, so that areas represent the flux, in accordance with equation (1) - (the transmission $\tau^* = 1$ - absorptivity)- . Since B is an exclusive function of the temperature at $z + \Delta z/2$, the ordinate (on right-hand side) is plotted as temperature corresponding to a linear scale in B. Incorporated into the chart is a nomogram based on Walshaw's (1957) absorption data, permitting a graphical evaluation of the absorptivity of any layer. The chart is entered from the left-hand ordinate at the calculated effective pressure (based on equation (2), or otherwise) between z and z_o, and with the ozone mass of the layer which must first be multiplied by 5/3. The dashed isopleths apply when the pressure ranges from 200 to 400 mb. When the abscissa (absorptivity of the layer in question) is thus found, the ordinate is determined by moving vertically to the temperature at z_o. A sample plot for the sounding of Fig. 2 a with a base temperature of 263 K is shown.

The suggestiveness of this radiation diagram, as of others, consits in permitting a qualitative survey of the effect of the relevant physical parameters. For instance, in the example illustrated, variation of the base temperature by some $\pm$ 20 K (corresponding to absence of cloud or rise in cloud-top level of some 3 km) would change the upward flux by some $\pm$ 50 % !

REFERENCES

Curtis, A.R. : 'Discussion of a paper by Goody', Quart. J. R. Meteor. Soc., 78, 638-640, 1952.

Elsasser, W.M. : 'Heat transfer by infrared radiation in the atmosphere', Harvard Meteor, Studies, No. 6, Harvard Univ. Press, 107, 1942.

Godson, W. L. : 'The computation of infrared transmission by atmospheric water vapour, J. Met., 12 272-284, 1955.

Goody, R.M. : 'A statistical model for water vapour absorption', Quart. J. R. Meteor. Soc. 78, 165-169, 1952 .

Hitschfeld, W. and J.T. Houghton : 'Radiation transfer in the lower stratosphere due to the 9.6 micron band of ozone ', Quart. J.R. Meteor .Soc. 78, 562-577, 1961.

Kaplan, L.D. : 'A method for calculation of infrared flux for use in numerical models of atmospheric motion' The atmosphere and the sea in motion. Rockfeller Inst. Press in assoc. with Oxford Univ Press. 170-177, 1959.

Kaplan, L.D. and D.F. Eggers : ' Intensity and line width of the 15 micron CO_2 band determined by a curve-of-growth method.' J. Chem.Phys. 25, 876-883, 1956.

Plass, G.N. : 'Useful representations for measurements of spectral band absorption', J. Opt. Soc. Amer., 50, 868-875, 1960.

Walshaw, C.D. : 'Integrated absorption by the 9.6 μ band of ozone', Quart. J.R. Meteor.Soc. ,83, 315-321, 1957.

Walshaw, C.D. and C.D. Rodgers : 'The effect of the Curtis -Godson approximation on the accuracy of radiative heating-rate calculations', Quart. J.R. Meteor, Soc., 89, 122-130, 1963.

Figure 3. Radiation chart for the 9.6 -micron band of ozone - a plot of blackbody flux against layer absorptivity. Blackbody flux is represented by absolute temperature scale at right. Ausiliary scales: at left, effective layer pressure; at far right, quantity to be added to upward flux determined in main part of diagram (milliwatts cm^{-2}), i.e. extension of area to 100% absorptivity. Isopleths are lines of constant ozone mass: solid lines correspond to pressure range from 0 to 200 mb ; dashed lines for pressure range from 200 to 400 mb.

An example is shown to calculate the net flux at 16 km on April 14, with a base temperature of 263 K. Upward flux is area under curve ABCD plus 0.125 milliwatts cm^{-2} ; downward flux is area under curve AEF. The numbers along the lines indicate the lower or upper limits of the layers whose other limit is 16 km.

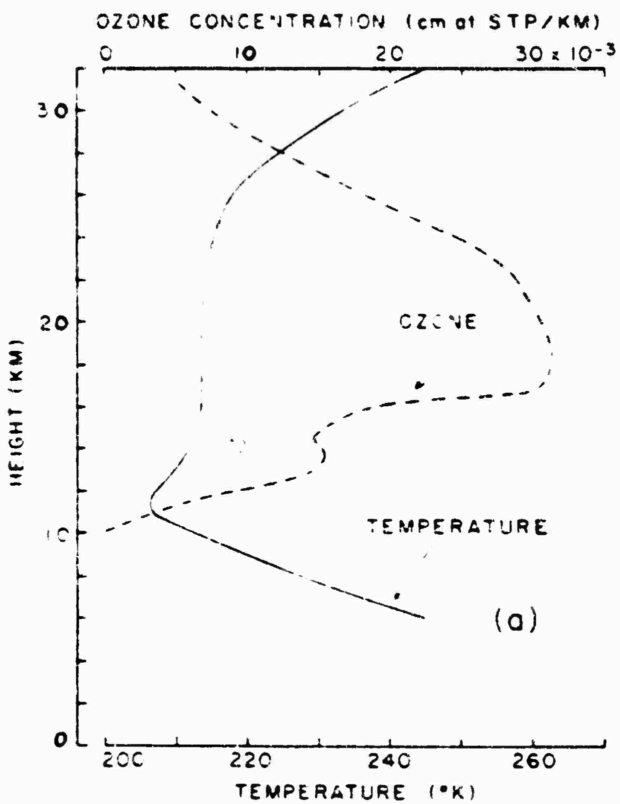

Figure 2 a
Vertical distribution of ozone and temperature for April 14 sounding

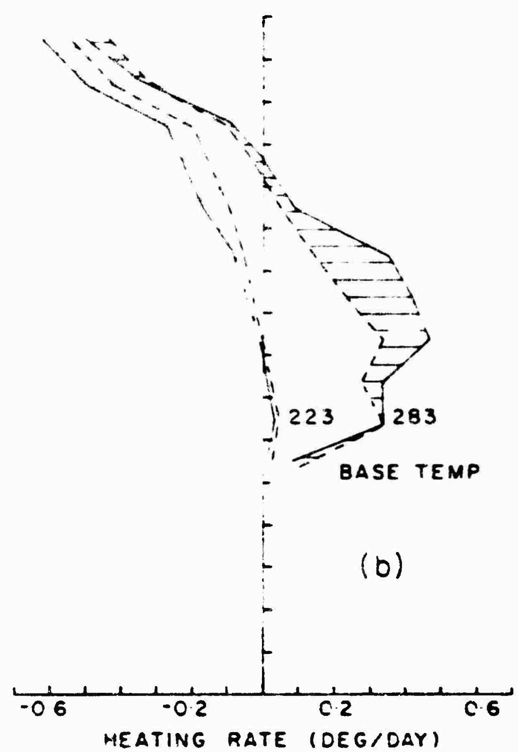

Figure 2 b
Comparison of Hitschfeld - Houghton heating rates (dashed lines) and present results (solid lines) for April 14.

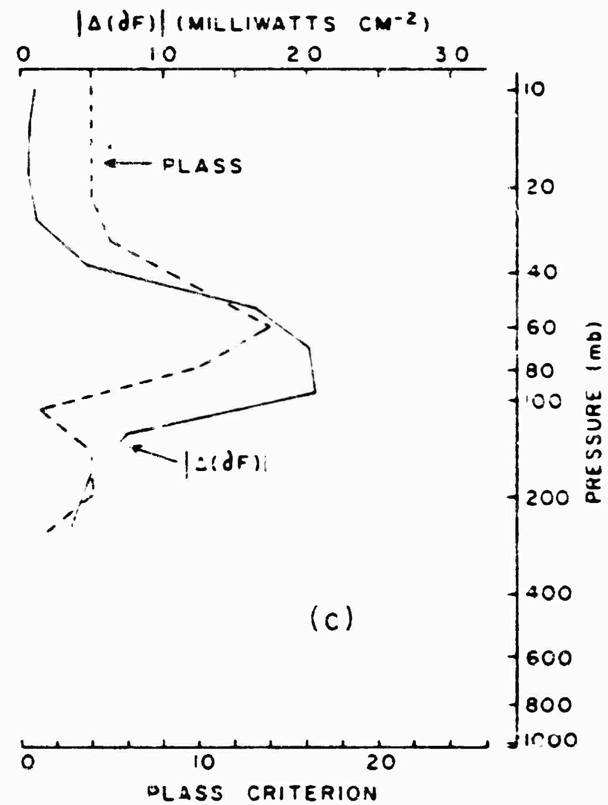

Figure 2 c
Vertical distributions of difference (absolute value) between Hitschfeld-Houghton and present flux values, and score from Plass' criteria.

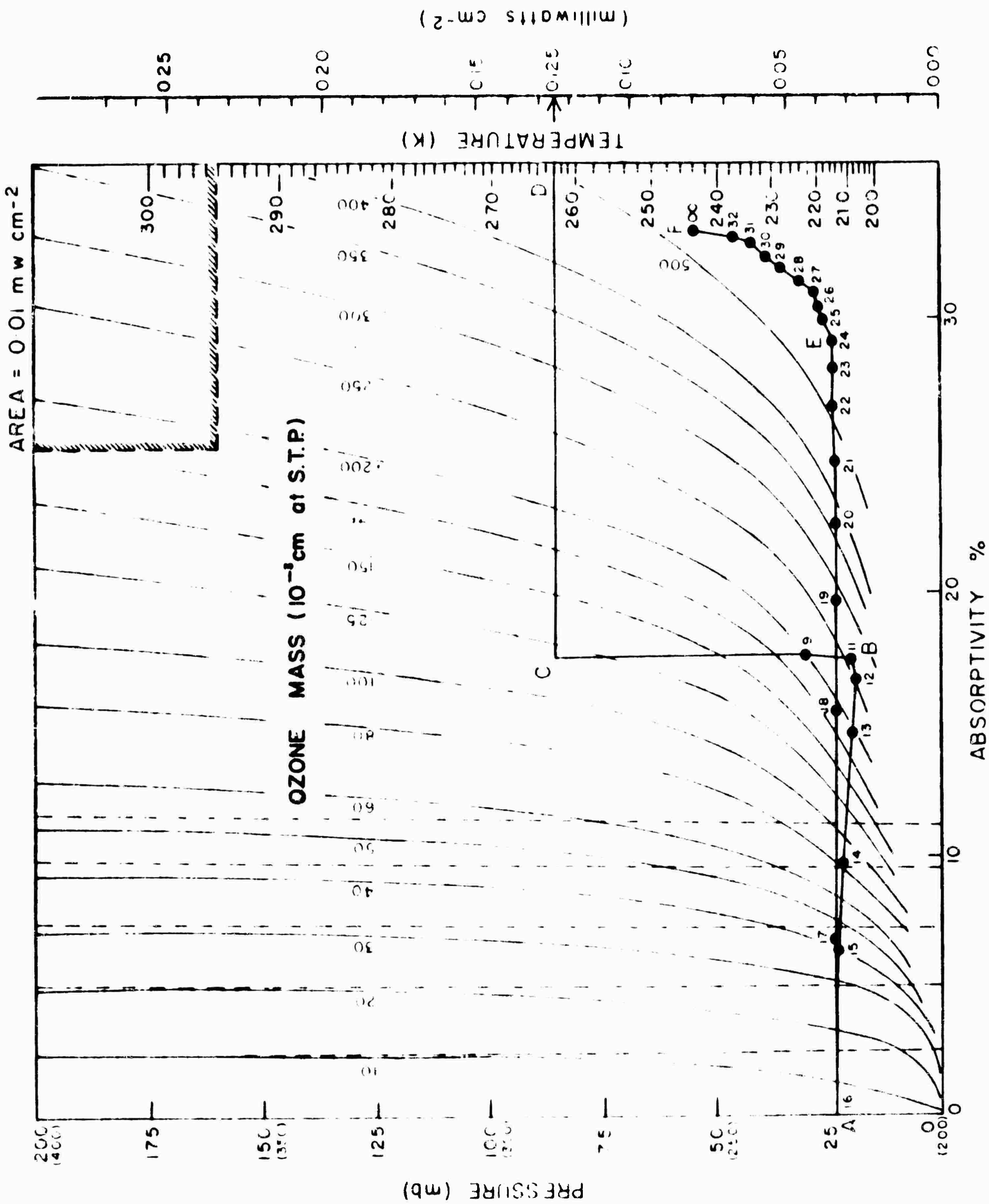

AREA = 0.01 mw cm-2
OZONE MASS (10-3 cm at S.T.P.)
TEMPERATURE (K)
(milliwatts cm-2)
PRESSURE (mb)
ABSORPTIVITY %

Figure 3

THE OZONE OF THE STRATOSPHERE AND ITS TRANSPORT

A. W. Brewer

The interest in atmospheric ozone lies primarily in the information it can give regarding transport processes in the stratosphere. The total amount of ozone is small ; only 2 or 3 molecules per million in the atmosphere are ozone. Additional interest arises due to its strong ultra violet absorption which causes high air temperatures at about 50 km and its infra red absorption which causes heating in special circumstances.

The ozone is created by the action of sunlight on the upper atmosphere. The ultra violet radiation does not penetrate too deeply, while the chemical reactions to create the ozone require the interaction of neutral air molecules . They therefore occur most readily at low levels where the air pressure is high. The combination of these effects gives a reasonably defined region of formation which is shown in Figure 1. It should be especially noted that the formation in the winter hemisphere is limited and is at high levels.

The total amount of ozone overhead can be measured spectrophotometrically by observing the cut off of the solar spectrum at 3000 Å with a refined U. V. spectrophotometer (a "Dobson"). If we do this we find that there are considerable day to day variations, and also a clear mean annual variation. The total amounts and the annual variation depend very much on the latitude as can be seen in Figure 2. Notice that inspite of the limited formation of ozone in winter the greatest amounts are found at high latitudes at the end of the winter night.

This shows that considerable transport occurs in the winter stratosphere; though conventionally the stratopphere is a quiescent region, in ra⁻iative equilibrium , free from substantial movements. To elucidate the problem we require to know exactly where the ozone is, and consequently considerable effort has gone into devising means of measuring the vertical distribution. The discussion given here is based on results obtained by an electro chemical sonde (Brewer and Milford) and measurements made with this instrument by M. Griggs.

Concerning day to day variations Figure 3 shows successive ozone ascents made at Liverpool , England , 54°N, in the spring of 1958. The total ozone measured at Oxford about 150 miles SSW of Liverpool is shown for each occasion. It is clear that the variations in the total arise through fluctuations in the concentration which can occur at almost any level reached by the balloons.

The cause of the annual variation may be seen by comparing the spring time ascents of Figure 3, with the ascents of Figure 4, which were made in autumn. The very much smaller amounts below 70 mb is obvious.

The reasons for the high total ozone at high latitudes and low ozone at low latitudes may be seen from the ascents plotted in Figure 5 in which ascents made at Malta, 37°N , may be compared with as ascents at Tromsø , 70°N both at approximately the same longitude. It is clear that there is extra ozone at levels below 50 mb.

We may use the ascents to draw a cross section showing the distribution of the ozone in the atmosphere. Figure 6 shows the isopleths of ozone mising ratio drawn from ascents for July 1958. The diagram also shows selected isentropic surfaces, and also, in the lower part of the diagram , the variation of absolute vorticity for non rotating samples of air . Notice that along the potential temperature surfaces high ozone and high vorticity are associated together at high latitude.

The march of events may reasonably be deduced to be : In the winter there is downward and poleward transport, to fill the lower stratosphere of temperate and polar regions. This transport must be very powerful and can hardly occur without corresponding transport of heat. This downward transport of heat would appear to absorb kinetic energy unless the ultimate source of the heat is at much lower levels. In the summer when the middle stratosphere is very quiescent the downward transport presumably stops. The ozone then leaks away , by mixing into the troposphere from the lower temperate stratosphere. Thus the region of high ozone shrinks and becomes much weaker and more localised at high latitudes, to be renewed next winter.

The day to day fluctuations arise because throughout the year the atmosphere moves about, either along isentropic surfaces or carrying isentropic surfaces with it, in the usual burley of the weather. This causes the day to day ozone changes as the cross section pattern is carried temporarily north and south in the various layers. In these movements potential vorticity is conserved but since vertical stretching and compression are difficult in the stratosphere vorticity is also substantially conserved, therefore high ozone corresponds to high vorticity (cyclonic conditions) and low ozone to low vorticity (anticyclonic) , a relation demonstrated by Normand in 1952 for total ozone. Griggs results , Table 1, show high positive correlations between local vorticity and local ozone concentration.

In spite of the large fluctuations the ozone does not completely leak away in the summer period of roughly 100 days. From the variance of ozone concentrations and the wind it is clear (as is perhaps well recognised) that the fluctuations must be waves with a correlation between ozone concentration and N to S wind velocity of less than about .05, but in winter special circumstances must apply to downward and poleward motions since the transport is able to fill the lower temperate stratosphere in spite of continued outward transport . This latter transport which is strong would appear the most difficult because of the strong downward heat flux which must accompany it while the former which can be along the isentropic surfaces would appear easy, yet it is relatively low. Why the contrast ?

Table 1

Coefficients of correlation (r) between ozone (o), vorticity (v), and temperature (t) , for three stratospheric levels.

	Level	$r_{o/v}$	$r_{v/t}$	$r_{o/t}$
	200 mb	.75	.48	.74
Spring	150 mb	.73	.50	.63
	100 mb	.75	.26	.35
	200 mb	.60	.70	.40
Autumn	150 mb	.42	.85	.32
	100 mb	.24	.59	.33

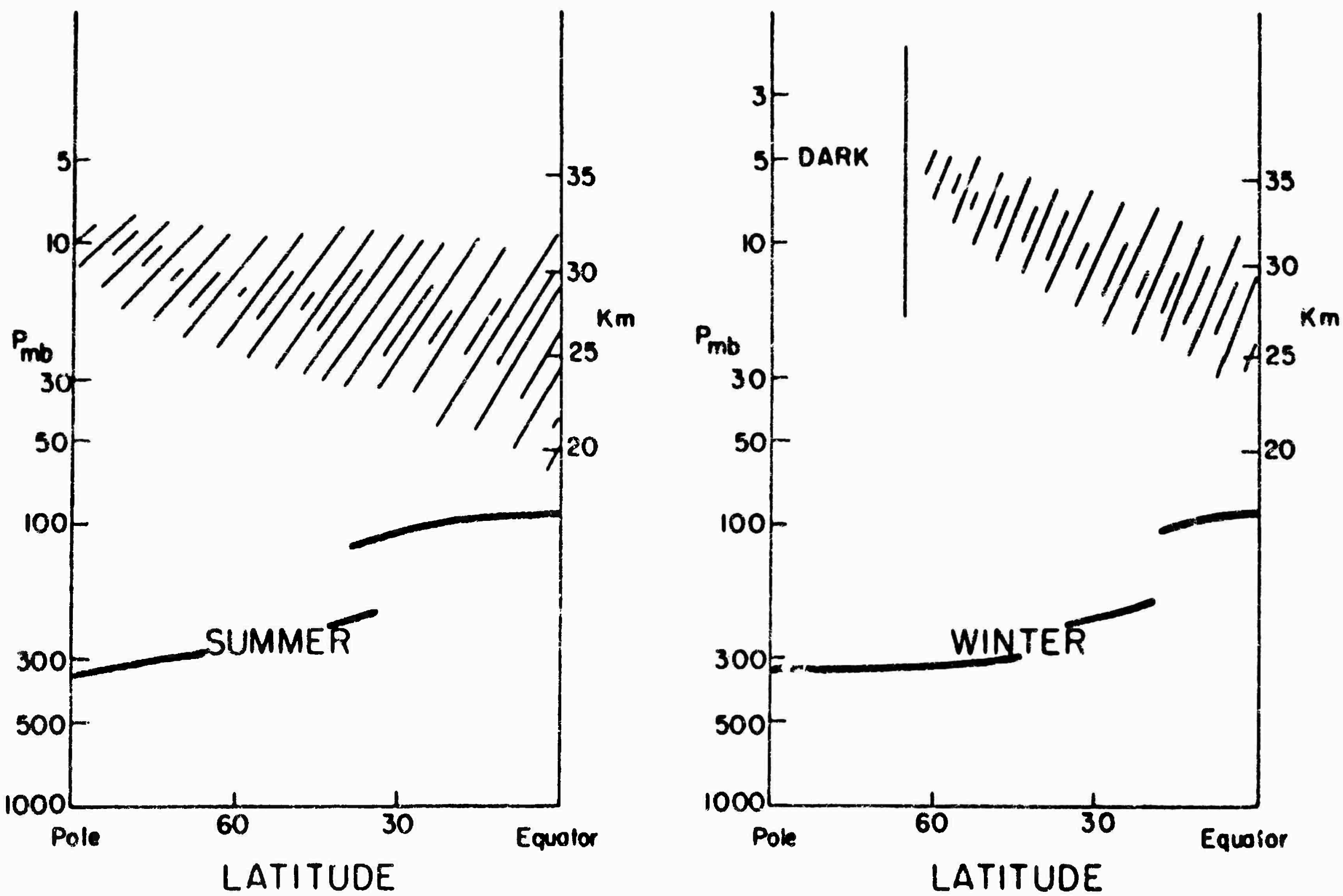

Fig. 1. Regions of ozone formation, ozone is stable below the layer or in the dark.

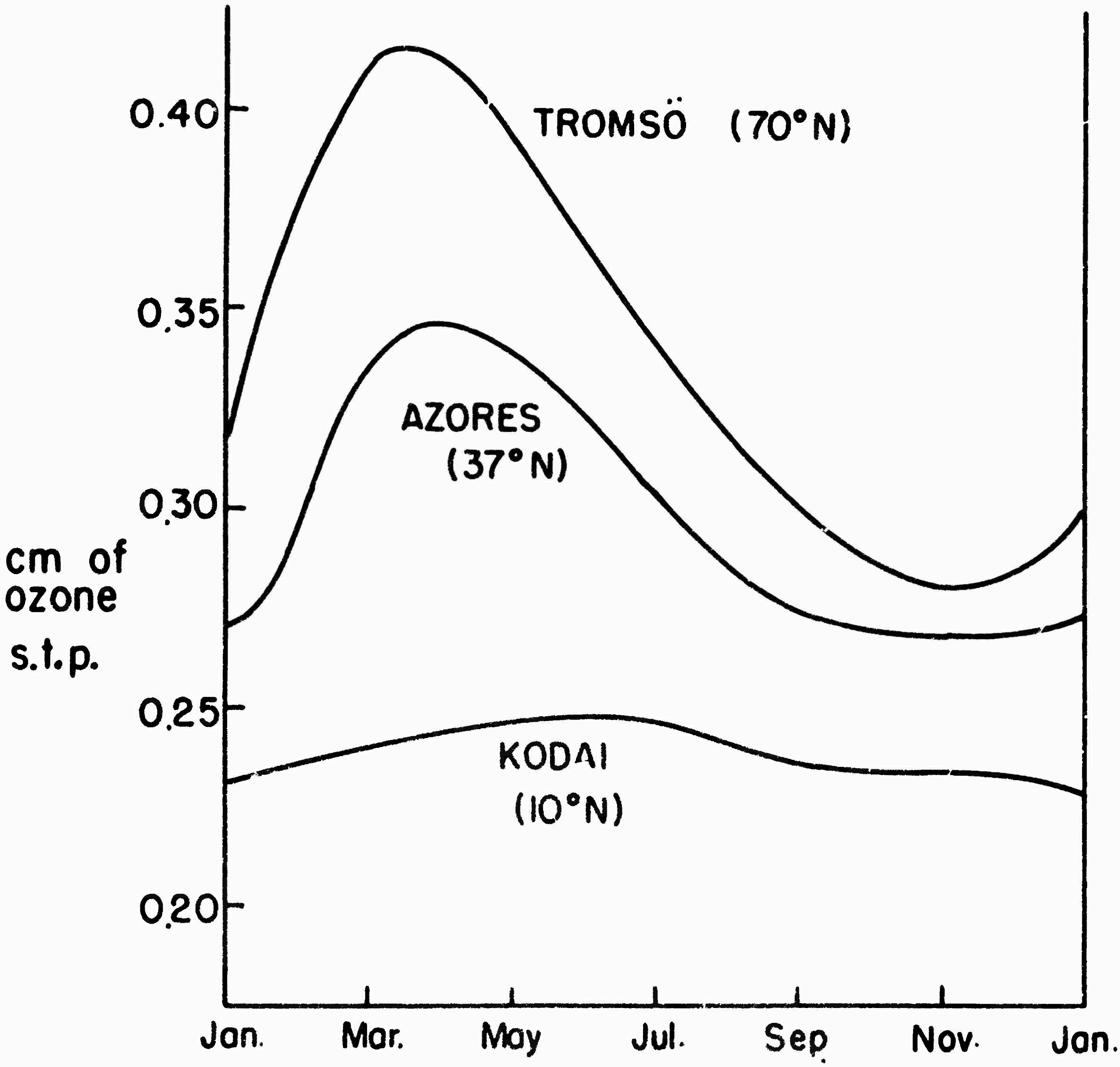

Fig. 2. Annual Variation of Total Ozone at Tromsö, Azores and Kodai

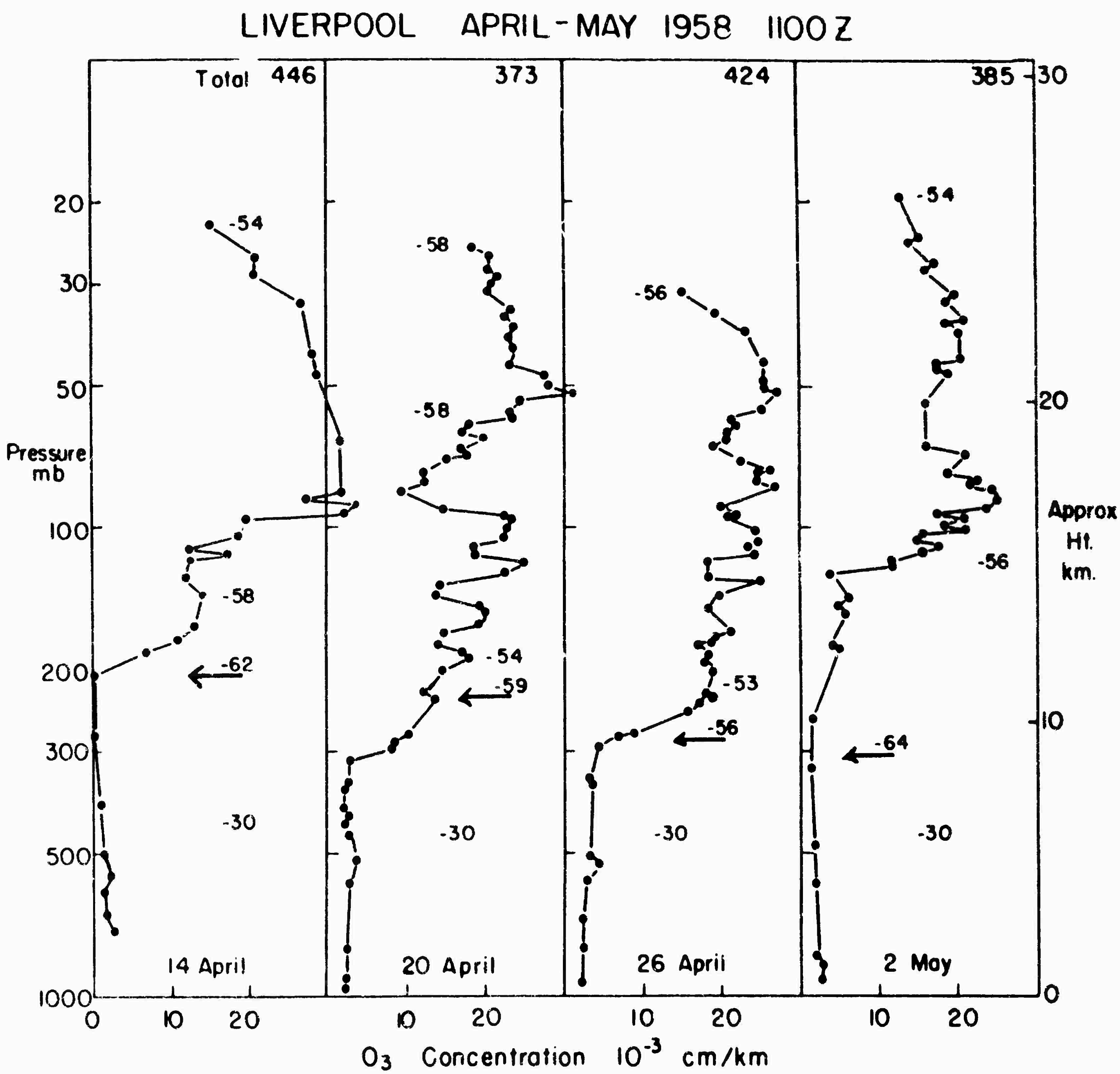

Fig 3 A Series of Ozone Ascents Made at Liverpool (54°N) in Spring 1958.

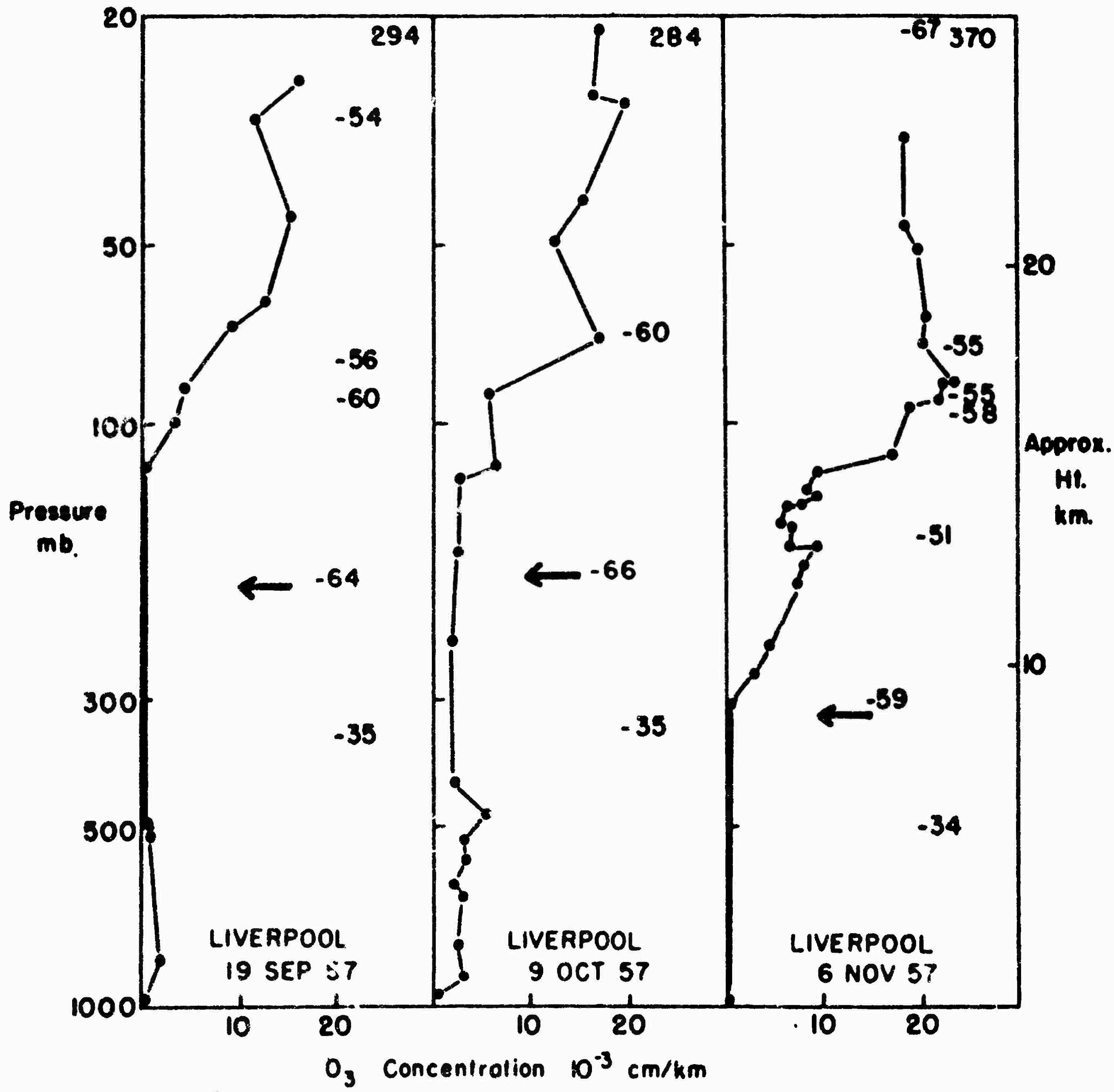

Fig. 4. A Series of Ozone Ascents Made at Liverpool in Autumn 1957.

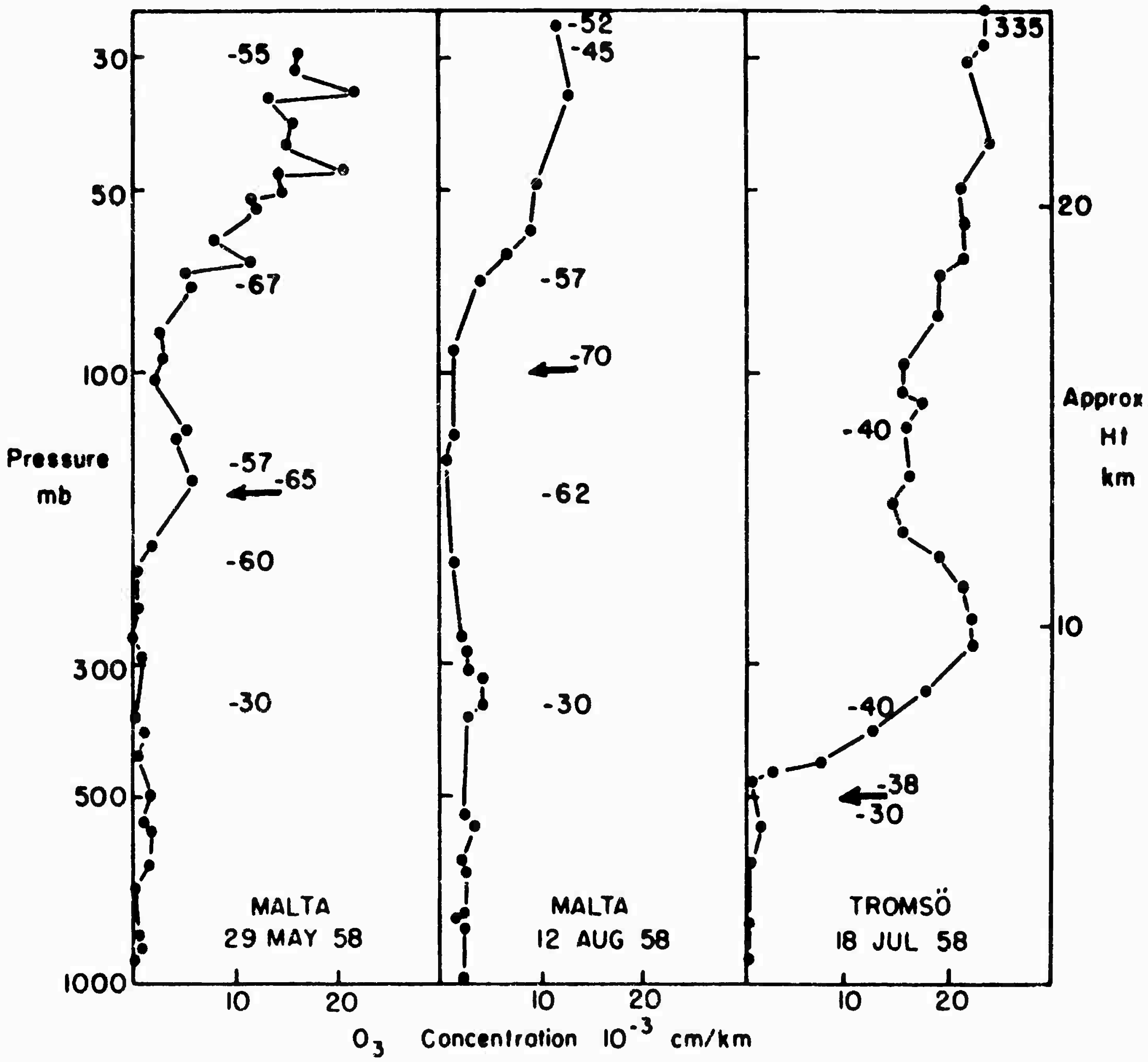

Fig. 5. Ozone Ascents from Malta (36°N) and Tromso (70°N) Showing the Latitude Variations

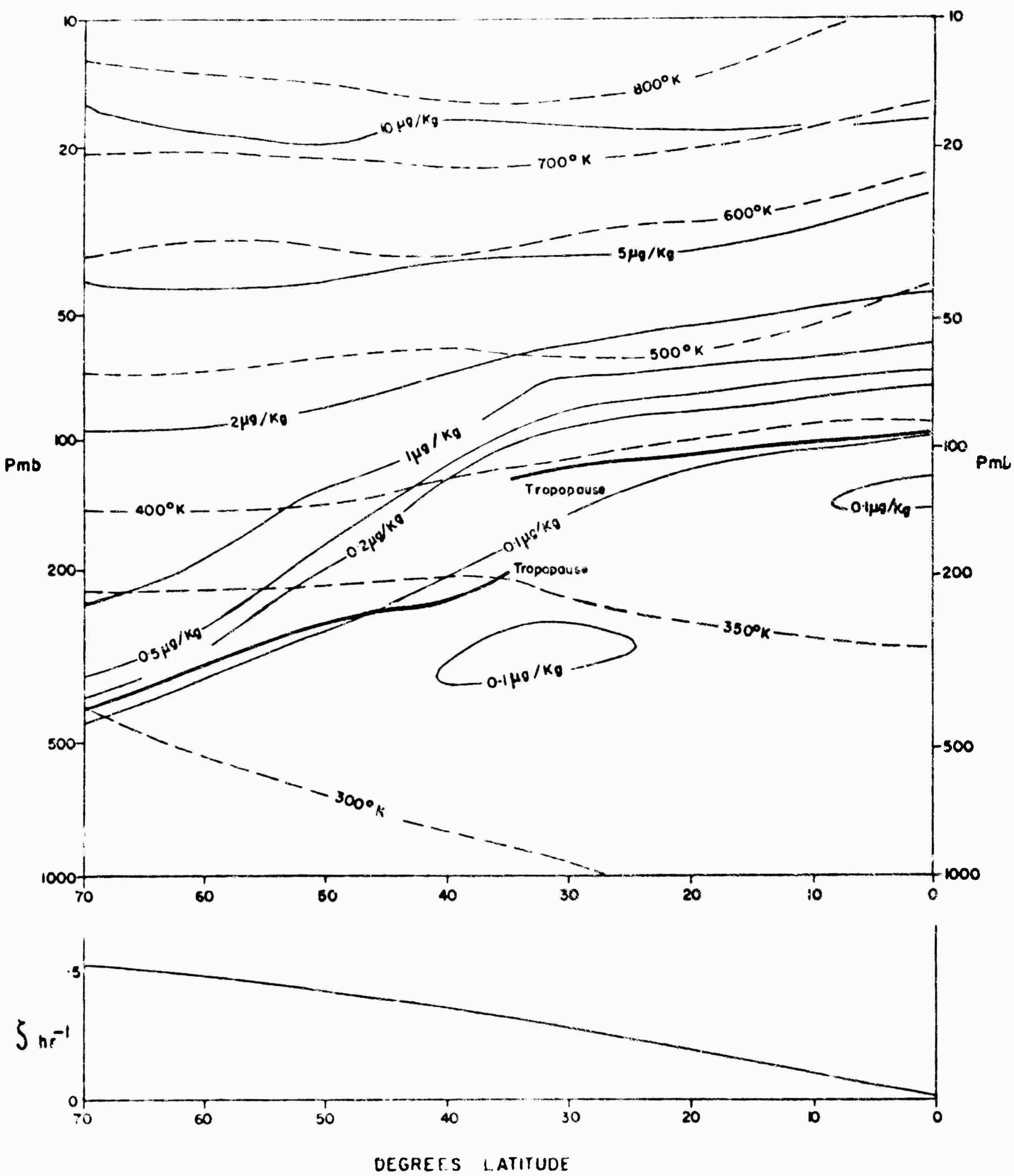

Fig 6. Above Cross section July–Aug. 1958, showing isopleths of ozone mixing ratio and potential temperature.

Below The vorticity of air with no relative rotation.
Along an isentropic surface high ozone concentration goes with high vorticity.

RADIOACTIVE TRACER RESULTS

E.A. Martell

A. RADIOACTIVE TRACER RESULTS ON POLAR STRATOSPHERE MIXING

In this discussion on polar stratosphere and in part B on equatorial stratosphere, I attempt to review and summarize what has been learned about stratospheric behaviour from recent radioactive tracer experiments. Radioactive cloud sources combine a number of special advantages for atmospheric tracing which are not afforded by chemical tracers like ozone : the radioactive point sources can be uniquely discriminated with high sensitivity and thus for large dilution factors and prolonged time periods. For a one megaton explosion as little as 10^{-21} of the cloud source can be detected on a time scale of weeks, and 10^{-18} over a period of decades. The possibilities of such tracers for the investigation of slow mixing, transport and deposition processes on a geophysical scale are obvious.

Following an introductory discussion of the physical properties of radioactive aerosols in the stratosphere, the main features of the rhodium-102 high altitude tracer experiment will be discussed. Selected fission product and induced radioisotope ratio data which serve to identify individual nuclear test series as sources also lend insight on stratospheric mixing processes and storage time. Isotope ratio data are suitable for tracing atmospheric processes over a time period up to several times the half-life of the shorter lived of the radioisotope pair. Carbon -14 and tritium studies are omitted from my discussion because they do not provide point source tracers in time and space. Current studies of the cosmic -ray spallation product distribution in the stratosphere (Drevinsky, 1963) are of limited usefulness because of substantial artificial production of sulfur-35 , phosphorus -32 and possibly others of the spallation products. Some useful stratospheric measurements of these natural radioactivities were made during the recent moratorium (Bhandari, 1963 and Rama , 1961). The basis and some possibilities for using cosmic ray produced radioisotopes for the investigation of atmospheric processes have been reported by Lal et al (1958, 1959, 1962).

Radioactive aerosol properties.

The physical properties of radioactive aerosols in the stratosphere and mesosphere determine the adequacy of aerosol sampling methods, the role of sedimentation in their downward transport, and thus the acceptability of radioactive aerosols as tracers for the study of atmospheric mixing and exchange processes at these levels. Radioactive aerosol size results obtained by impactor-filter balloon flights over Minneapolis, Minnesota and Hyderabad, India have been described elsewhere (Martell, 1961 , Drevinsky et al 1962).

These size distribution studies were carried out using a large-volume two-stage impactor based on the Junge impactor (Chagnon and Junge, 1961) and backed up by a polystyrene microfiber filter. Particles larger than 0.15 μ radius were collected on the first stage of the impactor, particles between 0.02 μ and 0.15 μ radius on the second stage, and smaller particles were deposited quantitatively on the background filter.

Representative results, shown in Fig. 1, show a marked trend with altitude. In the lower stratosphere about 90 percent of the radioactivity is associated with particles below 0.15 μ radius, with indications that it is largely attached to the natural sulfate aerosols near the peak in their number -distribution at about 0.1 μ radius. At altitudes of 90,000 to 100,000 feet some 60% to 80% of the radioactivity is associated with particles smaller than 0.02 μ radius (Fig 1). These experimental results show that sedimentation plays no significant role in the transport of radioactive aerosols within the mesosphere and stratosphere and across the tropopause. The suitability of radioactive aerosols as tracers for atmospheric circulation and mixing processes in the stratosphere and mesosphere cannot be doubted.

Rh-102 high altitude tracer:

Approximately 3 megacuries of rhodium-102 radioisotope were produced in a nuclear detonation at 43 kilometers altitude over Johnston Island (16 N, 170 W) on 11 August 1958. Details of the experiment and results are reported by Kalkstein (1962, 1963) and others (Leo and Walton, 1963). The nuclear debris cloud reportedly rose to an altitude between 100 and 150 kilometers. Most of the rhodium-102 distribution data were obtained at stratospheric levels below about 21 kilometers, the operational ceiling for U-2 sampling aircraft. A limited amount of less reliable data was obtained from balloon air filter samples up to 30 kilometers altitude. Thus the early mixing history of the rhodium-102 in the high atmosphere was not observed. However the results are consistent with initial dispersion of the rhodium-102 as individual oxide molecules or molecular cluster, gravitational sedimentation down to mesopause (near 80 kilometers altitude) in a few months, and subsequent turbulent horizontal and vertical mixing to produce approximately constant mixing ratio in a uniform world-wide layer down to the mesopeak (near 60 kilometers altitude).

The main features in the rhodium-102 tracer data obtained in the northern hemisphere stratosphere are shown in Fig. 2. These and the less abundant data for the southern hemisphere stratosphere (Kalkstein , 1962) that the initial downward mixing into the lower stratosphere takes place selectively at high latitudes in winter. Horizontal mixing in the lower stratosphere is shown to be rapid at the upper and middle latitudes down to 30 N. Mixing into the equatorial stratosphere below 20 kilometers is inhibited. The rhodium-102 concentrations near 20 kilometers in middle latitudes of the southern hemisphere are comparable to or higher than in the northern hemisphere. The approximately constant steady-state distribution in the lower stratosphere after early 1960 indicates a nearly constant vertical flux of rhodium-102 during periods of vertical mixing in winter and early spring. Rough estimation indicates a 5 to 20 year storage time for the rhodium-102 tracer. The transport of rhodium -102 across the tropopause and its rainout in the troposphere shows the expected seasonal variation with a marked spring peak (Leo and Walton, 1963).

Other radioactive tracer results

Both fission product and induced radioisotope ratio data have clarified features of the polar stratosphere behaviour. Material injected into the lower polar stratosphere as well as that which mixes into this region from lower latitudes and higher altitudes is transferred almost quantitatively into the troposphere in the early spring. The storage time increases markedly with altitude above about 20 kilometers. The recent total β radioactivity data obtained in the lower stratosphere best demonstrate the rapid lateral mixing within the lower stratosphere above above 30 N latitude.

B. RADIOACTIVE TRACER RESULTS ON EQUATORIAL STRATOSPHERE MIXING

The view that there is an organized meridional circulation in the stratosphere, with air rising through the tropopause and upwards into the equatorial stratosphere, first suggested by Brewer (1949)has received wide support. The observations of the tungsten-185 tracer by U-2 aircraft below 70,000 feet are however, best explained by large scale eddy-mixing along isentropic surfaces in the lower stratosphere (Feely and Spar 1960). Newell(1961 and 1962) discusses both the tracer and meteorological evidence and these appear to favour eddy-mixing processes but do not rule out the existence of small meridional motions. Further evidence which favours eddy -mixing , as against meridional circulation, in the equatorial stratosphere up to at least 30 kilometers is provided by equatorial balloon profile studies

(Drevinsky, Martell and Lal, 1962) and additional tungsten-185 data discussed below .

India profile

Vertical radioactivity profiles showing the total β activity and the rhodium-102 , strontium-90 and cerium-144 concentrations versus altitude over Hyderabad, India in April , 1961 are summarized in Fig. and are discussed in the last mentioned reference. These results are of special interest because they were obtained near the end of the nuclear test moratorium period , 2.5 years after the previous test (the October, 1958 Soviet tests) and nearly three years after the last equatorial tests (United States Hardtack tests, May-July 1958). The sharp increase in radioactivity concentration with altitude above the tropopause (Fig. 3) and the marked isotope variation with height augur against meridional transport with upward flow in the equatorial stratosphere. The isotope ratio variations indicate negligible vertical mixing and a stable stratification on a long time scale . The radioactivity profile is consistent with eddy-mixing along isentropic surfaces as the mechanism of transfer and with a marked increase in storage time with altitude from the tropopause to 30 kilometers.

Tungsten-185 results :

The Hardtack tests, May-July 1958, involved a number of shots which produced the 74-day half-life tungsten -185 radioactivity and injected it into several levels of the stratosphere at about 11 degrees N latitude . A considerable body of radio-tungsten data has been reported giving its subsequent distribution in the stratosphere (Stebbins, 1960, Kalkstein , 1962) in precipitation (Martell and Drevinsky 1962, Walton 1960) and in surface air (Lockhart et al 1960). U-2 aircraft observations show that the maximum in the tungsten-185 concentration persisted over the equatorial stratosphere near the point of injection (Stebbins, 1960) . The latitude distribution at 20 kilometers shows an almost inverse relation for the equatorial tungsten-185 and the high altitude rhodium-102 tracer , Fig. 4 . The stratospheric distribution pattern for the tungsten-185 is consistent with slow eddy-mixing along isentropic surfaces and with a transfer rate which rapid near the tropopause and decreases markedly with increasing altitude.

The 1959 spring peak for the tungsten-185 rainfall concentration is of special interest because such spring peaks in fallout have been associated with material originating in the lower polar stratosphere. The lack of vertical mixing in the equatorial stratosphere makes it necessary to consider the tungsten-185 source, produced in a number of shots of varying yield, as a multiple source. Such considerations, together with the spring 1959 rainfall data (Martell and Drevinsky, 1960) given in Table 1, afford a plausible explanation for the observed tungsten-185 peak. The origin of the strontium -89, Table 1, is the October 1958 Soviet test series. During the period April 6 to May 25, 1959, the time of the tungsten peak, the strontium-90 is fully accounted for by the Soviet tests. If the Sr^{89}/Sr^{90} ratio is taken as the maximum within uncertainties in the October, 1958 Soviet tests production ratio and production time, the amount of strontium-90 that can be associated with the Hardtack test origin remains too small for a W^{185}/Sr^{90} ratio equal to 380, the overall average for the Hardtack tests. However, the W^{185}/Sr^{90} ratio for Hardtack debris in the layer about 25 to 30 kilometers altitude is 1500. With this ratio during the April - May tungsten-185 peak, the data in Table 1 can be reconciled. It is concluded that the tungsten-185 in the layer about 25-30 kilometers was partially transferred into the polar stratosphere by eddy-mixing in isentropic layers and mixed downward behind the main 1959 spring peak of Soviet debris in the lower polar stratosphere. Thus the pattern of mixing and removal for material in the equatorial stratosphere above about 25 kilometers differs greatly from that near the tropopause.

<u>Seasonal variations.</u>

Seasonal variations in mixing within the stratosphere and across the tropopause as well as spring peaks in fallout have too often been explained by meridional circulation models. My initial explanation for such spring peaks was the essentially complete removal of material injected into the lower polar stratosphere following the later winter warming (Martell, 1959). Material which has mixed down into the lower polar stratosphere from higher altitudes, like the rhodium-102 tracer, and material which has mixed poleward from above 25 to 30 kilometers in the equatorial stratosphere also contribute to the spring peaks.

There is an interesting evidence of a seasonal alternation in the origin of stratospheric air which mixes across the tropopause. The isotope ratio data in rainfall during the period 1954-1958 show a dramatic shift in June or July of each year, with isotope ratios characteristic of the lower polar stratosphere in the first half of each year and of the lower equatorial stratosphere in the latter half of each year (Martell, 1959 b) . During the recent moratorium period a seasonal variation in the ratio of fission products in rains was carefully measured during 1960 and 1961 by Kuroda (1961). His Ce^{144}/Sr^{90} ratio peak occurs in the autumn and is consistent with Hardtack debris in the lower equatorial stratosphere, Fig. 3 . His minimum Ce^{144}/Sr^{90} ratio values, corresponding to debris of greatest age, occurs at the time of the spring peaks. This material is obviously a mixture of Ce^{144} and Sr^{90} from old sources in the higher stratosphere and the residual from the October, 1958 tests.

Concluding remarks

It is evident from the tungsten-185 results and other evidence given above, that eddy-mixing is the dominant mechanism of transfer within the stratosphere and that organized meridional circulations must be limited in significance even on a long time scale. The stratification of the equatorial stratosphere is well preserved, without vertical mixing or vertical displacement. At 25-30 kilometers and above the pattern of exchange with the troposphere is similar : horizontal eddy-mixing at altitude , and vertical mixing at high latitudes in winter, extending

Table 1. W^{185}, Sr^{89} and Sr^{90} in Bedford Rains, March - June, 1959 (19,22)

Sample No.	Collection Period	W^{185}	Sr^{89}	Sr^{90}	October 1958 Sr^{90}*	Hardtack Sr^{90}**
170	24 Feb-2 Mar	53.5 ± 3.6	540 ± 110	24.6 ± 1.4	20 ± 4	1.53 ± 0.11
171	2 - 4 Mar	48.8 ± 4.5	368 ± 10	19.7 ± 1.6	14.1 ± 0.4	1.44 ± 0.14
172	4 - 9 Mar	50.3 ± 3.4	310 ± 63	23.7 ± 2.4	12.4 ± 2.6	1.55 ± 0.11
182-3	6 - 13 Apr	65.6 ± 13	535 ± 17	21.6 ± 2.7	34.5 ± 2	2.8 ± 0.6
184-5	13-21 Apr	57.4 ± 1.5	399 ± 15	15.6 ± 1.3	28 ± 2	2.6 ± 0.1
187-8	27-29 Apr	81.5 ± 4.5	236 ± 30	13.1 ± 2.5	19.3 ± 3	4.08 ± 0.23
189	29 Apr-6 May	143 ± 5	303 ± 46	26.[illegible] ± 3.5	26.4 ± 4.0	7.5 ± 0.3
191-2	13-20 May	168 ± 34	292 ± 64	41.6 ± 4.4	30 ± 7	9.7 ± 2.0
193	20-25 May	29.8 ± 3.5	340 ± 50	23.9 ± 3.5	38.6 ± 6	1.83 ± 0.22
194	25 May-3 June	6.8 ± 1.4	40.7 ± 8.5	5.57 ± 0.32	5.2 ± 1.2	0.45 ± 0.10
196	8-15 June	35.1 ± 1.9	97.4 ± 7.1	19.6 ± 0.9	14.6 ± 1.2	2.64 ± 0.15
197	15-18 June	127 ± 15	185 ± 15	34.1 ± 3.8	30 ± 2.5	9.9 ± 1.2
203	26-29 June	11.1 ± 1.4	60.0 ± 9.5	10.9 ± 2.2	11.3 ± 1.8	0.98 ± 0.13

* Based on activity ratio Sr^{89}/Sr^{90} = 170 on 10/15/58 and $t_{1/2}$ of Sr^{89} = 51 days.

** Based on activity ratio W^{185}/Sr^{90} = 380 on 6/15/58 and $t_{1/2}$ of W^{185} = 74 days.

downward across the tropopause in late winter. A seasonal variation in origin of the stratospheric air which mixes across the tropopause is indicated, with a high latitude origin from January to June and origin in the lower equatorial region (tropopause to about 25 kilometers) from July to December.

REFERENCES:

Bhandari, N. and Rama : 'Atmospheric circulation from observations of sodium -22 and other short-lived natural radioactivities', J. Geophys. Res. 68, 1959-1966 1963.

Chagnon, C. W. and C. E. Junge : 'The vertical distribution of submicron particles in the stratosphere', J. Meteor, 18, 746-752, 1961.

Drevinsky, P. J, and E. A. Martell : ' Preliminary results on the size and vertical distributions of residual nuclear debris in the stratosphere', Proc. AEC Conf. on Radioactive Fallout from Nuclear Weapons Tests Nov. 1961 ; AEC Rpt. TID-7632, Part 1, 1962.

Drevinsky, P. J., E. A. Martell and D. Lal : Chapter IV in Joint Indo-United States Balloon Flight Progam -1961. AFCRL -62-1135, 1962.

Drevinsky, P. J., J. T. Wasson, E. C. Couble and N. A. Dimond : 'Be^7, P 32, P^{33} and S^{35} -Stratospheric concentrations and artificial production ', in press J. Geophys. Res., 1963.

Feely, H. W., and J. Spar : ' Tungsten-185 from nuclear bomb tests as a tracer for stratospheric meteorology ', Nature 188, 1062, 1960.

Kalkstein, M. I. : 'Rhodium-102 high altitude tracer experiment', Science 137, 645-652, 1962.

Kalkstein, M. I. : 'Results for the Rh^{102} high altitude tracer experiment, I . Stratospheric concentrations ', AFCRL 62-460 (I), 1962.

Kalkstein, M.I. : Movement of material from high altitude deduced from tracer observations', J. Geophys. Res. 68, 3835-3839, 1963.

Kuroda, P.K. : 'Radioactive fallout ', Annual Rpt. to USAEC Contract AT-(40-1)-2529, December 1961.

Lal, D. : 'Cosmic ray produced radioisotopes for studying the general circulation in the atmosphere', Indian J. Meteor. Geophys. 10, 147-154, 1959.

Lal, D., P.K. Malhotra and B. Peters : 'On the production of radio-isotopes in the atmosphere by cosmic radiation and their application to meteorology ', J. Atm. Terr. Phys. 12, 306-328, 1958.

Lal, D. and B. Peters : 'Cosmic ray produced isotopes and their applications to problems in geophysics', Prog. Cos. -Ray Elem. -Part Phys. 6 , 1 - 74, 1962.

Leo, M.W.M. and A. Walton : 'Rhodium-102 fallout : variations in deposition and concentration in precipitation', Science 140, 1398-1400 , 1963

Lockhart , L.B. et al : 'Fission product radioactivity in the air along the 80th meridian (West) during 1959 ', J. Geophys. Res. 65, 3987 - 3997 , 1960.

Manson, J.E. : 'The interaction between radioactive and non-radioactive particles in the stratosphere ', AEC Rpt TID-7632, Part 1, Feb. 1962.

Martell, E.A. : 'Atmospheric aspects of strontium-90 fallout ', Science 129, 1197-1206, 1959 (a).

Martell, E.A. : 'Global fallout and its variability ', in Fallout from Nuclear Weapons Tests, JCAE 810-840, 1959. (b)

Martell, E.A. and P.J. Drevinsky : 'Atmospheric transport of artificial radioactivity ', Science 132 , 1523-1531 , 1960

Martell, E.A. : 'Evidence for high stratosphere holdup of nuclear bomb debris', Proc. Upper Atmos. Sampling Symp. April 1961, SCR-420 , Sandia Corp , July 1961.

Newell, R.E. : *Geofisica Pura e Applicata* 49, 137, 1961.

Newell, R.E. : 'Transfer through the tropopause and within the stratosphere', MIT Planetary Circulations Project 7, Oct. 1962.

Rama and M. Honda : 'Natural radioactivity in the atmosphere', *J. Geophys. Res.* 66, 3227-3231, 1961.

Stebbins, A.K. : Special report on the high altitude sampling program, DASA 532B , Washington 1960.

Walton, A. : *Nature* 188 , 220, 1960.

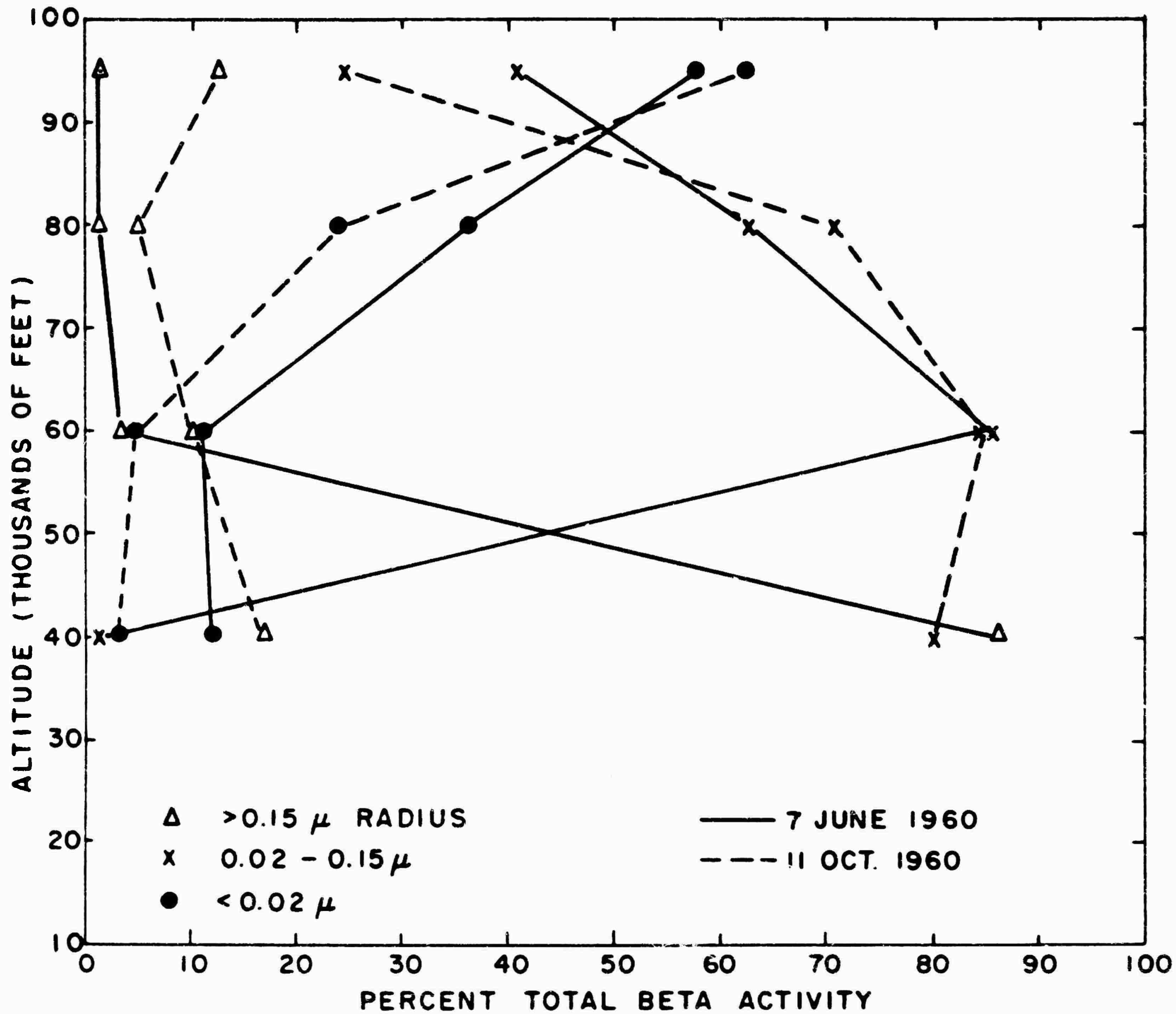

Figure 1. Size distribution of radioactive particles vs latitude in the stratosphere.

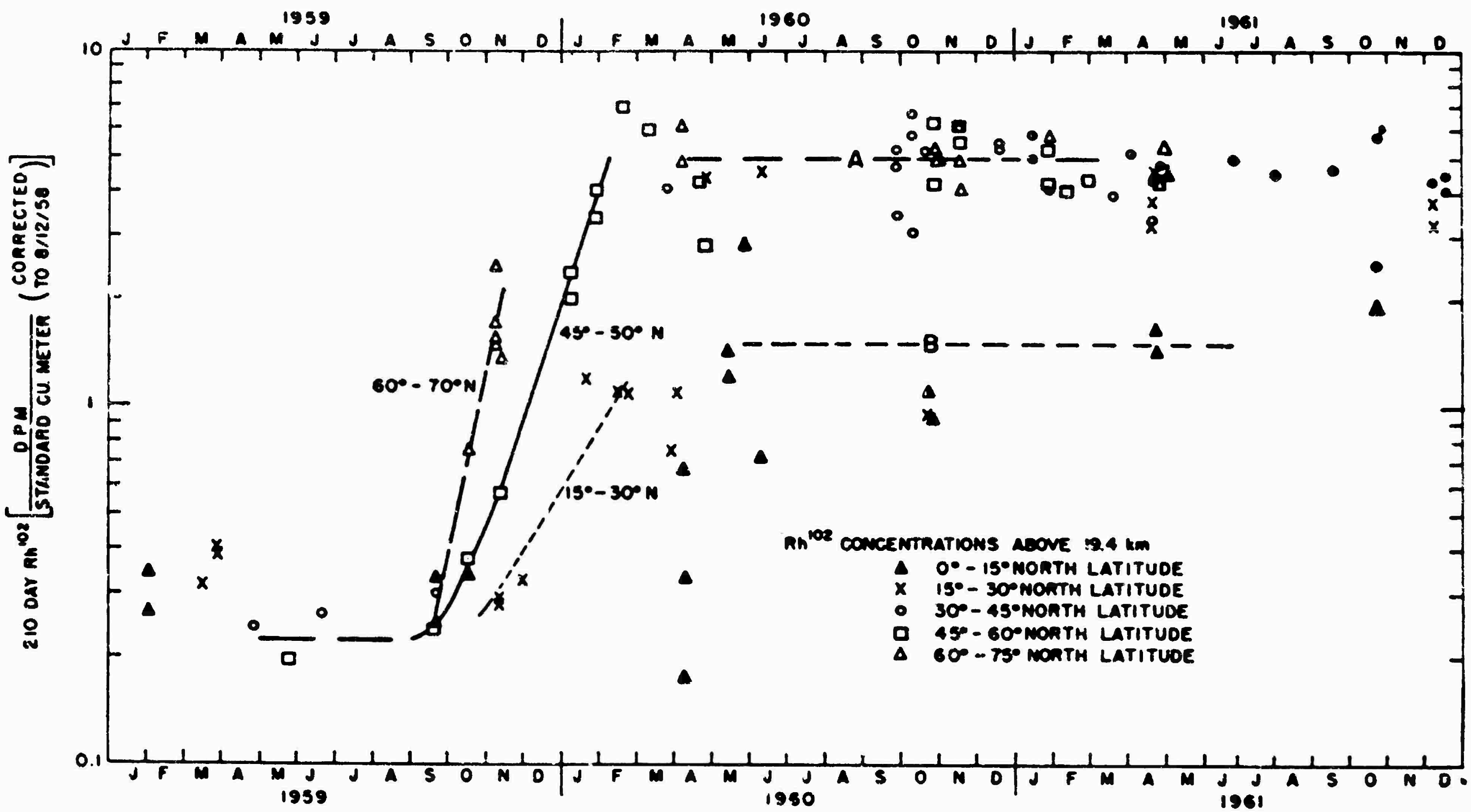

Figure 2. Rhodium-102 concentrations above 19.4 kilometers in the Northern Hemisphere (Dashed lines A and B represent approximate mean high latitude and low latitude concentrations, respectively.)

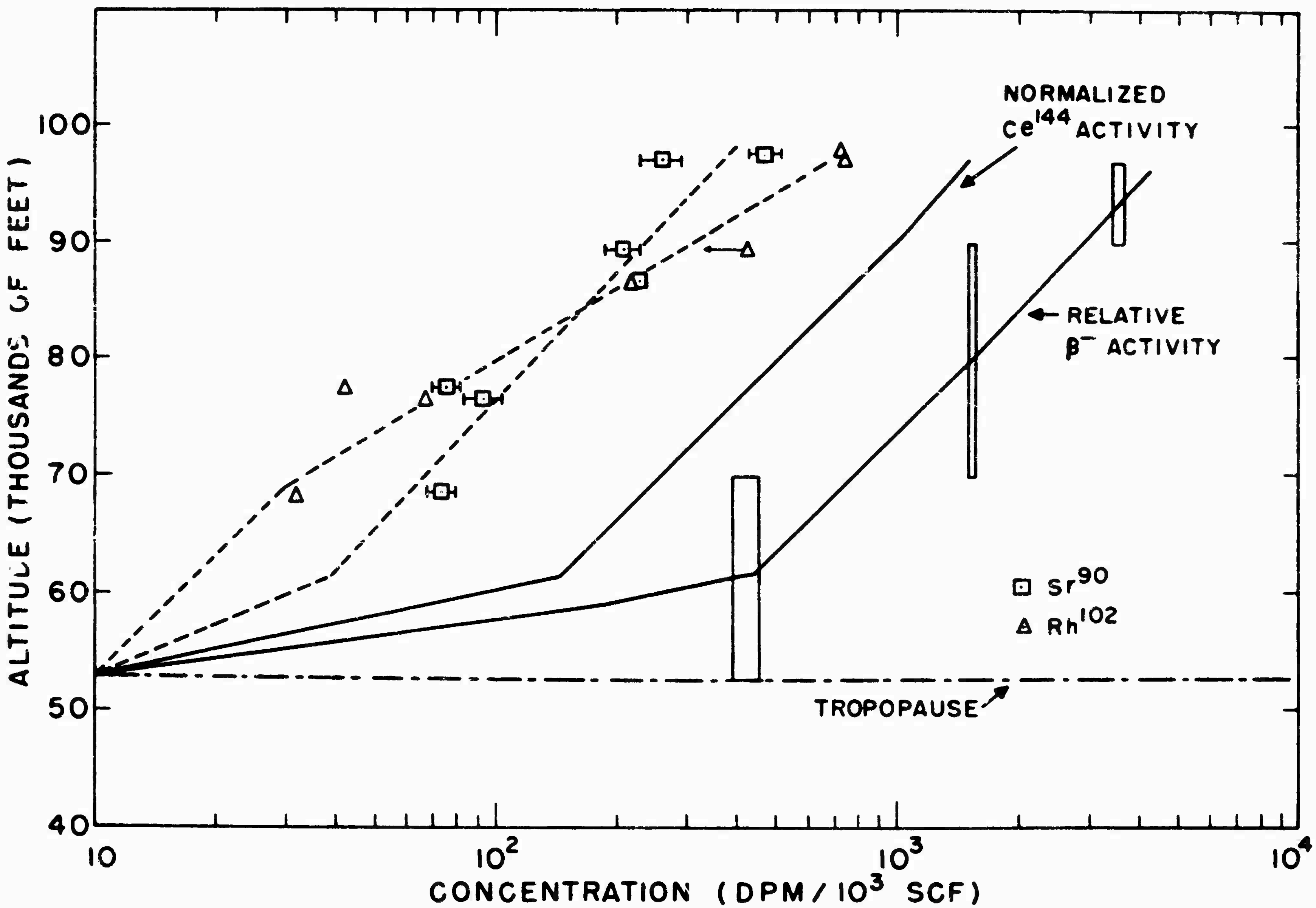

Figure 3. Concentrations of Ce^{144}, Sr^{90} and Rh^{102} vs altitude over Hyderabad, India, 20 April 1961.

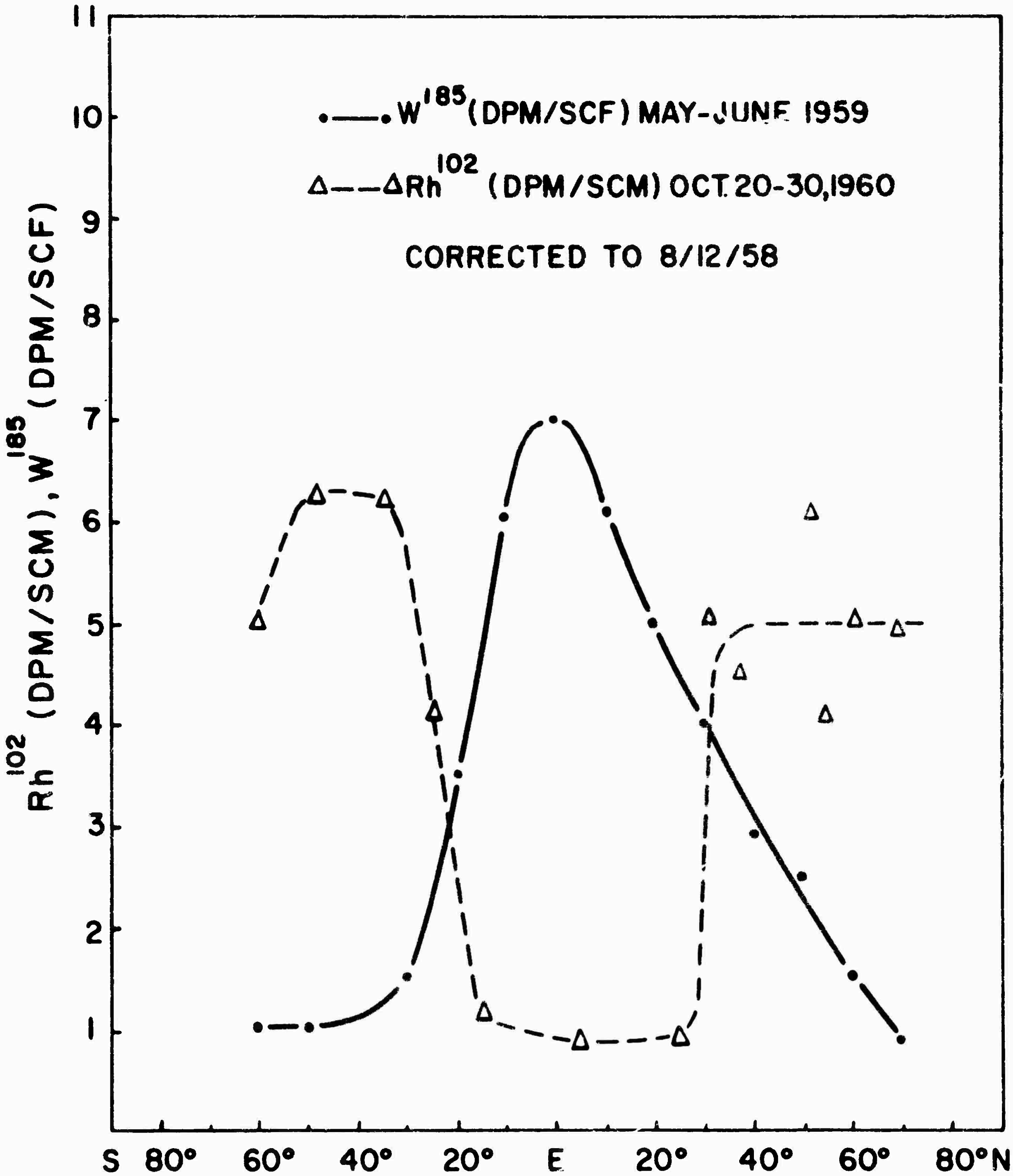

Figure 4. Latitude distribution of high altitude rhodium-102 and equatorial tungsten-185 at ~ 20 kilometers altitude.

THE DISTRIBUTION OF TOTAL OZONE

J. London

Although ozone is formed in the atmosphere as a result of photochemical processes, its geographic distribution and time variation are strongly modified by atmospheric transport processes. According to photochemical theory, the ozone concentration should increase with height to a maximum at about 25 to 30 km and then decrease above. Also, at all heights, there should be an equatorial maximum and at almost all heights and latitudes there should be a maximum during the summer. Observations made over the past thirty years of both total ozone and the vertical ozone distribution show that only at levels above about 35 km does the observed ozone distribution correspond to that predicted by photochemical theory. It is by now well established that the largest differences between observed and theoretical ozone amounts occur at high latitudes during the Winter and Spring. A time-latitude cross section of observed total ozone amounts (London, 1963) indicates minimum total ozone at the equator and increasing amounts poleward during all seasons. The maximum total ozone occurs at subpolar latitudes during the late Winter and Spring. The largest latitudinal gradients are found during the Spring in mid-latitude.

The following table gives a comparison between the photochemical equilibrium (theory) and observed amounts of total ozone (values are in 10^{-3} atmo-cm).

		0^{o}	30^{o}	60^{o}	80^{o}
Summer	Photochemical (theory)	345	400	204	105
	Obs.	255	290	345	345

Winter	Photochemical (theory)	345	167	027	--
	Obs.	240	285	372	362

For the hemispheric averages we have

	observed	theory
Winter	298	171
Spring	330	---
Summer	297	347
Fall	274	---
Annual	299	259

It is well known that variations of total ozone are closely related to the pressure distribution at the surface and aloft. In the troposphere low pressure areas are associated with high total ozone amounts and vice-versa. Recent studies of the 500 mb contour field as related to the total ozone distribution in Europe and mid-west U.S. have shown that the ozone distribution is best related to the contour pattern when the pressure system is extensive and quasi-stationary. An analysis of the distribution of total ozone over the Northern Hemisphere for each of the seasons shows that the total ozone is a minimum at equatorial latitudes and everywhere increases poleward. At the same time, however, there are marked longitudinal variations in the ozone patterns particularly at polar latitudes during the winter and spring. Strong ozone ridges are found over eastern North America, eastern Asia and central Europe. These ridges are closely related to the upper tropospheric and lower stratospheric contour patterns where contour troughs are found in the positions corresponding to the ozone ridges. Also ozone patterns are most pronounced during winter and early spring corresponding to the time when the upper level circulation patterns are best developed. It is obvious that the mean longitudinal variation of total ozone is associated with standing waves in the contour field of the lower stratosphere. The observed hemispheric distribution of ozone has been further discussed by London (1963).

It is of considerable interest and importance to understand by what methods the photochemistry and atmospheric transport combine to produce the observed ozone distribution.

As was pointed out above, ozone is formed in the stratosphere as a result of the near balance between the photochemical processes producing and those destroying ozone. Below about 35 km ozone is produced and destroyed very slowly. This is particularly so at high latitudes during the winter. Thus ozone which is transported vertically downward from its source region and poleward will persist for long periods of time despite the fact that the ozone concentration may be largely in excess of its photochemical equilibrium amount. As a result, ozone may be pumped downward and poleward by the action of the vertical and horizontal components of the vigorous stratospheric circulation during the winter. At the end of winter, the horizontal temperature gradients weaken and the stratospheric gradients weaken and the stratospheric circulation is characterized by weaker north-south transport. During the interval from spring to fall the ozone distribution tends to return to its photochemical equilibrium value. This return, however, is very slow in the lower stratosphere particularly in polar regions. The observed ozone distribution is then a result of both photochemical and stratospheric transport processes.

If we consider a quasi-static distribution of ozone (averaged for each season) we can write a differential equation for the equilibrium ozone amount as a function of the photochemical production and destruction and the mean and eddy components of the horizontal and vertical motions in the stratosphere. The resulting numerical solution after incorporating suitable assumptions of the various photochemical and atmospheric parameters, including the horizontal and vertical eddy exchange coefficients, reproduce the observed vertical, latitudinal and temporal distribution of ozone. That is, the resulting solution shows

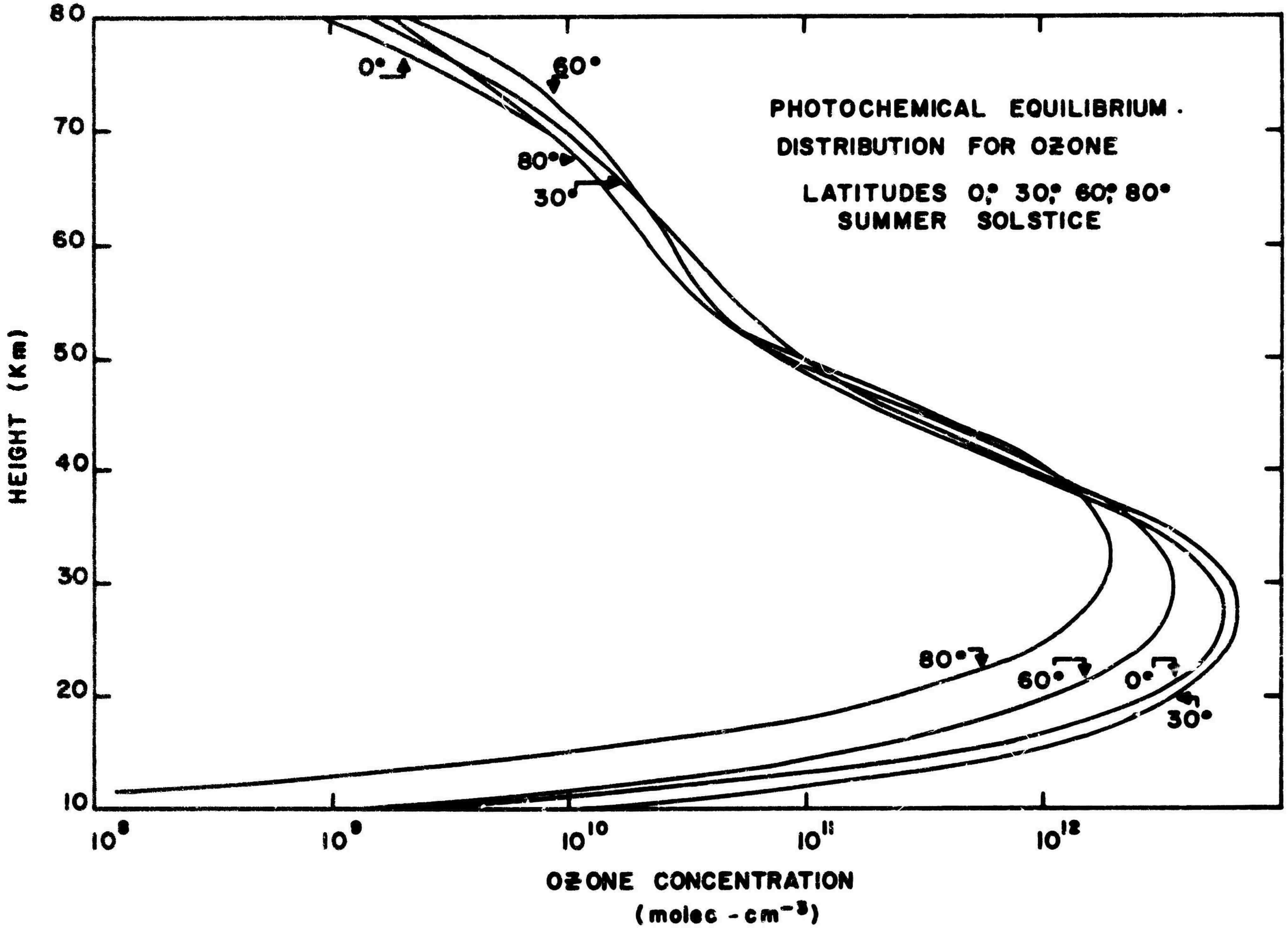
PHOTOCHEMICAL EQUILIBRIUM ·
DISTRIBUTION FOR OZONE
LATITUDES 0°, 30°, 60°, 80°
SUMMER SOLSTICE
HEIGHT (Km)
80
70
60
50
40
30
20
10
10^8
10^9
10^{10}
10^{11}
10^{12}
0°
60°
80°
30°
80°
60°
0°
30°
OZONE CONCENTRATION
(molec - cm^{-3})

Fig. 1

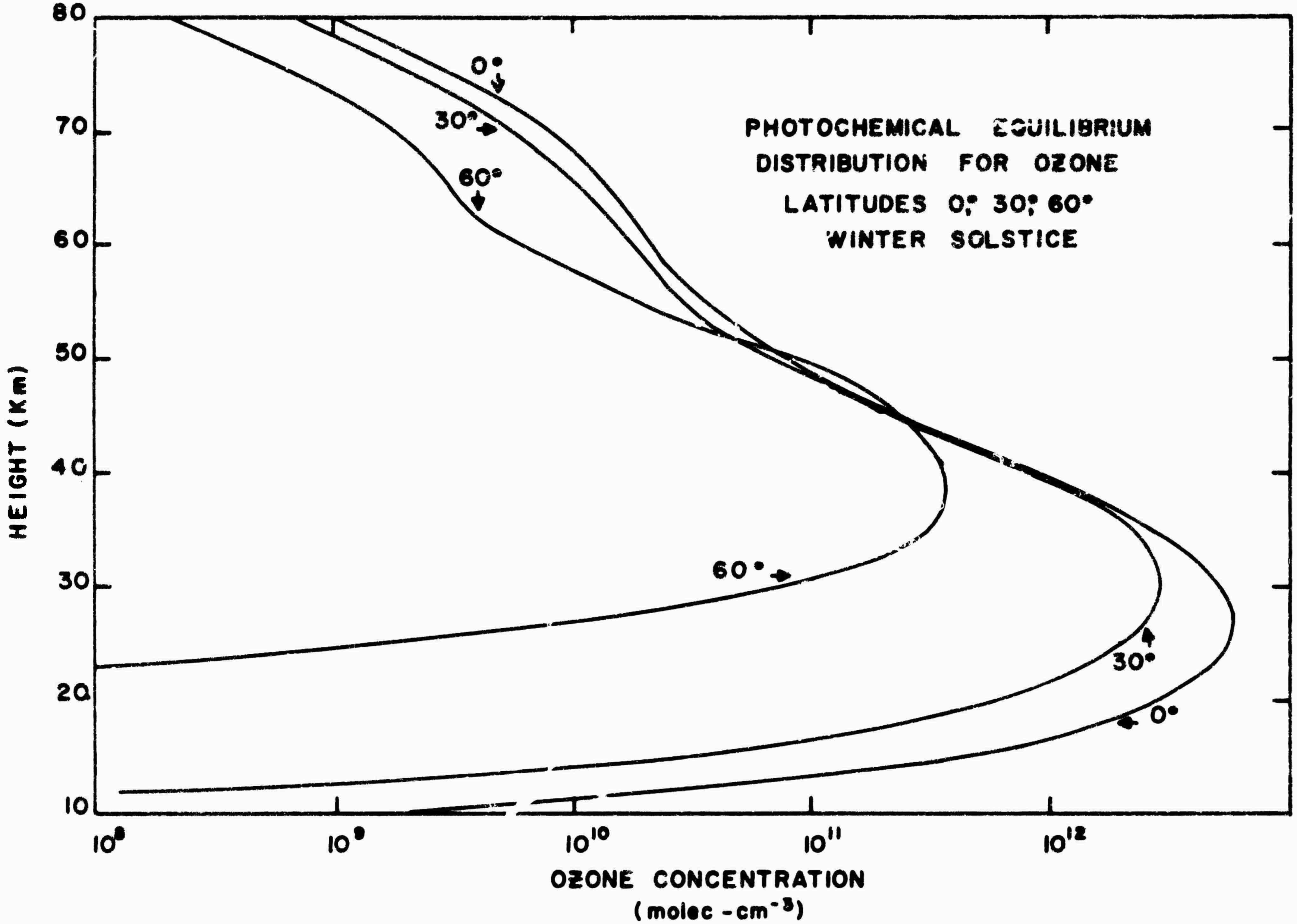
PHOTOCHEMICAL EQUILIBRIUM
DISTRIBUTION FOR OZONE
LATITUDES 0°, 30°, 60°
WINTER SOLSTICE
0°
30°
60°
60°
30°
0°
HEIGHT (Km)
80
70
60
50
40
30
20
10
10^8
10^9
10^{10}
10^{11}
10^{12}
OZONE CONCENTRATION
(molec - cm^{-3})

Fig. 2

a maximum during spring and minimum during fall as is observed. Details of the theoretical computations are given by Prabhakara (1962) and London and Prabhakara (1963).

REFERENCES :

London, J. : 'The distribution of total ozone in the northern hemisphere', (to be published in Beitrage zur Physik der Atmosphare, 1963).

London, J. and C. Prabhakara : ' The effect of stratospheric transport processes on the ozone distribution', Met. Abhandl. , Inst. f. Meteor. u. Geophys. Freien Universitat Berlin, XXXVI, 1963.

Prabhakara, C. : 'Effects of non-photochemical processes on the meridional distribution and total amount of ozone in the atmosphere', (Ph.D. thesis) Dept. of Meteorology and Oceanography, New York University, 1962 .

An Analysis of Ozonesonde Measurements Over North America

W. S. Hering

The development of an effective balloon-borne ozonesonde instrument by V. Regener (1960) has led to a systematic study of the vertical ozone distribution over North America. A network of eleven observational stations was established in January 1963 by the Air Force Cambridge Research Laboratories with the cooperation of the Air Weather Service, Canadian Meteorology Branch, and five universities in the United States. The 1963 schedule of ozonesonde measurements consists of ascents each Wednesday at 1200 Z at each of the stations listed in Table 1. In addition, a special synoptic series of daily observations were programmed for the period 29 April to 10 May.

Some of the general features of the vertical ozone distribution as revealed by the initial results from the network program are shown in Figures 1 -3.

Figure 1 shows the characteristic structure of the equatorial ozone profile during the late winter and spring 1963. Little variation is observed from week to week in the Canal Zone ascents. The ozone concentration remains low throughout the well-mixed troposphere. The profiles invariably show a rapid increase in ozone amount with elevation beginning abruptly at the equatorial tropopause and extending to the region of maximum partial pressure near the 20-mb level. Variations in the vertical ozone distribution are for the most part limited to small-scale oscillations and there is no evidence of significant impulsive vertical transport in the vicinity of the tropopause. The observed distribution tends to conform to the profile computed for the equatorial region from photochemical theory by London and Probhakara (1962), assuming equilibrium between ozone formation and distruction processes. Although many uncertainties remain in the photochemical calculations, the over-all deficit of observed ozone with respect to equilibrium amounts seems to be distributed over a large altitude range in the stratosphere.

The high latitude winter profiles present a totally different picture. As shown in Figure 2, the observed ozone concentrations in the lower and middle stratosphere in the polar region are very large in comparison with the indicated photochemical equilibrium values. Strong oscillations in the ozone profiles occur in association with the systematic northward and downward transport. The downward ozone flux in the lower stratosphere appears to be particularly significant above and on the poleward side of the zonal wind maximum in the upper troposphere. Major excursions of stratospheric ozone into the troposphere are rather infrequent and usually confined to the region immediately east and north of jet-stream troughs.

Figure 3 shows the average distribution of ozone particle pressure as observed for the months of January and February 1963 along the profile extending from the Canal Zone to Greenland. The level of maximum partial pressure is near 25 km over the equator sloping downward gradient in ozone concentration maintained in the tropopause-gap region is clearly evident on the mean cross section.

TABLE 1 Ozonesonde Network

Station	Latitude(deg.N)	Longitude(deg.N)
Albrook Fld, Canadal Zone (AWS)	9.6	79.6
Colorado State University, Fort Collins	40.6	105.1
Eielson AFB, Fairbanks, Alaska(AWS)	64.8	147.9
Florida State University, Tallahassee	30.4	84.3
Fort Churchill, Manitoba (Can. Met. Br.)	58.8	94.1
Goose Bay, Labrador (Can. Met. Br.)	53.3	60.4
L.G. Hanscom Fld., Bedford Mass.	42.5	71.3
Thule AFB, Greenland (AWS)	76.5	68.8
University of New Mexico, Albuquerque	35.0	106.6
University of Washington, Seattle	47.4	122.3
University of Wisconsin, Madison	43.1	89.4

REFERENCES

London, J. and C. Probhakara : 'Absorption processes in the stratosphere and mesosphere', Final Rpt. Contract No. AF 19(604)5492 , New York Univ., 1962.

Regener, V.H. : 'On a sensitive method for the recording of atmospheric ozone ,' J. Geos. Research, 65, No. 12, 1960.

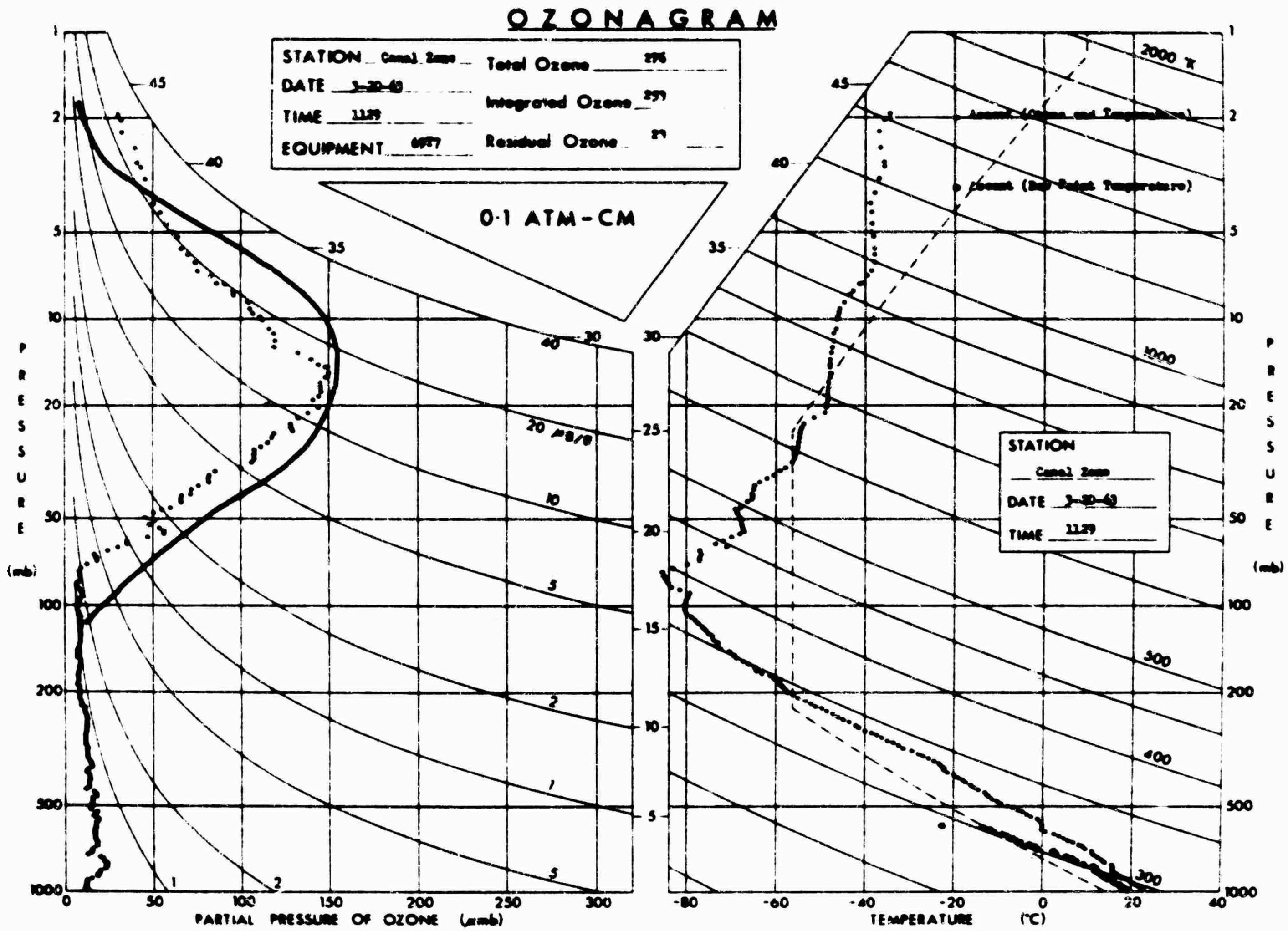

FIGURE 1

Ozone and temperature profiles(dotted lines) for Albrook Field , Canal Zone , on 20 March 1963. Dew point values are indicated by open circles. Heavy line gives the photochemical equilibrium distribution calculated by London and Probhakara.

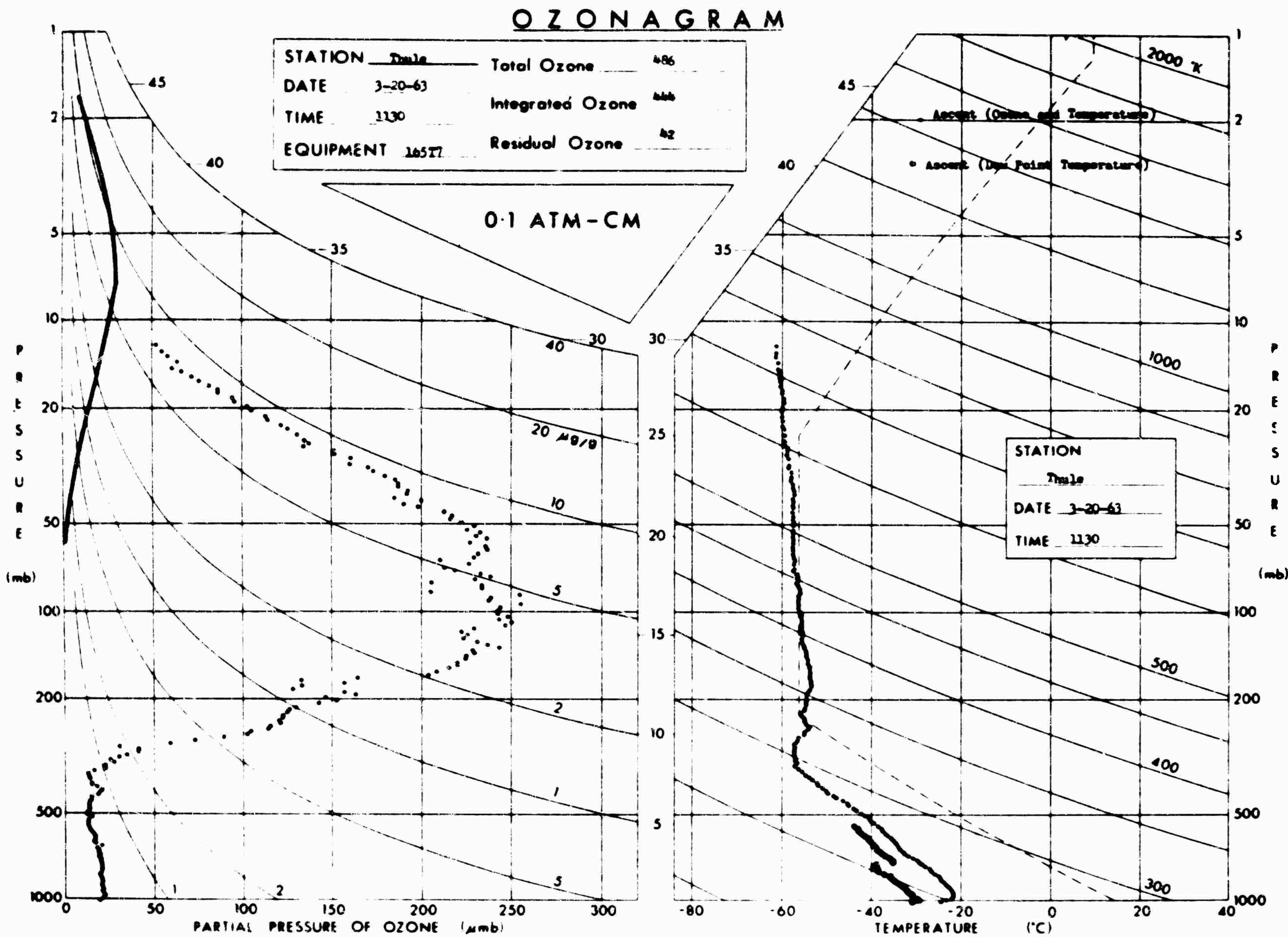

FIGURE 2

Ozonesonde and radiosonde observations for Thule AFB, Greenland, 20 March 1963

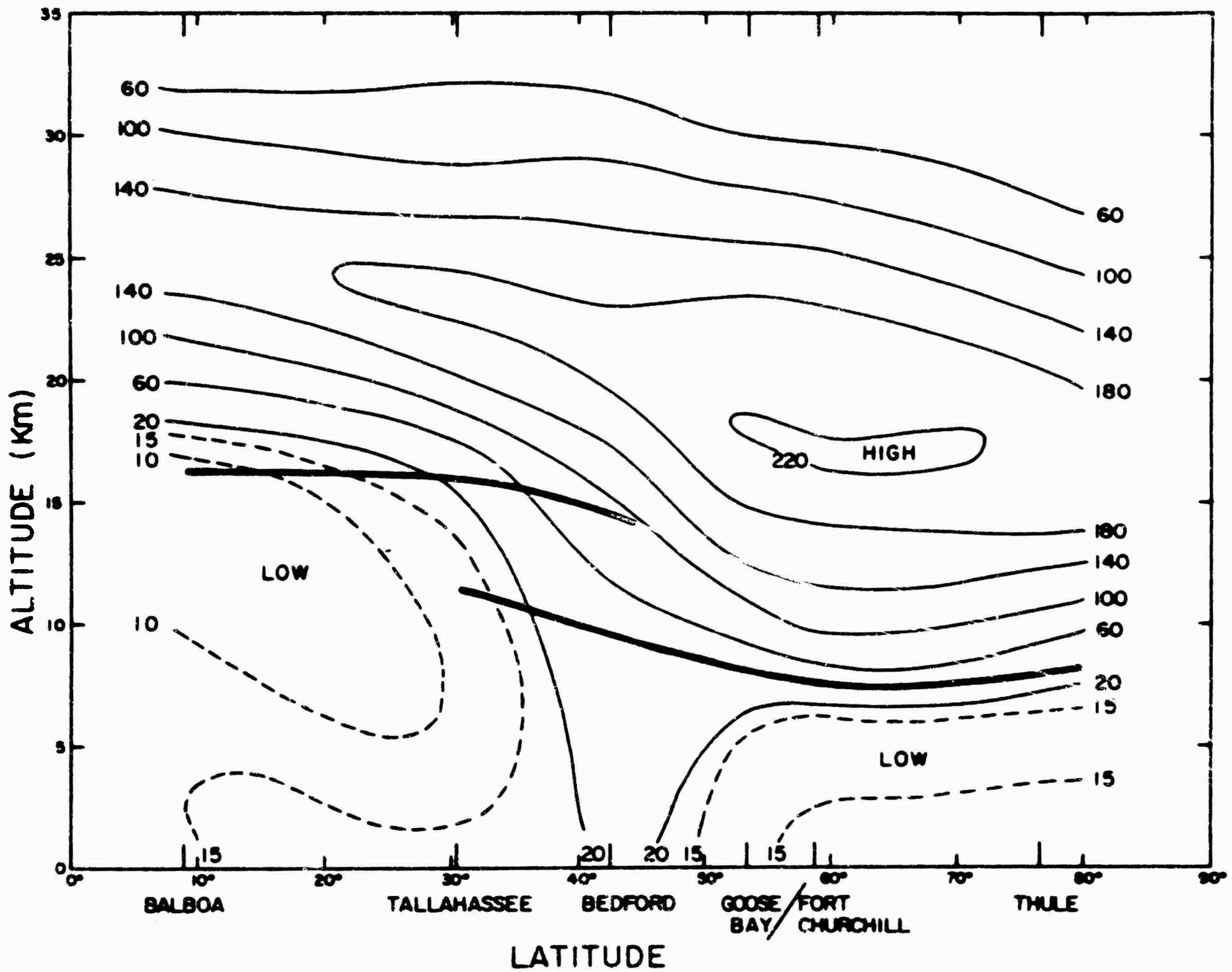

FIGURE 3

Average distribution of ozone partial pressure in micro-millibars for January and February 1963 for the cross section extending from the Canal Zone to Thule AFB, Greenland. The heavy line is the mean height of the tropopause as determined from the radiosonde observations obtained in conjunction with the ozonesonde ascents.

VARIATION OF TOTAL OZONE AND VERTICAL OZONE DISTRIBUTION

M. Shimizu

In order to separate and compare the effects of Ferrel disturbances and middle stratospheric phenomena on total ozone amounts correlation coefficients of O_3 vs H and O_3 vs Z were examined, using the linear regression equation $O_3 = a + bH + \underline{CZ}$, where H was the 500 mb height and Z the 30 - 100 mb thickness. Using data at Edmonton (Jan. 1959 - Dec. 1961) the calculation was carried out on both daily values and day-to-day changes; the former showed periodicities of about 8 and 17 days and the latter about 5 days. O_3 values used were 2-day running means of local noon observations; H and Z values were 0000Z values, unsmoothed.

Results show that roughly speaking, the :

1. O_3-H relationship is good from spring to autumn.
2. O_3-Z relationship for daily values is good from late summer to late winter and for day-to-day changes in autumn.
3. Correlation coefficients in winter vary widely year-to-year , depending on winter conditions.
4. Multiple correlation coefficients of O_3 on H and Z are nearly 0.7 - 0.8 for daily values and 0.6 - 0.7 for day-to-day changes throughout the year.

The seasonal character of the two effects on ozone values was examined by using the marches of the two partial correlation coefficients of O_3 - H (constant Z) and of O_3 -Z (constant H)(Fig. 1)

(a) In winter the middle stratospheric polar vortex affects total ozone amounts strongly giving good correlation of O_3 - Z. When the Ferrel jet retreated southward, as in 1959 - 60 winter, the

O_3 - Z correlation was poor, but when the Ferrel system remained over Edmonton, as in 1960 -61 winter, the O_3 - H correlation was as good as the O_3 - Z.

(b) In spring, after breakdown of the polar vortex, and as the Ferrel westerlies return to higher latitudes, the O_3 - Z relation becomes worse and the O_3 - H relation recovers.

(c) In summer , since the lower stratosphere is wholly governed by the Ferrel system , the O_3-H relation is fairly good. In July - August the O_3 - Z relation for daily values recovers, implying that longer period ozone change begins in the middle stratosphere, while the O_3 - Z relation for day-to-day changes recovers in September-October.

(d) In autumn the quasi-isothermal stratosphere, the minimal horizontal gradient of ozone and control by the Ferrel system of the middle stratosphere produce good correlations both of O_3 - H and O_3 - Z.

As an example of ozone-middle stratospheric relations, ozone changes during the sudden warming in January 1963 were studied (Fig. 2) . After the 14th, at Goose Bay, ozone amount and 50 mb temperature both decreased until the 20th. On the 20th, the warm centre at 30 mb made its closest approach to Goose Bay and the cold centre at 30 mb was near Edmonton. As the cold centre moved away from Edmonton, the warm centre approached Hudson Bay, ozone at Edmonton increased. At Goose Bay, the correlation coefficient between total ozone and 50 mb temperature in January was 0.97, suggesting that strong subsidence in the warm centre governed completely the ozone amount. At Edmonton, the correlation coefficient was only 0.36 , implying that the effect of advection was comparatively strong.

Using eleven vertical ozone distributions obtained by the ozonesonde observations at Goose Bay (Jan. 19th - Mar. 27th, 1963) ozone changes in late winter were examined. Mean ozone partial pressure had a maximum of about 230 mb close to the 50 mb level.

The level of maximum mixing ratio of about 10 mg/g was found usually near 25 km. Variability of ozone partial pressure (or mixing ratio) was large in the lower stratosphere, corresponding to a secondary maximum of vertical ozone distribution. When the tropopause was low, ozone amounts in the 200 - 500 mb layer increased. The ozone amount in the 30 mb-tropopause layer accounted for more than 90% of the change of total ozone. Even middle stratospheric ozone in the 30 - 100 mb layer had a good correlation with 500 mb height, because the Ferrel system expanded up to the middle stratosphere.

Figure 1. The changes of partial correlation coefficients from January - February 1959 to November - December 1961 at Edmonton. $r_{23.1}$ and $r'_{23.1}$ are the correlations between 30-100 mb thickness and ozone amount keeping 500 mb height constant, for daily values and for day-to-day changes, respectively. $r_{13.2}$ and $r'_{13.2}$ are the correlations between 500 mb height and ozone amount keeping 30 - 100 mb thickness constant, for daily values and for day-to-day changes respectively.

Figure 2. Left : Total ozone amounts and 50 mb temperatures at Goose Bay and Edmonton in January 1963.
Right: Movements of the warm centres and cold centres at 30 mb level, during the sudden warming.

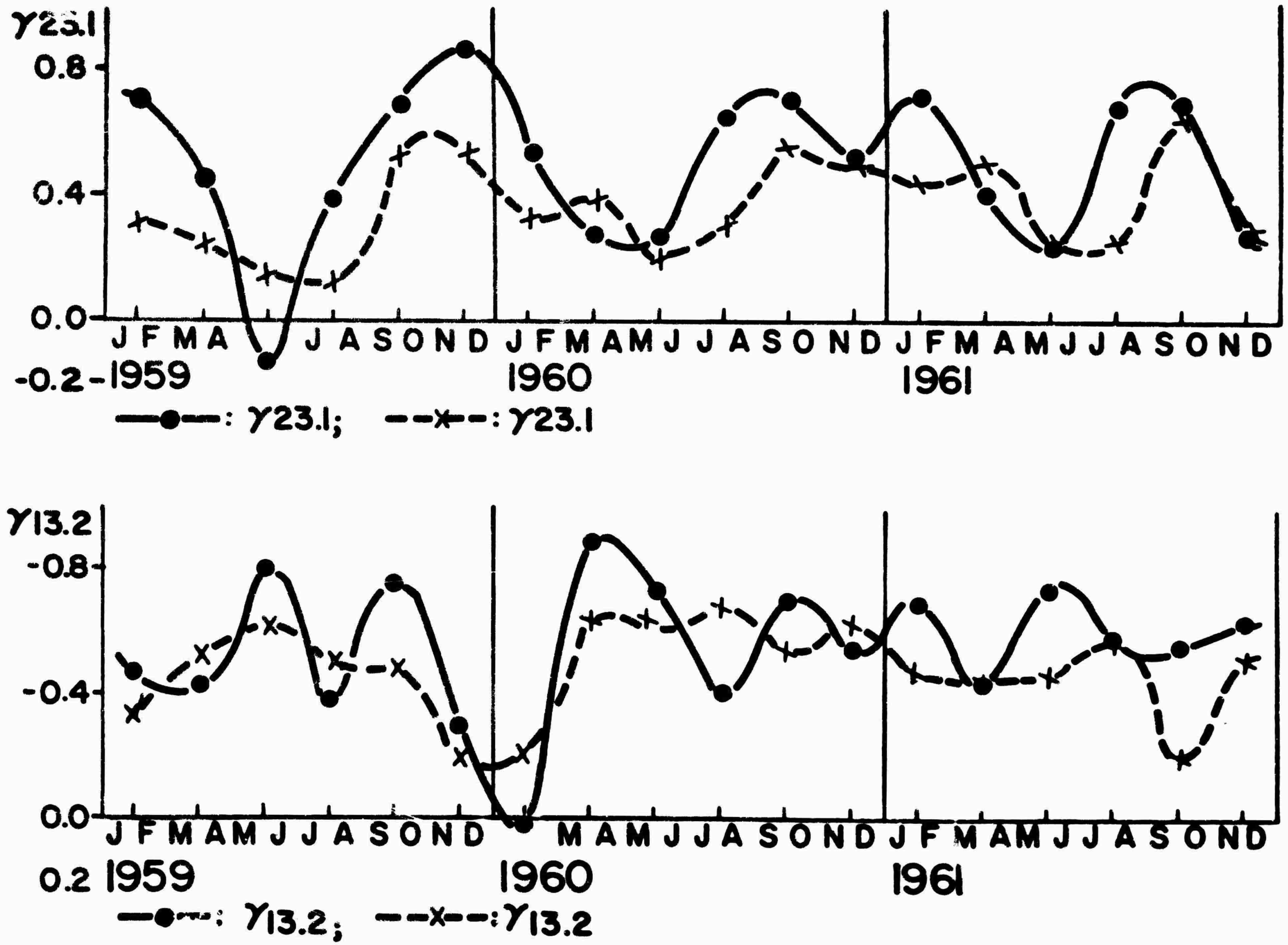
γ23.1
0.8
0.4
0.0
-0.2
J F M A J A S O N D J F M A M J J A S O N D J F M A M J J A S O N D
1959
1960
1961
—●—: γ23.1; --×--: γ23.1
γ13.2
-0.8
-0.4
0.0
0.2
J F M A M J J A S O N D M A M J J A S O N D J F M A M J J A S O N D
1959
1960
1961
—●—: γ13.2; --×--: γ13.2

FIGURE 1.

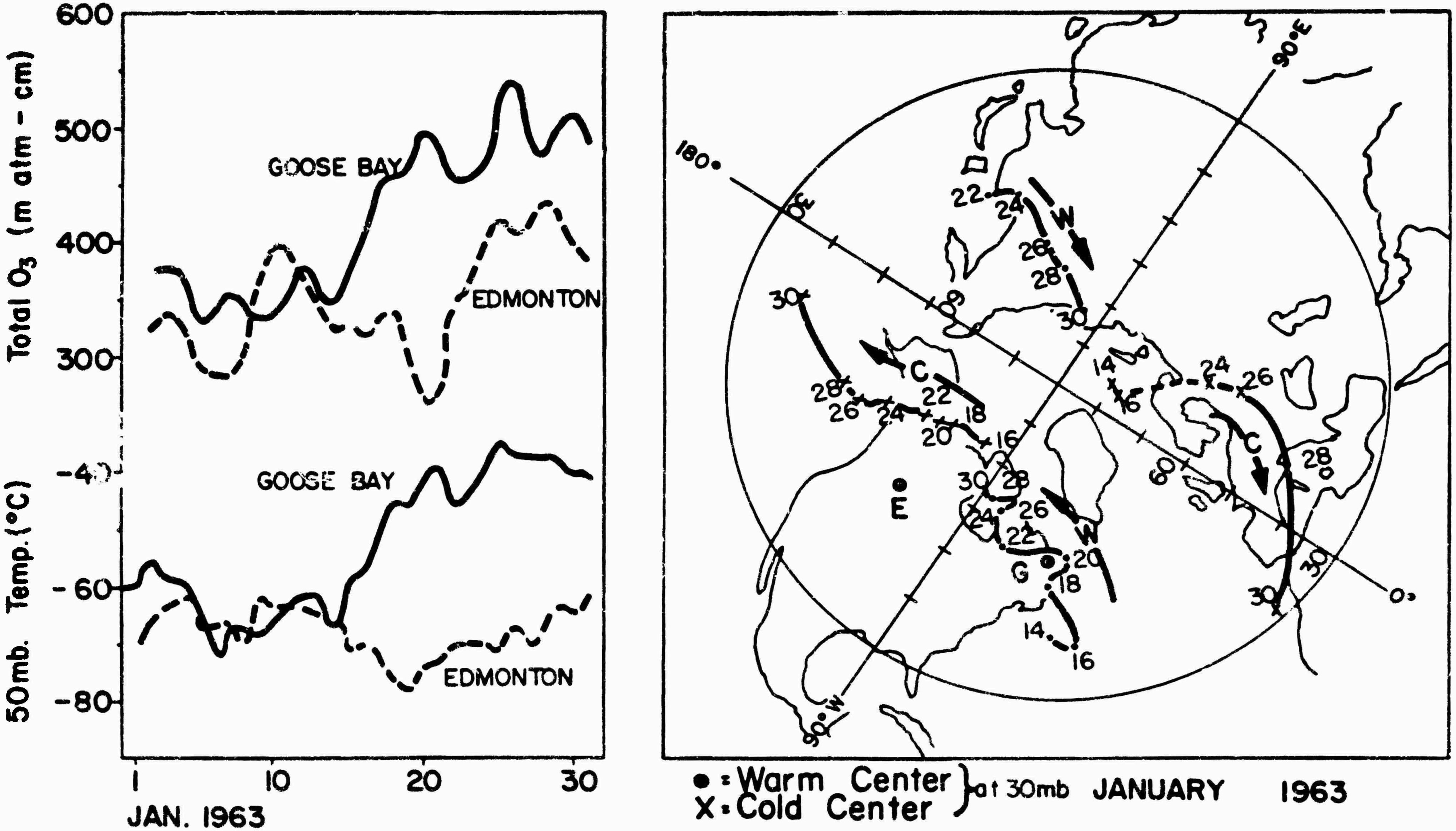

Total O_3 (m atm - cm)
50mb. Temp. (°C)
600
500
400
300
-40
-60
-80
GOOSE BAY
EDMONTON
GOOSE BAY
EDMONTON
1
10
20
30
JAN. 1963
180°
90°E
0°
90°W
W
C
C
W
E
G
● : Warm Center
X : Cold Center
at 30mb
JANUARY 1963

FIGURE 2.

PRELIMINARY AIRCRAFT OBSERVATIONS OF OZONE IN THE STRATOSPHERE

S. Penn

The first measurements of ozone taken along nearly horizontal trajectories in the middle stratosphere were presented. The Regener instrument which is employed in the A.F. C.R. L. ozone programme was used. These aircraft flights are part of that programme.

Four flights were analyzed, one from Florida to Boston, the second from southern California to Florida, the third from Florida to Wisconsin, and the fourth from Florida to Kentucky. Observations were made every 15 seconds; however, the analyses are based upon observations taken every third minute or about 20 miles apart. The values have not been smoothed, and each measurement represents an air strip about 0.1 miles long.

From the flight of February 8, 1963, Florida to Boston at 62 to 68 mb, the data *proved to be very reliable when one compared values from the northward flight with those from the return southward flight. The 50-mb flow and ozone cross-section for this case are shown in Figs. 1 and 2.

The flight of February 6, 1963, from Edwards AFB, California, to Florida is shown on the 50-mb map in Fig. 3. The measured ozone mixing ration in this flight increases in northern New Mexico from 2.2 to 3.8 μg/gm. In the southeastern U.S.A. it shows a strong north-south gradient as indicated by the 4.0 μg/g value in South Carolina which decreases rapidly to 3.3 μg/g at the

* Ozone in parts per million (μg/g)

southern end of the flight (off the coast of northern Florida). Trajectory considerations seem to account for these variations, with the high concentrations associated with air which has had a long history from the north.

The Florida-Wisconsin return flight on February 13, 1963 proceeding northward at 63 mb and returning at 56 mb pointed to a large variation in ozone in the vicinity of Atlanta, Ga. Amounts to the north of this zone were uniformly low. Again trajectory considerations indicate that Atlanta is near a confluence zone with the larger ozone concentrations representing flow about a Canadian vortex.

On February 15, 1963, the aircraft made two return flights between Atlanta, Georgia and Louisville, Kentucky at heights between 70 and 50 mb. At 70 mb a strong gradient of ozone was found from Atlanta to Nashville, Tennessee. At 50 mb there was little variation in the ozone concentration. Here two trajectory considerations from the 50 and 100 mb levels suggest that a confluence zone is present at 70 mb in the vicinity of Atlanta, Georgia.

<u>Figure 1.</u> This chart shows the 50 mb isotherms and streamlines. The flight track is along the east coast at 62-68 mb with ozone concentrations (μg/ g) at significant points.

<u>Figure 2.</u> A return flight record of ozone concentrations is shown, with dots indicating the northward track and X's the southward track.

<u>Figure 3.</u> This chart shows a track from California to Florida. Bold numbers are ozone concentrations with the pressure height of each observation beneath. Balloon network data are also plotted, and underlined figures show vertical displacements in mb/day. Tallahassee, Florida (4.0) shows a "normal" concentration of ozone.

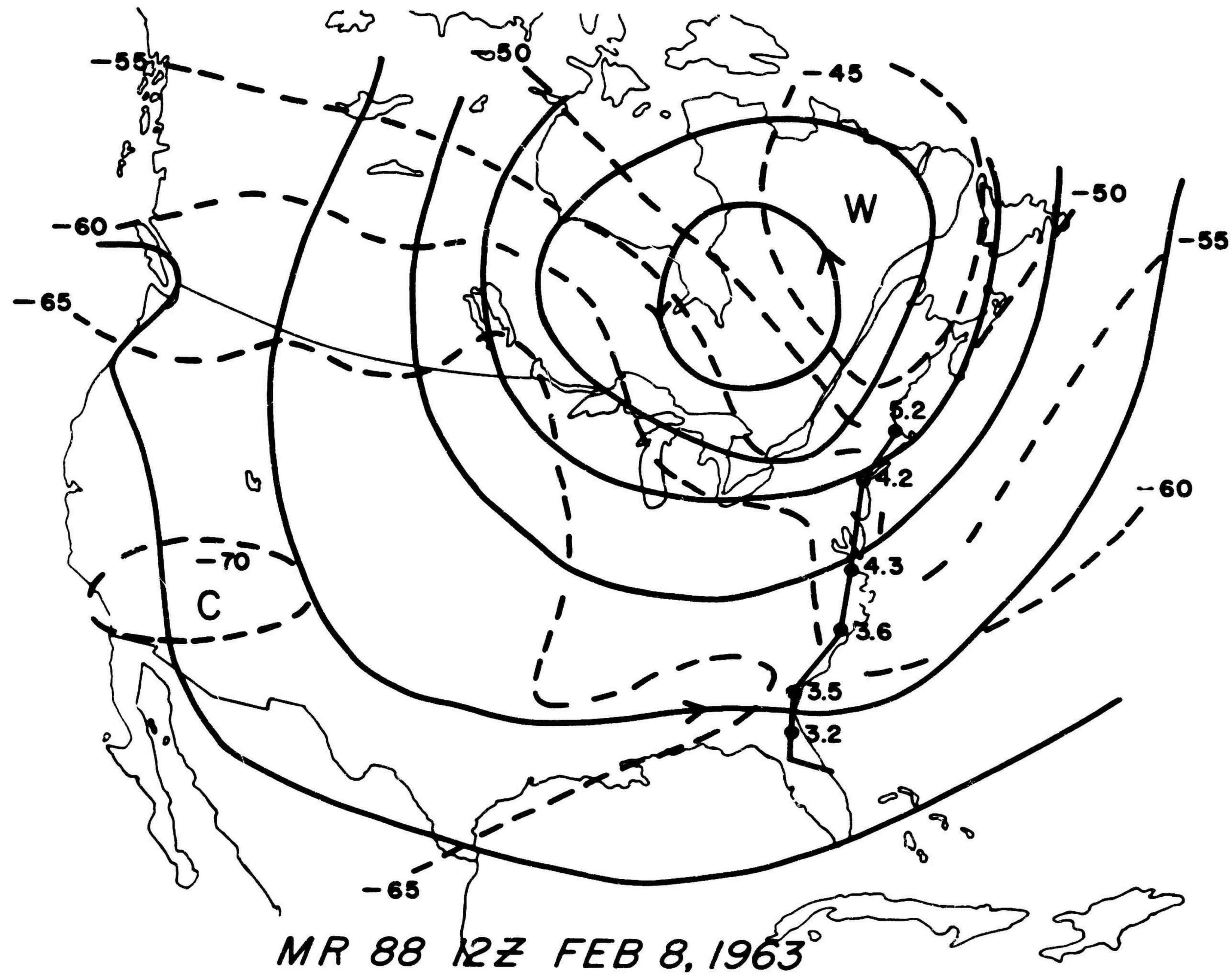

FIGURE 1.

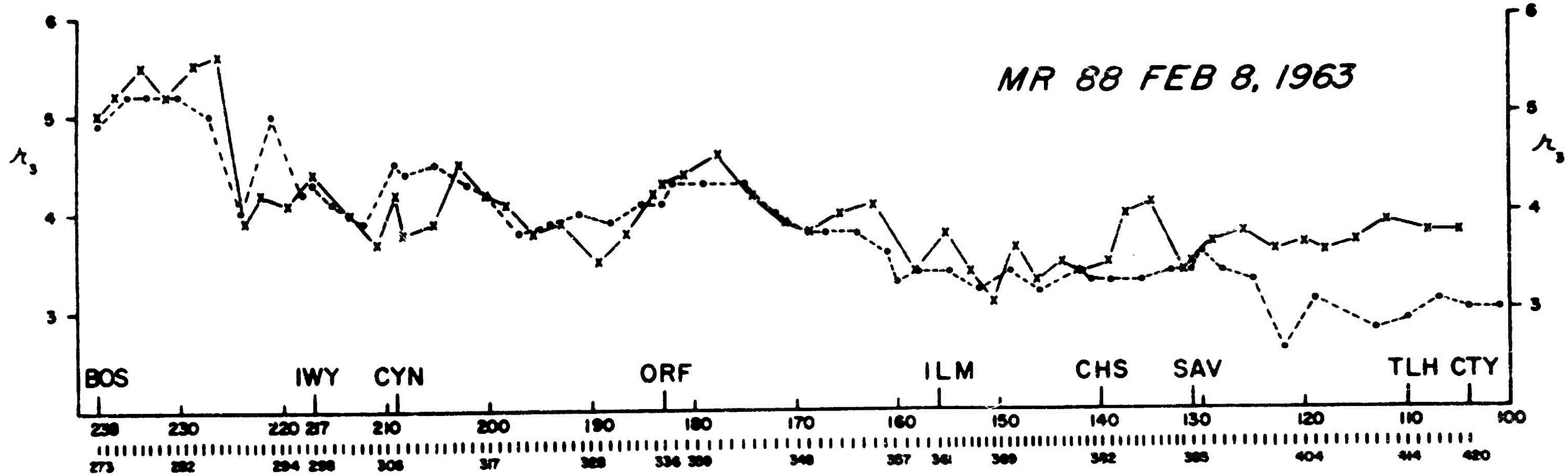

FIGURE 2.

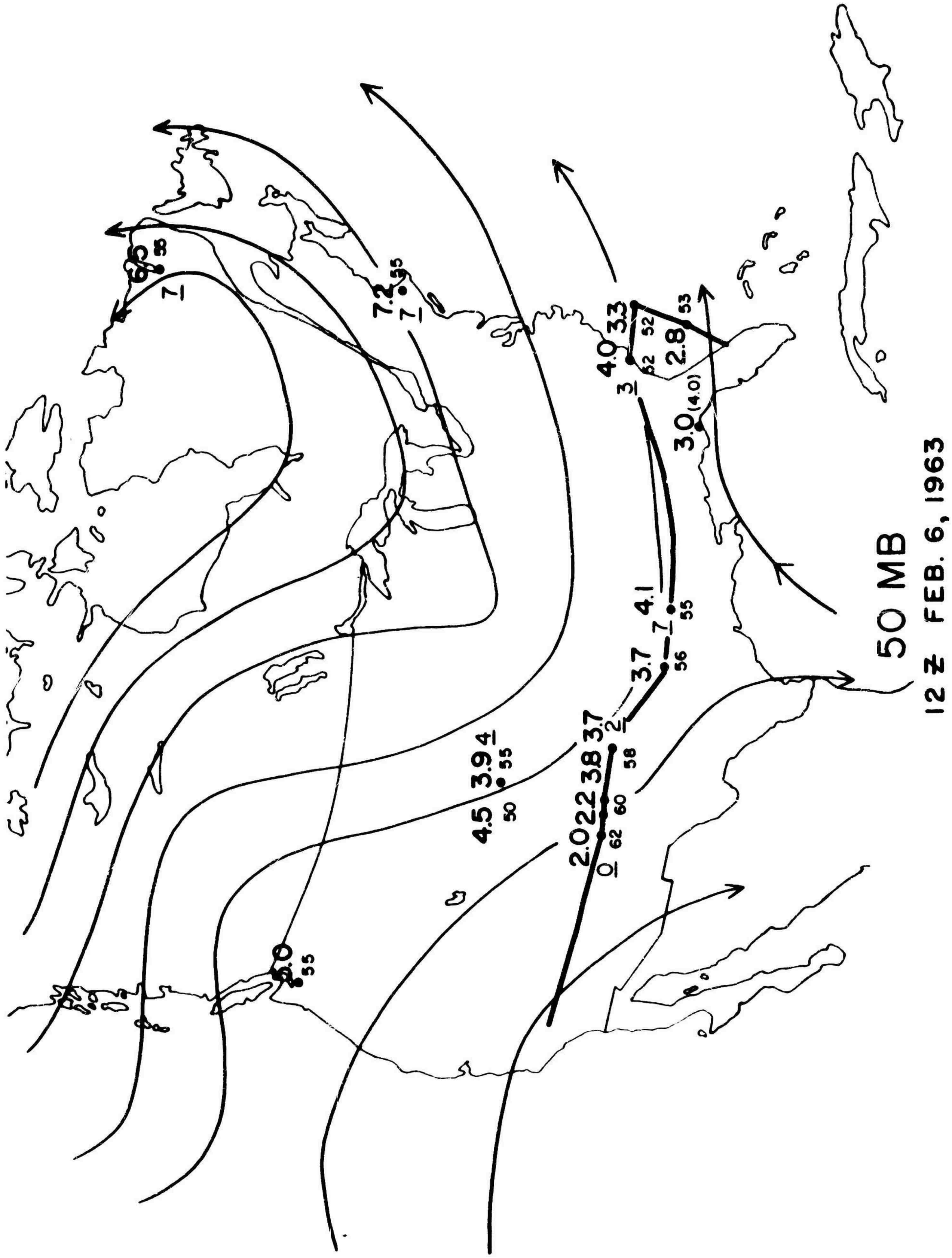

FIGURE 3.

RECENT OZONE OBSERVATIONS IN THE ANTARCTIC STRATOSPHERE

W.S. Weyant

A review of some Antarctic ozone measurements during the past few years was presented. The 1958 Halley Bay ozonesonde observations (MacDowall and Smith 1962) were briefly discussed; it was noted that these observations, using instruments of the Brewer type, indicated that the first sharp increase in ozone content with height coincided with the tropopause, except for the flight of October 30, 1958, when the increase began in the upper troposphere well below the indicated tropopause level. The results of the Little America V Dobson observations for the IGY period were also discussed, particularly the increase of ozone from September to a maximum in November corresponding to the spring stratospheric warming, and a dropping off to summer values of total ozone on the order of .31 cm (Wexler et al., 1960).

In 1962 a program of ozonesonde observations, using instruments of the Regener type, was instituted at Amundsen-Scott (South Pole) and Hallet Stations in Antarctica, and the program was extended to include Wilkes Station in 1963. Ozonogram plots of some of these soundings were presented; it was noted that while the absolute amounts of ozone measured might be subjected to considerable error, their relative distribution in the vertical and the heights of maximum ozone concentrations seemed quite reliable. The height of the maximum partial pressure of ozone was located generally between 100 and 60 millibars (about 14 to 18 km.) throughout the year. At the South Pole, the height of this maximum, near 60 millibars in August, gradually lowered to about 100 millibars by late October, but a November 16 ascent showed the maximum again at 56 millibars. The rapid spring warming of the lower stratosphere occurred during the second week in November, 1962, at the South Pole. It was also noted that several of the soundings showed an increase in ozone concentrations in the upper troposphere, while in the remainder the first increase with height coincided with the tropopause level. Both Hallett and Pole Stations showed a tropospheric increase to be more common in the February to June period, while from July to November the increase coincided with the tropopause level in most cases.

Finally, the planned ozone observational programme for U.S. Antarctic stations during the Internation Quiet Sun Years of 1964-65 was described. Ozone measurement programmes will be confined to Byrd Station (80 S 120 W) and the South Pole Station during this period; each of these stations will take continuous measurements of surface ozone concentrations and also observations of total ozone with Dobson ozone spectrophotometers when possible. Ozonesonde flights will be made at least once weekly at each station throughout the period, and three times weekly during certain specified weeks. In addition to providing further information about ozone concentrations and their changes in the Antarctic atmosphere, the flights will be scheduled to fit into a meridional line of such observations extending from the Arctic to the South Pole.

REFERENCES :

MacDowall, J. and J.A. Smith : ' Ozone Soundings', The Royal Soc. Internat'l Geophys. Year Antarctic Exp., Halley Bay, 1955-59, Vol. 3, 98 - 110. The Royal Society , London 1962.

Wexler, H. , W.B. Moreland and W.S. Weyant : 'A preliminary report on ozone observations at Little America, Antarctica', Monthly Weather Review, 1960, 43 - 54.

ANTARCTIC MICROMETEOROLOGY and CLIMATOLOGY

P. C. Dalrymple

The Quartermaster Research and Engineering Center in Natick, Massachusetts, conducted the micrometeorology programs in glaciology at Little America V in 1957 and at the South Pole in 1958 as part of the USNC-IGY program in Antarctica.

The two types of temperature sensors used at the South Pole (shielded No. 40-gauge copper constantan thermocouples and protected No. 30-gauge copper constantan thermocouples) have been tested at the University of Michigan in a wind tunnel. It was shown that the maximum radiation errors occur with low solar angles, high solar intensities, low wind speeds, and with the wind parallel to the sensors, and that these errors can be as much as 2C degrees. The temperatures measured at subsurface and above surface during the period without sun by the protected probes were shown to be accurate within a tenth of a degree centigrade. Monthly mean temperatures were presented for all depths and heights measured at the South Pole in 1958. Each mean temperature was computed from approximately 12,000 observations during the month (Table 1).

Wind speeds were measured by a Beckman and Whitley wind system with a 6-channel counter system. Over 1400 wind speed profiles were measured at the South Pole in 1958. Anemometer levels were maintained at 800, 400, 200, 100, and 50 centimeters and another set of cups was placed close to the surface for experimental purposes. Monthly mean wind speed profiles are shown for all eleven months of data. (Table 2). Anemometer cups placed with their centers 4 centi-

TABLE 1

MONTHLY MEAN TEMPERATURES (-°C)
(SOUTH POLE, 1958)

A. Surface and Above

	Surface	3cm	6cm	12cm	25cm	50cm	100cm	200cm	400cm	800cm
Feb	36.20	36.03	36.18	36.37	36.47	36.45	36.40	36.38	36.23	35.95
Mar	56.05	55.70	55.68	55.63	55.59	55.56	55.39	55.25	54.92	54.29
Apr	64.11	63.66	63.57	63.50	63.44	63.36	63.23	63.09	62.80	62.00
May	59.78	59.03	58.60	58.40	58.34	58.18	58.02	57.88	57.61	57.03
Jun	63.29	63.10	62.16	61.30	61.68	61.58	61.42	61.30	61.03	60.53
Jul	59.43	58.95	58.82	58.66	58.57	58.45	58.32	58.19	57.99	57.53
Aug	63.95	63.33	63.12	62.92	62.81	62.71	62.58	62.42	62.18	61.43
Sep	60.72	60.18	59.21	58.72	58.52	58.39	58.27	58.08	57.75	56.99
Oct	49.97	49.34	49.56	50.06	50.01	49.96	49.91	49.77	49.61	49.23
Nov	37.71	38.64	38.99	39.17	39.20	39.18	39.11	39.10	39.03	38.95

B. Subsurface

	-800cm	-250cm	-50cm	-25cm	-10cm	-5cm	-2cm
Feb	51.79	43.56	35.90	35.89	36.16	36.58	36.75
Mar	51.41	44.16	48.38	49.59	52.64	54.80	56.16
Apr	50.69	47.03	57.40	58.61	61.20	62.93	63.88
May	50.28	50.23	56.95	57.88	58.69	59.10	59.31
Jun	50.16	51.52	59.03	61.11	62.03	62.56	62.87
Jul	50.25	52.75	56.89	57.31	57.58	57.86	58.05
Aug	50.37	53.28	59.30	62.00	63.01	63.34	63.87
Sep	50.56	53.94	57.63	58.33	58.85	59.44	59.72
Oct	50.56	53.71	53.44	51.75	51.28	50.94	50.83
Nov	50.98	52.98	46.13	42.14	40.69	39.77	39.22

TABLE 2

MONTHLY MEAN WIND SPEED PROFIL-
(Height, cm - Speed, cm/sec)

	No. of Profiles	Hgt.	Speed	Hgt.	Speed	Hgt.	Speed	Hgt.	Speed	Hgt.	Speed
JAN	67	49.1	529.0	99.1	577.1	199.1	619.6	399.1	699.1	799.1	712.8
FEB	83	44.0	296.[illegible]	94.0	328.0	194.0	359.7	394.0	398.8	794.0	458.0
MAR	83	43.3	344.2	93.3	382.7	193.4	422.3	394.1	483.8	797.3	569.9
APR	83	53.8	340.6	103.8	373.1	203.8	412.8	404.8	479.0	804.0	573.6
MAY	70	56.0	553.0	106.0	600.1	206.0	651.8	406.0	719.0	806.0	797.2
JUN	96	49.0	470.9	99.0	519.9	199.0	575.4	399.0	636.2	799.0	728.7
JUL	106	49.2	589.5	98.7	649.7	198.7	705.5	390.1	774.3	790.1	358.5
AUG	129	47.9	417.3	99.2	464.7	194.4	515.3	385.1	573.6	785.6	663.0
SEP	137	44.7	530.8	96.5	554.8	189.5	660.5	381.1	694.8	781.4	779.4
OCT	133	42.6	517.8	92.6	559.8	185.6	605.9	382.6	670.9	776.6	755.0
NOV	86	47.4	369.4	97.4	398.8	194.7	431.5	393.5	469.1	791.2	514.8

meters above the surface yielded logarithmic results. Monthly plots of mean wind speed profiles show that logarithmic conditions existed in the first eight meters during mid-summer, and that profiles were logarithmic only to 200 or 400 centimeters, depending upon stability, during the winter months (Fig. 1).

Surface inversions in the lower eight meters were related to the overall inversions. The total inversion at interior stations in East Antarctica showed higher inversions of greater intensity than those measured at the South Pole and Byrd stations. The average mid-winter inversion at Vostok is approximately 1000 meters in depth and of 23 C degrees in intensity, while at Byrd the average mid-winter inversion is approximately 600 meters in depth and 12 C in intensity. The maximum inversions to eight meters at the South Pole were 13 to 15 C degrees.

A comparison of firn temperature versus mean annual temperatures for Byrd. South Pole, Komsomolskaya, Vostok, and Pionerskaya show that Byrd's firn and mean annual temperatures are within a tenth of a centigrade degree. while the firn temperatures for the other sites are from 0.9 to 1.7 of a centigrade degree colder. It was proposed that this colder temperature would more closely approximate the mean annual temperature of the snow surface.

The main emphasis for albedo measurements was placed on the differences between the measured values. The Russian albedo measurements for Vostok, Sovietskaya, Komsomolskaya, and Pionerskaya, are higher during the spring than during the fall, a condition which is just the reverse of that experienced at the South Pole. The differences are believed to be the result of different methods of measurements. The snow surface is considerably rougher at the end of the winter period with higher winds than they are at the end of summer and one would normally expect a higher albedo in late summer when the surface is smoother.

Climatic classifications for the Antarctic were discussed, and a new climatic breakdown was presented for the Antarctic Plateau. This region was defined on the basis of elevation and slope (1500 feet and less than a one degree slope in West Antarctica and 2000 feet and less than a one degree slope in East Antarctica). Four climatic regions were presented for the Antarctic Plateau : Cold Central Core, Cold Interior, Cold Katabatic, and Cold Transitional. The difference from one climatic region to another is basically one of extremes. Temperature, wind speed, and solar radiation are presented as the most important climatic elements for the polar regions. The one element which unites the four regions into a whole is windchill, where comparable values are obtained for all interior stations because of the higher wind speeds associated with the less cold temperatures near the coast.

The analyses of the micrometeorological data were presented in two additional lectures by Dr. Heinz H. Lettau, University of Wisconsin, who served as both a consultant and an expert to the data reduction and analyses project conducted at the Quartermaster Research and Engineering Center.

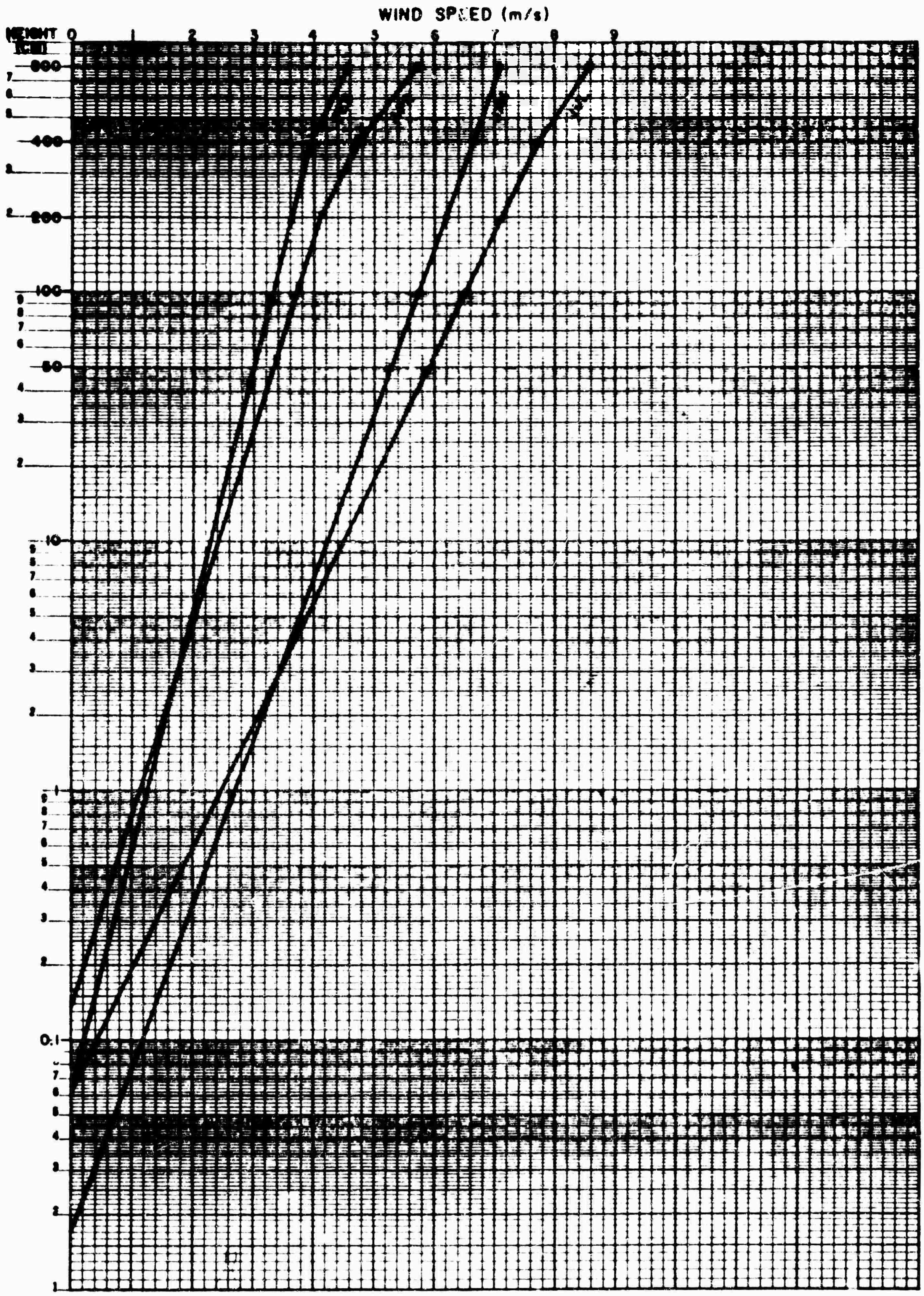

FIG. 1 MONTHLY MEAN WIND PROFILES

SEASONAL TRENDS IN ENERGY BUDGET TERMS OF THE SNOW SURFACE AT THE SOUTH POLE, 1958.

$$R_o = Q_o + S_o + E_o$$

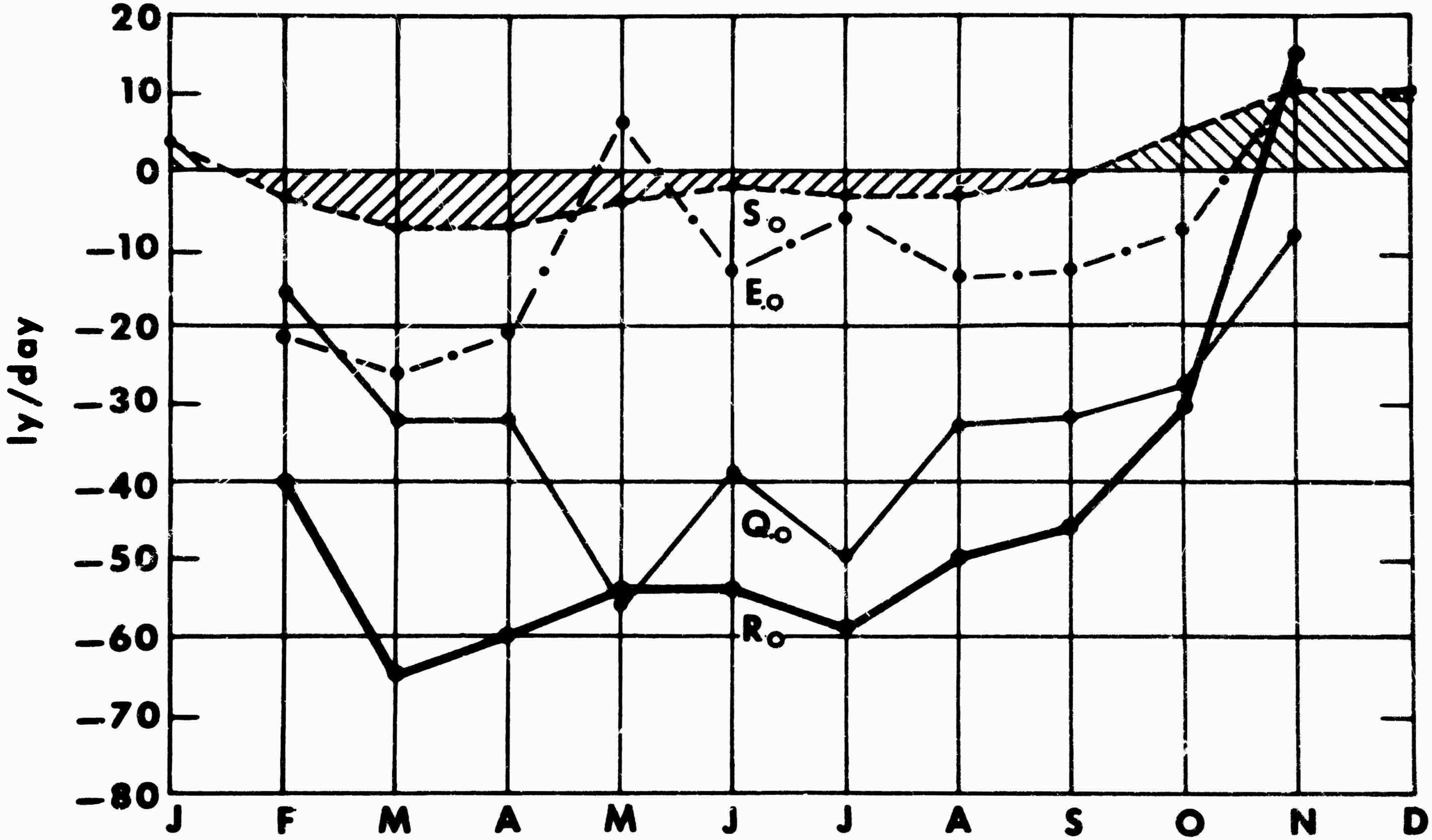

FIGURE 2.

CORRESPONDENCE BETWEEN THEORETICAL MODELS AND ACTUAL OBSERVATIONS IN ARCTIC MICROMETEOROLOGY

H.H. Lettau

In comparison with micrometeorological experience at temperate and low latitudes (where one deals, typically, with strong diurnal variations of thermal stratification over a variety of surface covers, ranging from forest canopies to desert ground, with emphasis on lapse conditions), one could say that arctic micrometeorology will be concerned, typically, with inversion conditions over relatively uniform snow and ice surfaces. For example, of the total of more than 1400 hourly mean wind profiles observed by Dalrymple (1961) during the 1958 South Pole Micrometeorology Program, at Amundsen-Scott Station, less than 2% showed lapse cases; strong to moderate inversion was the prevailing condition.

The exceptional quantity and high quality of the South Pole data permitted an unusually detailed and systematic analysis of the curvature characteristics of micrometeorological wind (V) and potential temperature (θ) profiles. Profile curvature is measured by the Deacon numbers which are formally defined as De, or β, or $\beta_V = -zV''/V'$; and DE, or $\beta_\theta = -z\theta''/\theta'$, where the primes denote partial differentiation with respect to height (z). These numbers are a function of stability, measured by the Richardson number Ri $= g\theta'/T_m V'^2$, where g = gravity, and T_m = absolute mean layer temperature. For detail, reference is made to Dalrymple, Lettau and Wollaston (1963). An example of a typical condition at the South Pole is illustrated in Fig. 1. The graphs are based on the average of 30 runs, each of which is represented by an hourly mean wind and temperature profile producing an effective $\underline{Ri}_1$-value (at the 1 m level) between 0.023 and 0.025. It is interesting to note that the temperature profile (see the upper-right part of Fig. 1), for this stability, shows an inflection point between 2 and 3 m; consequently, β_θ goes through zero at this level. The Deacon number of the wind profile (β_V), however, stays positive. For the numerous cases with larger $\underline{Ri}_1$ the detailed analysis of the South Pole data has shown that, while β_θ can become significantly negative, β_V stays always positive; this Deacon number appears to be limited by a minimum value of about 0.25 and tends to increase further upwards once it has passed through this minimum value. For detail, reference can be made to Fig. 6 and Fig. 9 of the South Pole data-analysis report. These findings must be considered of great importance for the correspondence between theoretical models and actual profile data, not only in arctic micrometeorology, but quite in general .

It can be shown that the above described behaviour of curvature characteristics cannot be accounted for by a theoretical model of surface layer structure, or any modification or revision thereof, since the real cause must be sought in an effect of momentum-flux divergence. In other words, the re-curvature in the β_V-profile occurs outside the surface layer, the thickness of which may be reduced to less than 1 m in a strong inversion condition. In comparison with the temperature profile, this reduction is much more pronounced for the wind profile, because increasing $\underline{Ri}_1$, for constant horizontal pressure gradient , is invariably accompanied by a decrease of both surface drag (τ_o) and low-level wind speed (V); thus, the geostrophic departure of the surface wind must increase and, as a consequence of the equation of motion, the absolute value of $\partial \tau / \partial z$ increases; the end result is that $-\tau_o / (\partial \tau / \partial z)$, which determines the thickness of the surface layer, must decrease considerably with increasing stability. For a detailed discussion of this, and the corresponding behaviour of

β_V above the surface layer of a barotropic and adiabatic boundary layer, reference is made to Lettau (1962). In Section 3.7 of Dalrymple, Lettau and Wollaston (1963) it is demonstrated that in the lowest 1 to 2 m of the atmosphere the observed β_V versus Ri relationship agrees quite satisfactorily with the theoretical curve which according to Panofsky (1963), can be referred to as the "KEYPS" formula.

Among the practical applications of micrometeorological surface layer theory the most frequently demanded information concerns the surface value (Q_o) of convectional heat flux density (Q). A convenient approach is to estimate, first of all, the surface drag (τ_o) with the aid of wind profile theory using Karman's constant; then to apply a similarity hypothesis by writing $Q_o = - c_p \; \tau_o \; \gamma \; \theta' / V'$, where c_p = specific heat of the air, and $\gamma = K_Q/K_M$ = ratio of eddy diffusivities for heat and horizontal momentum. In diabatic surface layers the estimate of τ_o depends on the assumed analytical form of the wind profile , i.e., the manner in which surface roughness (z_o), zero-point displacement (d), and shearing velocity ($\sqrt{\tau_o / \rho}$) appear as factors in the wind profile function V (z).

For the estimate of Q_o with the above described method, Thornthwaite and Holzman (1939) , and later, Halstead (1954) used a model which, essentially, assumes that $\beta = 1$ in diabatic as well as adiabatic states. Deacon (1953) introduced a model in which $\beta = \beta_o$ = const, larger than unity for lapse and smaller than unity for inversion cases. In view of the analysis results derived from Dalrymple's extraordinarily detailed profile data in the lowest 8 m above the central Antarctic region, as exemplified, in part, by Fig. 1 , a new model is suggested, which is characterized by $\beta - 1$ being proportional to the distance from the lower boundary. For a schematic illustration of the new model, in comparison with Deacon's model, see Fig. 2. An advantage of the new model is that it permits readily the determination of a zero point correction for the anemometer mast, together with the numerical determination of z_o and τ_o and their statistical errors. A schematical chart which illustrates the steps of a practical evaluation of an observed wind profile is given in Fig. 3. The new model has been employed and tested in the analysis of the South Pole data. The results, when judged by various criteria such as, for example, that the aerodynamic surface roughness z_o should not depend significantly on stability, or that profile curvature variations should be continuous and systematic, etc., are encouraging. It can also be proven analytically that a linear dependency of β on height is - at least for inversion conditions - in tolerable agreement with direct mathematical consequences of the theoretical "KEYPS" formula.

The estimated value of heat flux at the surface will depend on the magnitude of wind shear and temperature gradient in the immediate vicinity of the actual interface. For the case of $Q_o \neq 0$, wind shear and temperature gradient are interrelated with each other. It can be shown that for inversional stratification Q_o is overestimated when one assumes logarithmic profile structure, i.e., $\beta = 1$, as in the models of Thornthwaite and Holzman, and of Halstead; the value of Q_o is underestimated, when one assumes the power law, i.e., $\beta = \beta_o < 1$, as in Deacon's model for inversional stratification. For lapse conditions the reversed statement would be true. In arctic meteorology the Thornthwaite-Holzman model has been most frequently employed; see, for example, Lister and Taylor (1961).

The validity of the above statement can be demonstrated by the evaluation of Q_o using, as an example, the data of the selected 30-run average illustrated in Fig. 1. No zero point displacement was found for this particular case, i.e., $d = 0$, while $z_c = 0.019$ cm. The results of Q_o estimates, expressed in ly/hours, and uniformly employing a 0.428 value of the Karman constant, and $\gamma = K_Q/K_M = 1$ (unless otherwise stated) were :

Thornthwaite and Holzman [1]	-1.4 ly/hour
Halstead [1] (for γ = 1.41)	-2.4 "
Halstead for γ = 1.00)	-1.7 "
Deacon [1] for β_o = 0.70)	-0.2 "
Dalrymple, Lettau and Wollaston [2]	-1.1 "
Liljequist (for V_{10} = 6.4 m/sec)	-2.2 "

The last line refers to the empirical relationship suggested by Liljequist (1956) in the analysis of the micrometeorological data at Maudheim, $Q_o = 0.0058\ V_{10}$ (ly/min), where V_{10} is the windspeed at 10 m, expressed in m/sec.

The method of Q_o estimates employed by Dalrymple , Lettau and Wollaston produced a satisfactory agreement with energy budget requirements for the South Pole region considering USWB net radiation data and independently derived sub-surface heat fluxes. This can be interpreted as meaning that Q_o -values estimated with the aid of the Deacon formula would be decisively too low, the others too high. In the past , such discrepancies were frequently removed by assuming a convenient γ - value (mostly $\gamma < 1$ in inversion conditions). Our conclusion is that $\gamma = 1$ is still a good assumption.

---

[1] using data at levels 50 and 100 cm.

[2] using data at levels 50, 100, and 200 cm.

REFERENCES :

Dalrymple, P.C. : 'South Pole micrometeorological program; part I data presentation,' Techn. Rept. ES-2, Earth Sciences Division, QM R & E Command, Natick, Mass., 1961.

Dalrymple, P.C., H.H. Lettau, and S.H. Wollaston : 'South Pole micrometeorological program ; part II :data analysis', Techn. Rept. ES-7, Earth Sciences Division, QM R & E Command, atick, Mass., 1963.

Deacon, E.L. : 'Vertical profiles of mean wind in the surface layers of the atmosphere,' Geophys. Memoirs, No. 91, 1953 .

Halstead, M.H. : 'The fluxes of momentum heat and water vapor in micrometeorology', Pub. in Climat. Vol. 1 No. 2 , Lab. of Climatology, The John Hopkins University, 1954 .

Lettau, H.H. : 'Notes on theoretical models of profile structure in the diabatic surface layer,' Section 10, Final Rept., Studies of the three-dimensional structure of the planetary boundary layer, Univ. of Wisconsin, 1962.

Lilijequist, G.H. : ' Energy Exchange of an Antarctic snow-field ', part I, Vol. II , Scientific results, Norwegian British-Swedish Antarctic Expedition 1949-1952, Oslo, 1956-57.

Lister, H. and P.F. Taylor : ' Heat balance and ablation on an Arctic glacier'. Meddelelser om Groenland, Vol. 158, No. 7, Koebenhavn, 1961.

Panofsky, H.A. : 'Determination of stress from wind and temperature measurements,' Quart. J. Royal Meteor. Soc. , Vol. 89, p. 85, 1963.

Thornthwaite, C.W., and B. Holzman : 'The determination of evaporation from land and water surfaces,' Monthly Weather Rev. , 67, 4 - 11, 1939.

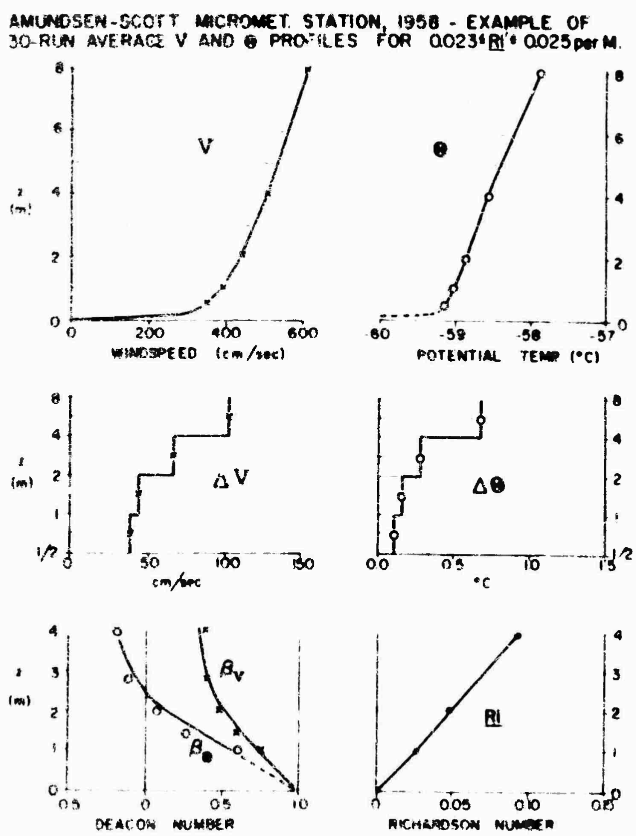

Figure 1. Example of 30-run averages of micrometeorological profiles of wind speed (V) and potential temperature (θ) in the lowest 8 m (in linear height scale) at Amundsen-Scott Station, 1958. This group comprises only those individual sets of hourly-mean V and θ which produced an effective Ri_1 number (at the 1 m level) Between 0.023 and 0.025. Profiles of vertical differences (over double-heights) are illustrated (in logarithmic height scale) in the center part, and profiles of Deacon and Richardson numbers (in linear height scale) in the lower part of this figure.

WIND PROFILE FORMULAS FOR THE SURFACE LAYER

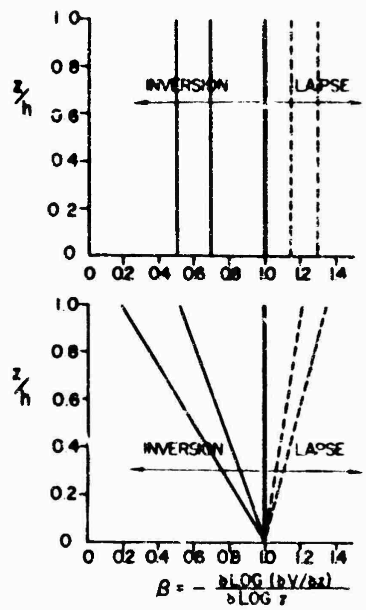

$(z \leq h)$

DEACON (1953): $\beta = \beta_0$

$$V = \frac{\sqrt{\tau_0/\rho}}{k(1-\beta_0)} \left[\left(\frac{z+z_0}{z_0}\right)^{1-\beta_0} - 1\right]$$

LETTAU (1963): $\beta = 1 + \beta'_0 z$

$$V = \frac{\sqrt{\tau_0/\rho}}{k}\left[\log_e \frac{z+z_0}{z_0} + \Phi\right], \text{ WHERE}$$

$$\Phi = \int_0^z \frac{e^{1-\beta}-1}{z+z_0}\,dz = 1-\beta + \frac{(1-\beta)^2}{4} + \frac{(1-\beta)^3}{18} + \cdots$$

Figure 2. Schematical comparison of two wind profile formulae for the atmospheric surface layer ($z \leq h$), in terms of curvature characteristics ($\beta = -zV'/V''$) versus relative height (z/h). Note that the 1963-model leads, analytically exact, to a form of the integral -diabatic influence function (Φ) which reduces to the "log + lin" -law if the deviation of β from unity remains relatively small.

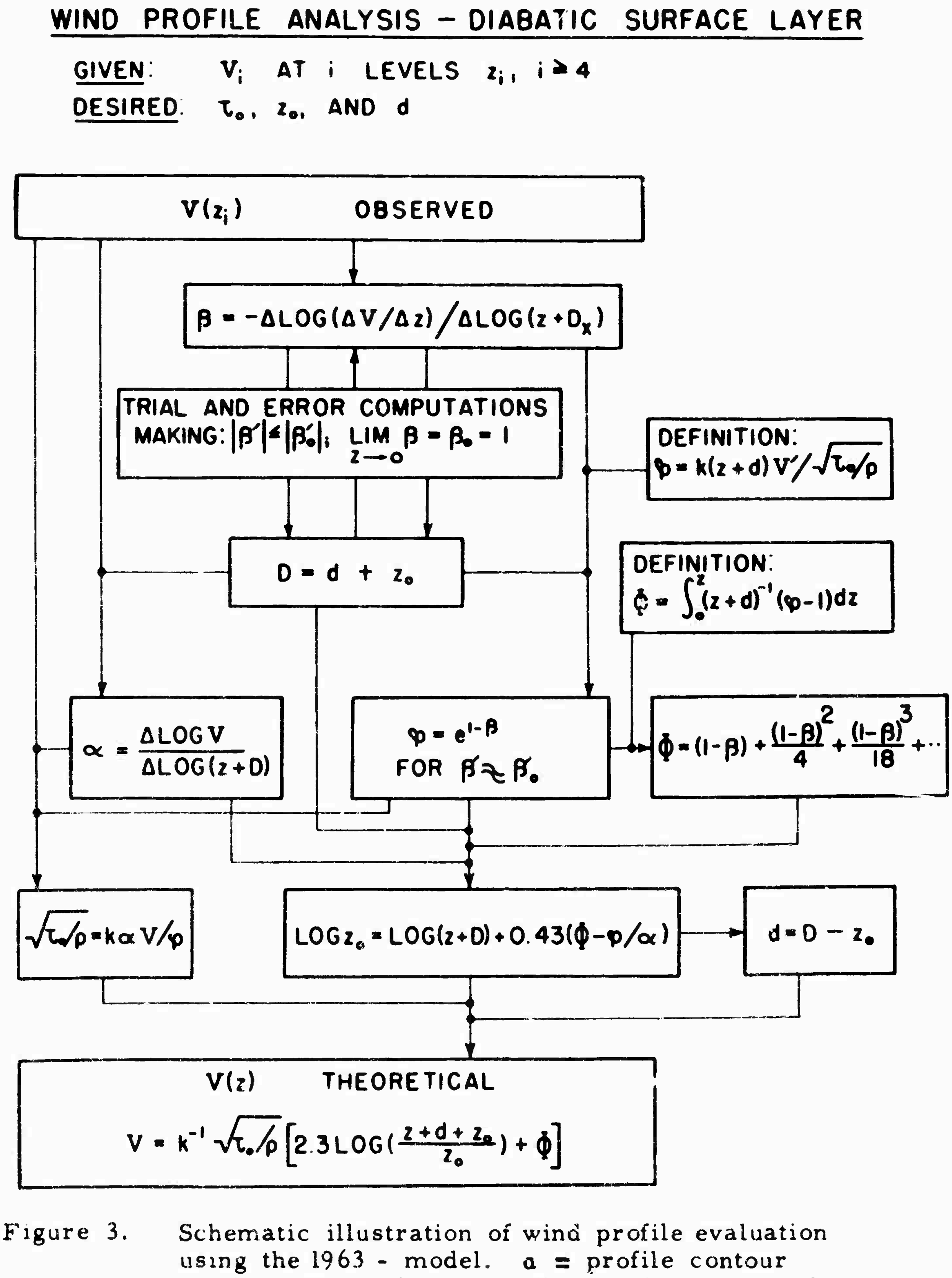

Figure 3. Schematic illustration of wind profile evaluation using the 1963 - model. α = profile contour number, φ = diabatic influence function, and Φ = integral -diabatic influence function.

HEAT BUDGET OF THE ARCTIC

E. Vowinckel and Svenn Orvig

The discussion of the heat budget of the Arctic presented at Stanstead was based partly on work which has already been published and which is listed in the references and partly on material under preparation for publication.

The energy exchange between the earth's surface and the atmosphere has been studied for the area north of 65 N, for every month of the year. Each term in the heat balance equation has been examined, beginning with the heat transport into the Arctic by ocean currents and the heat gain due to freezing and export of sea ice.

The solar radiation term was next studied, by calculating the loss of short wave radiation in the atmosphere and its reflection at the surface. Such calculations required knowledge of cloud type and amount over the Arctic throughout the year, as well as knowledge of albedo of various surfaces. Such studies were performed and published with values given for grid points for each month. The net result is a set of grid point values of absorbed solar radiation for each month, in the whole arctic area.

Next terrestrial radiation was examined. Reliable observations are available only for short wave radiation, and the long wave components must be obtained by application of radiation laws to the measured state of the atmosphere. Grid point values were obtained both for long wave radiation emitted from the ground and received at the ground from the atmosphere. The long wave radiation balance and the short wave absorbed radiation values give the total radiation balance at the surface throughout the year.

Next, it was of importance to know the radiation terms for the top of the troposphere, as only such values allow the determination of the enrgy gain and loss for the atmosphere-earth system as a whole. A comparison of the balance at the surface and at 300 mb makes possible some assessment of the magnitude of non-radiative processes. The radiation balance of the troposphere is obtained, and next the balance for the earth-atmosphere system. Characteristic radiation balance areas emerge and these are presented in maps and cross-sections.

Further studies of heat balance of the Arctic are under way. Such are evaporation and sensible heat flux studies, and an examination of energy transport to or from sub-surface layers. The average values of all of these terms should help in the understanding of the climate of the Arctic .

REFERENCES :

Boyes, G.A. : 'Meridional advection of moisture in the Arctic,' Arctic Met. Res. Gp. , Pub. in Met 57, McGill University, 42, 1963.

Larsson, P. : 'The distribution of albedo over Arctic surfaces', Geog. Rev. Vol.53, No. 4, 572-579 , 1963.

Larsson, R., and S. Orvig : ' Atlas of mean monthly albedo of Arctic surfaces ', Arctic Met. Res.Gp. Pub. in Met. 45, McGill University, 1961.

Vowinckel, E. : 'Cloud amount and type over the Arctic', Arctic Met.Res.Gp. Pub . in Met. 51, McGill University, 1962.

Vowinckel, E. : 'Ice transport between Greenland and Spitsbergen, and its causes ', Arctic Met. Res.Gp. Pub. in Met. 59, McGill University, 1963.

Vowinckel, E. and S. Orvig : ' Water balance and heat flow of the Arctic Ocean ', Arctic, Vol .15., No. 3, 205 - 223, 1962.

Vowinckel, E . and S. Orvig : 'Relation between solar radiation income and and cloud type in the Arctic ', J. Appl. Met., Vol. 1, No. 4 , 552-559, 1962.

Vowinckel, E. and S. Orvig : ' Insolation and absorbed solar radiation at the ground in the Arctic ', Arctic Met. Res. Gp. Pub. in Met 53, McGill University 1962.

Vowinckel , E. and S. Orvig : ' Long wave radiation and total radiation balance at the surface in the Arctic ', Arctic Met. Res.Gp. Pub. in Met 62, McGill University , 1963

Vowinckel, E. and S. Orvig : ' Radiation balance of the troposphere and of the system earth-atmosphere in the Arctic ', McGill University, in press.

AF Cambridge Research Laboratories, Bedford, Mass.
Contributions to the SEMINARS ON THE STRATOSPHERE AND MESOSPHERE AND POLAR METEOROLOGY,
July 7 - 19, 1963
F. K. Hare, Chairman, January 1964, 244 pp.
AFCRL 64-197 Unclassified Report

This report contains extended summaries of all the lectures presented at the meetings held at Stanstead in July 1963. Some summarize work already in print, and many contain material which has not yet been published. The summaries range over a wide variety of topics including polar micro-climatology, automatic data processing and computer applications to numerical weather prediction, atmospheric ozone, problems of atmospheric dynamics and energy and momentum studies, and atmospheric tides and gravity waves.

UNCLASSIFIED

1. Meteorology
2. Stratosphere and Mesosphere

I Hare, F.K.

UNCLASSIFIED

AF Cambridge Research Laboratories, Bedford, Mass.
Contributions to the SEMINARS ON THE STRATOSPHERE AND MESOSPHERE AND POLAR METEOROLOGY,
July 7-19, 1963
F. K. Hare, Chairman , January 1964, 244 pp.
AFCRL 64-197 Unclassified Report

This report contains extended summaries of all the lectures presented at the meetings held at Stanstead in July 1963. Some summarize work already in print, and many contain material which has not yet been published. The summaries range over a wide variety of topics including polar micro-climatology , automatic data processing an computer applications to numerical weather prediction, atmospheric ozone, problems of atmospheric dynamics and energy and momentum studies, and atmospheric tides and gravity waves.

UNCLASSIFIED

1. Meteorology
2. Stratosphere and Mesosphere

I Hare, F.K.

UNCLASSIFIED

AF Cambridge Research Laboratories, Bedford, Mass.
Contributions to the SEMINARS ON THE STRATOSPHERE AND MESOSPHERE AND POLAR METEOROLOGY,
July 7 -19, 1963.
F. K Hare, Chairman, January 1964, 244pp.
AFCRL 64-197 Unclassified Report

This report contains extended summaries of all the lectures presented at the meetings held at Stanstead in July 1963. Some summarize work already in print, and many contain material which has not yet been published. The summaries range over a wide variety of topics including polar micro-climatology, automatic data processing and computer applic tions to numerical weather prediction, atmospheric ozone, problems of atmospheric dynamics and energy and momentum studies, and atmospheric tides and gravity waves.

UNCLASSIFIED

1. Meteorology
2. Stratosphere and Mesosphere

I Hare, F.K.

UNCLASSIFIED

AF Cambridge Research Laboratories, Bedford, Mass.
Contributions to the SEMINARS ON THE STRATOSPHERE AND MESOSPHERE AND POLAR METEOROLOGY.
July 7 - 19, 1963
F. K. Hare, Chairman, January 1964, 244 pp.
AFCRL 64-197 Unclassified Report

This report contains extended summaries of all the lectures presented at the meetings held at Stanstead in July 1963. Some summarize work already in print, and many contain material which has not yet been published. The summaries range over a wide variety of topics including polar micro-climatology, automatic data processing and computer applications to numerical weather prediction, atmospheric ozone, problems of atmospheric dynamics and energy and momentum studies, and atmospheric tides and gravity waves.

UNCLASSIFIED

1. Meteorology
2. Stratosphere and Mesosphere

I Hare, F.K.

UNCLASSIFIED